Mucosal Associated Invariant T cells in Pulmonary Tissue Repair



A thesis submitted in fulfilment of the requirements

for the degree of Doctor of Philosophy in Clinical Medicine

Xiawei Zhang

St Cross College, Trinity term 2024

Supervised by Associate Professor Timothy Hinks, Professor Paul Klenerman

Mucosal Associated Invariant T cells in Pulmonary Tissue Repair

Xiawei Zhang, St Cross College, University of Oxford; Trinity Term 2024

Thesis submitted for the degree of Doctor of Philosophy in Clinical Medicine

Abstract

Mucosal-associated invariant T (MAIT) cells are the most abundant unconventional T cells in the lung and can respond to bacterial, fungal, and viral challenges. We and others have recently described a potential role in promoting tissue repair. However, it is unknown what role MAIT cells play during sterile lung tissue damage.

Both wild-type (WT) and MAIT-deficient *Mr1*$^{-/-}$ mice were challenged with bleomycin to assess MAIT cells' role in sterile lung tissue damage, which was characterised using histology and RT-qPCR. Flow cytometry, bulk and single-cell RNA sequencing (scRNA-seq), cell adoptive transfer and MERSCOPE spatial transcriptomic analysis were used to examine MAIT cells' coordination with other immune cells during lung tissue damage responses, which were further assessed by analysing published human scRNA-seq data from idiopathic pulmonary fibrosis (IPF) patient lungs.

In vivo bleomycin challenge caused significant recruitment and activation of pulmonary MAIT cells and induced their tissue repair program. *Mr1*$^{-/-}$ mice exhibited more severe weight loss and tissue damage post-bleomycin challenge compared with their WT counterparts. scRNA-seq cell-cell communication analysis reveals that the absence of MAIT cells disrupted lung cell interactions. MAIT cells drive the accumulation of type 1 conventional dendritic cells (cDC1), limiting tissue damage in a DNGR-1-dependent manner rather than altering cDC1 functionality. The heightened tissue damage and weight loss of *Mr1*$^{-/-}$ mice were rescued by adoptive transfer of fms-like tyrosine kinase-3 ligand-generated bone marrow-derived dendritic cells

(FLT3L-BMDC) but DNGR-1 blockade negated this effect. Human scRNA-seq data revealed activated lung MAIT cells and increased cDC populations in IPF patients.

The data suggest that MAIT cells enhance defence against sterile lung injury by fostering cDC1-driven anti-fibrotic pathways, suggesting their potential role in modulating fibrosis in human IPF.

Preface

This thesis contains materials that have been published in peer-reviewed journal or bioRxiv.

1. Timothy SC Hinks, Xiawei Zhang. MAIT Cell Activation and Functions. Frontiers in immunology 2020 May 27:11:1014. doi: 10.3389/fimmu.2020.01014.

2. Xiawei Zhang, Shuailin Li, Wojciech Lason, Maria Greco, Paul Klenerman, Timothy SC Hinks. MAIT cells protect against sterile lung injury. bioRxiv 2024.01.08.574631; doi: https://doi.org/10.1101/2024.01.08.574631

This thesis contains materials that were obtained in collaboration with other lab members:

1. The mouse lung single-cell RNA sequencing (scRNA-seq) dataset was generated with assistance from Wojciech Lason and Maria Greco.
2. MERSCOPE slides were prepared with assistance from Esther Bridges. MERSCOPE runs were conducted by Maria Greco and Paola Vargas Gutierrez.
3. The data analysis for the mouse lung scRNA-seq dataset, the published Human Lung Cell Atlas and the IPF Cell Atlas, and the MERSCOPE spatial transcriptomic data, was carried out in collaboration with Shuailin Li.

Acknowledgements

I extend my heartfelt thanks to the China Scholarship Council and the Nuffield Department of Clinical Medicine for their generous CSC-NDM studentship, making my DPhil endeavour possible.

I am immensely grateful to my supervisors, Timothy Hinks and Paul Klenerman. Your guidance and expertise have been indispensable for a rewarding DPhil journey. You have served as inspirational role models, and I am very lucky to have you as my supervisors. Your support has been my pillar through all the highs and lows over the last three years, giving me the courage to become independent and chase my aspirations. Having once dreaded public speaking, I can now address an audience of experts with poise, and for that transformation, I owe you a great debt.

My appreciation also goes to the brilliant scientists at the Respiratory Medicine Unit, especially Sophie Morgan, Wentao Chen and Jian Luo, whose guidance and encouragement during the initial stage of my DPhil journey have been invaluable. I would like to extend my gratitude to my lab mate Wojciech Lason for the engaging conversations, steadfast support, and the shared meals and gatherings. Thanks are due to my wonderful housemates, Wanlin He and Hong Sun. Arriving abroad during a lockdown was daunting, but the cherished moments we've shared have made everything worthwhile. Your help in settling in has meant the world to me. My heartfelt thanks go to my friend Harry Tian Hu for your constant help and support throughout my DPhil journey. The joyous days spent traveling together will always hold a special place in my memory.

To my family, my enduring inspiration, thank you for your constant encouragement. My mum and dad do not speak any English and may not fully understand my DPhil work, but your belief in my potential has always motivated me to do my best. I am ever thankful to my boyfriend, Shuailin, for your companionship on the challenging days and unwavering support with my projects. The joyful memories we created together were a cherished part of my DPhil journey.

Table of Contents

Abstract ..... **ii**

Preface ..... **iv**

Acknowledgements ..... **v**

Table of Contents ..... **vi**

Acronyms and abbreviations ..... **xii**

List of Figures ..... **xv**

List of Tables ..... **xxi**

1 INTRODUCTION **1**

1.1 The immune system and unconventional T cells 1

1.1.1 The immune system: a complex defence network 1

1.1.2 Conventional T cells: the adaptive response architects 1

1.1.3 Restriction molecules and the MHC paradigm 2

1.1.4 The growing family of unconventional T cells 2

1.1.5 Unconventional T cells: expanding the repertoire of immune recognition 3

1.1.6 MAIT cells in focus 3

1.2 MAIT cell activation 5

1.2.1 TCR mediated activation 5

1.2.2 TCR-independent activation 7

1.3 MAIT cell function in lung infection 10

1.3.1 Mycobacteria and pulmonary tuberculosis 10

1.3.2 *Francisella tularensis* and *Salmonella* Typhimurium 13

1.3.3 *Legionella pneumophila* and *longbeachae* 14

1.3.4 *Streptococcus pneumoniae* 15

1.3.5 Influenza A virus 16

1.3.6 SARS-COV-2 and COVID-19 17

1.4 MAIT cells function in other lung diseases 18

1.4.1 Asthma 18

1.4.2 Chronic obstructive pulmonary disease 20

1.4.3 Community-acquired pneumonia 22

1.4.4 Lung cystic fibrosis 22

1.4.5 Interstitial lung diseases 23

1.4.6 Pulmonary sarcoidosis 23

1.4.7 Lung cancer 24

1.5 MAIT cell function in tissue repair and homeostasis 25

1.6 Bleomycin-induced sterile lung injury mouse model 27

1.7 Research aims 29

1.7.1 Aim 1 29

1.7.2 Aim 2 30

1.7.3 Aim 3 30

2 MATERIALS AND METHODS 31

2.1 Murine models 31

2.2 Murine pulmonary MAIT cell expansion using *Salmonella* Typhimurium BRD509 32

2.3 Murine *in vivo* bleomycin challenge 32

2.4 Murine *in vivo* PR8 influenza A virus infection 33

2.4.1 Propagation, quantification and mouse infection of PR8 influenza A virus 33

2.4.2 Propagation of PR8 influenza virus in MDCK cells culture from virus stocks 33

2.4.3 Quantification of PR8 influenza viruses by 50% tissue culture infectious dose assay ($TCID_{50}$) 34

2.4.4 Quantification of PR8 influenza viruses by plaque assay 34

2.4.5 PR8 influenza virus infection 35

2.5 Flow cytometry analysis 35

2.5.1 Generation of human and murine MR1 tetramers 35

2.5.2 Antibodies staining for flow cytometry and cell sorting 36
2.6 Histology.....39
2.6.1 Making Formalin-Fixed, Paraffin Embedded Blocks.....39
2.6.2 Haematoxylin and Eosin staining 40
2.6.3 Trichrome staining.....41
2.6.4 Scoring 42
2.7 Hydroxyproline assay 43
2.7.1 Hydroxyproline Standards for Colorimetric Detection.....43
2.7.2 Sample Preparation 43
2.7.3 Assay Procedure.....44
2.8 RT-qPCR and bulk RNA sequencing 44
2.8.1 Total RNA extraction.....44
2.8.2 RNA integrity assessment.....44
2.8.3 RNA quantification, purity check and reverse transcription 45
2.8.4 Reverse transcription quantitative polymerase chain reaction (RT-qPCR).....45
2.8.5 cDNA library preparation, sequencing by Novogene.....46
2.8.6 Bulk RNA-sequencing data analysis 46
2.9 10x Genomics library generation, sequencing and computational analysis 47
2.9.1 GEM generation and barcoding.....48
2.9.2 Post GEM-RT clean-up and cDNA amplification 49
2.9.3 V(D)J amplification from cDNA 49
2.9.4 V(D)J library construction 49
2.9.5 5' Gene expression (GEX) library construction 50
2.9.6 Cell surface protein library construction.....50
2.9.7 Sequencing.....50
2.9.8 Computational analysis.....50
2.10 Analysis of human IPF scRNA-seq datasets in HLCA and IPF cell atlas.....53

2.11 Culture and adoptive transfer of Flt3 ligand-generated bone marrow-derived dendritic cells 54

2.12 MERSCOPE runs 54

2.12.1 Tissue sectioning 55

2.12.2 Deparaffinization and decrosslinking 56

2.12.3 Anchoring pre-treatment 56

2.12.4 Cell Boundary Staining 56

2.12.5 RNA anchoring 57

2.12.6 Gel embedding 58

2.12.7 Clearing 58

2.12.8 Probe hybridization 59

2.12.9 Imaging 59

2.12.10 MERSCOPE spatial transcriptomic data analysis 60

2.13 Isolation of human TCR Vα 7.2^{+} lymphocytes from peripheral blood and coculture with human fibroblast cell line 61

2.14 Data analysis and statistics 62

3 MAIT Cell Dynamics in Response to Bleomycin-Induced Sterile Lung Injury 63

3.1 Introduction 63

3.2 Aims 65

3.3 Results 65

3.3.1 Activated MAIT cells accumulate in the lung upon bleomycin treatment in a cytokine-dependent manner 65

3.3.2 Bleomycin challenge activates the tissue repair programme of MAIT cells ... 79

3.4 Discussion 104

3.5 Conclusion 105

4 MAIT Cells Protect Against Sterile Lung Injury 106

4.1 Introduction 106

4.1.1 MAIT cell communication with DC 106

4.1.2 Lung conventional dendritic cells 107

4.1.3 The role of cDC1 and DNGR-1 signalling in the regulation of lung tissue damage 108

4.2 Aim 110

4.3 Results 110

4.3.1 MAIT cell-deficient mice show dysregulated pulmonary immune responses upon bleomycin challenge 110

4.3.2 Early accumulation of pulmonary CD103+ type 1 DCs is impaired in *Mr1*$^{-/-}$ mice 124

4.3.3 Single-cell RNA Sequencing reveals diminished cDC1 proportions in *Mr1*$^{-/-}$ mice 130

4.3.4 Cell-cell communication analysis reveals MAIT cell impact on cellular interaction during bleomycin challenge 150

4.3.5 Adoptive transfer of Flt3 ligand-generated bone marrow-derived dendritic cells to *Mr1*$^{-/-}$ mice reverts weight loss and reduces tissue damage 159

4.3.6 Spatial transcriptomic analysis reveals co-localization of T cells and cDC1 164

4.4 Discussion 173

4.5 Conclusion 180

5 Insights into Human MAIT Cell Functionality in Tissue Repair 181

5.1 Introduction 181

5.2 Aims 182

5.3 Results 182

5.3.1 Human scRNA-sequencing datasets demonstrate differences in MAIT cells between IPF and non-fibrotic control lung tissues 182

5.3.2 An increase of cDC population in IPF patients' lung tissues 188

5.3.3 Human fibroblast cell line MRC-5 activated MAIT cells by 5-OP-RU antigen presentation 196

5.4 Discussion 199

5.5 Conclusion 200

6 DISCUSSION 201

7 REFERENCES 204

Acronyms and abbreviations

5-A-RU	5-amino-6-D-ribitylaminouracil
5-OE-RU	5-(2-oxoethylideneamino)-6-D-ribitylaminouracil
5-OP-RU	5-(2-oxopropylideneamino)-6-D-ribitylaminouracil
APC	Antigen-presenting cell
BAL	Bronchoalveolar lavage
BEC	Bronchial epithelial cell
BMDC	Bone marrow-derived dendritic cell
BTM	Blood transcriptional module
CAP	Community-acquired pneumonia
cDC	Conventional dendritic cell
CDP	Common dendritic cell precursor
CF	Cystic fibrosis
CFU	Colony forming unit
cGN	crescentic glomerulonephritis
CITE-seq	Cellular Indexing of Transcriptomes and Epitopes by Sequencing
CLR	C-type lectin receptor
COPD	Chronic obstructive pulmonary disease
CPE	Cytopathic effect
CSF2	Colony stimulating factor 2
CTLD	C-type lectin-like domain
DC	Dendritic cell
DEG	Differentially expressed genes
DMAB	4-(Dimethylamino)benzaldehyde
DNGR-1	Dendritic cell NK lectin group receptor-1
EDTA	Ethylenediamine tetraacetic acid
FBS	Foetal bovine serum
FC	Fold change
FEV1	Forced expiratory volume in one second
FFPE	Formalin-fixed paraffin-embedded
Flt3L	Fms-like tyrosine kinase-3 ligand
GO	Gene ontology
GSEA	Gene Set Enrichment Analysis

GVHD	Colonic graft versus host disease
HLCA	Human Lung Cell Atlas
ICOS	Inducible T cell co-stimulator
IFN	Interferon
IL	Interleukin
ILD	Interstitial lung disease
IPF	Idiopathic pulmonary fibrosis
LVS	Live vaccine strain
MAIT	Mucosal-associated invariant T
MDCK	Madin-Darby canine kidney
MEM	Modified Eagle's medium
MERFISH	Multiplexed error-robust fluorescence in situ hybridization
MHC	Major Histocompatibility Complex
MR1	MHC-related protein-1
NKT	Natural Killer T
NOD	Nonobese diabetic
NSCLC	Non-small cell lung cancer
NTHi	Non-typeable Haemophilus influenzae
OD	Optical density
PAMP	Pathogen-associated molecular pattern
PBS	Phosphate buffered saline
PD-1	Programmed cell death protein 1
PE	Phycoerythrin
PFU	Plaque forming units
PLZF	Promyelocytic leukaemia zinc finger
PRR	Pattern recognition receptors
pre-DC	Precursor dendritic cells
RORγt	Retinoic acid-related orphan receptor γt
ROS	Reactive oxygen species
RT	Room temperature
RT-qPCR	Reverse transcription quantitative polymerase chain reaction
scRNA-seq	Single-cell RNA sequencing
T-bet	T-box expressed in T cell

TB	Tuberculosis
TCR	T cell receptor
TL1A	TNF-like protein 1A
TLR	Toll-like receptor
TNF	Tumour necrosis factor
TPCK	Tosyl phenylalanyl chloromethyl ketone
UMAP	Uniform Manifold Approximation and Projection
β-ME	2-mercaptoethanol

List of Figures

Figure 1.1 MAIT cell activation. 9

Figure 3.1 Gating scheme for the identification of MAIT cells. 66

Figure 3.2 *In vivo* bleomycin challenge induces accumulation of pulmonary MAIT cells in naïve mice. 67

Figure 3.3 Raw absolute cell number data for Figure 3.2A and B. 68

Figure 3.4 *In vivo* bleomycin challenge induces activation of pulmonary MAIT cells in naïve mice. 69

Figure 3.5 Schematic of protocol of murine study. 71

Figure 3.6 Temporal dynamics of MAIT cells in pulmonary immune response to *Salmonella* Typhimurium infection. 72

Figure 3.7 *In vivo* bleomycin challenge induces accumulation of pulmonary MAIT cells in *Salmonella* Typhimurium BRD509 infected mice. 74

Figure 3.8 *In vivo* bleomycin challenge induces activation of pulmonary MAIT cells in *Salmonella* Typhimurium BRD509 infected mice. 76

Figure 3.9 Cytokine-modulated accumulation and activation of pulmonary MAIT cells upon bleomycin stimulation.....78

Figure 3.10 Differential gene expression analysis of lung MAIT cells in bleomycin-challenged mice. 81

Figure 3.11 Upregulated GO terms in lung MAIT cells at day 3 post bleomycin challenge. .82

Figure 3.12 Heatmap depicting expression of cytokines and chemokines in lung MAIT cells post bleomycin challenge. 83

Figure 3.13 Cytokine profile of *ex vivo* pulmonary MAIT cells following bleomycin-induced lung injury. 84

Figure 3.14 Gene set enrichment analysis for tissue repair gene signature (Linehan *et al.*, 2018) of lung MAIT cells at day 3 post-bleomycin challenge. 88

Figure 3.15 Gene expression profile of pulmonary MAIT cells following bleomycin-induced lung injury. 91

Figure 3.16 Differential gene expression analysis of lung MAIT cells in PR8 IAV-infected mice. 94

Figure 3.17 Upregulated GO terms in lung MAIT cells at day 3 post-PR8 IAV infection. 95

Figure 3.18 Time-series analysis showing the gene alteration trends of PR8 IAV-infected mice MAIT cells. 96

Figure 3.19 Gene set enrichment analysis for tissue repair gene signature (Linehan *et al.*, 2018) of lung MAIT cells post-PR8 IAV infection. 100

Figure 4.1 *Mr1*$^{-/-}$ mice show more severe weight loss and tissue damage than WT mice post bleomycin challenge. 111

Figure 4.2 Body weight loss expressed as a percentage of the weight before bleomycin challenge. 113

Figure 4.3 Flow cytometry gating strategy for the identification of pulmonary myeloid cells and lymphocytes. 116

Figure 4.4 Frequencies of indicated cell types (percentages of parent) in in WT and *Mr1*$^{-/-}$ mice lungs after bleomycin challenge.....118

Figure 4.5 Frequencies of indicated cell types (percentages of total live immune cells) in in WT and *Mr1*$^{-/-}$ mice lungs after bleomycin challenge. 120

Figure 4.6 Dysregulated immune responses in the lungs of MAIT cell-deficient mice following bleomycin challenge. 122

Figure 4.7 Heatmap depicting relative expression of selected genes in mice lungs (*Mr1*$^{-/-}$ versus WT).....124

Figure 4.8 Early accumulation of CD103+ type 1 dendritic cells in the lungs upon bleomycin challenge is impaired in *Mr1*$^{-/-}$ mice.....125

Figure 4.9 Expression of activation markers on lung cDC1 cells post-bleomycin challenge. 129

Figure 4.10 Single-cell RNA-sequencing analysis of total lung cells post-bleomycin challenge. 132

Figure 4.11 Dot plot showing the top discriminative gene sets for each cell lineage compared with every other lineage.....135

Figure 4.12 Proportion distribution and absolute number of the 27 cell lineages in each sample. 137

Figure 4.13 UMAP analysis showing presence of MAIT cells in both WT and *Mr1*$^{-/-}$ mice. 139

Figure 4.14 Cell type distribution in both WT and *Mr1*$^{-/-}$ mouse lungs post-bleomycin challenge. 141

Figure 4.15 Differential gene expression in dendritic cell and macrophage populations in *Mr1*$^{-/-}$ vs. WT mice in response to bleomycin. 145

Figure 4.16 Differentiation trajectories and gene expression patterns of pre-DCs to cDC1 and cDC2 in WT and *Mr1*$^{-/-}$ mouse lungs. 146

Figure 4.17 Volcano plots showing pre-DC-specific DEGs. 147

Figure 4.18 Gene Set Enrichment Analysis in lung cells of *Mr1*$^{-/-}$ and WT mice post-bleomycin challenge. 150

Figure 4.19 Cell-cell communication analysis reveals MAIT cell impact on cellular interaction during bleomycin challenge. 153

Figure 4.20 Dot plots showing predicted interactions between epithelial cells (sender cell) and other cell types (Factor 8) before and post bleomycin challenge in both WT and *Mr1*$^{-/-}$ mice. 155

Figure 4.21 Interactions of T cells with myeloid cells pre- and post-bleomycin challenge in both WT and *Mr1*$^{-/-}$ mice. 159

Figure 4.22 Adoptive transfer of bone marrow-derived dendritic cells (BMDC) to *Mr1*$^{-/-}$ mice reverts weight loss and reduces tissue damage. 161

Figure 4.23 Flow cytometry plots of bone marrow-derived dendritic cells. 163

Figure 4.24 MERSCOPE experimental scheme. 166

Figure 4.25 Annotation of major cell types in mouse lungs pre- and post-bleomycin challenge. 168

Figure 4.26 Spatial distribution of different cell types in the WT mouse lung pre-bleomycin challenge. 170

Figure 4.27 Spatial distribution of T cells and cDC1 the WT mouse lung pre-bleomycin challenge. 172

Figure 4.28 Differential expression of inflammatory markers *Il6* and *Ccl2* in lung cell types pre- and post-bleomycin challenge. 176

Figure 5.1 Differential gene expression in IPF patient lung MAIT cells. 184

Figure 5.2 Analysis of DEGs for overrepresentation of blood transcriptional modules (BTM). 187

Figure 5.3 Analyses and frequencies of indicated cell types in in the GSE135893 dataset. .190

Figure 5.4 Frequencies of indicated cell types in in the GSE136831 dataset. 192

Figure 5.5 Interaction between MAIT cells and cDCs, and macrophages, and monocytes in the lungs of IPF patients and healthy controls. 194

Figure 5.6 Representative flow plot showing the gating strategy of human MAIT cells ($CD3^+$ TCR $V\alpha7.2^+$ $CD161^+$ cells).....197

Figure 5.7 Human fibroblast cell line MRC-5 activated MAIT cells by 5-OP-RU antigen presentation. 198

Figure 6.1 Model for how MAIT cells contribute to protection against bleomycin-induced lung tissue damage. 201

List of Tables

Table 2-1 Flow cytometry reagents 37

Table 2-2 Characterisation of the modified Ashcroft scoring scale 42

Table 3-1 Tissue repair gene signature 64

Table 3-2 Top 20 upregulated and downregulated DEGs of MAIT cells, *Salmonella* Typhimurium BRD509 pre-infected, WT bleomycin-challenged versus WT unchallenged ..85

Table 3-3 Top 20 upregulated and downregulated DEGs of MAIT cells, Naïve WT bleomycin-challenged versus WT unchallenged 91

Table 3-4 Top 20 upregulated GO terms of Clusters 1-5 in time-series analysis.....97

Table 3-5 Top 20 upregulated and downregulated DEGs of MAIT cells, *Salmonella* Typhimurium BRD509 pre-infected, WT PR8 virus infected versus WT B6 uninfected.....102

Table 4-1 Top 20 upregulated and downregulated DEGs of total lung, *Salmonella* Typhimurium BRD509 pre-infected, *Mr1*$^{-/-}$ versus WT B6 127

Table 5-1 DEGs of MAIT cells, IPF vs Control.....184

1 INTRODUCTION

1.1 The immune system and unconventional T cells

1.1.1 The immune system: a complex defence network

Life, in its myriad forms, is persistently challenged by a multitude of pathogens. At the core of survival lies the immune system, an intricate network of cells, tissues, and organs that co-ordinate defences against these infectious agents. The immune system is fundamentally divided into two synergistic arms: the innate and adaptive immune responses. The innate immune system acts as the first line of defence, providing immediate protection by specifically recognising broadly conserved pathogen-associated molecular patterns (PAMPs) through pattern recognition receptors (PRRs). The adaptive immune system, in contrast, offers a highly specialised response, capable of targeting specific pathogens and retaining memory for more robust reactions upon re-exposure.

1.1.2 Conventional T cells: the adaptive response architects

T lymphocytes are important players within the adaptive landscape. Conventional T cells, typically identified by their surface proteins CD4+ and CD8+, orchestrate immune responses through a complex recognition process of antigens presented by Major Histocompatibility Complex (MHC) molecules (Zamoyska, 1998). CD4+ T cells, often termed helper T cells, primarily respond to antigens presented by MHC class II molecules, aiding in the activation of other immune cells. Conversely, CD8+ T cells, or cytotoxic T cells, respond to antigens presented by MHC class I molecules, directly destroying infected host cells. The specificity of this interaction is conferred by T cell receptors (TCRs), which undergo a developmental process of rearrangement to recognise a vast array of antigens (Shinkai *et al.*, 1992).

1.1.3 Restriction molecules and the MHC paradigm

The concept of restriction is important to T cell-mediated immunity, wherein the TCRs recognise a complex of antigenic peptide and MHC molecule, not the antigen alone. This molecular handshake ensures that T cells are activated only in the correct context of antigen presentation, a process critical for self-tolerance and precise immune targeting. MHC class I molecules are ubiquitous amongst nucleated cells and present endogenous antigens, typically signalling viral infection. MHC class II molecules are restricted to professional antigen-presenting cells (APCs) like dendritic cells (DCs), macrophages, and B cells, presenting exogenous antigens for immune surveillance (Steimle *et al.*, 1994).

1.1.4 The growing family of unconventional T cells

Unlike conventional T cells, unconventional counterparts are not restricted to classical MHC molecules. This diverse group includes cells that interact with a variety of other antigen-presenting molecules, such as CD1a, CD1b, CD1c, HLA-E, and MHC-related protein-1 (MR1), which present lipid and metabolite antigens rather than peptide antigens. These cells contribute to immune responses against a wide array of pathogens and are implicated in tumour immunity, autoimmune diseases, and transplant rejection. The exploration of unconventional T cells has opened new avenues for immunotherapy, as their unique antigen recognition and rapid response characteristics offer potential for targeted treatments. A comprehensive review by Godfrey *et al*.(Godfrey *et al.*, 2015) illustrates the interplay between these unconventional cells and APCs, providing a diagrammatic summary that encapsulates the complexity and potential of these interactions for therapeutic exploitation.

1.1.5 Unconventional T cells: expanding the repertoire of immune recognition

While conventional T cells, with their diverse TCR repertoire, are central to adaptive immunity's targeted responses to pathogens, unconventional T cells such as mucosal-associated invariant T (MAIT) cells, Type I and Type II Natural Killer T (NKT) cells and γδ T cells, offer an immediate form of defence. These unconventional T cells are defined by a more restricted TCR diversity and their ability to recognise non-peptide antigens, often outside the classical MHC pathway. For instance, NKT cells are activated by lipid antigens presented by CD1d, γδ T cells can directly respond to certain non-peptide antigens, and MAIT cells detect vitamin B metabolites presented by the MR1 molecule (Godfrey *et al.*, 2015).

Unconventional T cells are notable for acting quickly against pathogenic threats. This contrasts with the conventional T cells' strategy, which depends on variable TCRs to recognise peptides presented by classical MHC molecules. For example, while conventional T cells expand in response to specific antigens and create memory cells for quicker future responses, MAIT cells' semi-invariant TCRs, which recognise a conserved set of microbial-derived metabolites, allow for a more immediate protective response without the need for prior sensitisation or clonal expansion. This evolutionary strategy showcases the unique niche MAIT cells occupy, ready to provide a rapid first line of defence. The ability of unconventional T cells to quickly recognise and respond to a broad range of biosynthetic pathways positions them as essential components of the innate immune response, thereby augmenting the adaptive capabilities of conventional T cells (Godfrey *et al.*, 2015; Mayassi *et al.*, 2021).

1.1.6 MAIT cells in focus

As mentioned above, as a unique niche within the unconventional T cell family, MAIT cells are innate-like T cells defined by their semi-invariant αβ TCR which recognises small-molecule biosynthetic derivatives of riboflavin synthesis (Corbett *et al.*, 2014; Eckle *et al.*,

2015; Kjer-Nielsen *et al.*, 2012) presented on the restriction molecule MR1 (Hashimoto *et al.*, 1995; Treiner *et al.*, 2003). MAIT cells were described in 1999 (Tilloy *et al.*, 1999) based on their TCR comprising a semi-invariant TCR-α chain – usually Vα7.2–Jα33/12/20 in humans, Vα19–Jα33 in mice – predominantly associated with the β-chains Vβ2/Vβ13 in humans and Vβ6/Vβ8 in mice (Lepore *et al.*, 2014; Reantragoon *et al.*, 2013; Tilloy *et al.*, 1999). The TCR sequences characteristic of MAIT cells are predominantly derived from a process known as 'convergent recombination'. This mechanism facilitates the preferential generation of MAIT cell TCRs, underlining a genetic predisposition towards producing these sequences. Such a process suggests that the diversity typically required for antigen specificity in T cells is, for MAIT cells, to a significant extent innately programmed within the germline DNA. Consequently, MAIT cells exhibit a consistent TCR repertoire, optimised for rapid immune responses to a broad array of microbial species (Greenaway *et al.*, 2013).

The biosynthetic pathway of riboflavin (vitamin B2) in many bacteria and yeasts is an important source of ligands for MAIT cell activation (Chua *et al.*, 2012; Gold *et al.*, 2013; Kjer-Nielsen *et al.*, 2012; Le Bourhis *et al.*, 2010; Maggio *et al.*, 2015). During this process, the intermediate 5-amino-6-D-ribitylaminouracil (5-A-RU) non-enzymatically condenses with glyoxal or methylglyoxal, yielding the transient ligands 5-(2-oxopropylideneamino)-6-D-ribitylaminouracil (5-OP-RU) and 5-(2-oxoethylideneamino)-6-D-ribitylaminouracil (5-OE-RU) (Eckle *et al.*, 2015; Mak *et al.*, 2017). These ligands, while inherently unstable, are stabilised upon binding to MR1 through Schiff base formation, facilitating MAIT cell detection. This pathway is absent from mammals; therefore, its immune detection allows effective host-pathogen discrimination. The identification of these ligands was achieved through a technique where MR1, refolded with β2 microglobulin, captured these metabolites from bacterial cultures, confirming the MR1-dependent antigen presentation mechanism important for MAIT cell activation (Corbett *et al.*, 2014; Kjer-Nielsen *et al.*, 2012).

Occupying mucosal sites such as the gut, lung and skin, MAIT cells are poised for early response to microbial invasion, bridging innate and adaptive immune functions. The following sections will discuss the activation, function, and clinical implications of MAIT cells, further elucidating their role in human health and disease.

1.2 MAIT cell activation

1.2.1 TCR mediated activation

MAIT cells can be activated in response to TCR ligation by riboflavin intermediates presented on MR1, under co-stimulatory signals from specific cytokines or toll-like receptors (TLR) (Chen *et al.*, 2017). Activated cells expand substantially inducing a rapid innate-like immune response and effector functions including anti-microbial cytotoxic products, inflammatory chemokines and cytokines.

The metabolites 5-OP-RU and 5-OE-RU are central to the riboflavin biosynthesis (Corbett *et al.*, 2014; Eckle *et al.*, 2015; Soudais *et al.*, 2015). The gene *RibD*, vital for producing 5-A-RU, is linked to the activation of MAIT cells (Hartmann *et al.*, 2018). Therefore, bacteria with the riboflavin pathway, such as *Escherichia*, *Lactobacillus*, *Staphylococcus* (Le Bourhis *et al.*, 2010), *Shigella flexneri* (Le Bourhis *et al.*, 2013), *Salmonella*, *Clostridioides* (Bernal *et al.*, 2018; Kjer-Nielsen *et al.*, 2012; Le Bourhis *et al.*, 2010) and *Mycobacteri*a (Gold *et al.*, 2010), as well as riboflavin-synthesizing fungi like *Saccharomyces* (Le Bourhis *et al.*, 2010), *Candida* (Le Bourhis *et al.*, 2010; Meermeier *et al.*, 2018), and *Aspergillus* (Jahreis *et al.*, 2018), can trigger a MAIT cell response through MR1. In contrast, bacteria lacking this pathway, like *Enterococcus faecalis* (Le Bourhis *et al.*, 2010) and *Listeria monocytogenes* (Gold *et al.*, 2010), cannot activate MAIT cells directly.

Unlike conventional T cells, which recognise peptide antigens presented by MHC molecules, MAIT cells are restricted by MR1, a non-polymorphic, β2-microglobulin-associated antigen-presenting molecule, extensively expressed across various tissues (Hashimoto *et al.*, 1995; Riegert *et al.*, 1998). While recycling of the MR1 molecule can take place (Harriff *et al.*, 2016), the majority of MR1 molecules are broken down and reinternalized intracellularly, facilitating MR1's swift presentation of extracellular riboflavin antigens and the rapid activation of MAIT cells (McWilliam *et al.*, 2016). Furthermore, MR1-mediated MAIT cell activation is influenced by NF-κB signalling (Ussher *et al.*, 2016). Various APC, including DCs (Gold *et al.*, 2010; van Wilgenburg *et al.*, 2016), monocytes (Dusseaux *et al.*, 2011; Le Bourhis *et al.*, 2010), macrophages (van Wilgenburg *et al.*, 2016), B cells (Jeffery *et al.*, 2016; Salerno-Goncalves *et al.*, 2014), and non-bone marrow-derived cells like epithelial cells (Gold *et al.*, 2010; Jeffery *et al.*, 2016), can present antigens via MR1 to activate MAIT cells (H. Wang *et al.*, 2019).

MR1-TCR signalling on its own is inadequate to fully activate MAIT cells. They also require co-stimulation (Chen *et al.*, 2017; Slichter *et al.*, 2016; Turtle *et al.*, 2011; H. Wang *et al.*, 2019) via CD28 (Turtle *et al.*, 2011), TLR agonists, bacterial products, or cytokines (Chen *et al.*, 2017). These cytokines include interleukin (IL)-7 (Leeansyah *et al.*, 2015; Tang *et al.*, 2013), tumour necrosis factor (TNF) (Banki *et al.*, 2019), type-I interferons (IFNs) (Lamichhane, Galvin*, et al.*, 2019), IL-1β and/or IL-23 (Tang *et al.*, 2013; H. Wang *et al.*, 2019). MAIT cells express various cytokine receptors, including IL-7R, IL-12R, IL-15R, IL-18R, and IL-23R (Dusseaux *et al.*, 2011; Le Bourhis *et al.*, 2010; H. Wang *et al.*, 2019). IL-7 amplifies MAIT cell responses to bacteria and bolsters cytotoxicity (Leeansyah *et al.*, 2015). IL-12 and IL-18 reinforce MR1-dependent bacterial MAIT cell activation (Sattler *et al.*, 2015; Ussher *et al.*, 2016). Agonists of the pattern recognition receptors TLR1, TLR2 and TLR6 in humans (Ussher *et al.*, 2016), and TLR3, TLR4, TLR6/2 and TLR9 in mice (Chen *et al.*, 2017; Hinks *et al.*, 2019), mainly drive MAIT cell activation indirectly by activating APCs, which enhances MR1

presentation, stimulates cytotoxic molecules, boosts inflammatory cytokines or increases co-stimulatory ligands (Chen *et al.*, 2017; Liu & Brutkiewicz, 2017; Ussher *et al.*, 2014; Ussher *et al.*, 2016). Furthermore, the inducible T cell co-stimulator (ICOS), which MAIT cells express at high levels, is needed for optimal activation and sustaining the expression of retinoic acid-related orphan receptor γt (RORγt) (H. Wang *et al.*, 2019), the master transcription factor for Type 17 cell differentiation.

1.2.2 TCR-independent activation

Even in absence of TCR-mediated antigen recognition, MAIT cells can also be activated partially by cytokines, such as IL-7, IL-12, IL-15, IL-18 and type-I IFNs, broadening the potential range of pathogens to which MAIT cells can respond to include viruses (Loh *et al.*, 2016; Ussher *et al.*, 2018; van Wilgenburg *et al.*, 2018; van Wilgenburg *et al.*, 2016). IL-7 has the capacity to trigger the expression of cytolytic effector molecules (Leeansyah *et al.*, 2015). IL-12 or IL-15 in tandem with IL-18, produced by APCs in response to TLR ligands, can directly prompt MAIT cells to generate IFN-γ (Jo *et al.*, 2014; Ussher *et al.*, 2014; van Wilgenburg *et al.*, 2016) and release granzyme B and perforin (Sattler *et al.*, 2015). IFN-α/β on its own can activate MAIT cells but doesn't lead to cytokine production or the elevation of co-stimulatory molecules (Lamichhane, Galvin*, et al.*, 2019). Type-I IFNs only trigger significant IFN-γ and granzyme B production when paired with IL-12 or IL-18 (van Wilgenburg *et al.*, 2016). Similarly, the gut-associated pro-inflammatory cytokine, TNF-like protein 1A (TL1A/TNFSF15), activates MAIT cells when combined with IL-12 and IL-18 (Leng *et al.*, 2019).

Both TCR-mediated and independent activation mechanisms collaborate for optimal MAIT cell activation, as shown in Figure 1. Following stimulation, there is an upsurge in the expression of activation markers CD69 and CD25, the degranulation marker CD107a (Dias *et*

al., 2016; Le Bourhis *et al.*, 2013; Le Bourhis *et al.*, 2010), production of cytotoxic agents like perforin and granzyme B (Dusseaux *et al.*, 2011; Kurioka *et al.*, 2014; Leeansyah *et al.*, 2015), secretion of pro-inflammatory cytokines such as IFN-γ, TNF, IL-17 and colony stimulating factor 2 (CSF2/GM-CSF) (Chua *et al.*, 2012; Dusseaux *et al.*, 2011; Le Bourhis *et al.*, 2010) and release of chemokines like XCL1, CCL3, CCL4 and CXCL16 (Hinks *et al.*, 2019; Slichter *et al.*, 2016). MAIT cells deploy antimicrobial actions not merely through direct recognition and eradication of infected cells but also indirectly by, for instance, recruiting neutrophils (Lamichhane, Schneider*, et al.*, 2019), augmenting bactericidal activity in phagocytes (Davey *et al.*, 2014), stimulating IFN-γ production from DCs (van Wilgenburg *et al.*, 2016), and promoting monocyte to DC differentiation (Meierovics & Cowley, 2016). Though there is a substantial overlap in transcriptional and functional profiles, the two activation modes do exhibit differences. TCR stimulation typically triggers a swifter immune response along with the production of numerous pro-inflammatory cytokines and chemokines compared to cytokine stimulation in isolation. Increased expression of RORγt and cytokines IL-17A, TNF, and CSF2 is observed with TCR-mediated activation, aligning with a Tc17-like phenotype (Hinks *et al.*, 2019; Lamichhane, Schneider*, et al.*, 2019; Wang *et al.*, 2018). On the other hand, TCR-independent activation is characterised by IFN-γ, perforin, and granzyme B, overseen by the master transcription factors promyelocytic leukaemia zinc finger (PLZF) (Hinks *et al.*, 2019) and T-box expressed in T cells (T-bet) (Lamichhane, Schneider*, et al.*, 2019), fitting a Tc1-like profile. Crucially, it is the TCR-dependent activation that initiates a tissue-repair programme (Hinks *et al.*, 2019; Lamichhane, Schneider*, et al.*, 2019; Leng *et al.*, 2019).

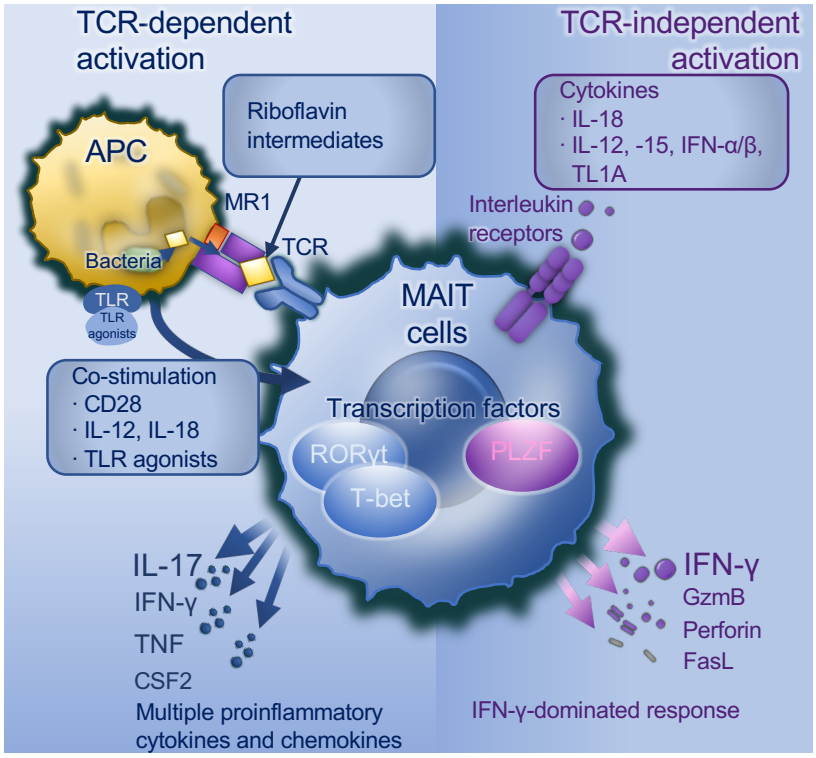

Figure 1.1 MAIT cell activation.

TCR-dependent activation requires microbially-derived riboflavin intermediates such as 5-OP-RU to be presented on MR1 to a MAIT cell TCR in conjunction with co-stimulation. Co-stimulation may include CD28 and/or cytokines particularly IL-12/-18, and can be induced by danger signals including TLR agonists (in mice TLRs 3, 4, 6/2 or 9, in human TLRs 1, 2, or 6). TCR dependent activation induces a strong and broad production of proinflammatory cytokines and chemokines, dominated by IL-17A under the control of the transcription factor RORγt. TCR-independent activation is driven by IL-18 in synergy with IL-12, or -15, or IFN-α or -β, and potentiated by TL1A. This activates a more modest cytokine response dominated by IFN-γ under the control of PLZF. Abbreviations: APC, antigen-presenting cell; CD, cluster of differentiation; CSF2, colony stimulating factor 2 (GM-CSF); GzmB, granzyme B; IFN, interferon; IL, interleukin; MAIT, mucosal associated invariant T; MR1, major histocompatibility complex-related protein-1; PLZF, Promyelocytic leukaemia zinc finger

protein; RORγt, retinoic acid-related orphan receptor gamma; TCR, T cell receptor; TL1A, tumour necrosis factor (TNF)-like protein 1A (TNFSF15); TLR, toll-like receptor. Figure from Frontiers Media S.A. Hinks (Hinks & Zhang, 2020).

1.3 MAIT cell function in lung infection

1.3.1 Mycobacteria and pulmonary tuberculosis

A wide range of bacterial and fungal pathogens have been shown to activate MAIT cells *in vitro*. These pathogens all express the riboflavin pathway triggering TCR-dependent activation. MAIT cells co-cultured with bacterially-infected monocytes (Dusseaux *et al.*, 2011; Le Bourhis *et al.*, 2010; Shaler *et al.*, 2017; van Wilgenburg *et al.*, 2016) or *M. tuberculosis*-infected lung epithelial cell lines (Gold *et al.*, 2010) release IFN-γ in an MR1-dependent manner. Beyond this canonical recognition route, MR1-independent activation has been observed after BCG vaccination, suggesting alternative pathways of MAIT cell engagement (Suliman *et al.*, 2019).

There is potent inhibition of *Mycobacterium bovis* BCG growth within macrophages when co-cultured with MAIT cells (Chua *et al.*, 2012). It has been demonstrated that MAIT cell TCR-transgenic mice had enhanced protection against *E. coli* or *Mycobacterium abscessus* infection compared to $Mr1^{-/-}$ transgenics (Le Bourhis *et al.*, 2010). In this study, the Vα19i-Tg mice, which express the Vα19-Jα33 TCR – MAIT TCRα chain – across all T cells, were the main model for researching MAIT cells prior to MR1 tetramers (Kawachi *et al.*, 2006). Despite the absence of MR1, $Mr1^{-/-}$ mice still produce mature T cells, implying that some Vα19i-Tg TCRs may be conventional MHC-restricted (Martin *et al.*, 2009). It is therefore important to compare Vα19i-Tg $Mr1^{+/+}$ and $Mr1^{-/-}$ mice to accurately determine MAIT-specific effects. The MR1

tetramer has since shown that Vα19i-Tg T cells are distinct from native MAIT cells (Rahimpour *et al.*, 2015), and so data from this model should be interpreted with caution.

MAIT cells exhibit innate recognition of *M. tuberculosis*, observable even in cord blood, indicating an early defence role (Gold *et al.*, 2013). However, the intricate relationship between MAIT cells and pulmonary tuberculosis (TB) progression presents challenges in determining a definitive role for MAIT cells against TB. Clonal expansion of MAIT cells has been observed in the airways of individuals with TB (Wong *et al.*, 2019). Conversely, the prevalence of MAIT cells in both human and non-human primate granulomas is relatively low (Gideon *et al.*, 2022). Increasing the frequency of MAIT cells in mice with 5-OP-RU significantly enhanced the control of *M. tuberculosis*. When mice with chronic *M. tuberculosis* infection were treated with 5-OP-RU, there was a tenfold reduction in bacterial loads within three weeks, and this reduction was dependent on the presence of IL-17A (Shunsuke Sakai *et al.*, 2021). Nevertheless, applying a similar strategy in macaques led to an unexpected dampening of the MAIT response without impacting the bacterial load (S. Sakai *et al.*, 2021). Hence, the roles of MAIT cells in the control of *M. tuberculosis* infection remain ambiguous, with their *in vivo* significance being difficult to determine, potentially owing to immunological redundancy that may conceal the contributions of MAIT cells. This redundancy, as discussed by Wang *et al.* (Wang *et al.*, 2018), might hide the impact of MAIT cells, becoming apparent only under severe conditions, such as high infectious burdens or when specific immunity is compromised. Accordingly, understanding the exact function of MAIT cells in the clinical trajectory of TB requires careful interpretation.

Definitive human evidence of MAIT cell protection against TB is lacking, although there are important correlative, observational data. In the case of active pulmonary TB in children, there is a notable reduction of MAIT cells within both peripheral blood and lung tissues (Le Bourhis

et al., 2010; Malka-Ruimy *et al.*, 2019), whereas a 5-fold increase in the frequencies of these cells are documented during latent TB infection (Paquin-Proulx *et al.*, 2018). This contrast indicates a potential dual role of MAIT cells: while they may contribute to immune protection during the latent phase, their reduced presence in active TB might reflect an impaired defensive response. The observed difference in MAIT cell prevalence between latent and active TB phases suggests a complex role for MAIT cells in TB pathogenesis. During latent TB, the presence of MAIT cells could be instrumental in containing the infection, implying a protective immune function. Conversely, their diminished numbers in active TB cases may indicate a compromised immune defence, potentially contributing to disease progression. However, the relationship between MAIT cell frequencies and TB status is not straightforward. Since 90% of individuals control TB successfully for life, and no longitudinal studies have tracked MAIT cell counts in lung tissue before, during, and after the transition to active TB (Jilani *et al.*, 2024), it is challenging to discern whether low MAIT cell counts are a cause or a result of the disease activation. It is possible that individuals with inherently lower MAIT cell counts are more likely to be among the 10% who progress from latent to active TB. This correlation might be causative, with low MAIT cells leading to insufficient immune response; consequential, where active TB suppresses MAIT cell numbers; or merely an epiphenomenon, where MAIT cell levels are an incidental finding unrelated to disease outcomes. Further research is required to understand the temporal changes in MAIT cell counts and to distinguish between these possibilities, thereby clarifying the role of MAIT cells in the pathogenesis of TB.

The immune competency of MAIT cells in active TB is further complicated by a subdued IFN-γ response, which persists despite the presence of auxiliary signals from cytokines like IL-15 (Jiang, Yang*, et al.*, 2016). In TB patients, MAIT cells show significant downregulation of genes important for an effective immune response, as compared to healthy individuals. This includes genes coding for cytokines and cytotoxic molecules such as IFN-γ, TNF-α, IL-17F,

as well as granulysin and granzyme B, which are essential for the targeted killing of infected cells (Jiang, Yang*, et al.*, 2016).

Paradoxically, in the specific microenvironment of tuberculous pleural effusions, MAIT cells exhibit a robust IFN-γ response, alongside enhanced cytotoxic and IL-17 responses to *M. tuberculosis* antigens, surpassing the activity seen in peripheral blood. The potency of this response is modulated by cytokines, particularly IL-2, IL-12, and IL-18, and is inversely related to TB severity, suggesting a localized protective role in the pleura (Jiang, Chen*, et al.*, 2016). It should be noted that pleural TB is a paucibacillary form of the disease, where the immune reaction is dominant rather than uncontrolled microbial expansion, and MAIT cell activity likely reflects attempts at effective immune control. Additionally, MAIT cells within pleural effusions are characterized by an upregulation of programmed cell death protein 1 (PD-1) expression, which correlates with disease severity, and elevated production of cytokines CXCL13 and IL-21, underscoring a multifaceted response to the pathogen (Jiang *et al.*, 2020).

1.3.2 *Francisella tularensis* and *Salmonella* Typhimurium

Francisella tularensis is the aetiological pathogen in tularaemia, a rare, opportunistic disease amongst people exposed to wild animals in North America. Its most severe presentation as pneumonia carries a mortality risk of up to 60% (Ellis *et al.*, 2002; Oyston, 2008), and despite its rarity, the potential to be weaponised makes it of interest in relation to biosecurity. While overall incidence has decreased over the past hundred years, occasional outbreaks still occur (Keim *et al.*, 2007).

Research has shown that MAIT cell expansion *in vivo* is mostly induced by intracellular pathogens. Notably, in a murine model, acute intranasal infection with the live vaccine strain (LVS) of *Francisella tularensis*, an uncommon opportunistic pathogen, results in significant pulmonary MAIT cell proliferation (Meierovics *et al.*, 2013). These cells produce IFN-γ, IL-

17, TNF, and inducible nitric oxide synthase (Meierovics *et al.*, 2013), as well as GM-CSF, which aids in attracting inflammatory monocytes to the lungs (Meierovics & Cowley, 2016). The essential role of MAIT cells in mucosal immunity, particularly when CD4+ and CD8+ T cells are depleted, is highlighted by the decreased resistance to *Francisella tularensis* LVS infection in MAIT cell-deficient *Mr1*$^{-/-}$ mice. MAIT cells inhibit the growth of LVS-infected monocytes by releasing IFN-γ, TNF-α, and nitric oxide, a response dependent on MR1 and modulated by IL-12 and IL-18 (Jesteadt *et al.*, 2018; Meierovics *et al.*, 2013).

In another model of intracellular lung infection, intranasal exposure to *Salmonella enterica serovar* Typhimurium prompts a swift and sustained increase in MAIT cell frequencies within the lungs, which can constitute up to half of all pulmonary αβ T cells (Chen *et al.*, 2017). Whilst *Salmonella* is never a natural respiratory pathogen, this model was selected initially because it was with *Salmonella* Typhimurium that experiments *in vitro* first showed the requirement of an intact microbial riboflavin pathway to activate MAIT cells and it has since proved a robust and versatile model for pulmonary MAIT cell expansion (Chen *et al.*, 2017). Clearance of *Salmonella* Typhimurium does not solely rely on MAIT cells, indicating the presence of compensatory mechanisms by conventional T cells (Chen *et al.*, 2017). *Mr1*$^{-/-}$ mice show compromised microbial control in infections with *Francisella tularensis* (Meierovics *et al.*, 2013; Meierovics & Cowley, 2016), *M. abscessus* (Le Bourhis *et al.*, 2010), and *M. bovis* BCG (Chua *et al.*, 2012), underscoring the importance of MAIT cells in combating intracellular bacterial infections.

1.3.3 *Legionella pneumophila* and *longbeachae*

The first demonstration of MAIT cell protection *in vivo* against a major human pathogen was with *Legionella.* In a mouse model of Legionnaire's disease, human MAIT cells were activated *in vitro* by two significant strains of *Legionella*: *pneumophila* and *longbeachae* (Wang *et al.*,

2018). *L. longbeachae,* which of the two strains is more pathogenic in mice, induced rapid pulmonary MAIT cell expansion, by up to 580-fold over 7 days, which persisted long-term, with a similar effect observed with *L. pneumophila*. The expansion resulted from MAIT cell proliferation within the lungs and lymph nodes. *Mr1*$^{-/-}$ mice had delayed bacterial clearance at days 10-14 post-infection, although in both models this effect was small, due to immunological redundancy. Transferring MR1-5-OP-RU positive MAIT cells into *Rag2*$^{-/-}\gamma C^{-/-}$ mice which lack T, B and NK cells led to a full recovery from lethal *L. longbeachae* infection (Wang *et al.*, 2018). The protection primarily depended on MAIT cell-produced IFN-γ, secondarily on GM-CSF, but not on perforin or granzyme (Wang *et al.*, 2018). *Legionella* infects inflammatory cells, particularly neutrophils and macrophages, rather than epithelia and it is likely MAIT-derived IFN-γ limits intracellular growth of bacteria in these cells through multiple mechanisms including enhancement of oxidative burst, nitric oxide production, antigen presentation, phagocytosis and upregulation of CD80/86 co-stimulation, cytokines and chemokines (Ellis & Beaman, 2004).

1.3.4 *Streptococcus pneumoniae*

Streptococcus pneumoniae has a poor capacity to activate MAIT cells when the APC is a monocyte or monocyte cell line, and this activation is dependent on cytokines rather than MR1 (Kurioka *et al.*, 2018), perhaps because of monocytes' poor phagocytic and antigen-presenting capacity (Kamphorst *et al.*, 2010; Samstein *et al.*, 2013). Conversely, *S. pneumoniae* does induce MR1-dependent activation in the presence of monocyte-derived macrophages, which have a greater phagocytic capacity (Kurioka *et al.*, 2018). Likewise, *S. pneumoniae* activates MAIT cells in the presence of human monocyte-derived DCs, in an MR1-dependent manner, with the extent of activation correlating with the activity of the RibD operon (Hartmann *et al.*,

2018). In co-culture, MAIT cells reduce growth of *S. pneumoniae* within infected primary bronchial epithelial cells.

1.3.5 Influenza A virus

Due to their ability for rapid cytokine-mediated activation, MAIT cells play an important role in the body's early anti-viral defence ahead of the conventional T cell response, which typically takes 4-7 days to develop. Virus-induced activation of CD161+ Vα7.2+ MAIT cells was observed *in vivo* in human peripheral blood MAIT cells during clinical infection of influenza A, dengue and hepatitis C (van Wilgenburg *et al.*, 2016). During each infection *in vivo*, activation of MAIT cells was indicated by an upregulation of CD38 and granzyme B, while *in vitro*, MAIT cells increased the expression of CD69 and IFN-γ in the presence of virally infected APCs. Similar findings were observed in a separate report of patients hospitalized with the H7N9 strain of influenza A virus, and interestingly higher MAIT cell frequencies were associated with subsequent recovery (Loh *et al.*, 2016).

Although clinical observations suggest a correlation between virus-induced MAIT cell activation and disease outcomes, they fall short of establishing causality. Neither of the above referenced studies has conclusively determined whether the effects of such activation are beneficial, bolstering antiviral defenses, or detrimental, exacerbating immune pathology or potentially enhancing a cytokine storm that could be fatal during acute influenza infections. To determine whether these correlations were protective or deleterious required *in vivo* experimental challenge. MAIT cells proved important in the immune response against lethal influenza, accumulating and activating in the lungs earlier than conventional CD8+ T cells post-infection. Increased presence and upregulation of activation markers CD25, CD69, and granzyme B in MAIT cells occur at least 48 hours prior to such changes in conventional T cells. IL-12 primarily drives this activation, with IL-15, IL-18, and IFN-α also playing roles (van

Wilgenburg *et al.*, 2018). The essential function of MAIT cells is evident as *Mr1*$^{-/-}$ mice, deficient in MAIT cells, experience greater weight loss and higher mortality rates, which are alleviated by transplanting pulmonary MAIT cells, thereby confirming their protective role. Enhancing airway MAIT cell numbers through pre-exposure to inhaled MAIT cell ligands could offer clinical benefits, a strategy that warrants further investigation through clinical trials (Hinks, 2021). This is backed by evidence that microbial exposures influence MAIT cells' abundance and activity within tissues, which is important for modulating immune responses to injury and promoting tissue repair (Constantinides *et al.*, 2019). Besides, in the context of immune-mediated kidney disease – crescentic glomerulonephritis (cGN) – MAIT cells exhibit a protective role by expressing both pro- and anti-inflammatory mediators, interacting with renal mononuclear phagocytes to suppress inflammatory progression. Moreover, pharmacological activation of MAIT cells has shown potential in attenuating cGN, indicating their therapeutic value in immune-mediated conditions (Gnirck *et al.*, 2023).

1.3.6 SARS-COV-2 and COVID-19

Observational studies suggest that MAIT cells modulate the clinical outcomes and fatality risk associated with COVID-19, which is caused by SARS-CoV-2. Key observations include a reduction in MAIT cell frequency and an increase in activation markers (CD38, CD69, HLA-DR) in the blood of COVID-19 patients, alongside a functional impairment manifested by diminished granzyme B, perforin and TNF-α (Carissimo *et al.*, 2020; Deschler *et al.*, 2021) (Flament *et al.*, 2021; Hubrack *et al.*, 2021; Parrot *et al.*, 2020; Ren *et al.*, 2021). Pyroptotic MAIT cells, rather than apoptotic, predominate, indicating pyroptosis as a key mechanism of MAIT cell depletion in SARS-CoV-2 infection (Shi *et al.*, 2021). Furthermore, MAIT cell depletion in peripheral blood also likely results from their migration to inflamed lungs, evidenced by higher MAIT cell frequencies in bronchoalveolar lavage (BAL) fluid, pleural

fluid, and endotracheal aspirates (Jouan *et al.*, 2020; Parrot *et al.*, 2020; Ren *et al.*, 2021). Transcriptomic analyses demonstrate a proinflammatory IL-17A bias of MAIT cells in the airways of these patients (Parrot *et al.*, 2020). Certain MAIT cell phenotypes are linked to worse outcomes in patients. These include MAIT cells with heightened cytotoxic capabilities, as indicated by increased granzyme B production (Flament *et al.*, 2021) and MAIT cells expressing high levels of CD69 (Youngs *et al.*, 2021) and low levels of CXCR3 (Parrot *et al.*, 2020). Additionally, there is a positive correlation between HLA-DR expression on MAIT cells and the Simplified Acute Physiology Score II, linking MAIT cell activation to disease severity (Deschler *et al.*, 2021). Other observational studies also indicate that MAIT cells could play a protective role in COVID-19. A higher early post-admission count of CD69+ MAIT cells in peripheral blood is linked to better oxygenation status on day 7. Furthermore, the level of CD69 on MAIT and iNKT cells has a direct correlation with the PaO2/FiO2 ratio (ratio of arterial oxygen partial pressure to fractional inspired oxygen), a key indicator of acute respiratory distress syndrome severity, in patients with COVID-19 (Jouan *et al.*, 2020). Proof of a causative link between MAIT cell activation and outcomes will require an *in vivo* challenge model.

1.4 MAIT cells function in other lung diseases

MAIT cells are particularly abundant in the lung, comprising up to 10% of all pulmonary T cells in a healthy human (Hinks *et al.*, 2016; Hinks *et al.*, 2015). Might MAIT cells be important in more common respiratory diseases?

1.4.1 Asthma

Asthma is a chronic airway inflammatory disease affecting 1-29% of the population in different countries (Venkatesan, 2023). The first descriptions of human airway MAIT cells showed that they were markedly reduced in blood, sputum and bronchial biopsies in steroid-treated asthma

and in chronic obstructive pulmonary disease (Hinks *et al.*, 2016; Hinks *et al.*, 2015). Recent paediatric studies (Lezmi *et al.*, 2018; Lezmi *et al.*, 2019) have identified an elevated frequency of circulating IL-17 producing MAIT cells, in children with severe asthma exacerbations. There is a notable correlation between the prevalence of IL-17 producing MAIT cells and the severity of asthma exacerbations, as well as an inverse relationship with the Asthma Control Test (ACT) scores, suggesting that higher levels of IL-17 producing MAIT cells are indicative of poorer asthma control (Lezmi *et al.*, 2018; Wen *et al.*, 2022).

Further research has demonstrated that therapeutic corticosteroids significantly reduce MAIT cell frequencies in asthma patients (Hinks *et al.*, 2015). This reduction was particularly pronounced in the peripheral blood and sputum of asthmatic patients with moderate to severe symptoms, highlighting a negative correlation between MAIT cell levels and clinical severity. Additionally, the proportion of $CD69^+$ MAIT cells has been negatively correlated with forced expiratory volume in one second (FEV1) in asthmatic patients, pointing towards a potential link with airflow limitation (Ishimori *et al.*, 2017). In neutrophilic asthma patients, circulating MAIT cells exhibit increased activation (evidenced by elevated CD69 expression) and signs of depletion (increased PD-1 expression and early apoptotic cells), in comparison to healthy individuals (Wen *et al.*, 2022). These findings collectively point to a pro-inflammatory role of MAIT cells in the pathophysiology of asthma.

In murine models, repeated allergen exposure resulted in a notable reduction of MAIT cell populations, with the decrease not being mitigated by steroid treatment. Proinflammatory T cells contributed to this reduction, yet reintroducing CD4+ T cells could replenish MAIT cell levels. Mice deficient in MAIT cells ($Mr1^{-/-}$) exhibited enhanced ILC2 responses and subsequent airway inflammation and hyperresponsiveness after allergen exposure, such as to *Alternaria*. However, when MAIT cells were transferred into these mice, ILC2-mediated

responses and associated airway symptoms were significantly reduced. Moreover, MAIT cells in both humans and mice expressed high levels of IL4I1, an anti-inflammatory agent, which upon administration, downregulated IL-5 and IL-13 in lung ILC2s, indicating that IL4I1 modulates ILC2 activity (Ye *et al.*, 2020). It was further confirmed that MAIT cells reduced allergic airway inflammation by inhibiting the production of cytokines and proliferation of ILC2s (Shimizu *et al.*, 2022).

These findings suggest a dual role for MAIT cells: a specific contribution of IL-17 producing MAIT cells to disease severity and pathophysiology in asthma and a general protective effect against chronic inflammation in experimental model of asthma.

1.4.2 Chronic obstructive pulmonary disease

Chronic obstructive pulmonary disease (COPD) is characterised by chronic respiratory symptoms due to abnormalities of the airways and/or alveoli that cause persistent, progressive airflow obstruction (Celli *et al.*, 2022). In COPD, research has identified a significant depletion of CD8+ and double-negative MAIT cells in the peripheral blood, with this decrease being more prominent in moderate to severe stages of the disease (Kwon *et al.*, 2016; Szabó *et al.*, 2017). This reduction in MAIT cells parallels the severity of COPD, evidenced by correlations with clinical measures such as the post-bronchodilator FEV1/ forced vital capacity (FVC) ratio and C-reactive protein levels (Kwon *et al.*, 2016). COPD patients also exhibit MAIT cells with an increased IL-17 production, indicative of a Th17 phenotype, which interestingly correlates positively with the FEV1/FVC ratio (Qiu *et al.*, 2021). Furthermore, low MAIT cell counts have been linked to a higher risk of hospitalisation for COPD patients, and those hospitalised have more activated MAIT cells, as shown by elevated CD38 expression and a tendency for increased LAG-3 expression (Pincikova *et al.*, 2022). Huber and colleagues explored the impact of smoking and COPD on the dynamics between bronchial epithelial cells (BECs) and

MAIT cells. Their research revealed that BECs from COPD patients trigger increased activation of MAIT cells without a corresponding rise in MR1 protein levels, in contrast to cells from healthy individuals or current smokers. Additionally, exposure to cigarette smoke extract generally diminished the activation of MAIT cells by bacteria-exposed epithelial cells, indicating a potential pathway for enhanced bacterial colonisation in the airways of smokers (Huber *et al.*, 2023). These findings highlight the intricate interactions between BECs and the immune system in COPD progression and infection susceptibility. They reveal that dysregulated MAIT cell activation contributes to inflammation and exacerbations in COPD, suggesting that MAIT cells could serve as potential biomarkers for monitoring COPD progression and acute episodes.

Inhaled corticosteroids are found to compromise MAIT cell efficacy in COPD patients, evidenced by diminished frequencies and a decreased IFN-γ response to nontypeable haemophilus influenzae (NTHi) exposure. Given MAIT cells' capacity to produce IFN-γ in response to macrophage-presented NTHi antigens, they are implicated in defending against NTHi – the most prevalent COPD pathogen. Consequently, steroid therapy may inadvertently elevate pneumonia risk by attenuating MAIT cell-mediated immunity (Hinks *et al.*, 2016).

In summary, these findings implicate MAIT cells in multiple roles in COPD progression and response to treatment. Diminished MAIT cell counts are closely linked with disease severity, inflammation, and airway obstruction. Additionally, corticosteroid treatments, while beneficial for managing COPD symptoms, may paradoxically weaken MAIT cell functions, potentially increasing susceptibility to infections like pneumonia, thereby complicating COPD management, and cautioning against indiscriminate, non-biomarker-directed prescription of corticosteroids.

1.4.3 Community-acquired pneumonia

Community-acquired pneumonia (CAP) is a prevalent acute infection that often leads to hospital admission, primarily due to pathogens like *Streptococcus pneumoniae*, influenza A, *Mycoplasma pneumoniae,* and *Chlamydophila pneumoniae*. Severe cases of CAP can result in acute respiratory distress, cardiac failure, multi-organ dysfunction, and death *(Brown, 2012)*. In CAP patients, there was a significant reduction in the frequency of MAIT cells in the peripheral blood, alongside increased activation of these cells. Despite heightened activation, MAIT cells from CAP patients showed a diminished capacity to produce key cytokines such as IFN-γ, TNF-α, and IL-17A (Ouyang *et al.*, 2021). Besides, higher levels of MAIT cells in the sputum are associated with less severe symptoms and shorter hospital stays, suggesting a protective role (Hannaway *et al.*, 2020). There is also a positive correlation between MAIT cell abundance and neutrophil infiltration, indicating a collaborative immune response (Hannaway *et al.*, 2020). In children with severe CAP, MAIT cells within the BAL, not in the bloodstream, were actively producing IL-17, implicating their involvement in CAP's inflammation. Notably, the IL-17+ to IFN-γ+ ratio in MAIT cells was significantly higher in severe CAP than in less severe cases, indicating a potential shift toward a pathogenic role of IL-17 producing MAIT cells in more severe infections (Lu *et al.*, 2020).

1.4.4 Lung cystic fibrosis

Cystic fibrosis (CF) is an inherited genetic disorder that causes sticky mucus to build up in the lungs and digestive system (Shteinberg *et al.*, 2021). In young CF patients, MAIT cells represent the predominant unconventional T cell population in BAL (McElroy *et al.*, 2022). CF patients have markedly fewer MAIT cells in their peripheral blood compared to healthy individuals (Pauline *et al.*, 2021; Smith *et al.*, 2014), with the lowest counts found in those with *Pseudomonas aeruginosa* infections or undergoing treatment for pulmonary exacerbations

(Smith *et al.*, 2014). This deficit correlates strongly with increased severity of lung disease in CF (Smith *et al.*, 2014).

1.4.5 Interstitial lung diseases

Interstitial lung disease (ILD), or diffuse parenchymal diseases, are a heterogeneous group of disorders characterised by fibrosis (scarring) of the lungs (Wijsenbeek *et al.*, 2022). As the most common form of ILD, idiopathic pulmonary fibrosis (IPF) is a severe, chronic disorder marked by unexplained thickening and stiffening of the tissue surrounding the lungs' air sacs, or alveoli, which leads to progressively worsening dyspnea, diffuse interstitial infiltrates, restrictive lung impairment, and diminished gas exchange (Ryu *et al.*, 1998). To date, there has been limited literature examining the function of MAIT cells in ILD. One important study reported decreased counts of MAIT cells in the peripheral blood of IPF patients, suggesting a potential migration to the lungs (Zhao *et al.*, 2023).

1.4.6 Pulmonary sarcoidosis

Sarcoidosis is a rare disease that causes granulomas to develop in the organs of the body (Spagnolo *et al.*, 2018). In patients with lung sarcoidosis, MAIT cells were found in lower proportions in peripheral blood but showed higher levels of activation markers CD69 and PD-1 compared to healthy individuals. When comparing peripheral blood MAIT cells to those found in the BAL fluid of these patients, there was a significant increase in both the abundance and activation level of MAIT cells in the lungs, especially in patients with parenchymal infiltration. A significant correlation was observed between the activation marker CD69 on MAIT cells and clinical biomarkers such as angiotensin-converting enzyme and soluble IL-2 receptor, indicating that MAIT cell activity may be reflective of the disease's activity in sarcoidosis (Matsuyama *et al.*, 2019).

1.4.7 Lung cancer

MAIT cells in lung tumours exhibit dual roles, acting as both tumour promoters and inhibitors. This behaviour is influenced by their activation state, cytokine presence, and interactions with other immune cells. In mucosal-associated cancers like lung, gastric, and colon cancers, circulating MAIT cells are less prevalent than in healthy individuals. Despite their reduced numbers, these cells can produce important cytokines such as IFN-γ, IL-17, or TNF-α. A notable link exists between low MAIT cell levels and advanced cancer stage markers, suggesting their involvement in progression of mucosal-associated cancers (Won *et al.*, 2016).

In non-small cell lung cancer (NSCLC), MAIT cells are abundant in tumour lesions and migrate from blood via the CCR6-CCL20 axis. Both peripheral and tumour-infiltrating MAIT cells in NSCLC show an exhausted phenotype with increased PD-1, TIM-3, IL-17A, and decreased IFN-γ. Circulating MAIT cells with cytotoxic capabilities indicate potential response to anti-PD-1 therapy in NSCLC. Reprogrammed MAIT cells (m-reMAIT cells) have shown tumour growth inhibition in lung metastasis models and extended survival in mice. These cells, when combined with NK cells, enhance cytolytic activity and produce Th1 and Th17 cytokines, suggesting a role in tumour immune response enhancement (Sugimoto *et al.*, 2022).

Activated and expanded MAIT cells, stimulated by 5-OP-RU and TLR9 agonist CpG, have demonstrated a broad anti-tumour response in various murine cancer models including lung and liver metastasis. The anti-tumour effect of MAIT cells does not depend on direct MAIT-cell TCR and MR1 tumour cell interaction (Ruf *et al.*, 2021). Lower circulating MAIT cell frequencies correlate with improved progression-free survival in lung cancer patients (Q. Zhang *et al.*, 2022).

Contrary to data supporting their protective role, *Mr1*$^{-/-}$ mice showed reduced tumour growth and lung metastasis, dependent on NK cells, CD8+ T cells, and IFN-γ. Introducing MAIT cells

back into these mice reversed this reduction (Yan *et al.*, 2020). Another study highlights the complex role of MAIT cells in tumour immunity. *Mr1*$^{-/-}$ mice showed improved control over metastatic B16F10 tumour growth. Conversely, activating MAIT cells by exposing tumour cells to the antigen 5-OP-RU markedly reduced metastasis, an effect largely attributed to the consequent activation of NK cells (Petley *et al.*, 2021).

In summary, MAIT cells in lung cancer have a complex, multifaceted role. Understanding their exact impact on tumour progression and treatment response is essential for future therapeutic strategies. The ability of MAIT cells to alternate between tumour-promoting and inhibitory functions opens avenues for lung cancer treatment, especially through approaches like reprogramming and genetic engineering.

1.5 MAIT cell function in tissue repair and homeostasis

Owing to their anatomical placement and resemblance to other tissue-resident lymphocytes (Hinks *et al.*, 2019), and to transcriptomic data, MAIT cells have been proposed to contribute to tissue protection (Constantinides *et al.*, 2019; Lamichhane, Galvin*, et al.*, 2019; Leng *et al.*, 2019). We have used a transcriptomic approach on sorted MR1-tetramer+ cells to define the activated MAIT cell transcriptome in humans and mice (Hinks *et al.*, 2019). We have found that TCR-mediated activation prompts both species to express a tissue-repair programme, upregulating genes like *TNF*, *CSF2*, *HIF1A*, among others. Previously, this transcriptional programme has been linked to skin-homing Tc17 cells, which commensal flora induce, and which have facilitated epithelial wound repair in mice (Linehan *et al.*, 2018). Although such Tc17 cells were H2-M3 restricted – absent in humans – MAIT cells likely share this reparative capacity. Our comparative analysis has revealed that activated MAIT cells bear the closest similarity to these Tc17 cells (Hinks *et al.*, 2019). We have observed this repair programme in TCR-stimulated MAIT cells, a response absent in cytokine-only stimulation (Lamichhane,

Schneider*, et al.*, 2019; Leng *et al.*, 2019). Finally, MAIT cell supernatants have been shown to expedite wound closure in intestinal epithelial cell line systems (Leng *et al.*, 2019).

Subsequent *in vivo* research has demonstrated that exposing germ-free mice to *Staphylococcus epidermidis*, a common skin commensal, results in the expansion of MAIT cells in the skin and the activation of their tissue repair capabilities. These cells, primarily found near the dermal-epidermal junction, require 5-OP-RU and MR1 for their proliferation. Furthermore, they have been shown to expedite healing of biopsy-induced skin wounds, an effect that is amplified by topical 5-OP-RU application (Constantinides *et al.*, 2019).

While most transcriptomic analyses in the existing literature have focused on the tissue repair programme of MAIT cells under an MR1-TCR dependent activation pathway, recent research has suggested that cytokine involvement might also play a significant role (du Halgouet *et al.*, 2023). Using a mouse model to simulate full-thickness skin injury, it has been shown that MAIT cells are pre-programmed for tissue repair. After an injury, MAIT cells have been found to support the healing process by promoting the proliferation of keratinocytes, and their migration to wound sites is governed by the CXCR6 chemokine receptor rather than traditional TCR signals. Furthermore, the secretion of amphiregulin by MAIT cells post-injury has been identified as critical to the healing process. Importantly, the maintenance of the repair function does not depend on sustained TCR activation, indicating a TCR-independent pathway in MAIT cell-mediated tissue repair. These insights could have significant implications for the development of new regenerative therapies (du Halgouet *et al.*, 2023).

Whilst the importance of MAIT cells in tissue repair is implied by data from the skin model, MAIT cells are very abundant in the lung and there exist no *in vivo* data exploring the immunological significance of this function in respiratory health. I hypothesised that the MAIT cell tissue repair programme could be activated locally and contribute to protection in the lung

during tissue injury. Therefore, I aimed to use an *in vivo* challenge model to define the role of MAIT cells in pulmonary tissue repair.

1.6 Bleomycin-induced sterile lung injury mouse model

Bleomycin sulphate is a water-soluble antineoplastic glycopeptide derived from the actinobacterium *Streptomyces verticillus* (Umezawa *et al.*, 1966). Bleomycin exhibits unique antitumor properties through its binding to deoxyribonucleic acid (DNA)'s guanosine-cytosine-rich sequences. Its antitumor mechanism involves the 'S' tripeptide and bithiazole rings, which partially intercalate into DNA, while a cluster of five nitrogen atoms binds metals such as iron and copper. The iron-bound molecular oxygen generates highly reactive free radicals, causing DNA single-strand breaks at 3'-4' bonds in deoxyribose, resulting in free base propenals, predominantly thymine. This activity is particularly pronounced during the M and G2 phases of the cell cycle, proving more effective against actively dividing cells than resting ones (Moseley, 1989; Twentyman, 1983) and it leads to cytotoxicity, cell death, and a sterile inflammatory response, which subsequently progresses to fibrosis due to the accumulation of extracellular matrix proteins (Hay *et al.*, 1991).

Key factors in bleomycin-induced lung injury include cytokines, superoxide and hydroxide free radicals, which are particularly potent due to low levels of bleomycin hydrolase in the lung, especially within type II pneumocytes (Adamson & Bowden, 1979; Hay *et al.*, 1991; Sleijfer, 2001). Bleomycin hydrolase is an enzyme that hydrolyses the L-amino alanine moiety of bleomycin, inhibiting the binding of metals such as iron and thus reducing oxidative stress (Twentyman, 1983). This mechanism of action highlights why lung cells are particularly susceptible to bleomycin's toxic effects during mitosis and underscores its utility in lung injury model induction.

Acute inflammation is key in the development of bleomycin-induced lung injury, primarily involving mononuclear macrophages, lymphocytes, and neutrophils (Hay *et al.*, 1987). Key inflammatory cytokines involved in bleomycin-induced lung injury include IL-1β, IL-18 (Hoshino *et al.*, 2009), TNF (Ortiz *et al.*, 1998), IL-33 (D. Li *et al.*, 2014), IL-12 (Sakamoto *et al.*, 2002), IL-22 (Sonnenberg *et al.*, 2010), IL-13 (Nie *et al.*, 2019), IL-17A, TGF-*β* (Mi *et al.*, 2011; Wilson *et al.*, 2010), and IL-6 (Karmiol *et al.*, 1993; Saito *et al.*, 2008; Scheule *et al.*, 1992). These cytokines initiate lymphocyte activation and increase adhesion molecules on endothelial cells, facilitating inflammatory infiltration and endothelial damage via the Fas-FasL pathway (Kuwano *et al.*, 1999). Research indicates that uric acid and ATP, released from lung cells damaged by bleomycin, serve as primary endogenous danger signals, triggering mitochondrial reactive oxygen species (ROS) generation and activate the NALP3 inflammasome. This activation is characterised by the maturation of procaspase-1, which leads to IL-1β production and subsequent lung fibrosis (Gasse *et al.*, 2009; Kim *et al.*, 2016; Riteau *et al.*, 2010). Furthermore, IL-1β activates the IL-1R1/MyD88 complex in tissue resident cells, particularly lung epithelial cells, triggering NF-κB activation. This cascade promotes inflammation in bleomycin-induced lung pathology, characterised by neutrophil and lymphocyte recruitment and fibroblast activation (Gasse *et al.*, 2007). Additionally, bleomycin induces alveolar macrophages to produce hyaluronan, a key molecule in fibrotic lungs (Savani *et al.*, 2000).

The pathogenesis of bleomycin-induced lung injury typically manifests within 48 hours following intratracheal administration, a timeline that has been validated through histopathological analysis. This lung injury process is characterised by the deposition of matrix proteins and enhanced collagen deposition, leads to increased permeability and the influx of proteins and inflammatory cells into lung tissue. Continuous exposure to various mediators released from circulating cells and tissues at the injury site mirrors human lung fibrosis, making

this a robust model for studying pulmonary repair and diseases like idiopathic pulmonary fibrosis (IPF) (Moore & Hogaboam, 2008; Reinert *et al.*, 2013; Tashiro *et al.*, 2017).

The bleomycin-induced lung injury model demonstrates a bimodal disease progression: an acute inflammatory response within the first week, marked by cytokine release and inflammation, evolves into chronic fibrosis over two to three weeks, characterised by myofibroblast proliferation and further collagen deposition (Izbicki *et al.*, 2002; Williamson *et al.*, 2015). This pattern closely resembles the pathology in human patients and provides a valuable framework to explore the role of MAIT cells in lung tissue injury and repair.

1.7 Research aims

MAIT cells, which are particularly abundant in the lung, constitute up to 10% of all T cells in this organ in a healthy human (Hinks *et al.*, 2016; Hinks *et al.*, 2015). These cells are characterised by a semi-invariant αβ TCR and are the predominant T cell subset during the initial stages of an immune response. Whilst MAIT cells have extensive antimicrobial specificity, effectively combatting a wide range of bacterial, fungal, and viral pathogens, recent research suggests they also play a role in tissue protection and repair. However, the precise function of MAIT cells in sterile lung injury remains to be elucidated.

The primary goal of this thesis was to understand the mechanisms and pathophysiological consequences of the MAIT cell tissue repair programme in the lung. This goal was pursued through the investigation of three specific aims:

1.7.1 Aim 1

To characterise activation of a MAIT cell tissue repair programme over the time course of pulmonary injury in the airway and parenchymal lung tissue during

a. Viral infection with influenza A infection

b. Acute sterile lung injury induced by bleomycin

My hypotheses were that MAIT cells play an important role in limiting tissue damage and accelerating mucosal repair after acute viral pneumonia and sterile lung injury.

1.7.2 Aim 2

To determine the functional consequences of this MAIT cell activation in mice deficient in MAIT cells (*Mr1*$^{-/-}$) (Treiner *et al.*, 2003) or with therapeutically enhanced MAIT cell frequencies (using intranasal 5-OP-RU or direct microbial stimulation with intranasal *Salmonella enterica* serovar Typhimurium BRD509).

My hypotheses were that MAIT cell function can be enhanced by stimulation with synthetic MAIT cell ligands.

1.7.3 Aim 3

To explore the underlying mechanisms of MAIT cell activity in the context of tissue injury.

My hypotheses were that MAIT cells interact with other immune cells to mediate tissue protection in the context of sterile lung injury. This interaction might be important for the immune response, reducing damage, facilitating the repair and regeneration of lung tissue in the absence of infectious agents.

2 MATERIALS AND METHODS

2.1 Murine models

Murine models were required for the analysis of an immune response *in vivo*. Addressing the role of MAIT cells in lung tissue repair requires a fully functional immune system and an entire respiratory tract, precluding the possibility of *in vitro* analysis for such specific factors. Nonetheless, *in vitro* assays are used to confirm key findings. The adult mouse is recognised for its reliability in modelling innate and adaptive immune responses and considered the mammal of lowest sentience. A variety of highly relevant murine genetic knockout strains are available, notably the MAIT cell-deficient *Mr1*$^{-/-}$ mouse (Treiner *et al.*, 2003), which is important for this research. Moreover, reagents, antibodies, and the unique anti-MR1 tetramers have demonstrated reactivity in both mouse and human studies. Murine models are valuable in studying human-like immune responses, but their difference from human biology can limit the direct applicability of the results. Genetic and environmental variations in mice may not accurately reflect human tissue repair processes, necessitating cautious interpretation when extrapolating data to human clinical scenarios.

C57BL/6 mice (aged 8–10 weeks) were purchased from University of Oxford Biomedical Services, Charles River or Envigo. *Mr1*$^{-/-}$ mice (Treiner *et al.*, 2003) (kindly provided by Dr Claire Hutchings, University of Oxford, MGI ID: 3664578), *Il18r1*^{tm1Aki} mice (kindly provided by Prof Kevin Maloy, University of Oxford, MGI: 2136765), and *Ifnar1*^{tm1Agt} mice (kindly provided by Dr Claire Hutchings, University of Oxford, MGI ID: 1930950) were bred in house and used at 8-10 weeks of age. Sex and age were matched between groups. All mice were housed in specific pathogen-free conditions. For indicated experiments, C57BL/6 and *Mr1*$^{-/-}$ mice were co-housed for ≥ 28 days to normalize the microbiome between strains (Varelias *et al.*, 2018). All work was performed under UK Home Office license PPL P61FAD253 in

accordance with the UK Animal (Scientific Procedures) Act 1986. The maximum permissible weight loss threshold on this licence was 20% for *Salmonella enterica* serovar Typhimurium BRD509 infection and 15% for bleomycin challenge.

2.2 Murine pulmonary MAIT cell expansion using *Salmonella* Typhimurium BRD509

Salmonella Typhimurium BRD509 were prepared as previously described (van Wilgenburg *et al.*, 2018). *Salmonella* Typhimurium BRD509 were streaked on Luria Broth (LB) agar plates and plates incubated overnight at 37 ºC. A single colony was selected and inoculated to a 10 mL LB culture medium in a shaking incubator at 37ºC to ensure an optimal optical density (O.D.) reading for preparing the inoculum. The inoculum was prepared from the culture with an $O.D._{600nm}$ reading at 0.5. The required inoculum, in colony forming units (CFU) of bacteria, was calculated by estimating 1 O.D. = 5-10 × 10^8 CFU. The culture was diluted with phosphate buffered saline (PBS) to a final concentration of 2 × 10^7 CFU/mL, allowing 50 µL inoculum/mouse, i.e., 10^6 CFU/50 µL/mouse. Mice were infected i.n. with 10^6 CFU *Salmonella* Typhimurium BRD509 in 50 µL PBS under isoflurane anaesthesia. Mice were allowed to recover and monitored for 7 days to allow the infection to take its course and MAIT cell frequencies to expand from 1% to up to 20% of all alpha-beta T cells.

2.3 Murine *in vivo* bleomycin challenge

For the bleomycin challenge, mice were anaesthetized with isoflurane and treated intratracheally with 1.875 U/Kg (mice weight) of bleomycin sulphate (Apollo Scientific, Cat. No. BI3543) in 50 µL of PBS for *Salmonella* BRD509 pre-infected mice, or with 1.0 U/Kg of bleomycin sulphate in 50 µL of PBS for naïve mice without pre-infection.

2.4 Murine *in vivo* PR8 influenza A virus infection

2.4.1 Propagation, quantification and mouse infection of PR8 influenza A virus

Propagation, quantification and murine infection of PR8 influenza A virus were performed as previously described (Hinks *et al.*, 2020).

2.4.2 Propagation of PR8 influenza virus in MDCK cells culture from virus stocks

Madin-Darby canine kidney (MDCK) cells were cultured to about 80% confluent using DMEM with 10% foetal bovine serum (FBS) (MDCK cell growth medium) in 175-cm^2 tissue culture-treated flasks. Vials of influenza virus stock were thawed on ice, MDCK growth medium removed and the MDCK monolayer washed twice with room temperature (RT) PBS. Influenza virus samples were diluted in modified Eagle's medium (MEM) with 0.1% bovine serum albumin (BSA) and 2 µg /mL tosyl phenylalanyl chloromethyl ketone (TPCK)-trypsin (PR8 influenza virus growth medium), and the flask was inoculated with diluted PR8 influenza virus and rotated to cover the monolayer with inoculum. Inoculated flasks were incubated for 1 h at 37 ºC to allow the inoculum to adsorb, then a 20 mL virus growth medium was added to the inoculated flasks before incubating flasks at 37ºC. Cytopathic effect (CPE) of MDCK monolayer was observed daily. Cell culture supernatants were harvested when at least 75% of the cell monolayer was exhibiting CPE. Typical CPE by influenza viruses included rounding up of infected cells and detachment from culture flask. To harvest, the medium in the flask was decanted into a 50 mL Falcon tube, the supernatant centrifuged for 20 min at 800 × g, 4 ºC, to pellet cellular debris. Clarified supernatants were transferred into a fresh 15 mL tube. Tissue culture flasks were disposed of in an appropriate biological waste container and the supernatants were dispensed into sterile 2-mL cryovials and stored for up to 1 year at −80 ºC.

2.4.3 Quantification of PR8 influenza viruses by 50% tissue culture infectious dose assay ($TCID_{50}$)

MDCK cells were cultured to 80-90% confluent in a 96-well tissue culture plate. MDCK growth medium was removed from the plate and the cells were washed twice by adding 350 µL PR8 influenza virus growth medium to all wells. PR8 influenza virus stock was thawed on ice and diluted 1:100 in the influenza virus growth medium. 20 µL diluted virus was added to 12 columns of the 96-well flat-bottom tissue culture plate, creating a log10 dilution series, with no virus as the cell control for the assay. Plates were incubated for 1 h at 37 ºC. The inoculum was removed and gently washed once with a 250 µL influenza virus growth medium. 200 µL PR8 influenza virus growth medium was added to all wells and incubated up to 72 h at 37ºC observing for endpoints in CPE. CPE endpoints were recorded and $TCID_{50}$ titres were determined per 100 µL using the ReedMuench method.

2.4.4 Quantification of PR8 influenza viruses by plaque assay

MDCK cells were cultured to 80-90% confluent in a 12-well tissue culture plate. The MDCK growth medium was removed from the plates and the MDCK monolayer was washed three times with RT PBS, and a ten-fold dilution series was performed starting at 10^{-1} and diluting virus samples down to 10^{-10} in PR8 influenza virus growth medium. 12-well tissue culture wells were inoculated in duplicate with 100 µL diluted virus sample and the tissue culture plates rotated to cover monolayer with inoculum. The inoculated plates were incubated for 1 h at 37 ºC. The wells were washed twice with RT PBS, 2 × PR8 influenza virus growth medium mixed 1:1 with 1.6% agarose solution and 1 mL of agarose medium solution immediately added to each inoculated well, before being left to solidify at RT. The plates were incubated at 37 ºC, and the MDCK monolayer was observed daily with an inverted microscope for plaque formation. After 72 h, the agar plug was carefully removed from each well using sterile forceps

and the agar was disposed of in a biological waste container, carefully avoiding scratching the MDCK cell monolayer or letting the agar plugs rotate during removal. 1 mL 0.4% crystal violet solution was added to each well and incubated for 10 min at RT to stain the MDCK cell monolayer. The crystal violet solution was removed, and the wells were washed with 1 to 2 mL water to rinse away excess stain solution, the plates were left to dry, and plaques were counted in each well to determine the PFU per millilitre using the following formula: PFU/mL = (no. of plaques × dilution factor × 10).

2.4.5 PR8 influenza virus infection

The virus was thawed on ice and serial dilutions in sterile PBS were performed to achieve the desired inoculum. The virus was mixed by vortex before administering the inoculum. Male C57BL/6 mice between 8–10 weeks of age were anaesthetized with isoflurane then infected intranasally with 350 PFU of PR8 influenza virus in 50 µL of PBS. Mice were allowed to recover and monitored until recovery. Lung tissues were harvested at 0, 3, 5, 7 and 13 days after exposure.

2.5 Flow cytometry analysis

2.5.1 Generation of human and murine MR1 tetramers

Human and murine MR1-5-OP-RU and MR1-6-FP monomers were provided by the NIH Tetramer Facility. Tetramers were generated using Brilliant Violet 421 (BV421)-Streptavidin and Phycoerythrin (PE)-Streptavidin (BioLegend, Cat. No. 405225 and 405245, respectively) following the NIH Tetramer Facility's guidelines.

2.5.2 Antibodies staining for flow cytometry and cell sorting

Mice were euthanised with CO_2. Mice lungs were collagenase-digested, washed and lung single cell suspension was prepared as described previously (Hinks *et al.*, 2019). For measurement of intracellular markers, 1 × Brefeldin A (eBioscience™, Cat. No. 00-4506-51) was added 4 h before staining. Lung cells were blocked with anti-Fc receptor 2.4G2 and/or 6-FP tetramer for 15 min at RT, stained with viability dye, fluorescently labelled MR1 tetramer and/or flow cytometric antibodies for 20 min at RT. Staining antibodies, clones and concentrations are listed in table 1. Samples were washed in FACS buffer (PBS + 0.5% BSA + 2 mM ethylenediamine tetraacetic acid (EDTA)), and cells were fixed for 15 min RT using intracellular fixation buffer then washed twice with 1 × permeabilization buffer (eBioscience™, Cat. No. 00-8222-49 and 00-8333-56, respectively). Intracellular staining was performed overnight at 4 °C. Samples were subsequently washed twice and stored in FACS buffer at 4 °C until analysed on BD LSRII flow cytometer.

For live cell sorting on murine lung MAIT cells, lung single-cell suspension was purified with a 40%: 70% Percoll gradient. The sorting was conducted on a BD Aria III directly into 350 µL lysis buffer (Buffer RLT plus, supplemented with 10 µL 2-mercaptoethanol (β-ME) per 1 mL Buffer RLT plus from the QiaGen RNeasy Plus Micro Kit, Cat. No. 74034) and subsequently stored at -80 °C for future batch RNA extraction.

For multiparameter spectral flow cytometry analysis, the “AF as a tag” (AF) function was used in the SpectroFlo (Cytek Biosciences, CA) software (Chang *et al.*, 2023). 6 unique AF tags were disassociated from unstained mouse lung samples and included in the unmixing strategy.

Table 2-1 Flow cytometry reagents

No.	Antigen	Conjugation	Clone	Host	Reactivity	Isotype	Concentration	Catalogue number	Supplier
1	CD103	AF700	2 E7	Hamster	Mouse	Armenian Hamster IgG	1:100	121442	BioLegend
2	CD45	BUV395	30-F11	Rat	Mouse	Rat IgG2b, κ	1:100	564279	BD Biosciences
3	CD11c	APC/Fire™ 750	N418	Rat	Mouse	Armenian Hamster IgG	1:100	117352	Biolegend
4	CD19	BV480	1D3	Rat	Mouse	Lewis IgG2a, κ	1:100	566107	BD Biosciences
5	MERTK (Mer)	PE-Cy7	2B10C42	Rat	Mouse	Rat IgG2a, κ	1:100	151522	Biolegend
6	CD4	AF488	GK1.5	Rat	Mouse	Rat IgG2b, κ	1:100	100423	Biolegend
7	Ly-6G	BUV615	1A8	Rat	Mouse	Lewis IgG2a, κ	1:100	751263	BD Biosciences
8	Ly-6C	BV570	HK1.4	Rat	Mouse	Rat IgG2c, κ	1:100	128029	Biolegend
9	MHC II	BV650	M5/114.15.2	Rat	Mouse	Rat IgG2b, κ	1:100	107641	Biolegend
10	CD8a	BV605	53-6.7	Rat	Mouse	Rat IgG2a, κ	1:100	100744	Biolegend
11	CD11b	BV711	M1/70	Rat	Mouse/Human	Rat IgG2b, κ	1:100	101242	Biolegend
12	CD3	BV785	17A2	Rat	Mouse	Rat IgG2b, κ	1:100	100232	Biolegend
13	CD64	PE	X54-5/7.1	Mouse	Mouse	Mouse IgG1, κ	1:100	139304	Biolegend
14	NK1.1	PE/Cyanine5	PK136	Mouse	Mouse	Mouse IgG2a, κ	1:100	108716	Biolegend
15	CD44	BUV805	IM7	Rat	Mouse	Rat IgG2b, κ	1:100	741921	BD Biosciences
16	TCR γ/δ	BUV737	GL3	Hamster	Mouse	Armenian Hamster IgG2, κ	1:100	748991	Biolegend
17	CD19	PerCP Cy5.5	6D5	Rat	Mouse	Rat IgG2a, κ	1:100	115534	BioLegend
18	CD69	FITC	H1.2F3	Hamster	Mouse	Armenian Hamster IgG1, λ3	1:100	553236	BD Biosciences
19	TCRβ	PE-Cy7	H57-597	Hamster	Mouse	Armenian Hamster IgG2, λ1	1:100	560729	BD Biosciences
20	CD25	APC	PC61.5	Rat	Mouse	Rat IgG1, λ	1:100	17-0251-82	eBioscience™
21	CD45.2	BV711	104	Mouse	Mouse	Mouse SJL IgG2a, κ	1:100	563685	BD Biosciences

22	IFN-γ	BV650	XMG1.2	Rat	Mouse	Rat IgG1, κ	1:100	563854	BD Biosciences
23	IL-22	APC	Poly5164	Goat	Mouse	Polyclonal	1:100	516409	BioLegend
24	IL-10	APC-Cy7	JES5-16E3	Rat	Mouse	Rat IgG2b, κ	1:100	505010	BioLegend
25	IL-17A	PE	TC11-18H10.1	Rat	Mouse	Rat IgG1, κ	1:100	506904	BioLegend
26	GM-CSF	PE/Dazzle™ 594	MP1-22E9	Rat	Mouse	Rat IgG2a, κ	1:100	505422	BioLegend
27	SiglecH	PerCP Cy5.5	551	Rat	Mouse	Rat IgG1, κ	1:100	129614	BioLegend
28	CD45	FITC	30-F11	Rat	Mouse	Rat IgG2b, κ	1:100	103108	BioLegend
29	CD86	BV605	GL-1	Rat	Mouse	Rat IgG2a, κ	1:100	105037	BioLegend
30	CD40	PE/Cyanine5	44986	Rat	Mouse	Rat IgG2a, κ	1:100	124618	BioLegend
31	CD192	PE/Dazzle™ 594	SA203G11	Rat	Mouse	Rat IgG2b, κ	1:100	150636	BioLegend
32	CD192	APC/Fire™ 750	SA203G11	Rat	Mouse	Rat IgG2b, κ	1:100	150630	BioLegend
33	CD317	PE/Cyanine7	eBio927	Rat	Mouse	Rat IgG2b, κ	1:100	25-3172-82	eBioscience™
34	CD370	APC	7H11	Rat	Mouse	Rat IgG1, κ	1:100	143506	BioLegend
35	CD24	PE/Dazzle™ 594	M1/69	Rat	Mouse	Rat IgG2b, κ	1:100	101838	BioLegend
36	CD45.2	FITC	104	Mouse	Mouse	Mouse (SJL) IgG2a, κ	1:100	109806	BioLegend
37	CD45.1	BV785	A20	Mouse	Mouse	Mouse (A.SW) IgG2a, κ	1:100	110743	BioLegend
38	CD11c	PE	N418	Hamster	Mouse	Armenian Hamster IgG	1:100	117308	BioLegend
39	CD45R	BV421	RA3-6B2	Rat	Mouse	Rat IgG2a, κ	1:100	103251	BioLegend
40	Zombie NIR™ Fixable Viability Kit						1:1000	423106	BioLegend
41	Zombie Aqua™ Fixable Viability Kit						1:1000	423102	BioLegend
42	Zombie Yellow™ Fixable Viability Kit						1:1000	423104	BioLegend

2.6 Histology

2.6.1 Making Formalin-Fixed, Paraffin Embedded Blocks

The left lobes of the mice lungs were first fixed using 10% formalin (Sigma-Aldrich, Cat. HT501128-4L) for a duration exceeding 24 h. Following fixation, the lung tissue underwent a dehydration process with an ethanol gradient: initially treated with 75% ethanol for one hour, then with 85% ethanol for an additional hour. Subsequently, the sections were treated with 95% ethanol in three separate instances, each lasting 20 min, totalling one hour, and with 100% ethanol similarly in three instances for a total of one hour. Afterward, the fixed and dehydrated tissue were cleansed twice with Histo-Clear II (Scientific Laboratory Supplies Limited, Cat. NAT1334), each for 30 min, and then washed in paraffin across three intervals, totalling two hours together. The tissues were then embedded in paraffin utilizing the Leica EG 1160 paraffin embedding station, adhering to the published protocol (Sadeghipour & Babaheidarian, 2019).

Prior to the sectioning process, paraffin-embedded tissue blocks were cooled on ice to ensure the wax's firmness, which aids in procuring finer sections by bolstering the tissue specimen's harder components. A water bath was prepared with ultrapure water and heated to a temperature range of 40-45 °C. The sectioning blade was then secured in its holder, and the appropriate clearance angle was established. The paraffin block was mounted and aligned to facilitate a direct cut across the block. The blade was gradually brought close to the block, and several slender sections were incised to confirm correct alignment, adjusting as necessary. The block was methodically trimmed at a thickness between 10-30 μm to reveal the tissue surface

appropriate for cutting a representative section. The sections were then sliced to a thickness of approximately 4-5 µm.

Following the sectioning, the obtained ribbons were picked with tweezers and gently floated on the water bath's surface, allowing them to extend flat. These sections were then carefully separated with the tweezers. The sections were retrieved from the water bath using microscope slides and placed upright in a slide rack. This rack was transferred to an oven where the sections were dried, either overnight at 37 °C or for a period of 1 to 2 h at a higher temperature range of 55 °C. The slides were conserved at RT for future histology staining.

2.6.2 Haematoxylin and Eosin staining

Haematoxylin and eosin staining was performed using commercial kit (Abcam, Cat. No. ab245880) following manufacturer's instructions.

The tissue sections were deparaffinized in Histo-Clear II through two 10-min immersions. Gradual hydration was then achieved using graded ethanol: the sections were washed once in 100% ethanol for 2 min, followed by 95% ethanol for 2 min, 85% ethanol for 2 min, and finally 75% ethanol for 2 min. The sections were washed in deionized water twice for 5 min each, with stirring in between. Excess liquid was aspirated from the slides.

For haematoxylin and eosin staining, haematoxylin, Mayer's (Lillie's Modification), was applied to cover the tissue sections completely and was incubated for 5 minutes. The slides were then rinsed in two changes of distilled water to remove excess stain. Bluing Reagent was applied to cover the tissue sections and incubated for 10-15 s, followed by a rinse in two

changes of distilled water. The slides were dipped in absolute ethanol and the excess was blotted off.

Eosin Y Solution (Modified Alcoholic) was applied liberally to completely cover the tissue sections and allowed to incubate for 2-3 min. The slides were then rinsed using absolute ethanol and dehydrated in three changes of absolute ethanol. Finally, the slides were cleared and mounted in synthetic resin.

2.6.3 Trichrome staining

Trichrome staining was performed using commercial kit (Abcam, Cat. No. ab150686) following manufacturer's instructions.

Prior to utilization, all materials and reagents were equilibrated to RT and gently agitated. Sections were deparaffinized as required and then hydrated in distilled water. Bouin's Fluid was preheated to a temperature range of 56-64 °C within a water bath situated in a fume hood or a well-ventilated area. Slides were placed in the preheated Bouin's Fluid for 60 min, followed by a cooling period of 10 min. The slides were then rinsed in tap water until the sections appeared completely clear, and subsequently rinsed once in distilled water.

For staining, Weigert's (A) and Weigert's (B) solutions were mixed in equal parts, and slides were stained with the resultant working Weigert's Iron Haematoxylin for 5 min. The slides were then rinsed in running tap water for 2 min. Biebrich Scarlet/Acid Fuchsin Solution was applied to the slides for 15 min, followed by a rinse in distilled water. The differentiation process involved the slides being treated with Phosphomolybdic/Phosphotungstic Acid Solution for 10-15 min or until the collagen no longer presented red staining.

Subsequently, without a prior rinse, Aniline Blue Solution was applied to the slides for a duration of 5-10 min. The slides were rinsed in distilled water before a 1% Acetic Acid Solution was applied for 3-5 min. A rapid dehydration was achieved with two changes of 95% Alcohol and two changes of absolute ethanol. Finally, the slides were cleared in Histo-Clear II (Scientific Laboratory Supplies Limited, Cat. NAT1334) and mounted with a synthetic resin.

2.6.4 Scoring

The modified Ashcroft scoring system was employed for a semiquantitative analysis (Hübner *et al.*, 2008) to evaluate the extent of fibrosis.

Table 2-2 Characterisation of the modified Ashcroft scoring scale

Grade of Fibrosis	Modified Ashcroft scoring scale
0	Alveolar septa: No fibrotic burden at the flimsiest small lines in some alveolar walls Lung structure: Normal lung
1	Alveolar septa: Isolated gentle fibrotic changes (septum <3x thicker than normal) Lung structure: Alveoli partly enlarged and rarefied, but no fibrotic masses present
2	Alveolar septa: Clearly fibrotic changes (septum >3x thicker than normal) with knot-like formation but not connected to each other Lung structure: Alveoli partly enlarged and rarefied, but no fibrotic masses
3	Alveolar septa: Contiguous fibrotic walls (septum >3x thicker than normal) predominantly in whole microscopic field Lung structure: Alveoli partly enlarged and rarefied, but no fibrotic masses
4	Alveolar septa: Variable Lung structure: Single fibrotic masses (≤10% of microscopic field)
5	Alveolar septa: Variable Lung structure: Confluent fibrotic masses (>10% and ≤50% of microscopic field), Lung structure severely damaged but still preserved
6	Alveolar septa: Variable, mostly not existent Lung structure: Large contiguous fibrotic masses (>50% of microscopic field), Lung architecture mostly not preserved
7	Alveolar septa: Non-existent Lung structure: Alveoli nearly obliterated with fibrous masses but still up to five air bubbles
8	Alveolar septa: Non-existent Lung structure: Microscopic field with complete obliteration with fibrotic masses

From Hübner et.al., Biotechniques. 2008 Apr;44(4):507-11, 514-7.

2.7 Hydroxyproline assay

Hydroxyproline was measured using 10 mg of lung tissue using a hydroxyproline assay kit (Sigma-Aldrich, Cat. No. MAK008) per the manufacturer's instructions. Duplicate runs were performed for all samples and standards, utilizing ultrapure water for their preparation.

2.7.1 Hydroxyproline Standards for Colorimetric Detection

A 0.1 mg/mL standard solution was prepared by diluting 10 µL of the 1 mg/mL Hydroxyproline Standard Solution with 90 µL of water. Volumes of 0, 2, 4, 6, 8, and 10 µL from this solution were added into a 96-well plate, resulting in standards containing 0 (blank), 0.2, 0.4, 0.6, 0.8, and 1.0 µg/well of hydroxyproline, respectively.

2.7.2 Sample Preparation

10 mg of mouse lung tissue was homogenized in 100 µL of water and 100 µL of the sample was transferred to a pressure-tight polypropylene vial with a PTFE-lined cap. An equal volume of 12 M concentrated hydrochloric acid was added, the vial was sealed, and the contents were hydrolysed at 120 °C for 3 hours. After hydrolysis, the content was mixed and centrifuged at 10,000 x g for 3 minutes. A supernatant volume ranging from 10–50 µL was then transferred to a 96-well plate. All wells were dried in a 60 °C oven. For undetermined samples, multiple dilutions were tested to confirm that readings fell within the linear range of the standard curve.

2.7.3 Assay Procedure

A Chloramine T/Oxidation buffer mixture was prepared, allocating 100 µL for each reaction well; this entailed adding 6 µL of Chloramine T Concentrate to 94 µL of oxidation buffer, followed by thorough mixing. Similarly, a diluted 4-(Dimethylamino)benzaldehyde (DMAB) reagent was prepared, requiring 100 µL per reaction well, by combining 50 µL of DMAB Concentrate with 50 µL of Perchloric Acid/Isopropanol Solution. Subsequently, 100 µL of the Chloramine T/Oxidation Buffer Mixture was added to each well, and the plate was incubated at RT for 5 minutes. This was followed by the addition of 100 µL of the diluted DMAB reagent to each well, with incubation proceeding for 90 minutes at 60 °C. Absorbance was measured at a wavelength of 560 nm (A560).

2.8 RT-qPCR and bulk RNA sequencing

2.8.1 Total RNA extraction

RNA extraction was performed by single column centrifugation using the RNeasy® Plus Micro Kit (Qiagen, Cat No. 74034) following the manufacturer's protocol. The cell lysate was loaded onto the QIAshredder spin column, transferred to the gDNA Eliminator spin column, followed by the RNeasy MinElute spin column, then washed and eluted in RNase-free water.

2.8.2 RNA integrity assessment

RNA integrity was assessed by Agilent High Sensitivity RNA ScreenTape Assay on an Agilent 4200 TapeStation following the manufacturer's protocol (Agilent, Cat. No. 5067-5579, 5580 and 5581). RNA ScreenTape device was loaded into the TapeStation instrument, and reagents were equilibrated or thawed, vortexed and spun down before use. Samples and ladder were

denatured, loaded into the Agilent 4200 TapeStation, run and results were displayed by Agilent Tapestation Analysis Software.

2.8.3 RNA quantification, purity check and reverse transcription

For reverse transcription quantitative polymerase chain reaction (RT-qPCR) experiments, total lung RNA was extracted as described above. RNA quantity and quality were assessed using a Nanodrop 2000 (Thermo Scientific) following the manufacturer's protocol. Isolated RNA was converted to cDNA in preparation for qPCR using a High-Capacity cDNA Reverse Transcription Kit with RNase Inhibitor (Applied Biosystems, Cat. No. 4374966) following the manufacturer's protocol. Template RNA and reagents were thawed on ice. The reverse transcription reaction mix was prepared and incubated in the Programmable Thermal Controller as the following steps: Step 1: 25 °C, 10 min; Step 2: 37 °C, 120 min; Step 3: 85 °C, 5 min; Step 4: 4 °C, ∞.

2.8.4 Reverse transcription quantitative polymerase chain reaction (RT-qPCR)

For qPCR reactions, 2 × QuantiFast SYBR Green PCR Master Mix kit (QiaGen, Cat No. 204056) was used following the manufacturer's instructions. PCR reaction mix was prepared, mixed, and appropriate volumes were dispensed into the wells of a PCR plate. Template cDNA was added to the individual wells containing the reaction mix. The qPCR plate was loaded into a Bio-Rad CFX96. qPCR was performed following the manufacturer (Bio-Rad)'s instructions. Thermal cycling conditions were set up as the following steps: PCR initial heat activation: 95 °C, 5 min; 2-step cycling: Denaturation: 95 °C, 10 s; Combined annealing/extension: 60 °C, 30 s; 35-40 cycles in total.

2.8.5 cDNA library preparation, sequencing by Novogene

Total RNA was subsequently submitted to Novogene following their sample preparation and shipping instructions. All further laboratory work was performed by Novogene using their commercial protocol. RNA quality and quantity were assessed using the RNA ScreenTape Analysis. RNA was reverse transcribed, and cDNA amplified by reverse transcription with the NEBNext® Ultra™ II Directional RNA Library Prep Kit for Illumina® (NEB, Cat. No. E7760S), a low input method using NEB Next® Ultra RNA Library Prep Kit for Illumina® (NEB, Cat. No. 7530), or an ultra-low input method using TaKaRa SMART-Seq v4 Ultra Low Input RNA Kit for Sequencing (TaKaRa, Cat. No. 634889). First-strand cDNA synthesis and tailing by reverse transcription were performed using SMART (Switching Mechanism at 5' End of RNA Template) technology. Following first-strand synthesis, cDNA was amplified by PCR to produce the library. Quality control of the library was performed by quantification with a Qubit 2.0 fluorimeter and by qPCR. Insert size was measured by the Agilent 2100 Bioanalyzer automated gel electrophoresis system. The library was sequenced using the NovaSeq platform with Illumina sequencing technology to generate 150 bp paired-end reads.

2.8.6 Bulk RNA-sequencing data analysis

NovaSeq platform images were first converted into raw sequence reads via Illumina's CASAVA software, stored in FASTQ format. After filtering out low-quality and adapter reads, the remaining clean reads were mapped using STAR version 2.6.1 (Dobin *et al.*, 2013) against the *Mus musculus* GRCm38 reference genome (GenBank accession number GCA_000001635.2). Successful mapping was determined by a rate over 70%, with the results preserved as BAM files (Dündar *et al.*, 2019). Read quantification involved featureCounts

1.5.0 (Liao *et al.*, 2014), which converted BAM files to a table of gene IDs and counts per sample. Differential expression analysis was performed in in R (version 4.1.0) using DESeq2 (version 1.30.1) (Love *et al.*, 2014). Differentially expressed genes (DEGs) were defined as log2 fold-change > 1 and adjusted $P < 0.05$. VennDiagram (version 1.6.20). ggplot2 (version 3.2.1), pheatmap (version 1.4.3) and ggrepel (version 0.8.1) were used for data visualization. clusterProfiler (version 4.0) (Wu *et al.*, 2021) and Mfuzz (Kumar & M, 2007) were used for Gene Ontology (GO) enrichment and time-series analysis, respectively. Gene Set Enrichment Analysis (GSEA) was performed using GSEA software (version 4.1.0) (Subramanian *et al.*, 2005). Bulk RNA-seq data cell type deconvolution was performed utilising MUlti-Subject SIngle Cell deconvolution (MuSiC) method (X. Wang *et al.*, 2019). For this analysis, cell-type-specific gene expression data from a bleomycin-induced lung injury mouse model, acquired from the single-cell RNA-seq dataset (GSE141259) published by Strunz. M. *et al.* was used as the reference dataset (Strunz *et al.*, 2020).

2.9 10x Genomics library generation, sequencing and computational analysis

Sequencing libraries were generated using 10x Genomics Chromium Next GEM Single Cell 5' Reagent kit v2 (Dual Index) following manufacturer's instructions (CG000330 Rev D). ADT-labelled (BioLegend, Cat. No. 155861, 155863 and 199903) cells were loaded onto the Chromium iX (10x Genomics) at a concentration of ~1 x 10^6 cells/mL, with 50,000 cells loaded per channel. One channer was loaded per 2 mouse lung samples. Library generation was performed using Biomek FX^P Laboratory Automation Workstation (Beckman Coulter) at MRC Weatherall Institute of Molecular Medicine Single-Cell Facility (WIMM, University of Oxford). Library quality and concentration was assessed using a Bioanalyzer (Agilent) and

Qubit 2.0 Fluorometer (Thermo Fisher Scientific), respectively. An overview of the procedures for generating Single Cell 5' Gene Expression libraries, Single Cell TCR libraries, and Single Cell 5' Cell Surface Protein libraries is provided below.

2.9.1 GEM generation and barcoding

GEMs (Gel Bead-in-emulsions) were produced by combining Single Cell VDJ 5' Gel Beads, each containing a unique barcode, with a Master Mix that included cells labelled with cell surface proteins, and Partitioning Oil on the Chromium Next GEM Chip K. For single-cell resolution, cells were introduced at a limiting dilution to ensure that the majority of GEMs did not contain a cell, while the remainder predominantly contained only one cell. Once GEMs were formed, the Gel Beads were dissolved, and any co-partitioned cells were lysed. This process released Gel Bead primers that comprised an Illumina TruSeq Read 1 sequence, a 16 nt 10x Barcode, a 10 nt unique molecular identifier (UMI), and a 13 nt template switch oligo (TSO), which then mixed with the cell lysate and a Master Mix containing reverse transcription (RT) reagents and poly(dT) primers.

Subsequently, the cell lysate and released Gel Bead primers were incubated with the Master Mix, resulting in the production of 10x Barcoded, full-length cDNA from poly-adenylated mRNA. Concurrently, in the same partition, the Gel Bead primers also captured the cell surface protein Feature Barcode, which was conjugated to the antibody. This capture sequence included a Nextera Read 2 (Read 2N), a 15 nt Feature Barcode, and a Capture Sequence. Incubation of the GEMs with the Master Mix and RT reagents led to the synthesis of 10x Barcoded DNA from the cell surface protein Feature Barcode.

2.9.2 Post GEM-RT clean-up and cDNA amplification

After the GEM-RT reaction, GEMs were broken, and the mixtures were collected. The 10x Barcoded cDNA, synthesized from poly-adenylated mRNA, and the DNA corresponding to the cell surface protein Feature Barcode were then purified using silane magnetic beads. The barcoded cDNA and the Feature Barcode DNA underwent amplification to create sufficient material for multiple library constructions from the same set of cells, including TCR libraries, 5' Gene Expression libraries, and Cell Surface Protein libraries. Finally, the amplified cDNA and DNA were subjected to size selection.

2.9.3 V(D)J amplification from cDNA

Full-length cDNA, amplified from poly-adenylated mRNA and carrying 10x Barcodes, was enriched for full-length V(D)J segments. This enrichment was achieved via PCR amplification using primers specific to the constant regions of TCR.

2.9.4 V(D)J library construction

Enzymatic fragmentation and size selection were employed to produce variable length fragments that spanned the V(D)J segments of the TCR transcripts that had been amplified. Prior to the construction of the library, the P5, P7, i5, and i7 sample indexes, along with an Illumina R2 sequence (read 2 primer sequence), were appended. This was accomplished through a series of steps: End Repair, A-tailing, Adaptor Ligation, and Sample Index PCR. The resultant final libraries contained the P5 and P7 priming sites, which are integral for sequencing on Illumina platforms.

2.9.5 5’ Gene expression (GEX) library construction

The 5’ Gene Expression library was generated using amplified full-length cDNA derived from poly-adenylated mRNA. Enzymatic fragmentation and size selection were applied to refine the size of the cDNA amplicons in preparation for the construction of the 5’ gene expression library. The addition of P5, P7, i5, and i7 sample indexes, along with the Illumina R2 sequence (read 2 primer sequence), was accomplished through End Repair, A-tailing, Adaptor Ligation, and Sample Index PCR. The completed libraries incorporated the P5 and P7 priming sites.

2.9.6 Cell surface protein library construction

The Cell Surface Protein library was constructed using amplified DNA, which originated from Feature Barcodes of cell surface proteins labelled with antibodies. During library construction, P5, P7, i5, and i7 sample indexes, along with the Nextera Read 2 (Read 2N primer sequence), were incorporated via Sample Index PCR. The finalized libraries contained P5 and P7 priming sites.

2.9.7 Sequencing

Dual index Libraries were sequenced on an Illumina NovaSeq 6000 to a mean depth of 40,000 read pairs/cell for scRNA-seq, 10,000 read pairs/cell for Cite-seq or TCR-seq, performed at Novogene.

2.9.8 Computational analysis

10x Genomics cellranger analysis pipelines were used to generate single cell gene counts. Reads from gene expression and TCR library were aligned to the mouse mm10 reference genome (version 2020-A) and GRCm38 Mouse V(D)J Reference-7.0.0 (May 17, 2022),

respectively, and quantified using cellranger multi pipeline together with those from ADT library.

Hashtag oligo (HTO) data underwent a transformation using Seurat's centred log-ratio (CLR) transformation (Hao *et al.*, 2021). Demultiplexing of HTO hashtags was subsequently performed manually with CITEviz (Kong *et al.*, 2022), followed by normalisation of CITE-seq data via the dsb package (Mulè *et al.*, 2022). Ambient RNA was removed using decontX (Yang *et al.*, 2020). The RNA-seq data were then processed using Scanpy (Wolf *et al.*, 2018), which involved doublet removal with Scrublet (Wolock *et al.*, 2019) and cell filtering with specified thresholds for total counts (1,000 – 60,000), genes by counts (500 – 6,000), and mitochondrial counts (0 – 10%). The filtered data underwent normalization to achieve a total sum of 10,000 and were log-transformed with a pseudocount of 1. Highly variable genes were identified by setting the flavour to "cell_ranger". Normalised expression level for highly variable genes then underwent scaling by setting max_value to 10 and zero_center to False. Principal Component Analysis (PCA) was conducted, with the number of principal components set using the KneeLocator function. Cells from different mice were subsequently integrated using the Harmony algorithm (Korsunsky *et al.*, 2019). Neighbourhoods were identified with n_neighbors set to 5, followed by dimensionality reduction with Uniform Manifold Approximation and Projection (UMAP) (Becht *et al.*, 2019) and partitioning cell type with Leiden clustering at a resolution of 2.0 (Traag *et al.*, 2019). DEGs between cell types were identified using the rank_genes_groups function with a t-test. Cell clusters were identified using both RNA and protein expression data. T cells were further selected for reintegration and subset identification using the same method as previously stated, except that the clustering resolution was set to 1.0.

PCA on the overall transcriptome for each mouse was based on pseudobulk counts, computed by summing the counts of all cells in each mouse. Genes with low expression were filtered using filterByExpr in edgeR (version 3.36.0) (Robinson *et al.*, 2010) by setting min.count to 3, and using model matrix adjusted for time point and genotype. Normalisation factors were calculated using calcNormFactors in edgeR and the pseudocounts were then normalised using voom in limma (version 3.50.3) (Ritchie *et al.*, 2015).

MAIT cells and iNKT cells were identified using clonotypes.csv and filtered_contig_annotations.csv, based on the output generated by cellranger multi pipeline. A cell was designated as a MAIT cell if it was part of a clonotype that exhibits *Trav1* and *Traj33* expression. A cell was designated as an iNKT cell if it was part of a clonotype that exhibits *Trav11* and *Traj18* expression.

Differential gene expression between *Mr1*$^{-/-}$ and WT mice across various time points and cell types was analysed using DESeq2 (Love *et al.*, 2014) and pseudobulk counts, computed by summing the counts of all cells within each cell type for each mouse. Enriched gene sets were identified using the pre-ranked GSEA algorithm implemented in the FGSEA R package (Sergushichev, 2016). Genes were ranked with the log2 fold change for the relevant coefficient calculated by DESeq2. Enrichment was assessed with gene set list from MSigDB's Hallmark collection.

In the trajectory analysis of DC populations, Monocle 2 (Qiu *et al.*, 2017) (version 2.22.0) was utilized. The raw count data was processed to establish a CellDataSet object within Monocle 2 by setting the expressionFamily to a negative binomial distribution with a fixed variance. Cell ordering was achieved using genes identified by dpFeature. Dimension reduction for

visualization was carried out using DDRTree. Pre-cDCs were identified as the root_state during the cell ordering process. Trajectories were generated independently for cells from different groups. The expression profiles of selected genes in the two differentiation branches (cDC1 and cDC2) were visualized using the "plot_genes_branched_heatmap" function within the Monocle2 package (Qiu *et al.*, 2017).

2.10 Analysis of human IPF scRNA-seq datasets in HLCA and IPF cell atlas

Cells within the integrated Human Lung Cell Atlas (HLCA) and IPF cell atlas were assessed for *TRAV1-2* expression. Those exhibiting positive *TRAV1-2* expression levels were categorized as MAIT cells. The primary identification of MAIT cells was in GSE135893 (Habermann *et al.*, 2020), and only these MAIT cells were utilized in subsequent analyses. Differential gene expression between MAIT cells from IPF patients and those from healthy controls was determined using the FindMarkers function in Seurat (Hao *et al.*, 2021), with a pseudocount set to 1. For the overrepresentation test, modules in BTM (S. Li *et al.*, 2014) were employed, utilizing the enricher function in clusterProfiler (Wu *et al.*, 2021).

Both GSE135893 and GSE136831 (Adams *et al.*, 2020; Habermann *et al.*, 2020) were analysed in terms of immune cell composition changes, given that both datasets contained more than three samples from the IPF and healthy control groups, respectively. Marker genes for DC populations were derived from the original publication.

2.11 Culture and adoptive transfer of Flt3 ligand-generated bone marrow-derived dendritic cells

B6.SJL-Ptprc^{a} Pepc^{b}/BoyJ mice were used as donor mice and all donor mice were infected with 10^{6} CFU *Salmonella* Typhimurium BRD509 4 weeks before harvesting bone marrow cells. FLT3L- bone marrow-derived dendritic cells (BMDC) were generated by culture in RPMI complete containing murine fms-like tyrosine kinase-3 ligand (Flt3L) at 200 ng/mL and murine GM-CSF at 20 ng/mL as previously described (Sancho *et al.*, 2008). Dendritic cell NK lectin group receptor-1 (DNGR-1) was highly expressed in the MHCII^{+} CD11c^{+} CD24^{hi} subsets of Flt3L BMDCs, which correspond to the CD103^{+} subset of lung DCs. CD11c^{+} FLT3L-BMDCs were enriched using PE anti-mouse CD11c antibody (BioLegend, Cat. No. 117308) and anti-PE microbeads (Miltenyi Biotec, Cat. No. 130-048-801). 5×10^{5} FLT3L-BMDCs were given into each recipient *Mr1*$^{-/-}$ mouse intranasally (Srivastava *et al.*, 2016) at day 1 post-bleomycin challenge. When necessary, mice were treated i.p. with 100 µg of 7H11 anti-DNGR-1 blocking antibody or isotype-matched control (BioXCell, Cat. No. BE0305 and BE0088, respectively). Injections were administered daily from day -1 to day 10 post-bleomycin challenge.

2.12 MERSCOPE runs

MERSCOPE, a state-of-the-art spatial profiling technology housed within the WIMM Single Cell Facility of University of Oxford, enabled analysis of cellular complexity at a single-cell and even subcellular resolution in this mouse model. This platform leverages multiplexed error-robust fluorescence in situ hybridization (MERFISH) (Chen *et al.*, 2015) technology to detect even low-expressing genes at a spatial resolution down to 100 nanometres.

MERSCOPE runs were performed following MERSCOPE FFPE Tissue Sample Preparation User Guide (Vizgen, 91600112 Rev B). Workstations and tools were wiped with RNAse-removing solution and ethanol prior to each step.

2.12.1 Tissue sectioning

A 150-mm petri dish was filled with nuclease-free water and heated on a hot plate to achieve a temperature of 45 ± 2 °C. A pre-chilled cold plate was removed from a −20 °C freezer and placed on the bench. Subsequently, a 60-mm petri dish, filled with nuclease-free water, was placed on the cold plate. The formalin-fixed paraffin-embedded (FFPE) tissue block was then placed in the nuclease-free water within the petri dish on the cold plate for a duration of 10-20 min before sectioning commenced.

The microtome, forceps, dissecting needle, and other sectioning tools, along with the surrounding area, were cleaned with RNaseZap solution to create an RNase-free sectioning environment. The prepared FFPE tissue block was placed on the cleaned microtome. The top 50 µm of the block was sectioned and discarded to maximize RNA quality. The tissue block was then sectioned at a thickness of 5 µm. Using sectioning tools, the tissue sections were transferred into the 150-mm petri dish containing nuclease-free water at the temperature specified in the first step. A MERSCOPE FFPE Slide was positioned beneath the floating tissue section in the petri dish. A dissecting needle was used to guide the tissue section onto the middle of the slide. The slide was placed in an oven set to 55 °C and dried for 15 min, then left to dry at RT for an additional 1 to 2 h. Prior to storage, the absence of visible water droplets on the sample was confirmed. Finally, the sample was placed into a labelled 60-mm petri dish.

2.12.2 Deparaffinization and decrosslinking

Deparaffinization Buffer (500 µL) was added onto the centre of the tissue on the slide. The slide was then incubated at 55 °C for 5 min. This step was repeated twice at RT. The slide was washed with 5 mL of 100% ethanol, incubating for 2 min with intermittent lifting to wash underneath if necessary. This was repeated three times, and if oil droplets persisted, additional washes were performed. The slide was treated with a single wash with 90% ethanol for 2 min and another with 70% ethanol for 2 min. Deparaffinization was continued by aspirating the ethanol and adding 5 mL of Decrosslinking Buffer twice, with the petri dish placed on a heat pan set at 90 °C for 15 min.

2.12.3 Anchoring pre-treatment

The dish was removed and allowed to cool at RT for 5 min. It was then washed twice with 5 mL of Conditioning Buffer for 1 minute per wash. After the final aspiration, 5 mL of Conditioning Buffer was added and incubated at 37 °C for 30 min.

In preparation for anchoring, a buffer mix was created with 100 µL of Conditioning Buffer, 5 µL of Pre-Anchoring Buffer, and 5 µL of RNase Inhibitor. This mix (100 µL) was applied onto the sections and covered with parafilm. The petri dish was sealed with parafilm and incubated in a humidified chamber at 37 °C for 2 h.

2.12.4 Cell Boundary Staining

The Cell Boundary Stain Kit (PN 10400118) was employed. Parafilm was removed using tweezers, and the MERSCOPE FFPE Slide was incubated with 5 mL of PBS for exactly 2 minutes. The Blocking Solution, consisting of 100 µL Blocking Buffer Premix and 5 µL RNase

inhibitor, was prepared. After aspirating the PBS and leaving just enough to cover the tissue, 100 µL of Blocking Solution was applied to the tissue's centre. A 2×2 cm parafilm piece was then placed on the solution to eliminate air bubbles and spread the solution evenly. The slide was incubated at RT for 60 min.

Subsequently, the Primary Staining Solution was prepared by adding 1 µL of Cell Boundary Primary Stain Mix to the Blocking Solution components. After removing the parafilm and drying the slide slightly, 100 µL of the Primary Staining Solution was applied. The section was covered with a new piece of parafilm and incubated for another hour.

The parafilm was then removed, and the slide was washed three times with 5 mL of PBS, each for 5 min on a rocker. The Secondary Staining Solution was prepared like the Primary, replacing the Primary Stain Mix with the Secondary Stain Mix. After the last PBS wash, 100 µL of Secondary Staining Solution was applied, covered with parafilm, and incubated for 1 h. After incubation, the parafilm was removed, and the slide was washed three times with 5 mL of PBS, each for 5 min. The PBS was aspirated, and 5 mL of fixation buffer was applied for 15 min to fix the tissue. This was followed by two PBS washes, each for 5 min. The RNA Anchoring process was then initiated immediately.

2.12.5 RNA anchoring

For anchoring, PBS was removed, and 5 mL of Sample Prep Wash Buffer was added, followed by 5 mL of Formamide Wash Buffer, and incubated at 37 °C for 30 min. After ensuring the slide was dry, 100 µL of spun-down Anchoring Buffer was applied onto the tissue and covered with a 2 cm piece of parafilm. The petri dish was placed in a humidified container and incubated at 37 °C for 12-18 h.

2.12.6 Gel embedding

After an overnight incubation, the parafilm was removed using tweezers, and 5 mL of Formamide Wash Buffer was added to the sample. The sample was then incubated at 47 °C for 15 min within an incubator situated in a fume hood. Subsequently, a single wash was conducted using 5 mL of Sample Prep Wash Buffer, and the sample was incubated for an additional 2 min.

For RNA anchoring and gel embedding preparation, coverslips were prepared with Gel Slick solution, either leaving 100 µL on the samples for 10 min or pre-coating them. The coverslip was cleaned with a lens wipe before use. Gel Embedding Solution was prepared by mixing 5 mL of Gel Embedding Premix with 25 µL of 10% Ammonium Persulfate and 2.5 µL of TEMED.

The slide was dried with an aspirator, then 50 µL of Gel Embedding Solution was added onto the tissue. A Gel Slick-coated coverslip was placed on top of the slide, ensuring the absence of bubbles, and excess gel was aspirated from around the coverslip. A larger coverslip was used to cover all sections. The slide was incubated at RT for 1.5 h; if gel polymerization was incomplete after 1 h, incubation at 30 °C was carried out for a maximum of 2 h.

2.12.7 Clearing

The Clearing Premix was warmed at 37 °C for 30 min prior to use, ensuring it formed a clear solution. The Clearing Solution was then prepared by combining 5 mL of Clearing Premix with 50 µL of Proteinase K. Following this, 5 mL of the Clearing Solution was added to the sample. The lid of the petri dish was placed, and its exterior was sprayed with 70% ethanol for

sterilization. The petri dish was then sealed with parafilm and placed in a humidified cell culture incubator at 47 °C for a period of 24 h.

2.12.8 Probe hybridization

The Clearing Solution was aspirated, and the sample was washed three times with 5 mL of Sample Prep Wash Buffer. Each wash was followed by a 5-min incubation at RT on a rocker. Subsequently, 5 mL of Formamide Wash Buffer was added, and the sample was incubated at 37 °C for 30 min in an incubator within a fume hood. The Formamide Wash Buffer was first aspirated. The gel remained not completely dry for longer than 1 min.

Next, 100 µL of MERSCOPE Gene Panel Mix was applied to the centre of the gel. A 2×2 cm piece of parafilm was cut, gently placed onto the gel, avoiding the introduction of air bubbles. The petri dish was then closed, its exterior was sprayed with 70% ethanol for sterilization, and the dish was sealed with parafilm. The prepared sample was placed in a humidified cell culture incubator set at 37 °C for a minimum of 36 h and up to a maximum of 48 h.

2.12.9 Imaging

Post-encoding probe hybridization wash involved removing the parafilm and adding 5 mL of Formamide Wash Buffer, incubating at 47 °C for 30 min twice. Before imaging, DAPI and PolyT Staining Reagent were warmed at 37 °C for 10 min and gently vortexed, while the Imaging Buffer Activator and Imaging Buffer were thawed on ice and spun down.

Clearing solution was aspirated from the slide, followed by a wash with 5 mL of Sample Prep Wash Buffer. The slide was lifted with tweezers to wash underneath and incubated on a rocker at RT for 5 min. The wash was repeated without lifting the slide. Subsequently, 3 mL of the

DAPI and PolyT Staining Reagent were added, and the sample was incubated for 15 min on a rocker. The MERSCOPE chamber was cleaned with RNAse-removing solution and 80% ethanol, and the fluidic chamber was cleaned using lens paper with no particles present.

Following incubation, the staining reagent was removed, and 5 mL of Formamide Wash Buffer was added, incubating for 10 min on a rocker at RT. The buffer was aspirated, and 5 mL of Sample Prep Wash Buffer was added. Chamber assembly for the MERSCOPE was initiated on Kimtech wipes and lens tissue, ensuring no particles on the glass. Imaging Buffer Activator (25 μL) was added to the Imaging Buffer, pushed through the chamber with a syringe until no air bubbles were present. The bottom of the MERSCOPE chamber was cleaned with lens tissue before proceeding with MERSCOPE instructions.

2.12.10 MERSCOPE spatial transcriptomic data analysis

Raw data from MERSCOPE were decoded using MERSCOPE instrument and analysis computer, employing the default cell segmentation based on DAPI and cell boundary staining, as performed by Cellpose (Stringer *et al.*, 2021). This segmentation targeted the fourth z-plane of the eight available, with the determined cell borders extended to adjacent planes. This initial segmentation provided the foundational data for further segmentation with the transcript-based cell segmentation algorithm, Baysor (Petukhov *et al.*, 2022), executed within the Sopa framework (Blampey *et al.*, 2023). The Sopa algorithm first generated overlapping patches of transcripts and then ran Baysor on each of these small patches. patch-width-microns was set to 2000 and patch-overlap-microns was set to 0 when patches were generated. min_molecules_per_cell was set to 50, n_clusters was set to 8, prior_segmentation_confidence was set to 0.5 and force_2d was set to true while using Baysor. Cell segmentation from different

patches were then aggregated by setting min-transcripts to 100. The resulting cell-by-gene table was filtered to keep cells with total number of transcripts no less than 100.

The cell-by-gene table from different samples were concatenated and input into SCANPY (Wolf *et al.*, 2018) and Squidpy (Palla *et al.*, 2022) for further analysis. Briefly, the filtered data underwent normalisation to and were log-transformed with a pseudocount of 1. The normalised count matrix was then scaled and PCA was conducted, with the number of principal components set to 50 and max_value set to 10. Cells from different mice were subsequently integrated using the Harmony algorithm (Korsunsky *et al.*, 2019). Neighbourhoods were identified with n_neighbors set to 10 and n_pcs set to 20, followed by dimensionality reduction with UMAP (Becht *et al.*, 2019) and partitioning cell type with Leiden clustering at a resolution of 1.5 (Traag *et al.*, 2019). DEGs between cell types were identified using the rank_genes_groups function with a t-test. Cell clusters were then identified.

2.13 Isolation of human TCR Vα 7.2$^+$ lymphocytes from peripheral blood and coculture with human fibroblast cell line

Human PBMCs were isolated from whole blood by the density gradient centrifugation method. PBMCs were stained with TCR Vα 7.2-PE antibodies and conjugated with Miltenyi anti-PE beads, loaded onto the LS Columns on MACS Separator, and positively selected cells were collected. Human fibroblast cell line MRC-5 cells were cultured and seeded on 96-well flat-bottom cell plate until 80-90% confluency. Magnetically enriched TCR Vα 7.2$^+$ lymphocytes were added, and different stimulation conditions were applied to each well. Cells were cocultured for 24 h then stained with human MAIT cell surface antibodies. Cells were

fixed/permeabilized then stained with intracellular activation markers of MAIT cells. Cells were run on FACSAria II.

It is important to note a limitation in the method used: The TCR Vα7.2-antibody targets the Vα7.2 TCR α-chain segment, which, when paired with the Jα33 segment, forms an invariant TCR characteristic of MAIT cells. However, it is important to note that the Vα7.2 segment can also be expressed by conventional T cells (Park *et al.*, 2019). Consequently, the TCR Vα7.2-antibody, which is used to detect this segment, additionally stains a subset of conventional CD4 and CD8 T cells. To achieve unequivocal identification of MAIT cells, staining with the TCR Vα7.2-antibody should be combined with anti-CD161 or -IL18Ra staining.

2.14 Data analysis and statistics

Flow cytometry data were acquired on a BD LSRII Flow Cytometer (BD Biosciences) or Cytek Aurora (Cytek Biosciences) and processed in FlowJo version 10.8.1 (FlowJo, LLC) or SpectroFlo version 3.0.3 (Cytek Biosciences). All data was analysed in Prism version 9.2.0 (GraphPad) and RStudio version 1.4.1717. For *in vivo* mouse data analysis, various tests were deployed as required, including unpaired t tests, Mann-Whitney tests, one-way analysis of variance (ANOVA) with Dunnett's or Sidak's multiple comparisons, Kruskal-Wallis with Dunn's multiple comparisons, and two-way ANOVA with Sidak's multiple comparisons, Holm-Sidak's multiple comparisons or Fisher's LSD test. A *P* value less than 0.05 was considered significant.

3 MAIT Cell Dynamics in Response to Bleomycin-Induced Sterile Lung Injury

3.1 Introduction

As mentioned, in the context of inflammatory stimuli, MAIT cell activation is known to be triggered in at least two distinct ways: either through an MR1-TCR-dependent pathway, typically associated with antibacterial host defence, or via an MR1-TCR-independent route mediated by interleukins (IL-12/-15/-18) and type I interferon, which is often linked to antiviral responses (Hinks & Zhang, 2020). Bleomycin, a chemotherapeutic agent that induces lung inflammation and fibrosis, is utilised as a model to emulate conditions of non-infectious lung injury. This allows for a detailed exploration of the MAIT cell response during the initial phase of injury, subsequent tissue repair, and fibrogenesis. In this chapter, I investigated MAIT cells' response to bleomycin-induced acute lung injury. I quantified alterations in the lung MAIT cell populations in contrast to non-MAIT αβ T cells and examined the role of the cytokine environment in influencing MAIT cell dynamics.

I also investigated the induction of a tissue repair programme in MAIT cells following bleomycin-induced lung injury, an exploration inspired by prior findings in skin-homing Tc17 cells. These cells, linked to the presence of commensal flora, demonstrated a 'tissue repair' gene signature (Table 3-1), facilitating expedited repair of epithelial wounds. Remarkably, they exhibit similarities to non-classical T cells, sharing the type 17 cytokine profile and a restriction by H2-M3, an alternative MHC class I antigen presentation molecule. Our prior research employed GSEA to ascertain whether MAIT cells exhibit a similar, consistent transcriptional response indicative of tissue repair (Hinks *et al.*, 2019). We noted a significant enrichment of tissue repair-related genes in human MAIT cells post-stimulation with 5-OP-RU, a response

notably absent in CD3+ T cells following CD3/CD28 co-stimulation. Despite variations in species, analysis duration, and activation protocols, this gene set was even more prominently enriched in the MAIT cells of mice during acute *L. longbeachae* infection (Hinks *et al.*, 2019). Therefore, I asked whether this tissue repair phenotype was a shared transcriptional programme in MAIT cells during sterile injury.

Table 3-1 Tissue repair gene signature

Genes			
Flg	*Mmp13*	*Angpt4*	*Dll4*
Flg2	*Mmp15*	*Hgf*	*Jag1*
Furin	*Mmp25*	*Cyr61*	*Jag2*
Areg	*Mmp28*	*Inhba*	*Wnt1*
Bmp2	*Defb1*	*Inhbb*	*Wnt2*
Bmp4	*Defb6*	*Btc*	*Wnt2b*
Bmp7	*Epgn*	*Ereg*	*Wnt3*
Ngf	*Hbegf*	*Nrg1*	*Wnt3a*
Tgfa	*Egf*	*Nrg2*	*Wnt4*
Tgfb1	*Mmp1a*	*Nrg3*	*Wnt5a*
Tgfb2	*Mmp2*	*Nrg4*	*Wnt5b*
Tgfb3	*Tnf*	*Lep*	*Wnt6*
Pdgfa	*Il1a*	*Vegfb*	*Wnt7a*
Pdgfb	*Il1b*	*Vegfc*	*Wnt7b*
Csf2	*Csf1*	*Figf*	*Wnt8a*
Fgf1	*Ccl2*	*Pdgfc*	*Wnt8b*
Fgf2	*Ccl3*	*Hmgb1*	*Wnt9a*
Fgf7	*Cxcl1*	*Ptges2*	*Wnt9b*
Fgf10	*Cxcl2*	*Cxcl12*	*Wnt10a*
Fgf22	*Cxcl10*	*Shh*	*Wnt10b*
Igf1	*Cxcl15*	*Dhh*	*Wnt11*
Igf2	*Il6*	*Ihh*	*Wnt16*
Vegfa	*Pgf*	*Disp1*	*Chat*
Ctgf	*Angpt1*	*Dll1*	*Thbs1*
Mmp3	*Angpt2*	*Dll3*	*Hif1a*
Mmp10			

From Linehan JL, Cell. 2018 Feb 8;172(4):784-796.e18.

3.2 Aims

To investigate whether bleomycin-induced sterile lung injury could stimulate pulmonary MAIT cells *in vivo*, and transcriptomic profile of MAIT cells during this process.

3.3 Results

3.3.1 Activated MAIT cells accumulate in the lung upon bleomycin treatment in a cytokine-dependent manner

My initial objective was to establish whether sterile lung injury could stimulate pulmonary MAIT cells *in vivo*. I administered bleomycin intratracheally to C57BL/6 (wild type, WT) mice, to precipitate acute, sterile lung inflammation, followed by a tissue repair phase and subsequent fibrosis over a fortnight (Tashiro *et al.*, 2017). I detected an early surge of pulmonary MAIT cells (characterised as CD45.2^{+} TCRβ^{+} CD19^{-} MR1-5-OP-RU tetramer^{+} cells, Figure 3.1), peaking approximately three days post-challenge. By comparison, the peak number of non-MAIT αβ T cells occurred later at day 7 post-challenge (Figure 3.2 and Figure 3.3). On both day 3 and 5 post-challenge, the fold change in MAIT cell frequency was significantly higher than that in non-MAIT αβ T cells frequency (Figure 3.2). Moreover, pulmonary MAIT cell CD69 expression increased significantly at days 3 and 5 post challenge relative to unchallenged controls, and CD69 expression was significantly higher in MAIT cells than that in non-MAIT αβ T cells (Figure 3.4).

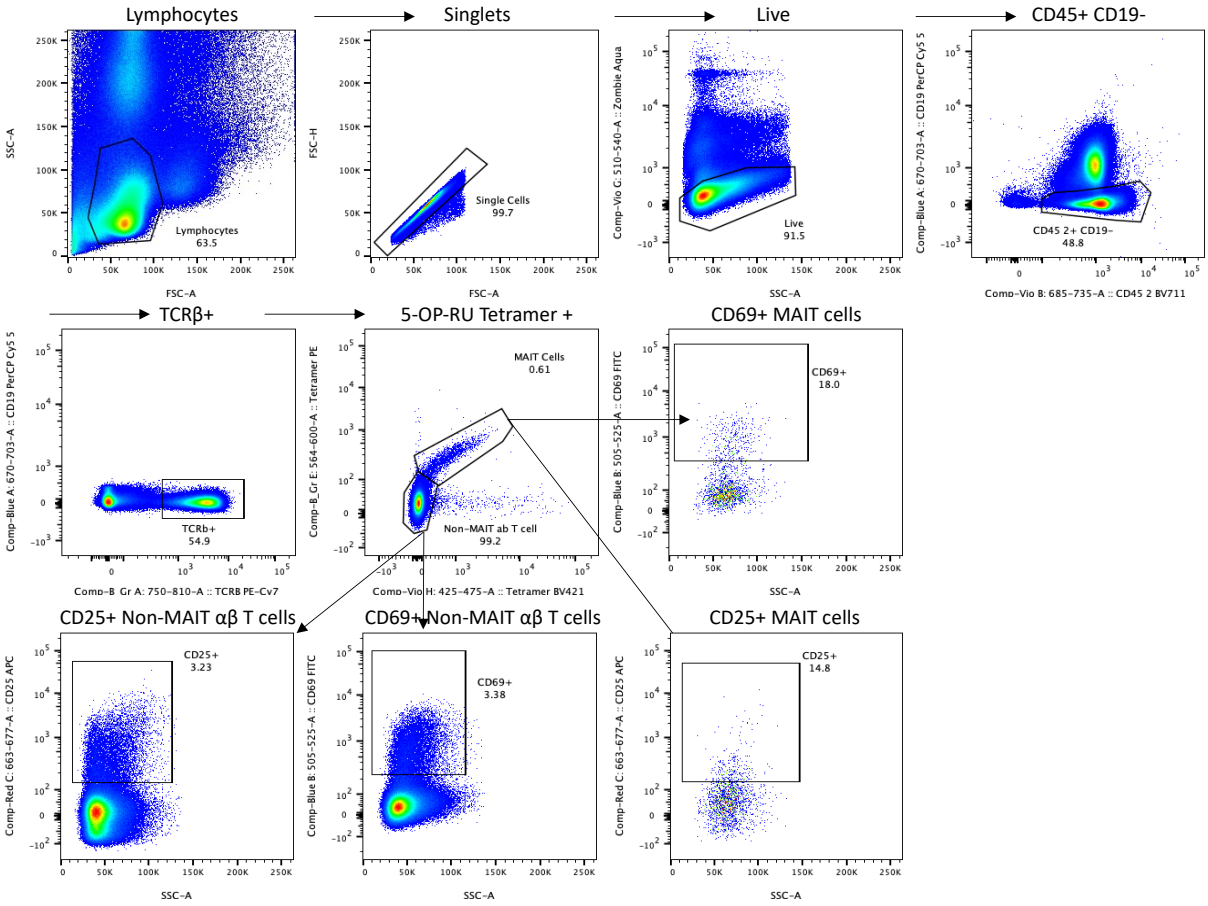

Figure 3.1 Gating scheme for the identification of MAIT cells.

Gating scheme for the identification of MAIT cells (TCRβ+ CD45.2+ CD19− MR1-5-OP-RU tetramer+ cells), and expression of CD25 and CD69 on MAIT and non-MAIT αβ T cells in naïve mice lung.

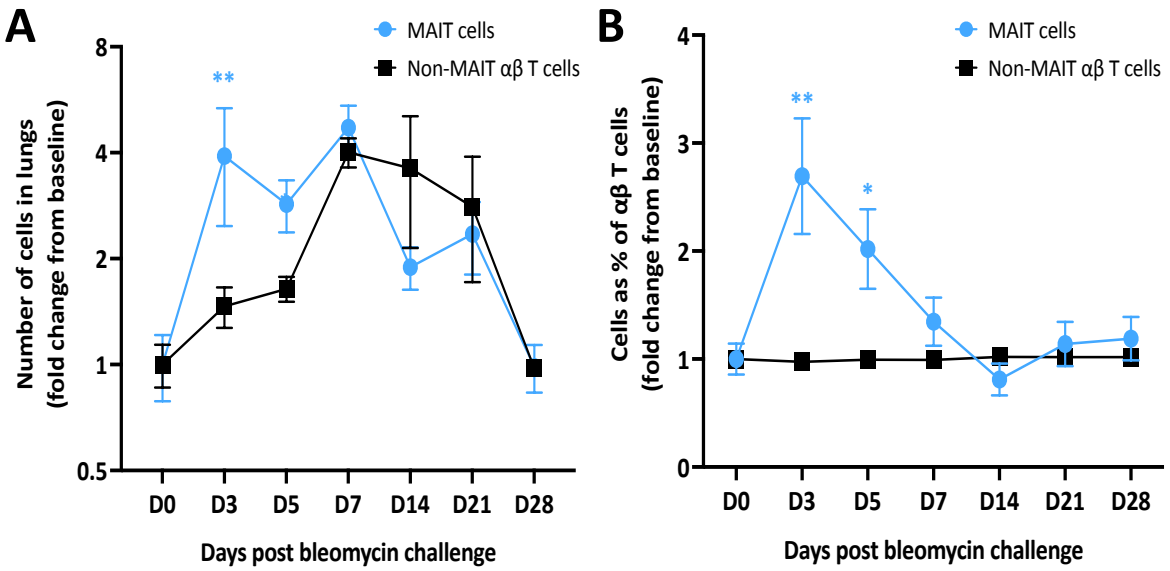

Figure 3.2 *In vivo* bleomycin challenge induces accumulation of pulmonary MAIT cells in naïve mice.

(**A**) Fold change in the absolute MAIT cell and non-MAIT αβ T cell number in the lungs of naïve mice post-bleomycin challenge, relative to unchallenged PBS controls (Day 0). Comparisons between MAIT cell subsets and non-MAIT αβ T cell subsets at individual time-points, were conducted using unpaired t tests or Mann-Whitney tests, $*P < 0.05$, $**P < 0.01$, $***P < 0.001$, $****P < 0.0001$. (**B**) Fold change in MAIT cell and non-MAIT αβ T cell frequency as the percentage of total pulmonary αβ T cells in the lungs of naïve mice relative to unchallenged controls. Comparisons between MAIT cell subsets and non-MAIT αβ T cell subsets at individual time-points, were conducted using unpaired t tests or Mann-Whitney tests, $*P < 0.05$, $**P < 0.01$, $***P < 0.001$, $****P < 0.0001$. The data are presented as the mean ± SEM of a single experiment, with 3-5 mice in each group.

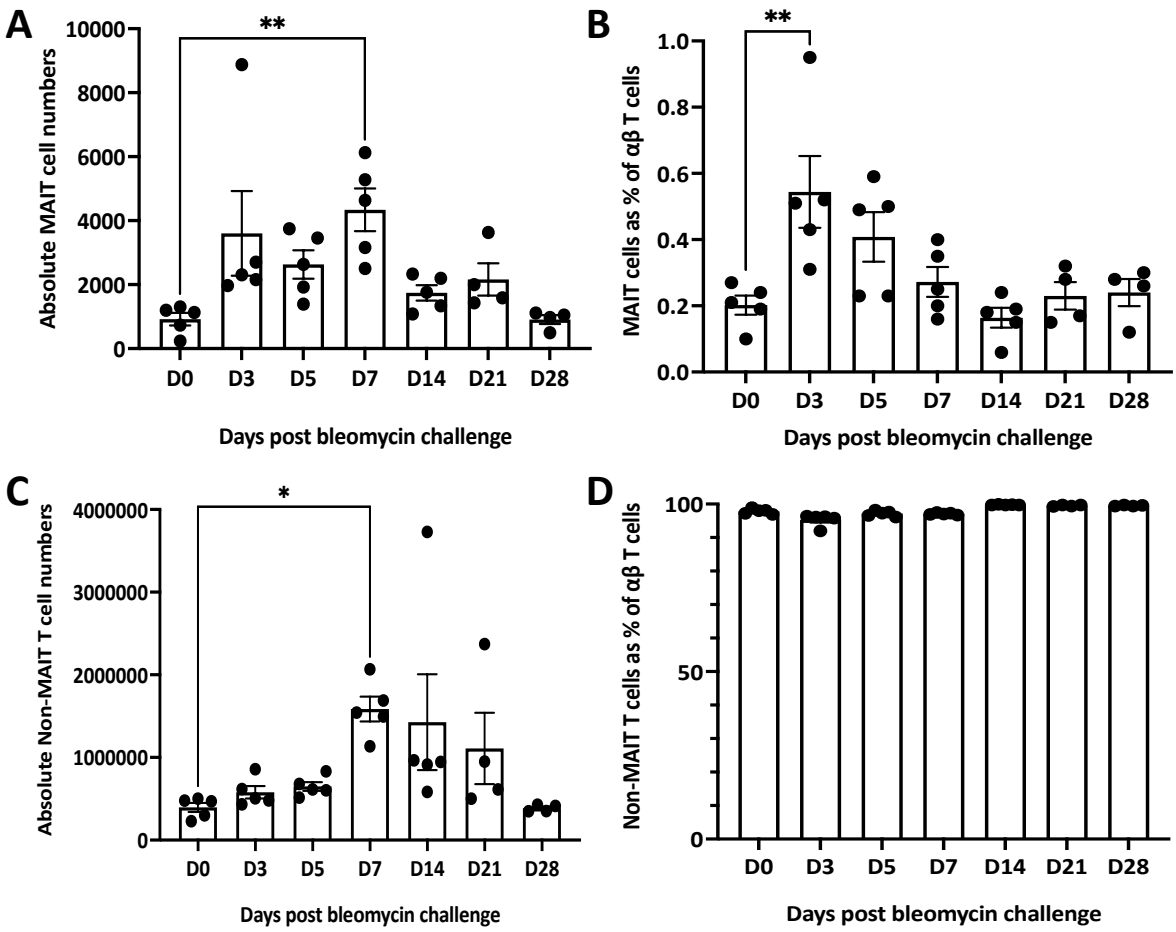

Figure 3.3 Raw absolute cell number data for Figure 3.2A and B.

Statistical comparisons across different timepoints post-bleomycin challenge and unchallenged PBS control were made using one-way ANOVA with Dunnett's or Dunn's multiple comparison tests, $*P < 0.05$, $**P < 0.01$, $***P < 0.001$, $****P < 0.0001$. The data are presented as the mean ± SEM of a single experiment, with 3-5 mice in each group.

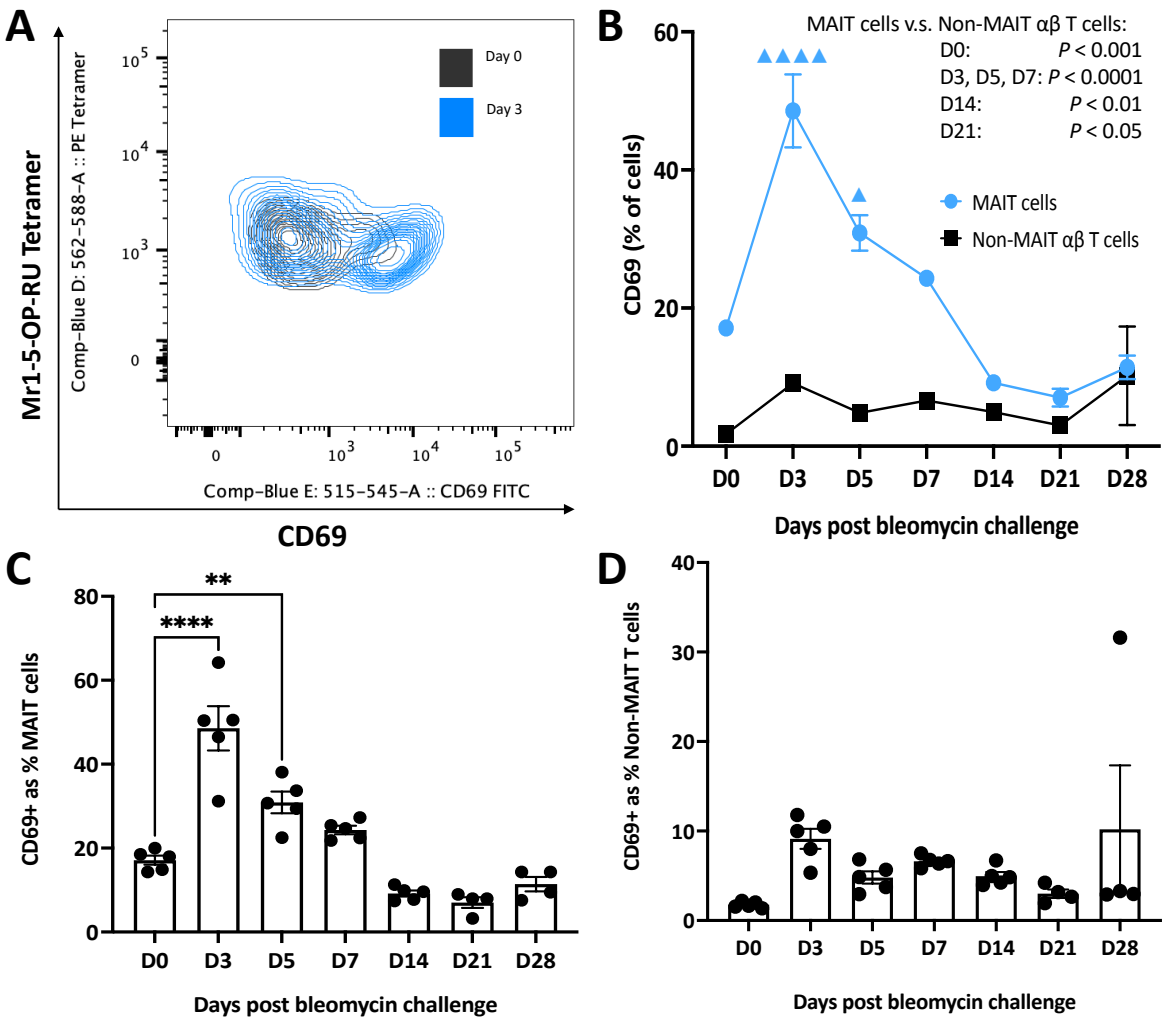

Figure 3.4 *In vivo* bleomycin challenge induces activation of pulmonary MAIT cells in naïve mice.

(**A**) Representative flow cytometry plot showing CD69 expression on MAIT cells. (**B**) Proportion of pulmonary MAIT cells and non-MAIT αβ T cells expressing CD69 in naïve mice. Annotated symbols in Figure 3.4B indicate statistical comparisons across different timepoints post-bleomycin challenge and unchallenged PBS controls, conducted using one-way ANOVA with Dunnett's or Dunn's multiple comparison tests, $^{▲}P < 0.05$, $^{▲▲}P < 0.01$, $^{▲▲▲}P < 0.001$, $^{▲▲▲▲}P < 0.0001$. The *P* value in Figure 3.4B shows the comparisons between MAIT cell

subsets and non-MAIT αβ T cell subsets at individual time-points, conducted using unpaired t tests or Mann-Whitney tests. (**C** and **D**) Raw absolute number data for Figure 3.4B. The data are presented as the mean ± SEM of a single experiment, with 3-5 mice in each group.

In nature, early life microbial exposures are essential for the development of MAIT cell populations. When mice have been raised in a specific pathogen free environment, MAIT cells constitute less than 1% of total pulmonary αβ T cells (Wang, 2018) but can be up to 10% in healthy humans (Hinks *et al.*, 2016; Hinks *et al.*, 2015). Therefore, I employed an established MAIT cell-enriched model by infecting WT C57BL/6 mice intranasally with 10^6 CFU *Salmonella enterica* serovar Typhimurium BRD509 four weeks prior to initial bleomycin challenge for clearer population delineation (Figure 3.5 and Figure 3.6) (Chen *et al.*, 2017; Riffelmacher *et al.*, 2023). This bacterial inoculum is rapidly cleared from the lungs but transiently provides the required combination of MAIT cell ligands and pathogen-associated molecular patterns necessary to produce rapid and lasting expansion of the MAIT cell population (Hinks *et al.*, 2020). While it was previously reported that post-*Salmonella* Typhimurium BRD509 infection MAIT cells adopt an effector memory phenotype, with relatively high baseline CD69 expression (Figure 3.6D) (Chen *et al.*, 2017), I still observed rapid MAIT cell accumulation, peaking on day 3 post-challenge (Figure 3.7), along with activation upon bleomycin stimulation, evidenced by significantly increased CD69 expression on day 3 and 7, compared to unchallenged PBS controls (Figure 3.8). Conversely, no significant changes were observed in either the accumulation or activation of non-MAIT αβ T cells post-bleomycin challenge (Figure 3.8). Collectively, these results indicate MAIT cells

accumulate and are activated early in the lungs following bleomycin-induced sterile injury of mice.

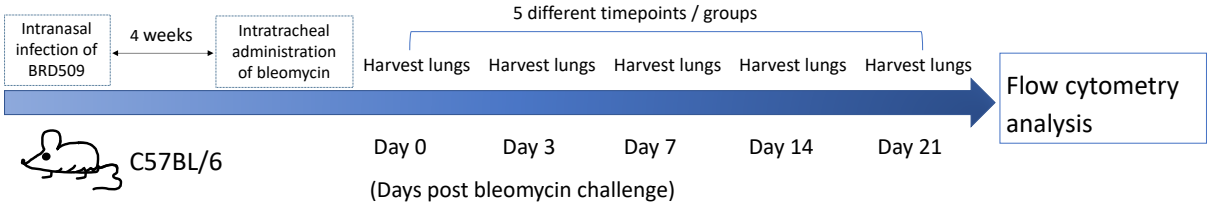

Figure 3.5 Schematic of protocol of murine study.

Both WT and *Mr1*$^{-/-}$ mice were infected with 10^6 CFU *Salmonella* Typhimurium BRD509 to augment the MAIT cell population, followed by intratracheal bleomycin administration. Mouse lung samples were collected at days 0, 3, 7, 14 and 21 after the challenge.

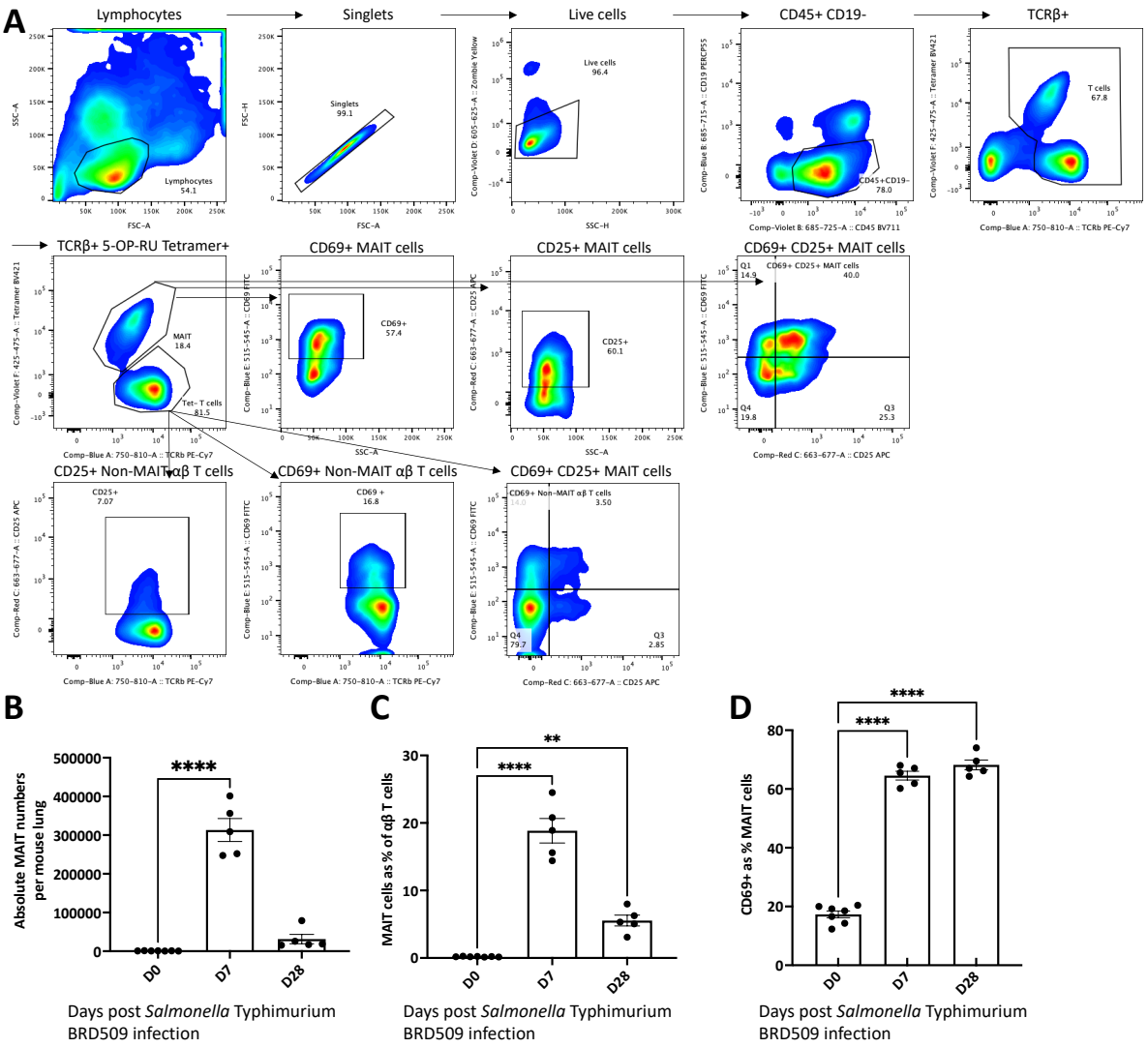

Figure 3.6 Temporal dynamics of MAIT cells in pulmonary immune response to *Salmonella* Typhimurium infection.

(**A**) Gating scheme for the identification of MAIT cells (TCRβ$^+$ CD45.2$^+$ CD19$^-$ MR1-5-OP-RU tetramer$^+$ cells), and expression of CD25 and CD69 on MAIT and non-MAIT αβ T cells in *Salmonella* Typhimurium BRD509 infected mice lung. (**B** and **C**) Bar plots showing the absolute MAIT cell numbers (**B**) and percentage of MAIT cells of total pulmonary αβ T cells (**C**) post BRD509 infection. (**D**) Proportion of pulmonary MAIT cells expressing CD69,

expressed as a percentage of pulmonary MAIT cells post BRD509 infection. Data (mean ± SEM) are one representative experiment of two independent experiments, with 5–7 mice per group in each replicate. Statistical significance tested by one-way ANOVA with Dunnett's multiple comparison tests. ** $P < 0.01$; **** $P < 0.0001$.

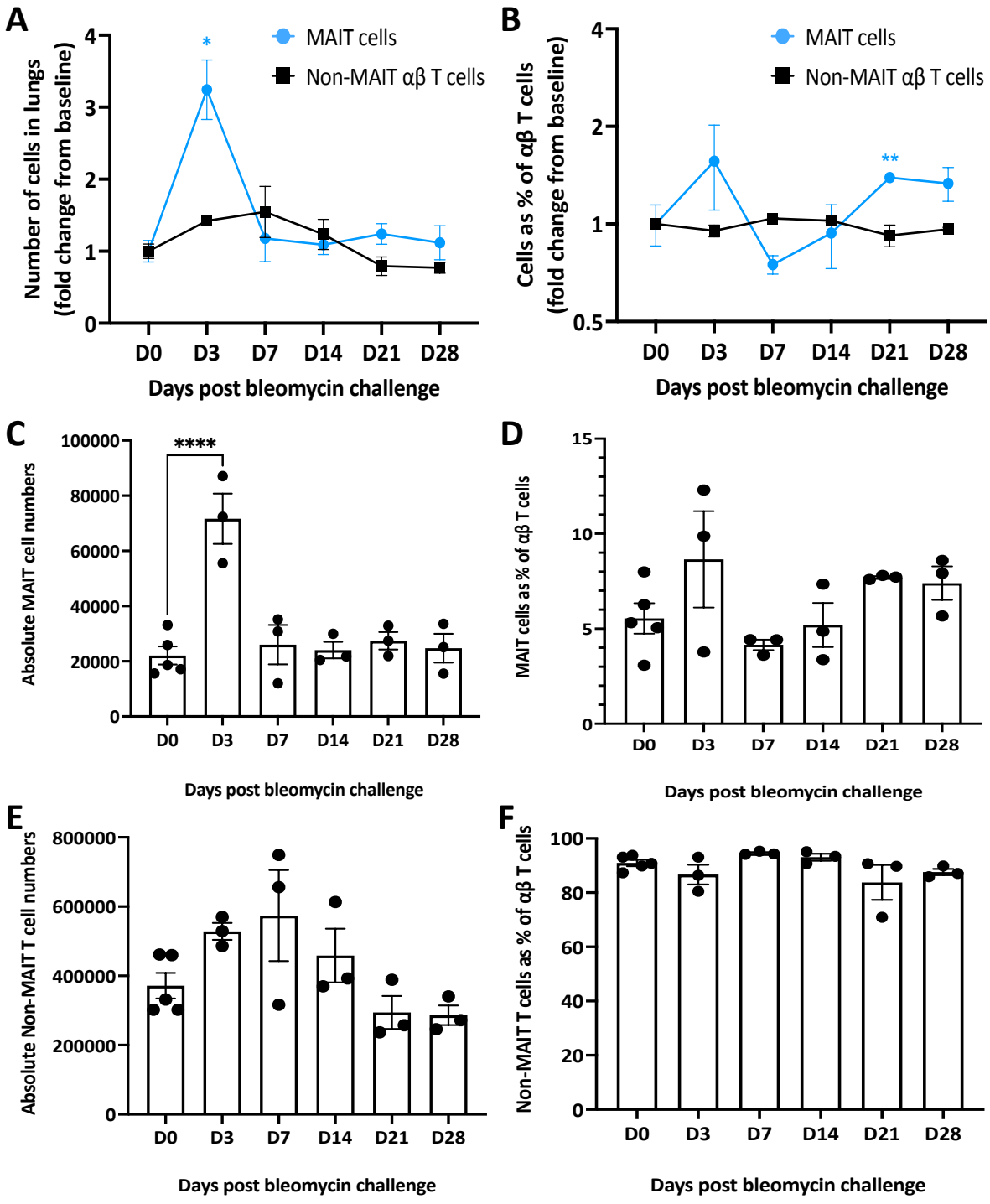

Figure 3.7 *In vivo* bleomycin challenge induces accumulation of pulmonary MAIT cells in *Salmonella* Typhimurium BRD509 infected mice.

(**A**) Fold change in the absolute MAIT cell and non-MAIT αβ T cell number in the lungs of **MAIT cell-boosted mice** (infected with *Salmonella* Typhimurium BRD509 four weeks prior to bleomycin challenge) post-bleomycin challenge, relative to unchallenged D0 controls (PBS). Comparisons between MAIT cell subsets and non-MAIT αβ T cell subsets at individual time-points, were conducted using unpaired t tests or Mann-Whitney tests, *$P < 0.05$, **$P < 0.01$, ***$P < 0.001$, ****$P < 0.0001$. (**B**) Fold change in MAIT cell and non-MAIT αβ T cell frequency as the percentage of total pulmonary αβ T cells in the lungs of **MAIT cell-boosted mice** post-bleomycin challenge, relative to unchallenged controls. Comparisons between MAIT cell subsets and non-MAIT αβ T cell subsets at individual time-points, were conducted using unpaired t tests or Mann-Whitney tests, *$P < 0.05$, **$P < 0.01$, ***$P < 0.001$, ****$P < 0.0001$. (**C** to **F**) Raw absolute number data for **Fig. 3.7A and B**. Statistical comparisons across different timepoints post-bleomycin challenge and unchallenged PBS control were made using one-way ANOVA with Dunnett's or Dunn's multiple comparison tests, *$P < 0.05$, **$P < 0.01$, ***$P < 0.001$, ****$P < 0.0001$. The data are presented as the mean ± SEM of a single experiment, with 3-5 mice in each group.

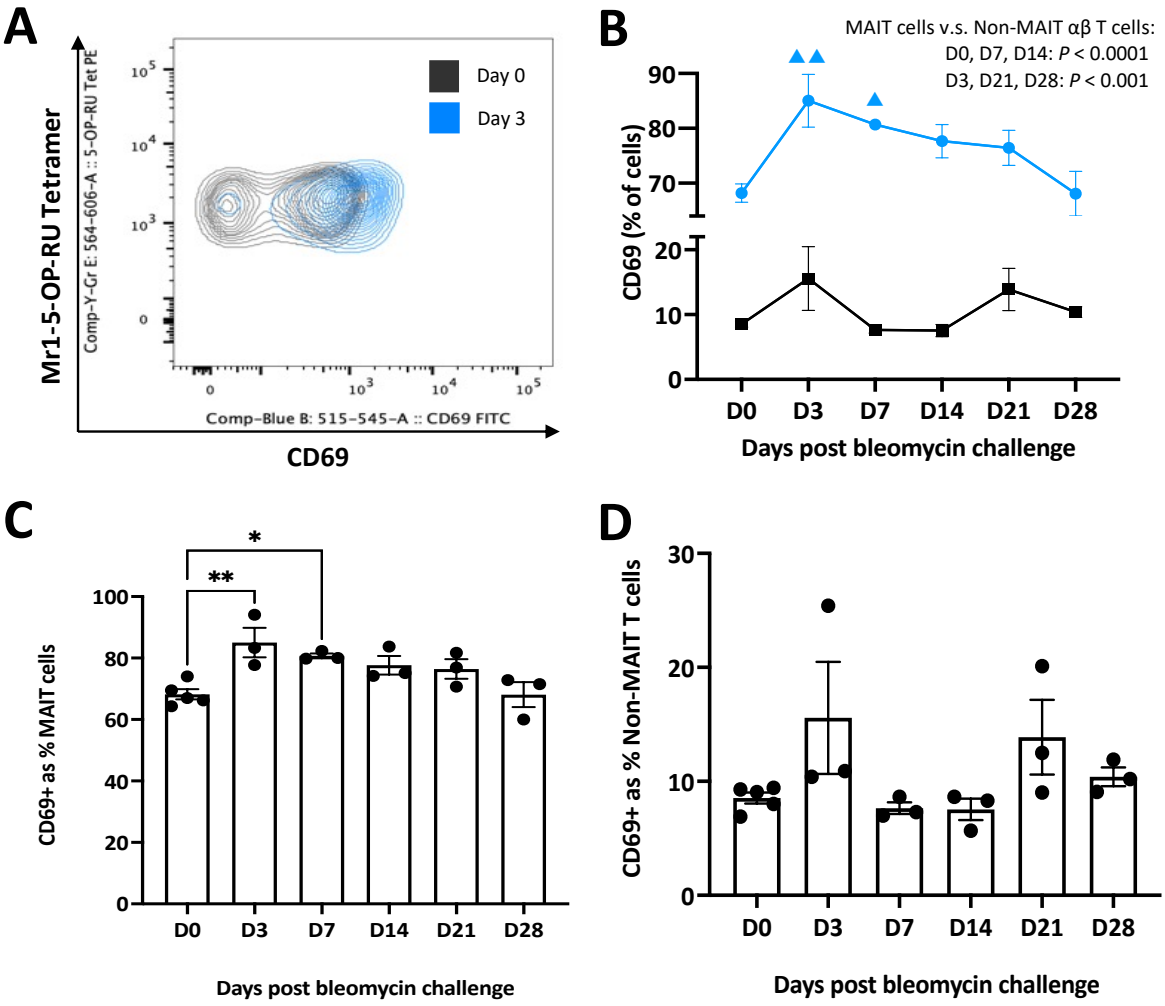

Figure 3.8 *In vivo* bleomycin challenge induces activation of pulmonary MAIT cells in *Salmonella* Typhimurium BRD509 infected mice.

(**A**) Representative flow cytometry plot showing CD69 expression on MAIT cells. (**B**) Proportion of pulmonary MAIT cells and non-MAIT αβ T cells expressing CD69. Annotated symbols in Figure 3.8B indicate statistical comparisons across different timepoints post-bleomycin challenge and unchallenged PBS controls, conducted using one-way ANOVA with Dunnett's or Dunn's multiple comparison tests, ▲$P < 0.05$, ▲▲$P < 0.01$, ▲▲▲$P < 0.001$, ▲▲▲▲$P < 0.0001$. The P value in Figure 3.8B shows comparisons between MAIT cell subsets

and non-MAIT αβ T cell subsets at individual time-points, conducted using unpaired t tests or Mann-Whitney tests. The data are presented as the mean ± SEM of a single experiment, with 3-5 mice in each group. (**C** and **D**) Raw absolute number data for **Fig. 3.8B.** The data are presented as the mean ± SEM of a single experiment, with 3-5 mice in each group.

As MAIT cells can be activated in a TCR-independent manner by cytokines, including interleukin (IL)-12, -15, -18, and type I interferon (IFN), in antiviral responses (Hinks & Zhang, 2020), I examined MAIT cell responses post bleomycin challenge utilising mouse strains deficient in the two most important of these pathways, IL-18R or IFN-αR without a preliminary MAIT boost. Relative to WT C57BL/6 mice, I observed a marked impairment in pulmonary MAIT cell accumulation on day 3 post-bleomycin in both IL-18R and IFNαR-deficient mice (Figure 3.9). Conversely MAIT cell activation was significantly impeded solely in the absence of IFNαR (Figure 3.9). These findings suggest bleomycin-induced MAIT cell activation is predominantly cytokine driven, with IFN-αR playing a key role.

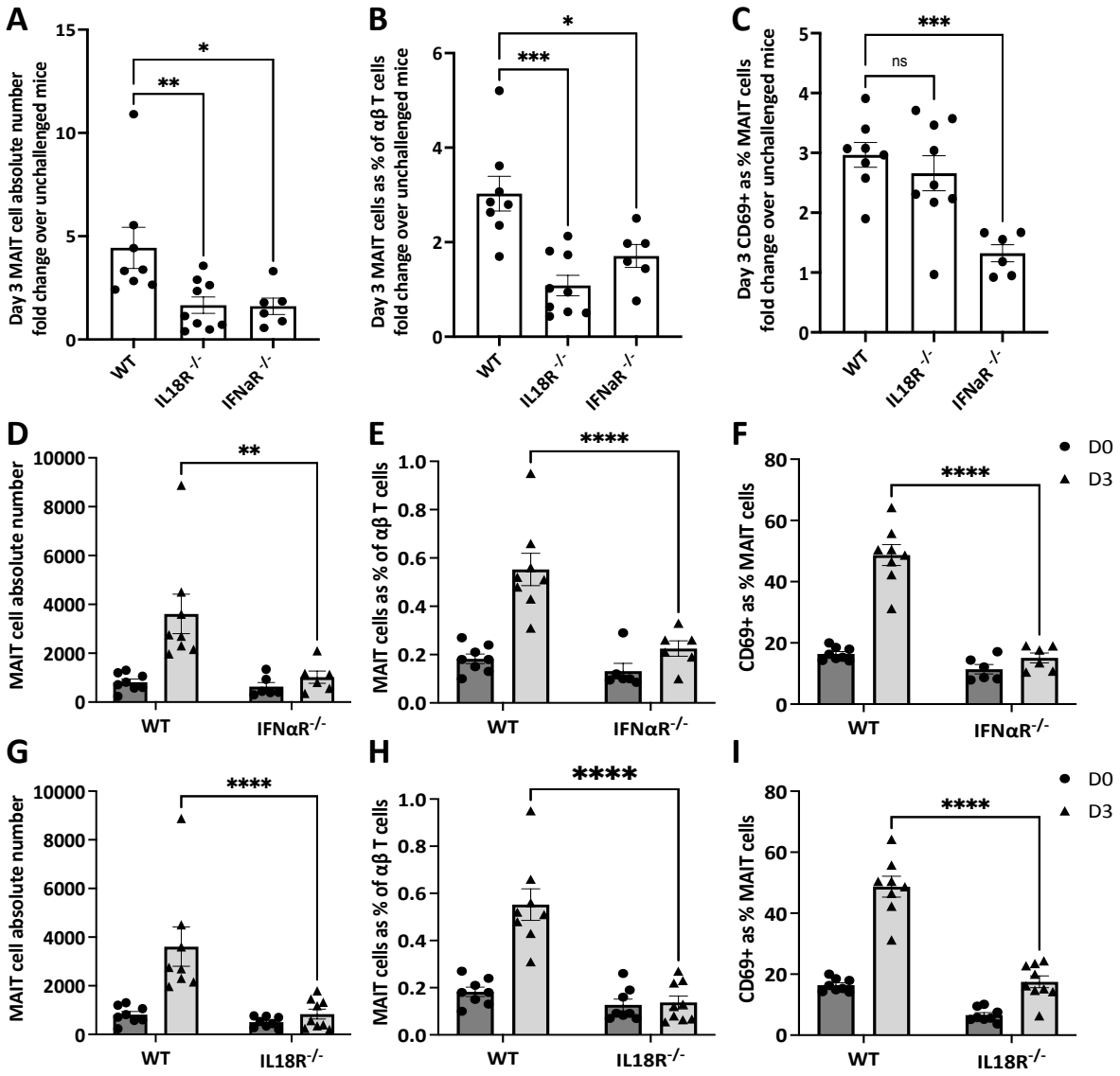

Figure 3.9 Cytokine-modulated accumulation and activation of pulmonary MAIT cells upon bleomycin stimulation

(**A**) Fold change in the number of pulmonary MAIT cells in naïve WT or cytokine receptor knock out mice on day 3 post-bleomycin challenge, relative to unchallenged controls. (**B**) Fold change in the frequency of MAIT cells as a percentage of total pulmonary αβ T cells in naïve WT or cytokine receptor knock out mice on day 3 post challenge, relative to unchallenged controls. (**C**) Fold change in the proportion of pulmonary MAIT cells expressing CD69 in naïve

WT or cytokine receptor knock out mice on day 3 post challenge, relative to unchallenged controls. Differences in significance between WT mice and cytokine receptor deficient mice were assessed using one-way ANOVA with Dunnett's multiple comparison tests. Data are mean ± SEM, pooled from three independent experiments, with 2–5 mice per group in each replicate; *$P < 0.05$, **$P < 0.01$, ***$P < 0.001$, ****$P < 0.0001$. (**D** to **I**) Raw absolute number data for **Fig. 3.9, A to C**. Statistical significance tested by two-way ANOVA with Holm-Sidak's multiple comparisons test; *$P < 0.05$, **$P < 0.01$, ***$P < 0.001$, ****$P < 0.0001$.

3.3.2 Bleomycin challenge activates the tissue repair programme of MAIT cells

A transcriptional programme related to tissue repair, initially identified in Tc17 cells (Linehan *et al.*, 2018), has been observed in both human MAIT cells following 5-OP-RU stimulation and mice lung MAIT cells during acute *L. longbeachae* infection (Hinks *et al.*, 2019). Consequently, I assessed whether bleomycin could activate the MAIT cell tissue repair programme after bleomycin challenge in lungs of *Salmonella* Typhimurium-treated mice using bulk RNA-seq of flow-sorted pulmonary MAIT cells. The numbers of DEGs in bleomycin-challenged lung MAIT cells compared with unchallenged controls, were 425 (361 up, 64 down), 1230 (399 up, 831 down), 0, 24 (4 up, 20 down) and 131 (40 up, 91 down) genes at day 3, 7, 14, 21 and 28 post-bleomycin challenge, respectively (Figure 3.10A, Table 3-2). Intriguingly, the top 15 upregulated genes in pulmonary MAIT cells at day 3 post-bleomycin included tissue-damage related genes such as *Col4α1*, *Col4α2*, *Ptger1*, and *Wwtr1* (Figure 3.10B). The predominant GO pathways upregulated in MAIT cells at day 3 post-bleomycin challenge compared to those from unchallenged mice were associated with the regulation of the defence

response, leukocyte differentiation, and response to viruses (Figure 3.11). I also observed a notable rise in the *Cd69* gene expression and a modest upregulation of several inflammatory cytokines, such as *Csf2*, *Ifn-γ*, *Tnf*, *Il17a*, *Il10* and *Il22*, in MAIT cells (Figure 3.12), and verified selected cytokines by flow cytometry (Figure 3.13).

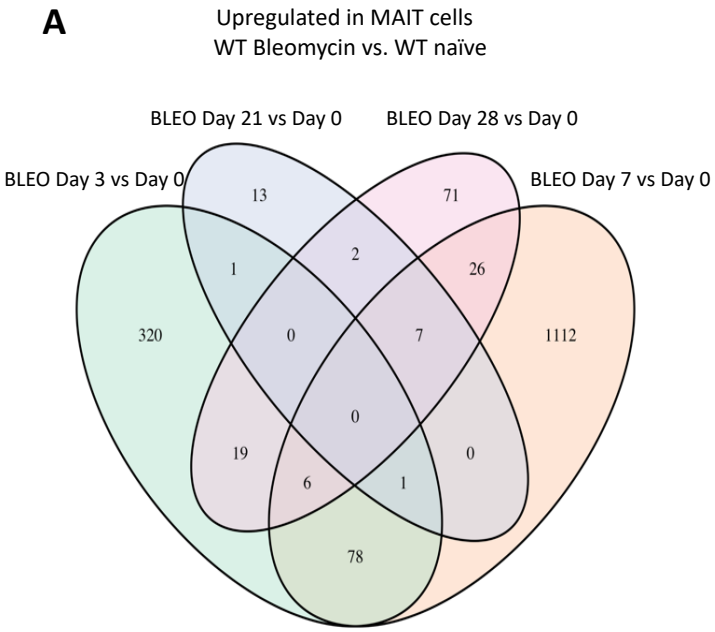

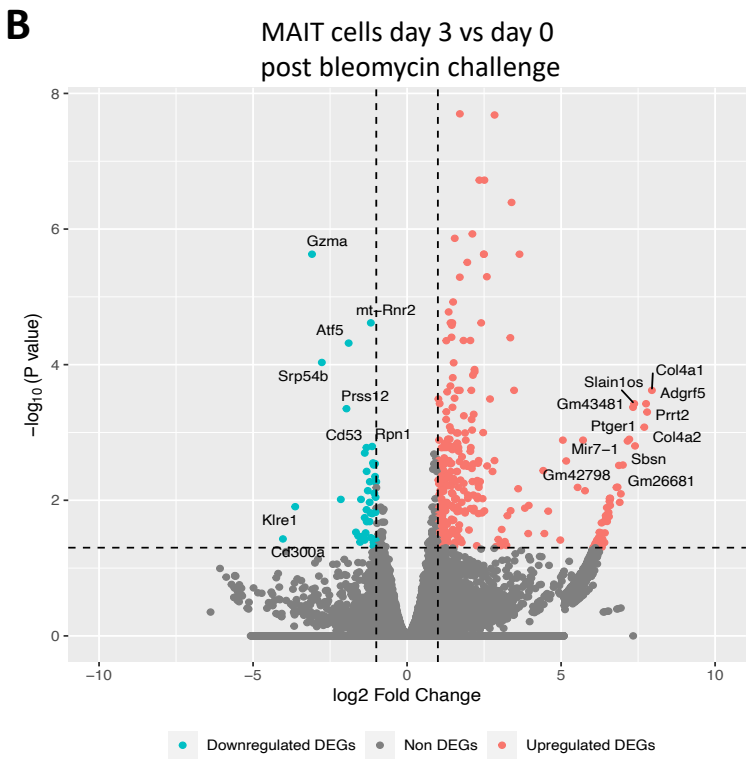

Figure 3.10 Differential gene expression analysis of lung MAIT cells in bleomycin-challenged mice.

(**A**) Venn diagram showing the overlap of genes up regulated in mice lung MAIT cells on day 3, 7, 21 and 28 post-bleomycin challenge, compared to unchallenged controls (n=3/group). (**B**) Volcano plot of DEGs [log2 fold change (FC) > 1, adjusted $P < 0.05$] of mouse lung MAIT cells on day 3 post-bleomycin challenge compared with unchallenged PBS controls. The top up and down-regulated genes are annotated. Horizontal line indicates *P* value threshold of 0.05. Vertical line indicates log2 fold change threshold of 1.

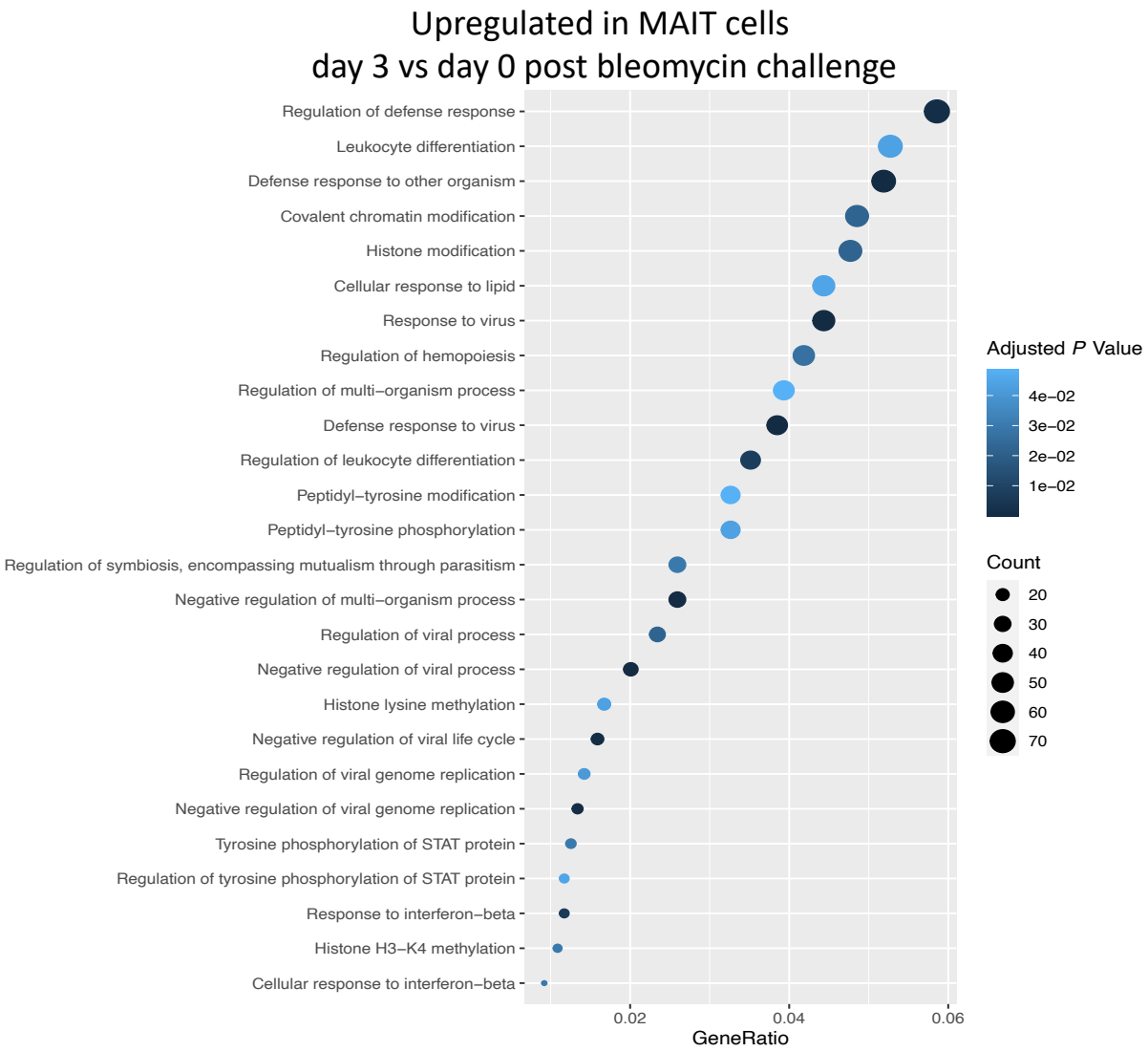

Figure 3.11 Upregulated GO terms in lung MAIT cells at day 3 post bleomycin challenge.

Top 25 significantly enriched ($P < 0.05$) pathways from Gene Ontology (GO) database (biological process) among upregulated DEGs in mouse lung MAIT cells at day 3 post-bleomycin challenge compared with unchallenged PBS controls. The colour intensity indicates the statistical significance of the enrichment, with the dot size representing the number of genes upregulated in each pathway. The x-axis illustrates the proportion of all DEGs included in each pathway (Gene Ratio).

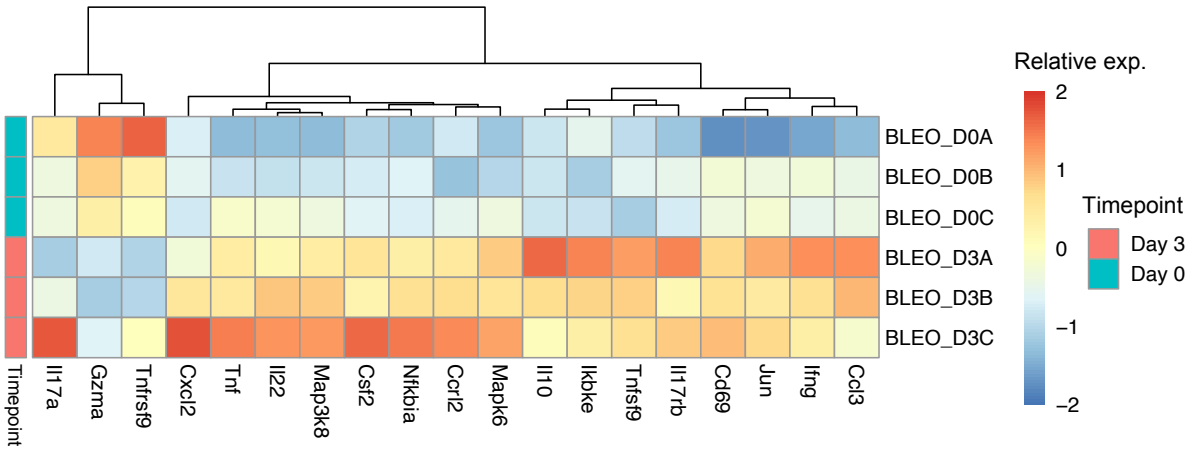

Figure 3.12 Heatmap depicting expression of cytokines and chemokines in lung MAIT cells post bleomycin challenge.

Cytokine and chemokine expression profiles in lung MAIT cells at days 0 (PBS control) and 3 post bleomycin challenge (red, highest expression; blue, lowest).

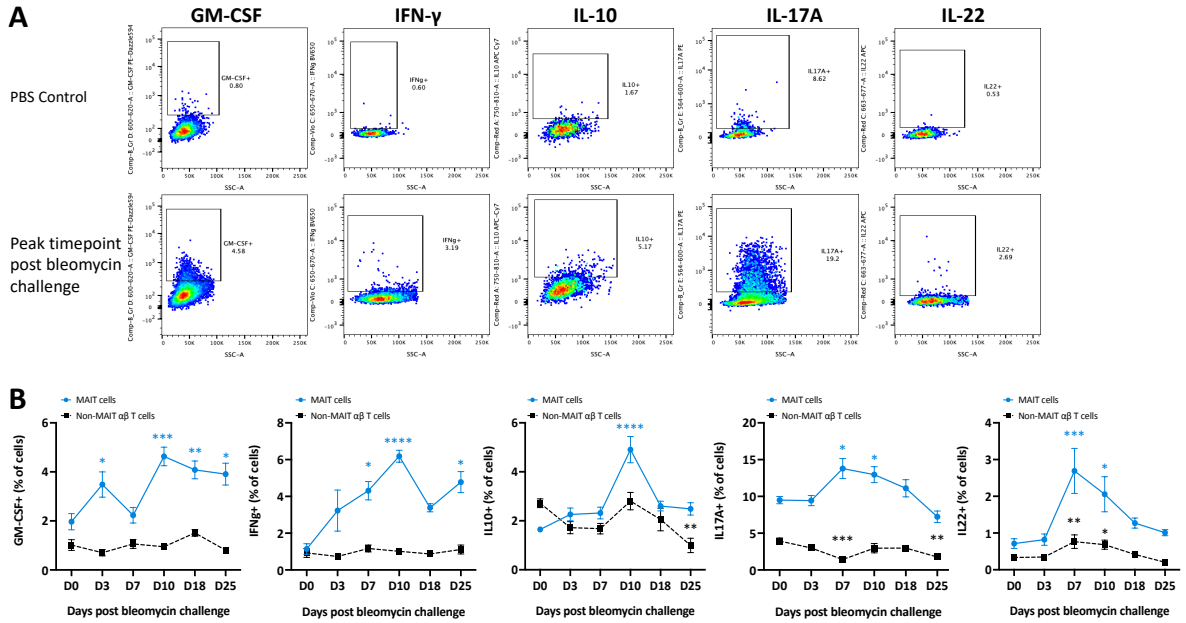

Figure 3.13 Cytokine profile of *ex vivo* pulmonary MAIT cells following bleomycin-induced lung injury.

(**A**) Flow cytometry plot illustrating the expression levels of GM-CSF, IFN-γ, IL-10, IL-17A, and IL-22 in lung MAIT cells from MAIT-cell enriched mice after bleomycin challenge. Peak response times to bleomycin for each cytokine are presented, with Day 10 for GM-CSF, IFN-γ, and IL-10, and Day 7 for IL-17A and IL-22. (**B**) Proportion of pulmonary MAIT cells expressing GM-CSF, IFN-γ, IL-10, IL17A and IL22 expressed as percentage of MAIT and non-MAIT αβ T cells. Graphs show combined data (mean ± SEM) from two independent experiments with similar results, with 3–5 mice per group in each replicate. Statistical tests compare each time-point with day 0 control in each subset by one-way ANOVA with Dunnett's multiple comparisons test or Kruskal-Wallis with Dunn's multiple comparisons test; $*P < 0.05$, $**P < 0.01$, $***P < 0.001$, $****P < 0.0001$.

Table 3-2 Top 20 upregulated and downregulated DEGs of MAIT cells, *Salmonella* Typhimurium BRD509 pre-infected, WT bleomycin-challenged versus WT unchallenged

MAIT Bleo D3 vs Bleo D0 DEG			**MAIT Bleo D7 vs Bleo D0 DEG**			**MAIT Bleo D21 vs Bleo D0 DEG**			**MAIT Bleo D28 vs Bleo D0 DEG**		
Gene	**Log2 Fold Change**	**Adjusted *P* value**	**Gene**	**Log2 Fold Change**	**Adjusted *P* value**	**Gene**	**Log2 Fold Change**	**Adjusted *P* value**	**Gene**	**Log2 Fold Change**	**Adjusted *P* value**
Col4a1	7.95	0.0002	*Rai14*	7.00	0.002	*Large1*	3.34	0.010	*Tcn2*	1.63	0.0013
Prrt2	7.79	0.0005	*Alas2*	6.88	0.005	*Trio*	1.03	0.03	*Rbm45*	1.26	0.0385
Adgrf5	7.76	0.0004	*Kif18b*	6.65	0.007	*Kmt2c*	0.86	0.03	*Lpcat3*	1.17	0.0045
Col4a2	7.70	0.0008	*Mybl1*	6.63	0.006	*Ccl5*	-1.10	0.003	*Enpp4*	1.15	0.0125
Sbsn	7.40	0.002	*Slamf6*	6.45	0.03	*mt-Co2*	-1.21	4.31E-06	*Dkkl1*	1.12	0.0063
Slain1os	7.38	0.0004	*Aqp1*	6.41	0.02	*mt-Atp6*	-1.30	6.87E-06	*Tmem50b*	1.10	0.0045
Ptger1	7.21	0.001	*Krt18*	6.38	0.01	*mt-Co3*	-1.33	4.31E-06	*Ccr8*	1.07	0.0207
Mir7-1	7.16	0.001	*Trav4n-4*	6.25	0.05	*Cd74*	-1.64	0.003	*Cyp51*	1.05	0.0102
Cav1	6.90	0.01	*Oscp1*	6.23	0.03	*H2-Eb1*	-2.00	0.04	*Stard4*	1.03	0.0352
CT571247.2	6.83	0.006	*Iqcg*	6.16	0.04	*Apoe*	-3.17	0.0002	*Ndrg1*	1.02	0.0063
Wwtr1	6.80	0.006	*Troap*	6.13	0.03	*Ccl6*	-3.51	0.04	*Fgl2*	1.01	0.0074
Trav13-2	6.60	0.009	*Snora78*	6.02	0.04	*Lyz2*	-4.28	0.03	*Psen2*	1.00	0.0241
Egr4	6.59	0.01	*Nid1*	6.01	0.04	*Fcgr3*	-5.39	0.03	*Trp53inp1*	0.99	0.0002
Mybl1	6.59	0.009	*Igsf23*	6.00	0.04	*Tyrobp*	-6.29	0.0001	*Crybg1*	0.97	0.0008
Mtss1l	6.57	0.01	*Hddc3*	5.81	0.01	*Wdfy4*	-6.73	0.04	*P2ry10*	0.91	0.0229
Timp3	6.56	0.02	*Olfml3*	4.96	0.03	*Sirpa*	-7.53	0.002	*Slc39a9*	0.90	0.0352
C530050E15Rik	6.49	0.02	*Bub1*	4.75	0.01	*Clec7a*	-8.36	2.11E-05	*Ctsc*	0.90	0.0267

Sema3c	6.46	0.02	*Ifit3*	4.63	2.47E-09	*Cybb*	-9.05	0.01	*Ndufa4*	0.88	0.0176
2610037D02Rik	6.45	0.02	*Stab2*	4.60	0.01				*Insig1*	0.86	0.0186
Cavin1	6.42	0.03	*Rilpl1*	3.80	0.01				*Ltb4r1*	0.86	0.0213
Slc7a5	-1.31	0.004	*Hist1h4k*	-5.18	0.02				*Arid4b*	-1.19	0.0176
Cyp51	-1.32	0.01	*Slc29a2*	-5.21	0.0002				*Rev3l*	-1.23	0.0179
Cd53	-1.32	0.002	*Slc1a4*	-5.33	0.02				*mt-Co2*	-1.23	0.0001
Pop4	-1.35	0.03	*Cyp2t4*	-5.53	0.03				*Rif1*	-1.24	0.0407
Rcn2	-1.37	0.002	*Nrip3*	-5.72	0.007				*Tagap*	-1.31	0.0018
Srxn1	-1.38	0.02	*Vpreb3*	-5.98	0.05				*Ppp1r15a*	-1.35	1.11E-06
Pcyox1	-1.38	0.04	*Fgf18*	-6.06	0.04				*Trib1*	-1.37	0.0373
Ndrg1	-1.41	0.04	*Ghrl*	-6.12	0.04				*Jarid2*	-1.38	0.0186
Trmt61b	-1.45	0.03	*Smpdl3b*	-6.19	0.03				*Tpr*	-1.47	0.0003
Tnfrsf9	-1.50	0.010	*Gstm1*	-6.20	0.03				*Plac8*	-1.51	0.0003
Sgip1	-1.53	0.04	*Rusc2*	-6.27	0.02				*Pak1*	-1.54	0.0447
Pak1	-1.58	0.03	*Tgm1*	-6.32	0.05				*Zfp36*	-1.59	1.35E-05
Mvk	-1.66	0.03	*Hist1h4n*	-6.39	0.02				*Cd74*	-1.67	5.13E-05
Atf5	-1.90	4.81E-05	*Igf2bp2*	-6.43	0.04				*Gadd45g*	-1.68	0.0074
Prss12	-1.97	0.0004	*Adgre4*	-6.51	0.02				*Rgs16*	-1.98	0.0034
Trib3	-2.15	0.010	*Mest*	-6.55	0.008				*Ifng*	-2.10	3.47E-07
Srp54b	-2.77	9.28E-05	*Ccr10*	-6.57	0.02				*Egr1*	-2.30	0.0356
Gzma	-3.09	2.35E-06	*Ankrd33b*	-6.66	0.008				*Ccl5*	-2.45	5.12E-09
Klre1	-3.63	0.01	*Gdpd1*	-6.67	0.008				*Hspa1b*	-2.64	0.0002
Cd300a	-4.03	0.04	*Gng4*	-7.43	0.0005				*Hspa1a*	-2.90	0.0003

I then conducted a GSEA to compare the TCR-triggered MAIT cell tissue repair gene signature (Hinks *et al.*, 2019; Lamichhane, Schneider*, et al.*, 2019; Leng *et al.*, 2019), previously characterised in response to commensal bacteria in H2-M3-restricted RORγt^{+} CD8^{+} T cells in murine skin (Linehan *et al.*, 2018), with the gene expression profile of pulmonary MAIT cells following bleomycin exposure. This revealed significant enrichment of the tissue repair gene set in MAIT cells at day 3 post-bleomycin challenge (Figure 3.14). These findings suggested that *in vivo* bleomycin challenge activates the tissue repair programme of MAIT cells.

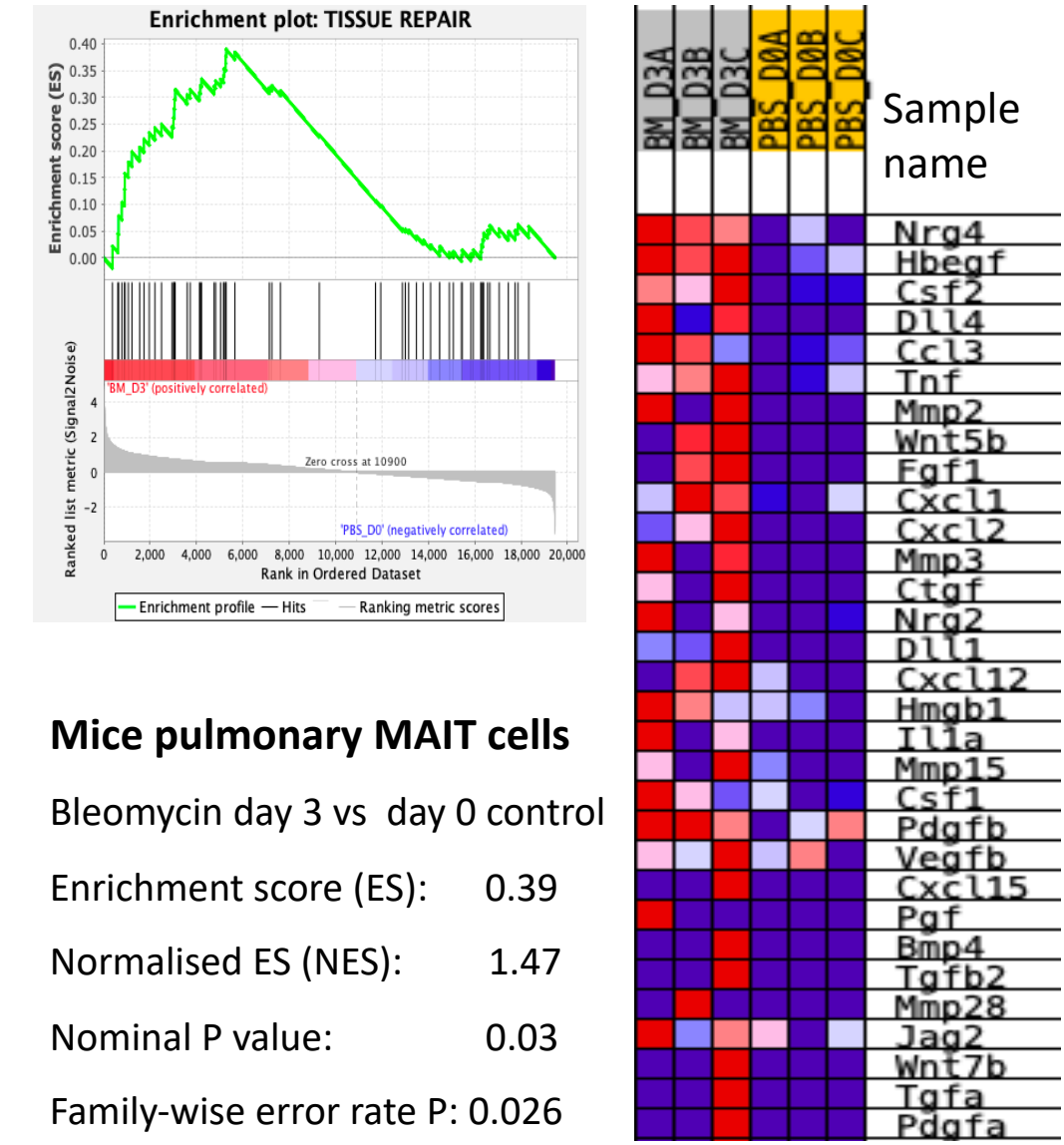

Figure 3.14 Gene set enrichment analysis for tissue repair gene signature (Linehan *et al.*, 2018) of lung MAIT cells at day 3 post-bleomycin challenge.

Heatmap showing the expression of leading-edge gene subsets in mice pulmonary MAIT cells at day 3 post-bleomycin challenge and unchallenged control (red indicates highest expression; blue indicates lowest).

To ascertain whether pre-infection with *Salmonella* Typhimurium BRD509 is essential for the enrichment of the tissue-repair gene set, I conducted bulk RNA sequencing using naïve MAIT cells at earlier timepoints post-bleomycin challenge, without pre-infection of *Salmonella* Typhimurium BRD509. I identified 544 and 339 differentially regulated genes in lung MAIT cells at day 3 and day 7 post-bleomycin challenge, respectively (Figure 3.15A, Table 3-3). The top predominant GO pathways upregulated in MAIT cells at day 3 post-bleomycin challenge, in comparison to those from unchallenged mice, were associated with the response to viruses, regulation of the inflammatory response, regulation of cytokine-mediated signalling pathways, and regulation of type I interferon production (Figure 3.15B). There was a trend towards the downregulation in the tissue repair gene set at day 3 post-bleomycin challenge ($P < 0.09$) (Figure 3.15C). To evaluate the consistency of DEGs in MAIT cells, both with and without pre-infection, I conducted a GO enrichment analysis on the DEGs shared by MAIT cells under both conditions (Day 3 post-bleomycin versus PBS control). The predominant GO pathways of shared upregulated genes in both conditions were the response to virus, positive regulation of the innate immune response, regulation of cytokine-mediated signalling pathways, and regulation of type I interferon production (Figure 3.15D), which are similar to the enriched GO terms in naïve MAIT cells. This suggests that the pre-infection did not significantly alter the profile of MAIT cells.

A MAIT cells day 3 vs day 0, post-bleomycin challenge (without pre-infection of *Salmonella* BRD509)

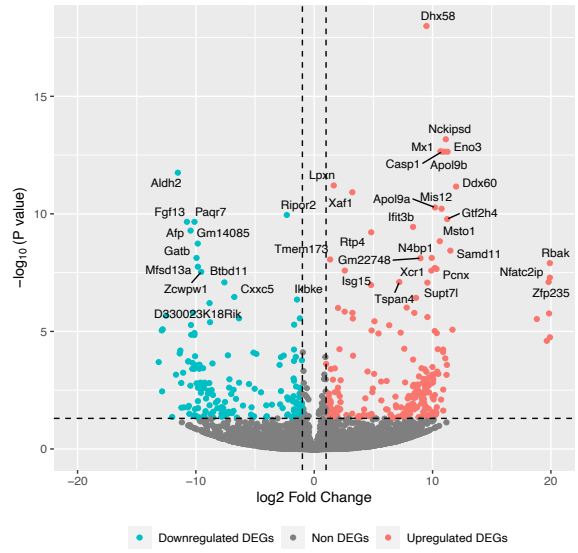

C Enrichment of tissue repair-related gene set

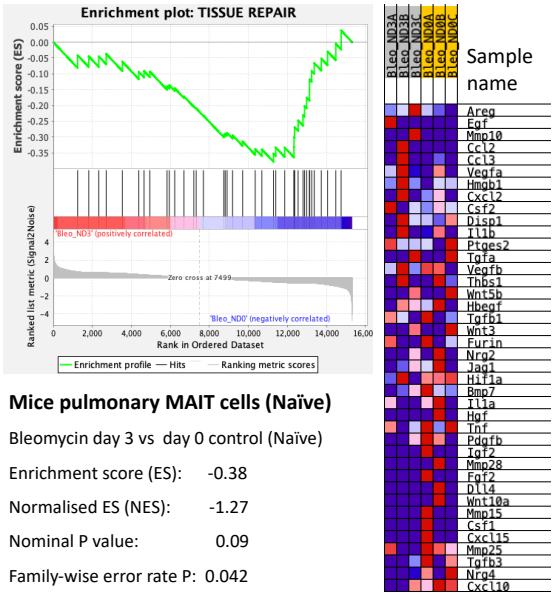

Mice pulmonary MAIT cells (Naïve)

Bleomycin day 3 vs day 0 control (Naïve)

Enrichment score (ES): -0.38

Normalised ES (NES): -1.27

Nominal P value: 0.09

Family-wise error rate P: 0.042

B Up-regulated in MAIT cells, day 3 vs day 0 post-bleomycin challenge (without pre-infection of *Salmonella* BRD509)

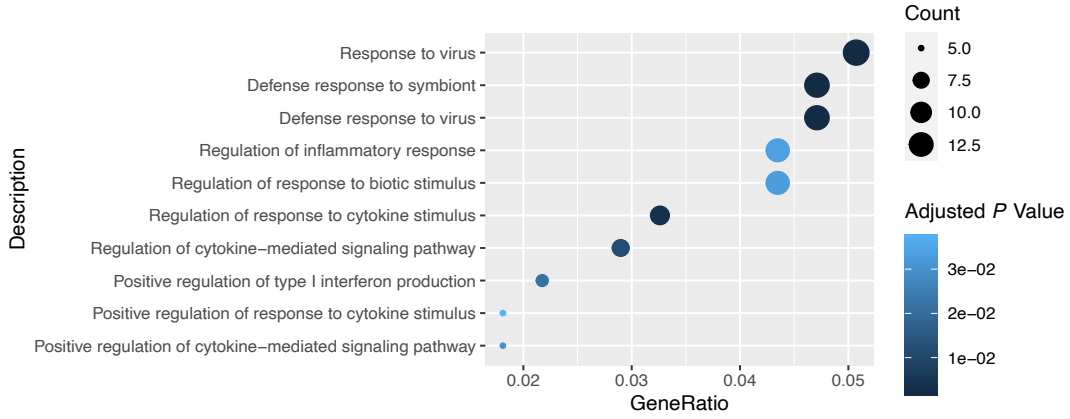

D Up-regulated in MAIT cells, day 3 vs day 0, post-bleomycin challenge GO enrichment analysis on the overlapped DEGs of MAIT cells with and without pre-infection

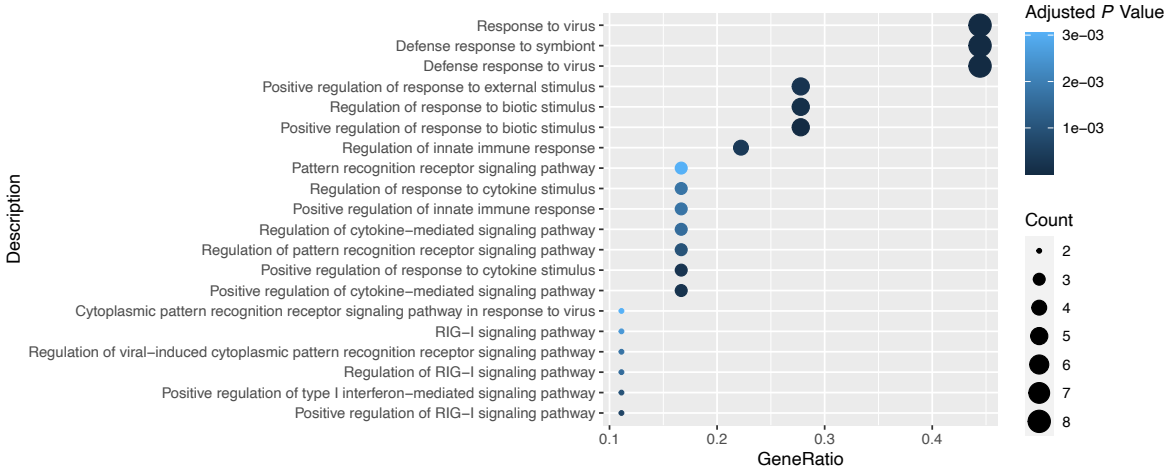

Figure 3.15 Gene expression profile of pulmonary MAIT cells following bleomycin-induced lung injury.

Experiments were conducted using naïve mice that had not undergone pre-infection of *Salmonella* Typhimurium BRD509. (**A**) Volcano plot of DEGs [log2 fold change (FC) > 1, adjusted $P < 0.05$] in mice lung MAIT cells on day 3 post-bleomycin challenge compared to PBS controls (n = 3 per group). The top up and down-regulated genes are annotated. Horizontal line indicates *P* value threshold of 0.05. Vertical line indicates log2 fold change threshold of 1. (**B**) All significantly enriched ($P < 0.05$) pathways from Gene Ontology (GO) database (biological process) in upregulated DEGs of mice lung MAIT cells at day 3 post-bleomycin challenge compared to PBS controls. (**C**) Gene set enrichment analysis (GSEA) for tissue repair gene signature (Linehan *et al.*, 2018) in mouse MAIT cells. Heatmap showing expression of leading-edge subset genes within the gene set (red, highest expression; blue, lowest) for mouse pulmonary MAIT cells at day 3 post-bleomycin challenge compared to PBS controls. (**D**) All significantly enriched ($P < 0.05$) pathways from GO database (biological process) in overlapped DEGs of MAIT cells on day 3 post-bleomycin challenge, with and without pre-infection.

Table 3-3 Top 20 upregulated and downregulated DEGs of MAIT cells, Naïve WT bleomycin-challenged versus WT unchallenged

Naïve MAIT Bleo D3 vs Bleo D0 DEG			**Naïve MAIT Bleo D7 vs Bleo D0 DEG**		
Gene	**Log2 Fold Change**	**Adjusted *P* value**	**Gene**	**Log2 Fold Change**	**Adjusted *P* value**
Ighmbp2	22.90850387	2.97E-12	*Klhdc10*	23.03211013	6.26E-10

Chst14	22.55067914	8.21E-07	*Ighmbp2*	22.93568183	4.95E-12
Kdm8	22.31049456	1.37E-08	*Mettl21a*	22.86283488	1.18E-09
Ncapg	22.14644235	1.31E-06	*Rbak*	22.78571342	7.98E-11
Cryzl2	22.09221647	1.40E-06	*Zfp712*	22.50035837	1.18E-09
Ccdc181	22.01707963	1.53E-06	*Gtf3c4*	22.48781825	1.60E-08
Gnb1l	22.00134941	4.92E-08	*Tpk1*	22.47676111	6.00E-09
Lrrc29	21.99819238	1.40E-07	*Dhx33*	22.33045573	7.06E-10
Lrrc20	21.91316395	1.72E-06	*Srbd1*	22.32266179	1.99E-06
Klhdc10	21.64988364	4.95E-09	*Ddias*	22.22612569	2.27E-06
Angel1	21.61739261	2.46E-06	*Aldoc*	22.16072137	2.40E-06
Gnb5	21.61556797	8.72E-09	*Ints6l*	22.15779319	2.40E-06
Mettl21a	21.59678071	7.49E-09	*Gnb1l*	22.13113564	6.45E-08
Calhm2	21.52939973	2.74E-06	*Tmed8*	22.08159867	8.25E-09
F2rl3	21.52028579	2.74E-06	*Angptl2*	22.0717123	8.06E-09
Boll	21.50439408	2.77E-06	*Dgcr8*	21.98365916	3.07E-06
Ehhadh	21.49714681	2.78E-06	*Camkk1*	21.9562475	8.06E-09
Ap4m1	21.38895946	3.08E-06	*Gnb5*	21.92762753	7.71E-09
Gbp2b	21.38326937	3.08E-06	*Cd200r4*	21.85851876	3.64E-06
Hmmr	21.37196948	8.46E-09	*Hmmr*	21.84337527	6.00E-09
Prdm16	-22.88860206	1.42E-09	*Fstl4*	-7.782032007	0.044080382
Wdr62	-22.91281535	5.16E-07	*Igsf5*	-9.875897652	0.001728574
Gm47586	-22.92641559	8.35E-10	*C5ar1*	-9.901127291	0.001182773
Acoxl	-22.98803306	4.73E-07	*Sirpb1b*	-10.06814757	0.030398679
Kif13b	-23.03860131	3.11E-08	*Slc37a2*	-10.42247016	0.001548588
Ncapg2	-23.08627753	4.15E-07	*Fgd2*	-10.62380788	0.000807983
Capn3	-23.161691	2.18E-13	*Blnk*	-10.66954332	0.000151939
Dclk2	-23.25113509	3.31E-07	*Clec4d*	-10.88521682	0.04869389
Pex1	-23.38960774	2.71E-07	*S100a9*	-13.55556284	0.002635861
Nek4	-23.6079024	1.97E-07	*S100a8*	-13.7924163	0.008337836
Abcb10	-23.6274759	1.93E-07	*Retnlg*	-22.67161361	1.28E-06
Smyd4	-23.67521665	9.19E-09	*Nphp4*	-23.09150394	2.71E-08
Perp	-23.70090885	1.73E-07	*Pi16*	-23.28403902	5.42E-07
Msl3l2	-23.7363051	1.66E-07	*Ifitm1*	-23.40864709	4.53E-07
Rnase6	-23.82784047	1.45E-07	*Clec4n*	-23.53947695	3.99E-07
Fignl1	-23.8417631	1.43E-07	*Mmp9*	-25.12459171	1.08E-09
Ccnf	-23.94589677	2.03E-08	*Pla2g7*	-25.67919581	3.03E-10
Zscan18	-24.02499691	1.09E-07	*Scd1*	-26.27224426	7.71E-09
Scd1	-26.00796403	7.69E-09	*Csf3r*	-26.27355234	1.10E-10
Igkv8-30	-27.04657383	1.75E-09	*Igkv8-30*	-27.37522561	1.65E-09

Current research indicates that MAIT cells are activated by MR1-TCR dependent or cytokine-dependent pathways; with the latter being key in antiviral response. Consequently, I further expanded my inquiry to investigate a different, albeit highly pertinent, condition of cytokine-dependent MAIT cell activation – viral infection. I performed bulk RNA-seq of MAIT cells isolated from the lungs of mice infected with 100 plaque forming units (PFU) of the mouse-adapted influenza virus strain A/Puerto Rico/8/34/1934 (PR8, H1N1). As expected, key upregulated genes included interferon-inducible genes, such as *Ifi205* and *Ifi44* (Figure 3.16, Table 3-5). Upregulated GO terms included those related to defence responses against viruses and other organisms (Figure 3.17). Intriguingly, the time-series analysis (Figure 3.18A, Table 3-4) revealed that tissue repair-related GO terms were exclusively found in Cluster 2, characterised by enriched GO terms like wound healing and regulation of cell morphogenesis (Figure 3.18, B and C). Importantly, the previously discussed tissue repair programme (Linehan *et al.*, 2018), was also activated in the MAIT cells at early timepoints post-infection (Figure 3.19), echoing the pattern I identified post-bleomycin, implying activation of this programme in both viral and sterile lung injury.

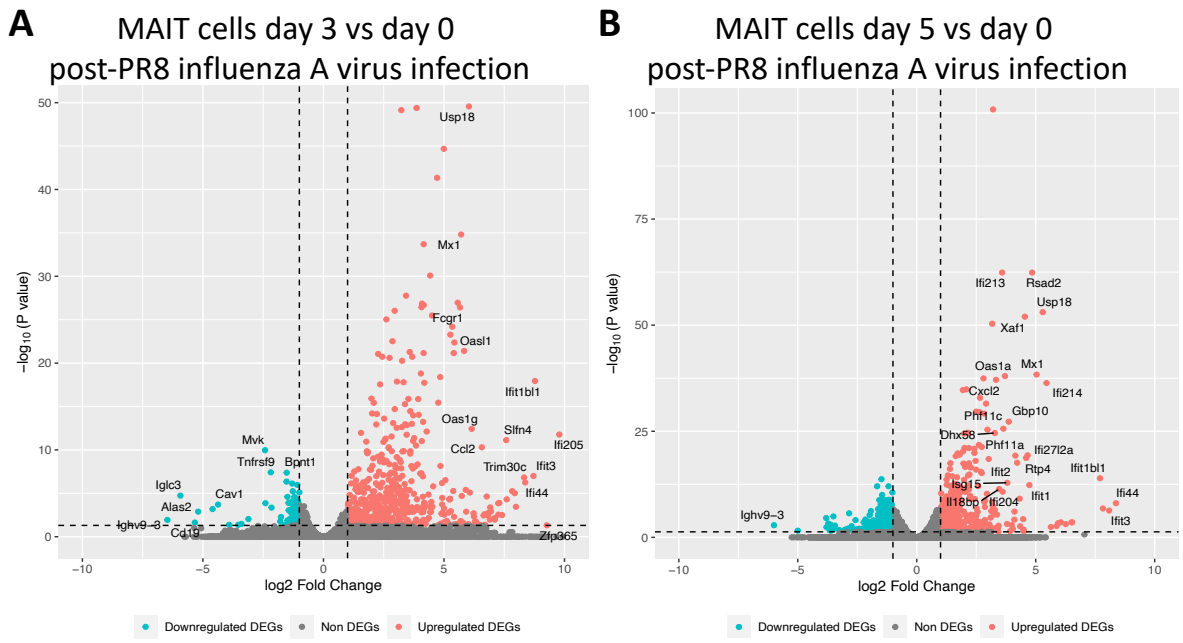

Figure 3.16 Differential gene expression analysis of lung MAIT cells in PR8 IAV-infected mice.

Volcano plot of differentially expressed genes (DEGs) [log2 fold change (FC) > 1, adjusted *P* < 0.05] in mice lung MAIT cells on day 3 (**A**) and 5 (**B**) post-PR8 IAV infection compared to uninfected controls (n=3/group). The top up and down-regulated genes are annotated. Horizontal line indicates *P* value threshold of 0.05. Vertical line indicates log2 fold change threshold of 1.

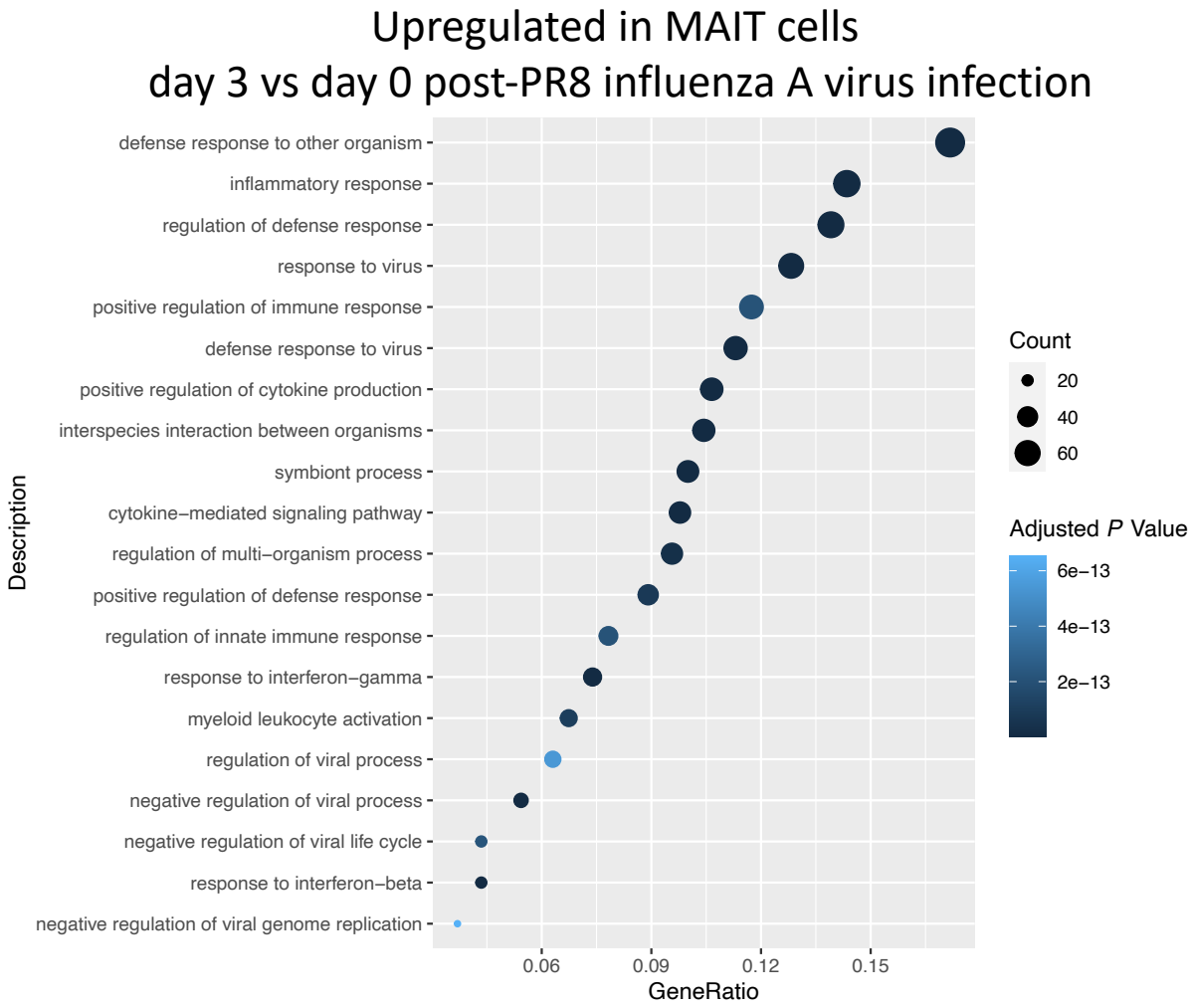

Figure 3.17 Upregulated GO terms in lung MAIT cells at day 3 post-PR8 IAV infection.

Top 25 significantly enriched ($P < 0.01$) pathways from Gene Ontology (GO) database (biological process) in upregulated DEGs of mice lung MAIT cells at day 3 post-PR8 IAV infection compared to uninfected controls (n=3/group). The colour intensity indicates the statistical significance of the upregulation, with the dot size representing the number of genes upregulated in each pathway. The x-axis illustrates the proportion of all differentially expressed genes included in each pathway (Gene Ratio).

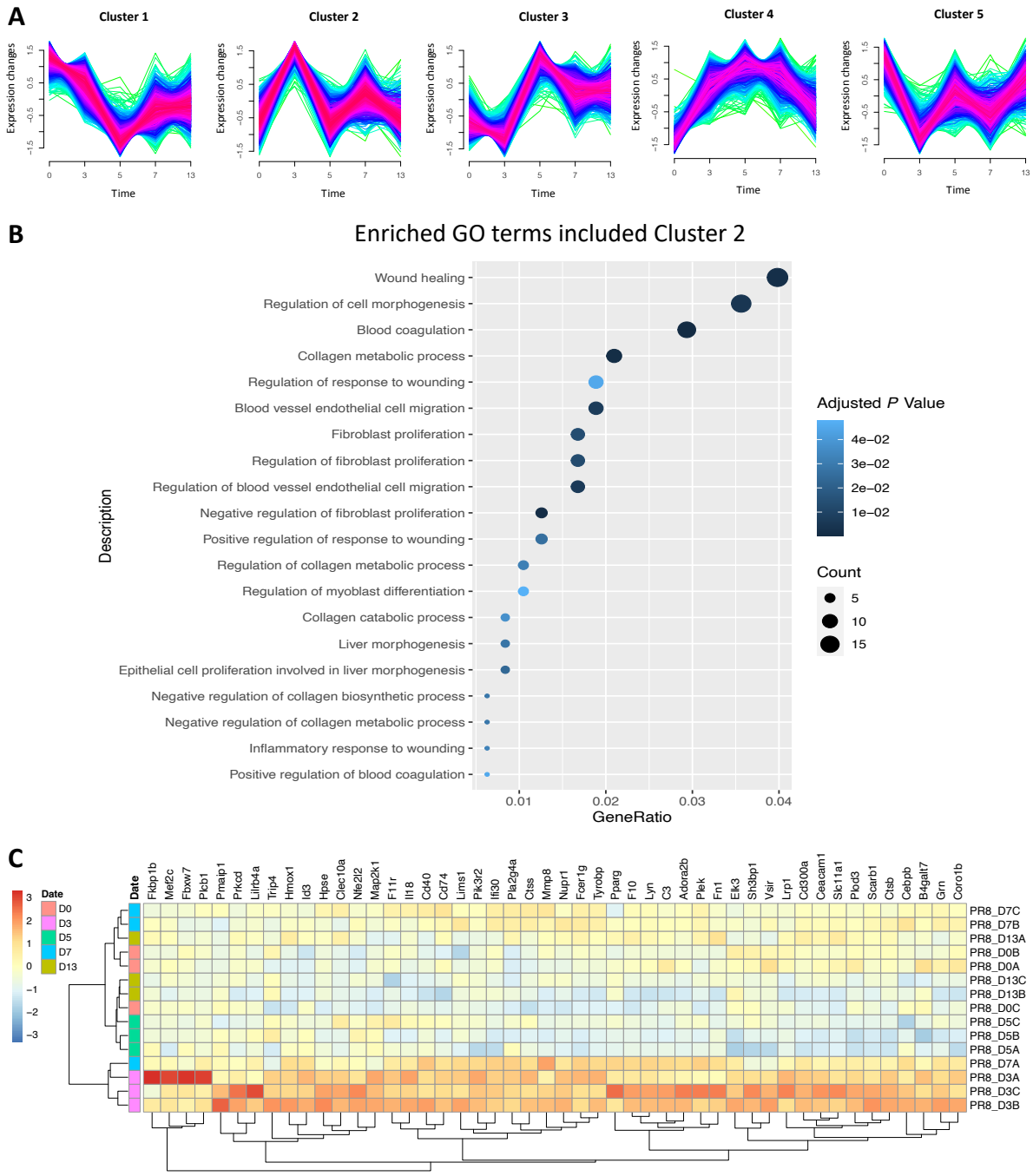

Figure 3.18 Time-series analysis showing the gene alteration trends of PR8 IAV-infected mice MAIT cells.

(**A**) Time-series expression of five gene clusters obtained from the time-series analysis. The different colours indicated the degree of match between changes of gene expression and the

major changes of the clusters. Red, blue and green represented high, moderate and low match degrees, respectively. (**B**) Tissue repair-related GO terms (biological process) enriched from genes in cluster 2. The colour intensity indicates the statistical significance of the upregulation, with the dot size representing the number of genes upregulated in each pathway. The x-axis illustrates the proportion of all differentially expressed genes included in each pathway (Gene Ratio). (**C**) Heatmap depicting relative expression of genes associated with tissue repair at different time points in Cluster 2.

Table 3-4 Top 20 upregulated GO terms of Clusters 1-5 in time-series analysis

Cluster 1				
ID	**Description**	**Gene Ratio**	**Adjusted *P* value**	**Count**
GO:0009101	glycoprotein biosynthetic process	30/644	7.26970481257564e-07	30
GO:0030258	lipid modification	28/644	1.06558930271979e-06	28
GO:0070085	glycosylation	25/644	1.14579072713681e-06	25
GO:0006644	phospholipid metabolic process	33/644	1.14579072713681e-06	33
GO:0009100	glycoprotein metabolic process	32/644	1.14579072713681e-06	32
GO:0006486	protein glycosylation	23/644	2.61270539714414e-06	23
GO:0043413	macromolecule glycosylation	23/644	2.61270539714414e-06	23
GO:0090407	organophosphate biosynthetic process	35/644	9.40890589930475e-06	35
GO:0008654	phospholipid biosynthetic process	20/644	6.24587308212728e-05	20
GO:0006650	glycerophospholipid metabolic process	25/644	6.24587308212728e-05	25
GO:0006631	fatty acid metabolic process	32/644	6.24587308212728e-05	32
GO:0046486	glycerolipid metabolic process	30/644	6.24587308212728e-05	30
GO:0019395	fatty acid oxidation	15/644	0.000107549	15
GO:0018209	peptidyl-serine modification	29/644	0.000110535	29
GO:0034440	lipid oxidation	15/644	0.000205337	15
GO:0044242	cellular lipid catabolic process	21/644	0.000205337	21
GO:0018105	peptidyl-serine phosphorylation	27/644	0.000217588	27
GO:0032868	response to insulin	22/644	0.000249484	22
GO:0032869	cellular response to insulin stimulus	20/644	0.000256026	20
GO:0016570	histone modification	32/644	0.000256026	32
Cluster 2				
GO:0001819	positive regulation of cytokine production	48/477	3.10626936818367e-17	48

GO:0002274	myeloid leukocyte activation	34/477	9.28222851136116e-16	34
GO:0032103	positive regulation of response to external stimulus	41/477	4.57635525229861e-14	41
GO:0019886	antigen processing and presentation of exogenous peptide antigen via MHC class II	11/477	9.11487912019089e-13	11
GO:0032635	interleukin-6 production	26/477	9.11487912019089e-13	26
GO:0002478	antigen processing and presentation of exogenous peptide antigen	13/477	9.11487912019089e-13	13
GO:0032755	positive regulation of interleukin-6 production	21/477	9.11487912019089e-13	21
GO:0050727	regulation of inflammatory response	35/477	3.32995005607443e-12	35
GO:0032602	chemokine production	20/477	6.96238415093925e-12	20
GO:0032675	regulation of interleukin-6 production	24/477	6.96238415093925e-12	24
GO:0031349	positive regulation of defense response	30/477	7.0787148108755e-12	30
GO:0019884	antigen processing and presentation of exogenous antigen	13/477	2.05689103991642e-11	13
GO:0002495	antigen processing and presentation of peptide antigen via MHC class II	11/477	2.230857900911e-11	11
GO:0002504	antigen processing and presentation of peptide or polysaccharide antigen via MHC class II	11/477	4.06727964515989e-11	11
GO:0006909	phagocytosis	34/477	4.18368099692314e-11	34
GO:0050900	leukocyte migration	34/477	4.97977606809536e-11	34
GO:0097529	myeloid leukocyte migration	26/477	1.82545792286702e-10	26
GO:0046651	lymphocyte proliferation	31/477	2.02586552210067e-10	31
GO:0032943	mononuclear cell proliferation	31/477	2.45764447638587e-10	31
GO:0070661	leukocyte proliferation	32/477	3.18983835131821e-10	32

	Cluster 3			
GO:0002181	cytoplasmic translation	29/439	3.34265351715269e-24	29
GO:0022613	ribonucleoprotein complex biogenesis	45/439	1.98065275183449e-18	45
GO:0042254	ribosome biogenesis	37/439	7.27287049902848e-17	37
GO:0042255	ribosome assembly	18/439	9.77284810006674e-14	18
GO:0022618	ribonucleoprotein complex assembly	25/439	1.56293216453025e-12	25
GO:0006364	rRNA processing	27/439	1.78006829461981e-12	27
GO:0071826	ribonucleoprotein complex subunit organization	25/439	2.91132597087945e-12	25
GO:0016072	rRNA metabolic process	27/439	3.89691599168285e-12	27
GO:0042274	ribosomal small subunit biogenesis	17/439	9.93178954114609e-12	17
GO:0008380	RNA splicing	35/439	1.13331494634441e-11	35
GO:0042273	ribosomal large subunit biogenesis	16/439	1.04546042870642e-10	16
GO:0000028	ribosomal small subunit assembly	10/439	4.56658772756301e-10	10
GO:0034470	ncRNA processing	31/439	4.56658772756301e-10	31
GO:0006397	mRNA processing	35/439	1.15585139163698e-09	35
GO:0034660	ncRNA metabolic process	32/439	2.84101987619283e-08	32
GO:0043484	regulation of RNA splicing	18/439	1.28762113243577e-07	18
GO:0000375	RNA splicing, via transesterification reactions	24/439	1.28762113243577e-07	24
GO:0000377	RNA splicing, via transesterification reactions with bulged adenosine as nucleophile	24/439	1.28762113243577e-07	24
GO:0000398	mRNA splicing, via spliceosome	24/439	1.28762113243577e-07	24
GO:0006417	regulation of translation	25/439	2.8010300144261e-06	25

	Cluster 4			
GO:0035456	response to interferon-beta	22/303	1.49220969675373e-23	22
GO:0035458	cellular response to interferon-beta	20/303	9.80410350481863e-23	20
GO:0009615	response to virus	37/303	2.53163644591194e-22	37
GO:0051607	defense response to virus	33/303	4.4304043429723e-21	33
GO:0140546	defense response to symbiont	33/303	4.4304043429723e-21	33
GO:0044403	biological process involved in symbiotic interaction	34/303	8.39808733235103e-16	34
GO:0002831	regulation of response to biotic stimulus	28/303	1.15247453925025e-13	28
GO:0043903	regulation of biological process involved in symbiotic interaction	21/303	1.36478931126219e-11	21
GO:0050792	regulation of viral process	20/303	3.11946096882172e-11	20
GO:0016032	viral process	26/303	3.83329217733911e-11	26
GO:0034341	response to interferon-gamma	18/303	5.90918390965273e-11	18
GO:0045088	regulation of innate immune response	20/303	9.47723393093119e-11	20
GO:0071346	cellular response to interferon-gamma	16/303	3.3838478057613e-10	16
GO:0002833	positive regulation of response to biotic stimulus	18/303	4.46929686077396e-10	18
GO:0001562	response to protozoan	11/303	4.57469040442108e-10	11
GO:1903900	regulation of viral life cycle	17/303	2.98465963326363e-09	17
GO:0042832	defense response to protozoan	10/303	3.66613815926634e-09	10
GO:0019058	viral life cycle	20/303	4.32831043681773e-09	20
GO:0045089	positive regulation of innate immune response	15/303	4.45125808606186e-09	15
GO:0048525	negative regulation of viral process	13/303	2.50916057120155e-08	13

	Cluster 5			
GO:0008380	RNA splicing	27/376	1.10783073392017e-06	27
GO:0006397	mRNA processing	28/376	5.25459767563476e-06	28
GO:0034660	ncRNA metabolic process	27/376	5.51204738175011e-06	27
GO:0022613	ribonucleoprotein complex biogenesis	24/376	5.46873682144832e-05	24
GO:0034470	ncRNA processing	22/376	6.37743901704956e-05	22
GO:0000375	RNA splicing, via transesterification reactions	19/376	6.44508875900345e-05	19
GO:0000377	RNA splicing, via transesterification reactions with bulged adenosine as nucleophile	19/376	6.44508875900345e-05	19
GO:0000398	mRNA splicing, via spliceosome	19/376	6.44508875900345e-05	19
GO:0034248	regulation of cellular amide metabolic process	22/376	0.000395878	22
GO:0042254	ribosome biogenesis	17/376	0.002401243	17
GO:0006364	rRNA processing	14/376	0.002466035	14
GO:0034504	protein localization to nucleus	17/376	0.002726205	17
GO:0034250	positive regulation of cellular amide metabolic process	12/376	0.003124697	12
GO:0016072	rRNA metabolic process	14/376	0.00314622	14
GO:0010612	regulation of cardiac muscle adaptation	4/376	0.003207206	4
GO:0006417	regulation of translation	18/376	0.003801347	18
GO:0016579	protein deubiquitination	10/376	0.003801347	10
GO:1903311	regulation of mRNA metabolic process	15/376	0.00456744	15
GO:0014745	negative regulation of muscle adaptation	4/376	0.00580446	4
GO:0045931	positive regulation of mitotic cell cycle	10/376	0.00580446	10

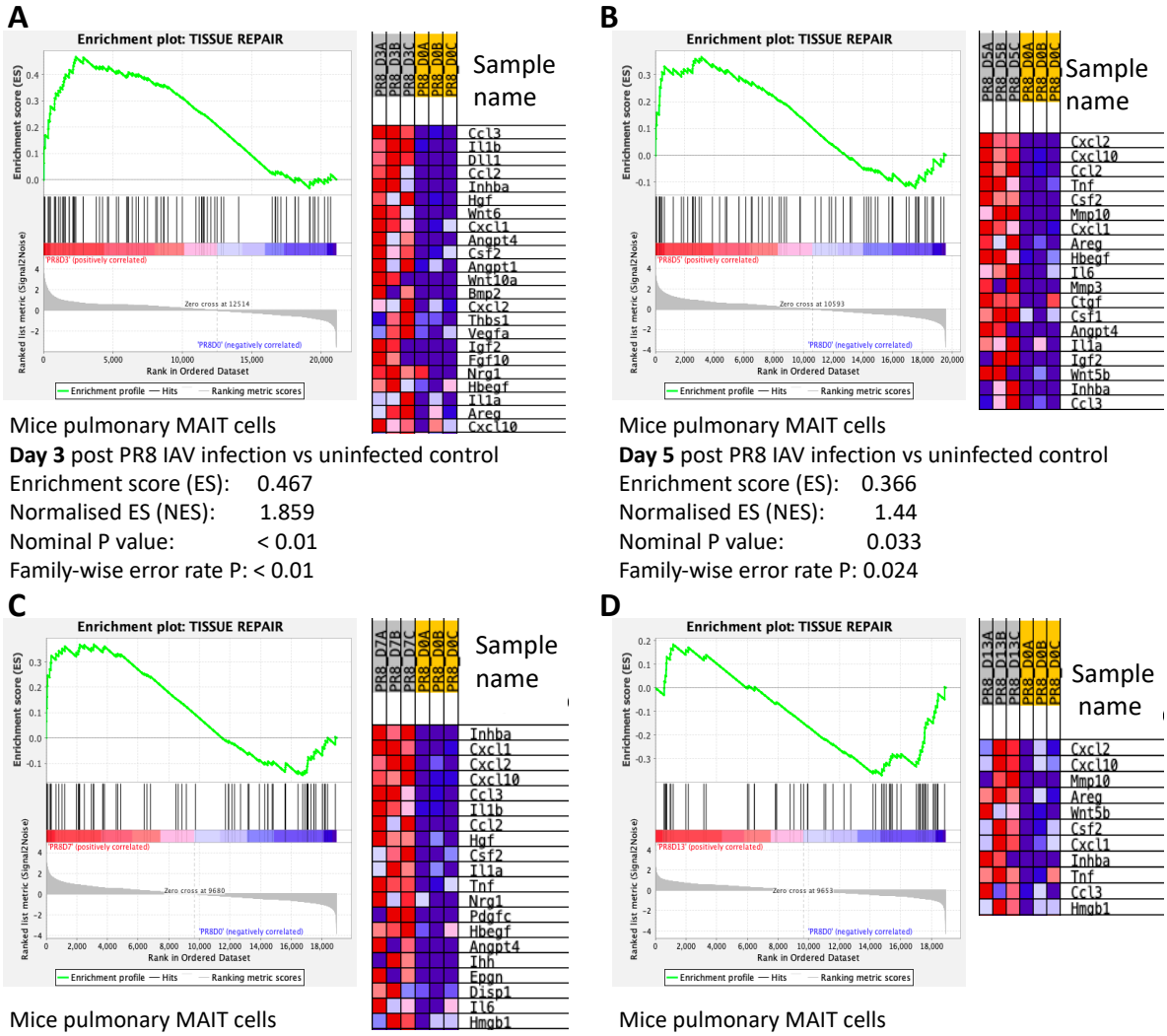

Mice pulmonary MAIT cells
Day 3 post PR8 IAV infection vs uninfected control
Enrichment score (ES): 0.467
Normalised ES (NES): 1.859
Nominal P value: < 0.01
Family-wise error rate P: < 0.01

Mice pulmonary MAIT cells
Day 5 post PR8 IAV infection vs uninfected control
Enrichment score (ES): 0.366
Normalised ES (NES): 1.44
Nominal P value: 0.033
Family-wise error rate P: 0.024

Mice pulmonary MAIT cells
Day 7 post PR8 IAV infection vs uninfected control
Enrichment score (ES): 0.369
Normalised ES (NES): 1.424
Nominal P value: 0.04
Family-wise error rate P: 0.028

Mice pulmonary MAIT cells
Day 13 post PR8 IAV infection vs uninfected control
Enrichment score (ES): -0.37
Normalised ES (NES): -1.57
Nominal P value: 0.008
Family-wise error rate P: 0.004

Figure 3.19 Gene set enrichment analysis for tissue repair gene signature (Linehan *et al.*, 2018) of lung MAIT cells post-PR8 IAV infection.

Heatmap showing expression of leading-edge subset genes within the gene set (red, highest expression; blue, lowest) for mouse pulmonary MAIT cells at day 3 (**A**), 5 (**B**), 7 (**C**) and 13 (**D**) post-PR8 IAV infection and uninfected control.

Table 3-5 Top 20 upregulated and downregulated DEGs of MAIT cells, *Salmonella* Typhimurium BRD509 pre-infected, WT PR8 virus infected versus WT B6 uninfected

MAIT PR8 D3 vs PR8 D0 DEG			**MAIT PR8 D5 vs PR8 D0 DEG**			**MAIT PR8 D7 vs PR8 D0 DEG**			**MAIT PR8 D13 vs PR8 D0 DEG**		
Gene	**Log2 Fold Change**	**Adjusted *P* value**	**Gene**	**Log2 Fold Change**	**Adjusted *P* value**	**Gene**	**Log2 Fold Change**	**Adjusted *P* value**	**Gene**	**Log2 Fold Change**	**Adjusted *P* value**
Ifit3b	11.50	4.73E-18	*Ifit3b*	11.50	4.73E-18	*Ifit3b*	11.50	4.73E-18	*Ifit1*	1.67	0.043
Ifi205	9.78	1.70E-12	*Ifi205*	9.78	1.70E-12	*Ifi205*	9.78	1.70E-12	*Pak1*	1.33	2.83E-05
Zfp365	9.27	0.049	*Zfp365*	9.27	0.049	*Zfp365*	9.27	0.049	*Cxcl2*	1.26	0.0044
Ifit1bl1	8.77	1.15E-18	*Ifit1bl1*	8.77	1.15E-18	*Ifit1bl1*	8.77	1.15E-18	*Cxcl3*	1.25	0.012
Ifit3	8.71	1.02E-07	*Ifit3*	8.71	1.02E-07	*Ifit3*	8.71	1.02E-07	*Gzmb*	1.16	3.82E-08
Ifi44	8.37	5.60E-07	*Ifi44*	8.37	5.60E-07	*Ifi44*	8.37	5.60E-07	*Gla*	1.16	1.60E-07
Trim30c	8.32	1.49E-07	*Trim30c*	8.32	1.49E-07	*Trim30c*	8.32	1.49E-07	*Uty*	1.15	2.13E-05
Dmxl2	7.99	0.00035777	*Dmxl2*	7.99	0.00035777	*Dmxl2*	7.99	0.00035777	*Rgs1*	1.14	6.67E-05
Tarm1	7.60	4.92E-05	*Tarm1*	7.60	4.92E-05	*Tarm1*	7.60	4.92E-05	*Dimt1*	1.12	0.012
Slfn4	7.58	7.52E-12	*Slfn4*	7.58	7.52E-12	*Slfn4*	7.58	7.52E-12	*C9orf72*	1.11	0.0007
Rasal1	7.41	0.003	*Rasal1*	7.41	0.003	*Rasal1*	7.41	0.003	*Gzmc*	1.11	0.0020
Clec10a	7.29	0.00012696	*Clec10a*	7.29	0.00012696	*Clec10a*	7.29	0.00012696	*Gas5*	1.10	0.024
Brd3os	7.26	0.00284105	*Brd3os*	7.26	0.00284105	*Brd3os*	7.26	0.00284105	*Eif2s3y*	1.08	0.0001
Apod	7.25	0.00014171	*Apod*	7.25	0.00014171	*Apod*	7.25	0.00014171	*Ifi213*	1.07	0.0053
Nos1ap	7.11	0.01	*Nos1ap*	7.11	0.01	*Nos1ap*	7.11	0.01	*Snhg15*	1.07	0.0059
Dlg2	7.10	0.007	*Dlg2*	7.10	0.007	*Dlg2*	7.10	0.007	*Gatad2b*	1.06	0.025
G530011O06Rik	6.95	0.00121259	*G530011O06Rik*	6.95	0.00121259	*G530011O06Rik*	6.95	0.00121259	*Bclaf3*	1.05	0.0079

Phf11d	6.92	0.00042334	*Phf11d*	6.92	0.00042334	*Phf11d*	6.92	0.00042334	*Malat1*	1.05	0.0001
Neo1	6.90	0.01	*Neo1*	6.90	0.01	*Neo1*	6.90	0.01	*Fam208b*	1.04	0.022
Spic	6.83	0.00183254	*Spic*	6.83	0.00183254	*Spic*	6.83	0.00183254	*Tgtp2*	1.03	0.0017
Nmrk1	-1.49	2.55E-05	*Nmrk1*	-1.49	2.55E-05	*Nmrk1*	-1.49	2.55E-05	*Rfx1*	-1.03	0.040
Cd200r1	-1.51	0.03	*Cd200r1*	-1.51	0.03	*Cd200r1*	-1.51	0.03	*Coro2b*	-1.04	0.0009
Bpnt1	-1.53	4.19E-08	*Bpnt1*	-1.53	4.19E-08	*Bpnt1*	-1.53	4.19E-08	*Plod1*	-1.04	0.0081
AI506816	-1.53	4.47E-07	*AI506816*	-1.53	4.47E-07	*AI506816*	-1.53	4.47E-07	*Pgap3*	-1.04	0.024
Cables1	-1.59	0.04	*Cables1*	-1.59	0.04	*Cables1*	-1.59	0.04	*Scap*	-1.04	0.010
Samd11	-1.79	0.02	*Samd11*	-1.79	0.02	*Samd11*	-1.79	0.02	*Chtf8*	-1.06	0.013
Prr7	-2.15	0.00044536	*Prr7*	-2.15	0.00044536	*Prr7*	-2.15	0.00044536	*Fig4*	-1.06	0.013
Tnfrsf9	-2.19	3.84E-08	*Tnfrsf9*	-2.19	3.84E-08	*Tnfrsf9*	-2.19	3.84E-08	*Slc9a1*	-1.11	0.011
Igsf5	-2.41	0.00013935	*Igsf5*	-2.41	0.00013935	*Igsf5*	-2.41	0.00013935	*Atp13a2*	-1.13	0.039
Mvk	-2.42	1.09E-10	*Mvk*	-2.42	1.09E-10	*Mvk*	-2.42	1.09E-10	*Syne3*	-1.13	0.0034
Jchain	-3.11	0.01	*Jchain*	-3.11	0.01	*Jchain*	-3.11	0.01	*Gdpd5*	-1.14	0.036
Ly6d	-3.40	0.03	*Ly6d*	-3.40	0.03	*Ly6d*	-3.40	0.03	*Cad*	-1.14	0.028
Mpzl2	-3.53	0.04	*Mpzl2*	-3.53	0.04	*Mpzl2*	-3.53	0.04	*Rnpepl1*	-1.16	0.0010
Ovol2	-3.91	0.04	*Ovol2*	-3.91	0.04	*Ovol2*	-3.91	0.04	*Arsa*	-1.17	0.0031
Cav1	-4.37	0.00019852	*Cav1*	-4.37	0.00019852	*Cav1*	-4.37	0.00019852	*Myo1c*	-1.23	0.024
Iglv1	-4.60	0.00064841	*Iglv1*	-4.60	0.00064841	*Iglv1*	-4.60	0.00064841	*Arid2*	-1.37	0.0010
Alas2	-5.20	0.0012915	*Alas2*	-5.20	0.0012915	*Alas2*	-5.20	0.0012915	*Plxdc2*	-1.48	0.0006
Cd19	-5.34	0.02	*Cd19*	-5.34	0.02	*Cd19*	-5.34	0.02	*Chst2*	-1.50	0.0054
Iglc3	-5.93	1.84E-05	*Iglc3*	-5.93	1.84E-05	*Iglc3*	-5.93	1.84E-05	*Prr7*	-1.54	0.0017
Ighv9-3	-6.47	0.01	*Ighv9-3*	-6.47	0.01	*Ighv9-3*	-6.47	0.01	*Gsn*	-1.91	6.54E-06

3.4 Discussion

In this study, I observed upregulation of CD69 in lung MAIT cells of mice subjected to bleomycin challenge. This activation manifested earlier and more intensely than in non-MAIT αβ T cells, underscoring the rapid response of MAIT cells to sterile injury. There was substantial impairment in MAIT cell accumulation in both *Il18r1*$^{-/-}$ *and Ifnar1*$^{-/-}$ mice, whilst MAIT cell CD69 upregulation was significantly impaired only in the *Ifnar1*$^{-/-}$ mice, consistent with our previous studies in murine influenza infection (van Wilgenburg *et al.*, 2018). Our findings suggest that bleomycin-induced responses are strongly cytokine-driven, with IFN-α emerging as the dominant activating cytokine in this model of sterile challenge.

Although MAIT cells have never been assessed in pulmonary fibrosis, murine skin resident MAIT cells exhibit a distinct tissue repair transcriptional signature (Constantinides *et al.*, 2019), similar to H2-M3 restricted CD8^{+} T cells (Linehan *et al.*, 2018), and seen in TCR-activated MAIT cells in humans and mice (Hinks *et al.*, 2019; Lamichhane, Schneider*, et al.*, 2019; Leng *et al.*, 2019), indicating their local repair programme similar to other tissue resident cell types. MAIT cells have also been implicated in models of collagen-induced arthritis (Chiba *et al.*, 2012) and chronic liver injury (Hegde *et al.*, 2018), where their absence diminished inflammation and pathology, and their presence intensified these conditions. Pharmacological inhibition of MAIT cells alleviated fibrosis, hinting at interactions with monocytes/macrophages (Mabire *et al.*, 2023).

While most transcriptomic analyses in existing literature have focused on the tissue repair programme of MAIT cells under an MR1-TCR dependent activation pathway, recent published research suggests that cytokine involvement might also play a role (du Halgouet *et al.*, 2023).

My research demonstrates for the first time that both a sterile chemical insult, namely a bleomycin challenge, and a viral infection can trigger such a tissue repair programme in a cytokine-dependent manner, suggesting a functional versatility and broader applicability of the underlying mechanisms governing MAIT cell activation than previously recognised. Specifically, the bleomycin challenge led to a transient activation of the tissue repair programme in MAIT cells, with notable upregulation by day 3. In contrast, a sustained activation was observed following PR8 challenge, persisting for at least seven days post-infection. Collectively, these results enriched the understanding of the dynamic role of MAIT cells in tissue repair processes. Future research would be valuable into the cytokine-dependent activation pathway and their connection to the tissue repair programme of MAIT cells.

3.5 Conclusion

- MAIT cells accumulate and are activated by bleomycin stimulation in a cytokine-dependent way.
- Both Bleomycin challenge and PR8 influenza virus infection activate the tissue repair programme of lung MAIT cells.

4 MAIT Cells Protect Against Sterile Lung Injury

4.1 Introduction

As mentioned, MAIT cells are abundant in the lung, implying an essential role for MAIT cells in pulmonary mucosal immunology, particularly during the initial stages of an immune response, yet our understanding of the full repertoire of MAIT cell functions remains incomplete, particularly in the context of tissue injury and repair. Increasing evidence implicates MAIT cells in bridging innate and adaptive immunity, an important role being the recruitment of other immune cells, particularly DC and monocytes during TCR-dependent (Meierovics *et al.*, 2013; Meierovics & Cowley, 2016; Philipp, 2020) and cytokine-dependent activation (Provine *et al.*, 2021; van Wilgenburg *et al.*, 2018).

4.1.1 MAIT cell communication with DC

MAIT cells highly express CD161 (NKR-P1A), a C-type lectin-like membrane receptor whose ligand is lectin-like transcript 1 (LLT1) found on activated B cells and TLR-activated DCs (Le Bourhis *et al.*, 2013). Prior studies have shown that communication with DC is important in responses of unconventional T cells to *S. pneumoniae (*Ivanov *et al., 2012)*, and it has been speculated that MAIT cell communication with DCs could be important for antimicrobial responses (Gold *et al.*, 2015; Sharma *et al.*, 2015), particularly MAIT cells promoting early differentiation of monocytes into DCs (Meierovics & Cowley, 2016), but they could also be relevant in sterile tissue injury.

4.1.2 Lung conventional dendritic cells

Strategically located within the airway epithelium and interstitium, pulmonary DCs bridge the external and internal environments (Holt *et al.*, 1989; von Garnier *et al.*, 2005). The lung features two distinct conventional DC subsets (cDC, $MHCII^+$ $CD11c^+$): $CD103^+$ type 1 cDC ($CD103^+$ $CD11b^{lo/-}$ $XCR1^+$ $DNGR\text{-}1^+$ $SIRP\text{-}\alpha^-$ $CX3CR1^-$ $F4/80^-$, cDC1) and $CD11b^+$ type 2 cDC ($CD11b^{hi}$ $CD103^-SIRP\text{-}\alpha^+$ $CX3CR1^+$ $F4/80^+$, cDC2) (Guilliams *et al.*, 2013). cDC1 specialize in cross-presenting antigens to $CD8^+$ T cells and promoting Th1 cells. In contrast, cDC2 excel at stimulating $CD4^+$ T cell responses, mainly Th2 or Th17 cells. Lung cDCs originate from common dendritic cell precursors (CDPs) in the bone marrow. These CDPs mature into precursor dendritic cells (pre-DCs), which migrate to the lungs through the bloodstream and differentiate into either cDC1 or cDC2 subsets guided by local signals and specific transcription factors (Liu *et al.*, 2009; Onai *et al.*, 2013; Schlitzer *et al.*, 2015).

DCs play a regulatory role in pulmonary fibrosis, accumulating in the lungs in idiopathic pulmonary fibrosis (IPF) patients (Greer *et al.*, 2014; Marchal-Sommé *et al.*, 2007; Tsoumakidou *et al.*, 2009) and in bleomycin mouse models (Bantsimba-Malanda *et al.*, 2010; Chakraborty *et al.*, 2017), whilst diminishing in the circulation (Galati *et al.*, 2020). Pulmonary cDC1s increase with bleomycin treatment but are reduced with transforming growth factor (TGF)-β inhibition, suggesting anti-inflammatory and anti-fibrotic roles in pulmonary fibrosis (Chakraborty *et al.*, 2017). Moreover, increased fibrosis severity and impaired lung function were seen in DC-deficient mice, but mitigated when DC counts were boosted (Tort Tarrés *et al.*, 2019), though their protective mechanism is still unclear.

4.1.3 The role of cDC1 and DNGR-1 signalling in the regulation of lung tissue damage

DNGR-1, encoded by Clec9a, is a C-type lectin receptor predominantly expressed on cDC1 in both mice and humans. Originally recognised for its association with dendritic cells, DNGR-1 has attracted considerable attention for its role in detecting and responding to cellular necrosis (Sancho *et al.*, 2009). The receptor binds to F-actin, typically sequestered within the intracellular milieu of healthy cells but becomes exposed during necrosis when plasma membrane integrity is compromised. Engagement with F-actin enables DNGR-1 to signal through SYK, facilitating the cross-presentation of antigens from necrotic cells (Sancho *et al.*, 2009; Zhang *et al.*, 2012). This process is crucial for initiating adaptive immune responses, particularly in tumour immunology (Cueto *et al.*, 2021; Giampazolias *et al.*, 2021; Lim *et al.*, 2022) and in combating viral infections including vaccinia virus (Iborra *et al.*, 2012), influenza A virus (Iborra *et al.*, 2016) and herpes simplex virus-1(Zelenay *et al.*, 2012). DNGR-1 has been suggested as a potential target for cancer immunotherapy and vaccine development (Henry *et al.*, 2023; Iborra *et al.*, 2012).

Beyond its established function in generating CD8+ T cell responses to antigens associated with dead cells, DNGR-1 is increasingly recognised for its role in moderating tissue damage in various pathological conditions (Del Fresno *et al.*, 2018). Mice deficient in DNGR-1 exhibit exacerbated neutrophil recruitment during caerulein-induced acute pancreatitis. Neutrophils, while essential for defending against infectious diseases, can also cause tissue damage. DNGR-1 serves to limit the recruitment of neutrophils to sterile injured tissues, thereby providing negative feedback to tissue damage. This effect is also observed in *Rag1*-deficient mice, which lack T and B cells, indicating that the function of DNGR-1 is independent of its role in antigen

cross-presentation (Del Fresno *et al.*, 2018). In kidney damage induced by *Candida albicans* infection, DNGR-1 mitigates neutrophil infiltration and subsequent tissue damage, reducing morbidity and mortality.

Neutrophils are identified as the principal mediators of increased immunopathology in DNGR-1-deficient mice, and their depletion in disease models prevents the escalation of tissue damage. Moreover, the administration of anti-DNGR-1 blocking antibodies mirrors the increased neutrophil infiltration observed in WT mice but not in *Batf3*-deficient mice, which underscores the importance of cDC1s in this process. Intriguingly, DNGR-1 activation does not prompt cytokine production in cDC1s (Sancho *et al.*, 2009; Zelenay *et al.*, 2012). However, when engaged with a synthetic ligand containing F-actin/myosin II (Schulz *et al.*, 2018), DNGR-1 attenuates the expression of pro-inflammatory genes, such as *Tnf*, *Cxcl2*, and *Egr2*, in cDC1s in response to whole glucan particles, a mimic for *C. albicans* recognition through Dectin-1 (Del Fresno *et al.*, 2018). Given that CXCL2 is a key chemokine driving neutrophil migration to sites of inflammation during *C. albicans* infection (Balish *et al.*, 1999) (Eash *et al.*, 2010), the use of pepducin, a peptide inhibitor of CXCR2 (the principal CXCL2 receptor), reverses the increased neutrophil recruitment in DNGR-1-deficient mice (Del Fresno *et al.*, 2018). Bone marrow chimera experiments have further clarified that *Cxcl2* expression by cDC1s is necessary for the pronounced neutrophilia in the absence of DNGR-1 (Del Fresno *et al.*, 2018). Hence, DNGR-1 plays a dual role: it contributes to adaptive immunity by promoting CD8+ T cell cross-priming and regulates innate immune responses by cDC1s by modulating inflammatory signals that govern neutrophil influx into injured tissues, suggesting a potential role of cDC1-DNGR-1 in modulating the balance between inflammation and fibrosis in the injured lung.

In this study, I aim for the first time to define the role of MAIT cells in sterile lung injury and to investigate the underlying mechanisms. I employed a model of lung injury using bleomycin: a potent chemotherapeutic agent, with a well-characterised side effect profile of acute lung injury, followed by a chronic phase with pathological hallmarks of human IPF *(Tashiro et al., 2017)*. I have discovered for the first-time an *in vivo* mechanism by which pulmonary MAIT cells make an important contribution to protection against sterile lung tissue damage in mice.

4.2 Aim

To understand MAIT cells' effects within the context of sterile lung injury induced by bleomycin treatment and explore potential mechanisms.

4.3 Results

4.3.1 MAIT cell-deficient mice show dysregulated pulmonary immune responses upon bleomycin challenge

I sought to determine whether the recruitment and activation of MAIT cells in response to bleomycin have an impact on the phenotype. To this end, I assessed weight loss and tissue damage between WT and MAIT cell-deficient *Mr1*$^{-/-}$ mice. Both WT and *Mr1*$^{-/-}$ mice were subjected to 10^6 CFU *Salmonella* Typhimurium BRD509 infection to expand the MAIT cell population followed by intratracheal bleomycin administration four weeks post-MAIT cell enrichment (Figure 3.5). Notably, *Mr1*$^{-/-}$ mice exhibited more substantial weight loss (Figure 4.1A), heightened tissue damage (Figure 4.1B), and increased gene expression of *Col1α1* and *Col3α1* compared to WT mice (Figure 4.1, C and D). Hydroxyproline levels in the lungs showed no significant difference between WT and *Mr1*$^{-/-}$ mice (Figure 4.1E).

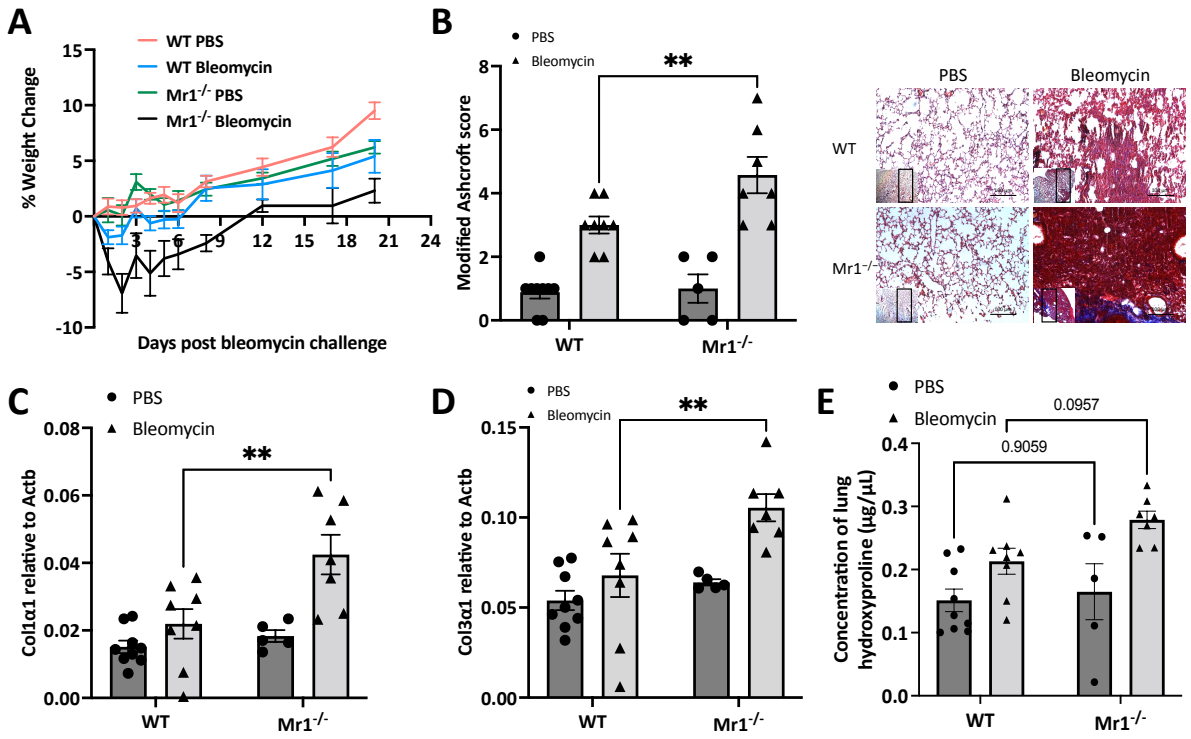

Figure 4.1 *Mr1*$^{-/-}$ mice show more severe weight loss and tissue damage than WT mice post bleomycin challenge.

(A) Body weight loss expressed as a percentage of the weight before bleomycin challenge. (**B** and **C**) Modified Ashcroft score (**B**) and representative images (**C**) of lung slices of PBS or bleomycin-challenged WT and *Mr1*$^{-/-}$ mice at day 21, stained with Masson's trichrome. (**D**) Gene expression of *Col1α1*, and *Col3α1* in lung homogenates of PBS or bleomycin-challenged WT and *Mr1*$^{-/-}$ mice at day 21. *Actb* was used as a housekeeping gene. (**E**) Hydroxyproline concentration in WT and *Mr1*$^{-/-}$ mice at D21 after bleomycin. Data (mean ± SEM) are one representative experiment of two independent experiments, with 5–9 mice per group in each

replicate. Statistical significance tested by two-way ANOVA with Holm-Sidak's multiple comparisons test.

To assess whether pre-infection with *Salmonella* Typhimurium BRD509 is necessary for the protective effects of MAIT cells, I evaluated weight loss in WT and *Mr1*$^{-/-}$ mice, without prior *Salmonella* Typhimurium BRD509 infection. Remarkably, even in the absence of pre-infection, *Mr1*$^{-/-}$ mice experienced significantly greater weight loss compared to WT mice (Figure 4.2). This indicates that the protective role of MAIT cells does not rely on prior infection with *Salmonella* Typhimurium BRD509. Given that the MAIT cell-boosted mouse model more accurately reflects MAIT cell frequencies seen in human lungs – where these cells account for up to 10% of the total T cell population – for subsequent experiments I continued to use this model with pre-infection to investigate the protective effects of MAIT cells in the context of bleomycin-induced lung injury.

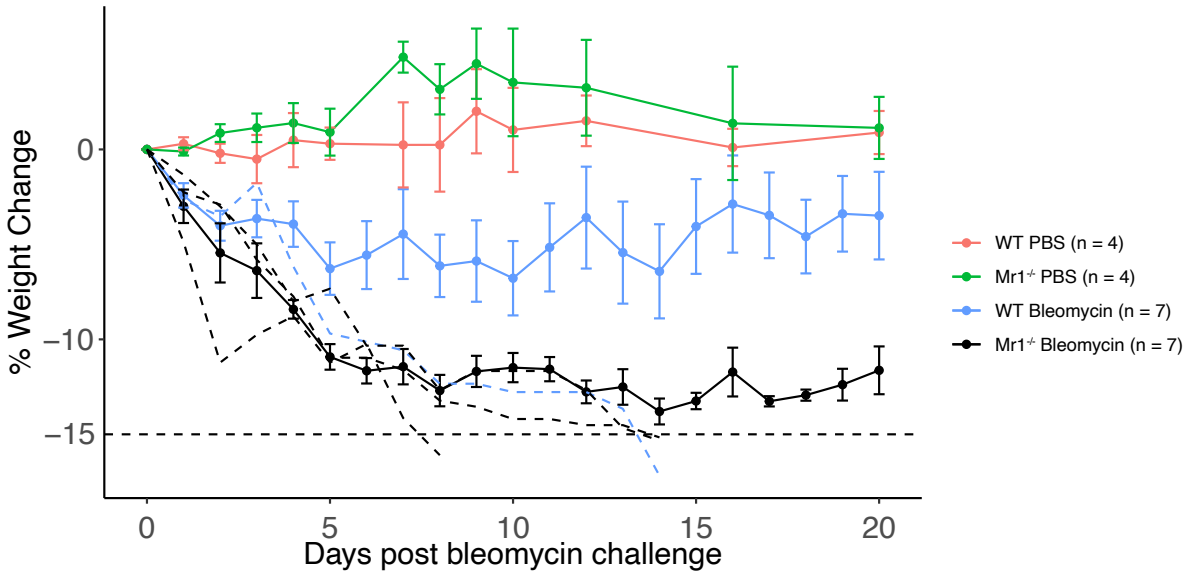

Figure 4.2 Body weight loss expressed as a percentage of the weight before bleomycin challenge.

Experiments were conducted using naïve mice that had not undergone pre-infection with *Salmonella* Typhimurium BRD509. Data are one representative experiment of two independent experiments, with 4–7 mice per group in each replicate. Graphs show mean weights ± SEM for all mice within the group, with individual plots (dotted line) for those animals that succumbed to the bleomycin challenge.

To elucidate the mechanism underlying the observed phenotypic differences, I evaluated immune cell infiltration between WT and *Mr1*$^{-/-}$ mouse lungs using spectral flow cytometry analysis (Cytek Aurora) following a published gating strategy (Svedberg *et al.*, 2019) (Figure 4.3). Lung samples were collected on days 0, 3, 7 and 10 post challenge (Figure 3.5). *Mr1*$^{-/-}$ mice exhibited a decreased frequency of DCs (MerTK^{-} CD11c^{+} MHCII^{+}) on days 3 and 7, and

an increased frequency of monocytes on day 3 post bleomycin challenge. Notably, differences in the frequencies of alveolar macrophages, interstitial macrophages, neutrophils, eosinophils, NK cells, NK T cells, $CD4^+$ T cells, $CD8^+$ T cells, and γδ-T cells post-challenge between WT and *Mr1*$^{-/-}$ mice were not statistically significant (Figure 4.4 and Figure 4.5).

Myeloid cells gating strategy

Debris clean → CD45+ → Singlets → Live cells → CD19- cells (Not Gate) → NK1.1- cells (Not Gate) → CD4- cells (Not Gate) → CD8- cells (Not Gate)

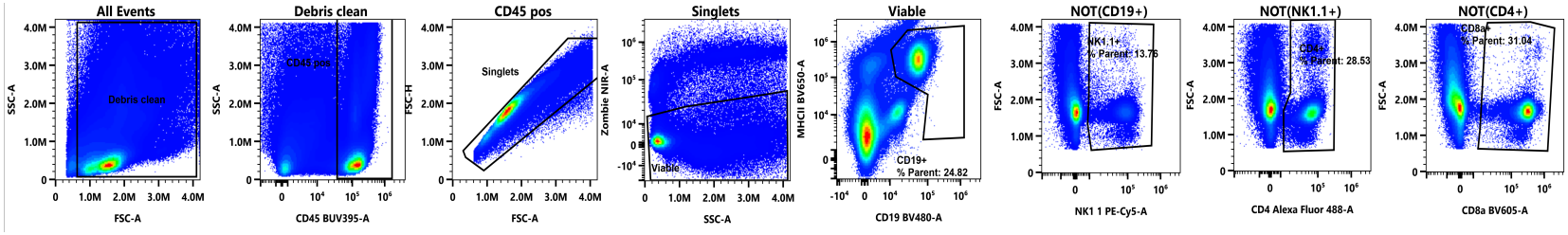

→ CD11b+ Ly6G+ Neutrophils → MerTK+ CD64+/ MerTK- cells (Not Neutrophils Gate) → AlvMs and IntMs

Siglec-F+ eosinophils → MHCII+ CD11C+ DCs (Not eosinophils Gate) → CD11b+ Ly6C+ monocytes (Not DCs Gate)

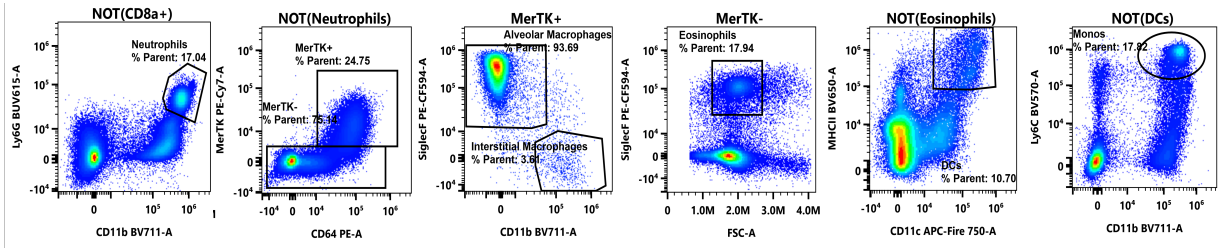

Lymphocytes gating strategy

CD11b- cells → Lymphocytes → Lymph singlets → B cells → NK/NK T cells CD3+ T cellls → γδ T cells → CD4/CD8+ T cells

Gated on CD45+ single live cells

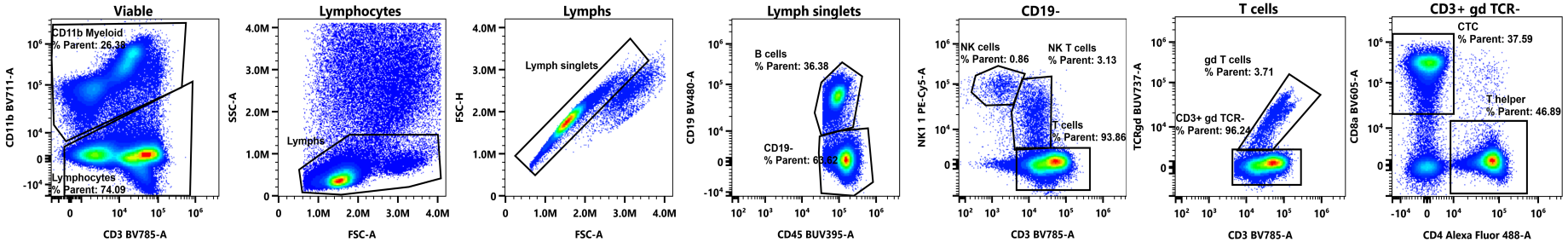

Figure 4.3 Flow cytometry gating strategy for the identification of pulmonary myeloid cells and lymphocytes.

Representative flow cytometry plots showing gating for cells isolated from mouse lung tissue to identify neutrophil ($CD11b^+$ $Ly6G^+$), eosinophil ($MerTK^-$ $Siglec\text{-}F^+$), alveolar macrophage ($MerTK^+$ $CD64^+$ $CD11b^-$ $Siglec\text{-}F^+$), interstitial macrophage ($MerTK^+$ $CD64^+$ $CD11b^+$ $SiglecF^-$), dendritic cell ($MerTK^-$ $CD11c^+$ $MHCII^+$), monocyte ($MerTK^-$ $CD64^+$ $CD11b^+$ $Ly6C^+$), B cell (CD3- CD19+), $CD4^+$ T cell ($CD3^+$ $CD19^-$ $CD4^+$), $CD8^+$ T cell ($CD3^+$ $CD19^-$ $CD8^+$), NK cells ($CD3^-$ $NK1.1^+$), NK T cell ($CD3^+$ $NK1.1^+$), and $\gamma\,\delta$-T cell (TCR $\gamma\,\delta^+$) populations.

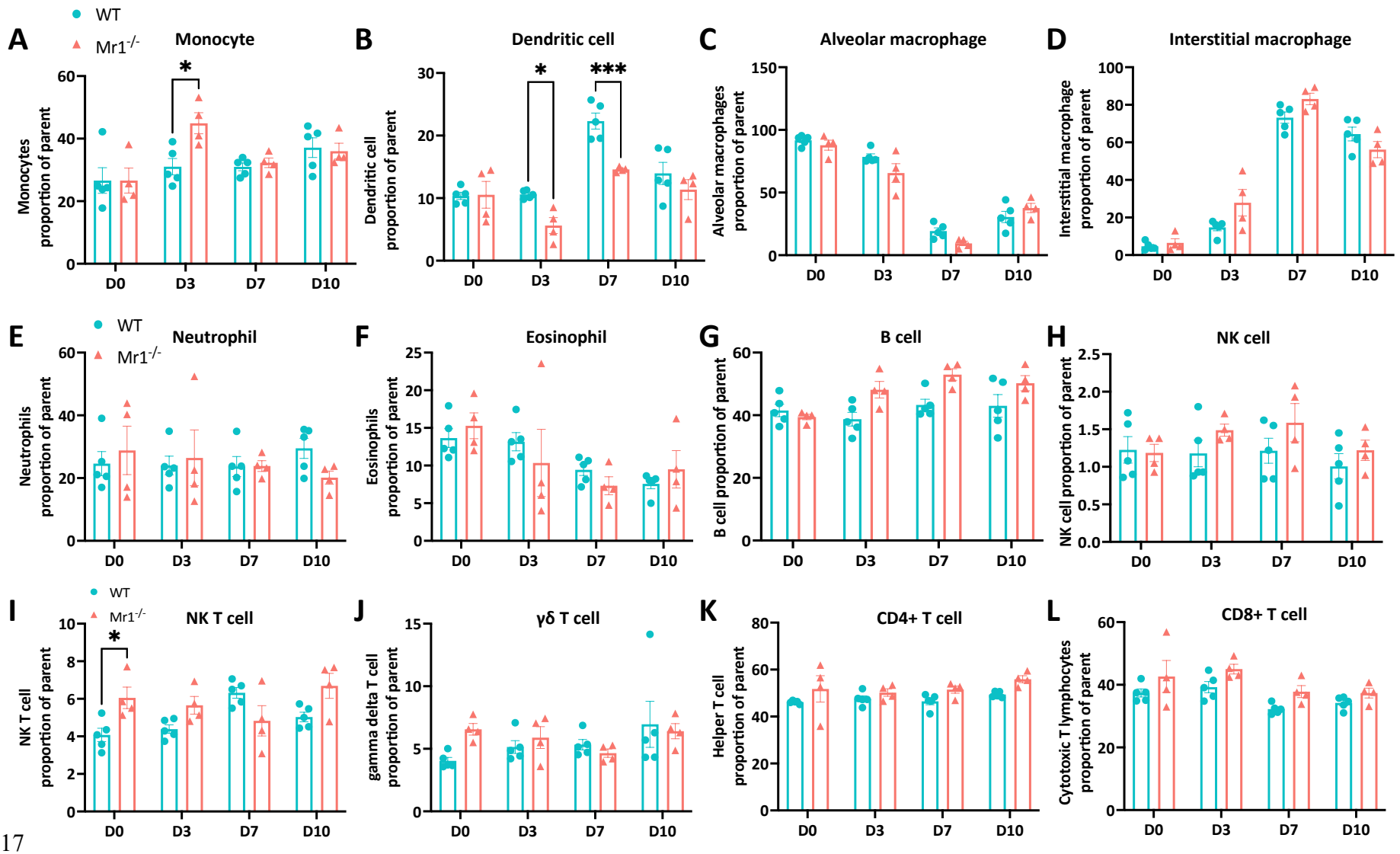
A
Monocyte
Monocytes proportion of parent
B
Dendritic cell
Dendritic cell proportion of parent
C
Alveolar macrophage
Alveolar macrophages proportion of parent
D
Interstitial macrophage
Interstitial macrophage proportion of parent
E
Neutrophil
Neutrophils proportion of parent
F
Eosinophil
Eosinophils proportion of parent
G
B cell
B cell proportion of parent
H
NK cell
NK cell proportion of parent
I
NK T cell
NK T cell proportion of parent
J
γδ T cell
gamma delta T cell proportion of parent
K
CD4+ T cell
Helper T cell proportion of parent
L
CD8+ T cell
Cytotoxic T lymphocytes proportion of parent
WT
Mr1-/-
D0
D3
D7
D10

Figure 4.4 Frequencies of indicated cell types (percentages of parent) in in WT and *Mr1*$^{-/-}$ mice lungs after bleomycin challenge.

Frequencies of monocyte (A), dendritic cell (B), alveolar macrophage (**C**), interstitial macrophage (**D**), neutrophil (**E**), eosinophil (**F**), B cell (**G**), NK cell (**H**), NK T cell (**I**), γ δ-T cell (**J**), helper T cell (**K**) and cytotoxic T cell (**L**) as percentages of parent in WT and *Mr1*$^{-/-}$ mice lungs after bleomycin challenge. Data are one representative experiment of two independent experiments, with 4–6 mice per group in each replicate. Graphs show mean ± SEM. Statistical significance tested by two-way ANOVA with Holm-Sidak's multiple comparisons test; **P* < 0.05, ***P* < 0.01, ****P* < 0.001.

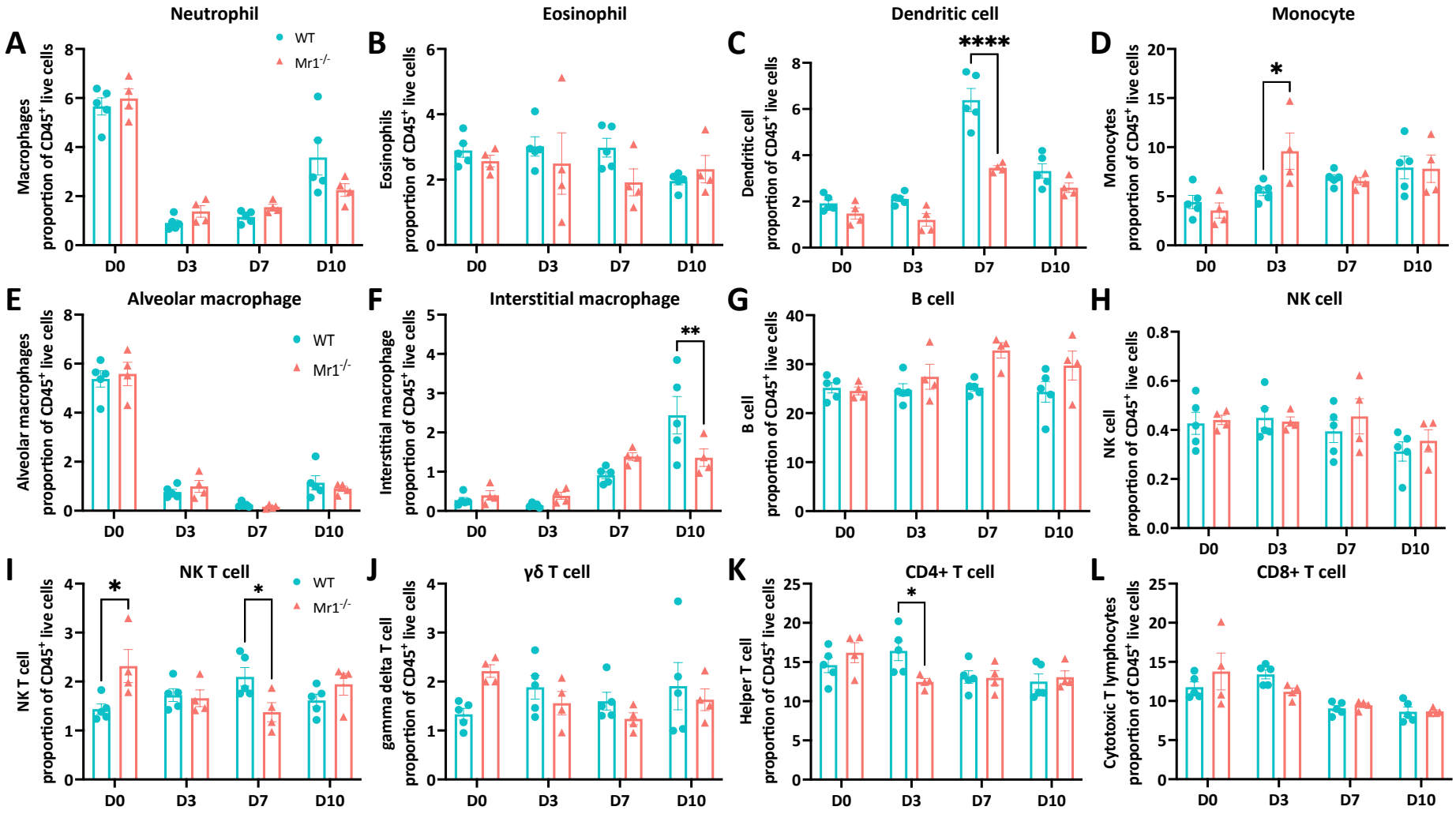
A
Neutrophil
Macrophages proportion of CD45+ live cells
WT
Mr1-/-
B
Eosinophil
Eosinophils proportion of CD45+ live cells
C
Dendritic cell
Dendritic cell proportion of CD45+ live cells
****
D
Monocyte
Monocytes proportion of CD45+ live cells
*
E
Alveolar macrophage
Alveolar macrophages proportion of CD45+ live cells
F
Interstitial macrophage
Interstitial macrophage proportion of CD45+ live cells
**
G
B cell
B cell proportion of CD45+ live cells
H
NK cell
NK cell proportion of CD45+ live cells
I
NK T cell
NK T cell proportion of CD45+ live cells
J
γδ T cell
gamma delta T cell proportion of CD45+ live cells
K
CD4+ T cell
Helper T cell proportion of CD45+ live cells
L
CD8+ T cell
Cytotoxic T lymphocytes proportion of CD45+ live cells
D0
D3
D7
D10

Figure 4.5 Frequencies of indicated cell types (percentages of total live immune cells) in in WT and *Mr1*$^{-/-}$ mice lungs after bleomycin challenge.

Frequencies of neutrophil (A), eosinophil (B), dendritic cell (C), monocyte (D), alveolar macrophage (E), interstitial macrophage (F), B cell (G), NK cell (H), NK T cell (I), γδ-T cell (J), helper T cell (K) and cytotoxic T cell (L) as percentages of total live immune cells (Live CD45+ cells) in WT and *Mr1*$^{-/-}$ mice lungs. Data are one representative experiment of two independent experiments, with 4–6 mice per group in each replicate. Graphs show mean ± SEM. Statistical significance tested by two-way ANOVA with Holm-Sidak's multiple comparisons test; $*P < 0.05$.

I then investigated the transcriptomic variations between WT and *Mr1*$^{-/-}$ mouse lungs. Accordingly, I obtained bulk RNA-seq data from whole lungs pre-infected with *Salmonella* Typhimurium BRD509 and challenged with bleomycin. Lung samples were collected on days 0, 3, 7, 14 and 21 post challenge (Figure 3.5). Compared with WT mice, 9 (3 up, 6 down), 1,729 (967 up, 762 down), 116 (54 up, 62 down), 173 (65 up, 108 down) and 192 (107 up, 85 down) genes were differentially expressed in *Mr1*$^{-/-}$ mice lungs at days 0, 3, 7, 14 and 21 post-bleomycin challenge, respectively (Figure 4.6A and B, and Table 4-1).

The gene expression of the chemokine *Ccl2* (monocyte chemoattractant protein-1, *Mcp-1*), which recruits myeloid cells to sites of inflammation, and the proinflammatory cytokine *Il6*, were prominently upregulated in *Mr1*$^{-/-}$ mice at day 3 (Figure 4.6B). Both CCL2 and IL-6 are known contributors to lung fibrosis (Liu *et al.*, 2007). GO enrichment analysis for biological processes (Ashburner *et al.*, 2000) revealed only 3 significantly enriched ($P < 0.05$) upregulated gene sets in *Mr1*$^{-/-}$ mice lungs versus WT mice lungs without bleomycin challenge (Figure 4.6C), but 1,526 significantly enriched gene sets at day 3 post-bleomycin, of which the top ranked terms include leukocyte migration, regulation of cytokine production, regulation of response to external stimulus, cell adhesion, migration and chemotaxis (Figure 4.6D).

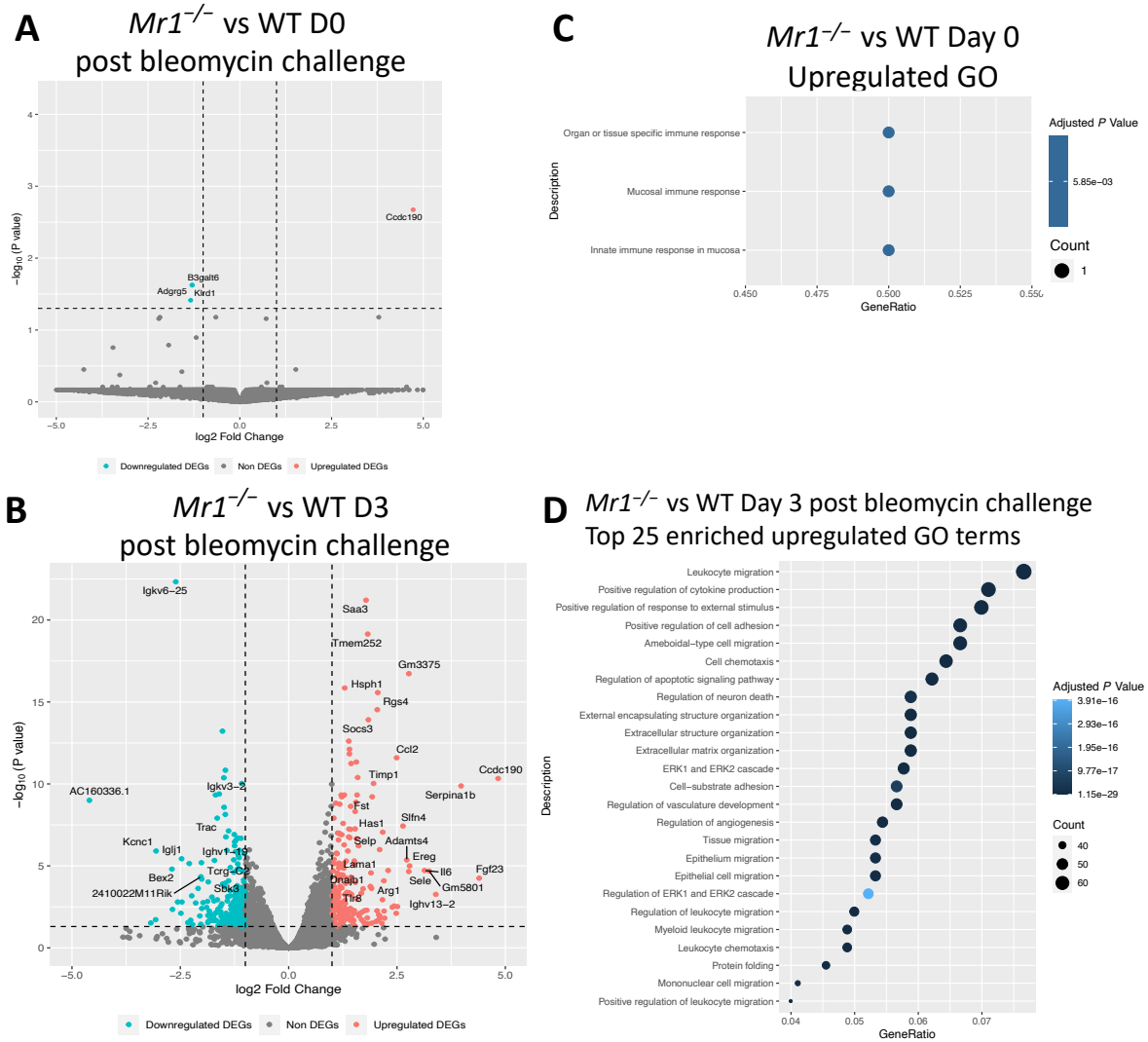

Figure 4.6 Dysregulated immune responses in the lungs of MAIT cell-deficient mice following bleomycin challenge.

(**A**)Volcano plot of DEGs [log2 fold change (FC) > 1, adjusted $P < 0.05$] in whole lung tissue from WT and *Mr1*$^{-/-}$ mice lungs without bleomycin challenge (Day 0) (n=3/group). All up and down-regulated genes are labelled. Horizontal line indicates *P* value threshold of 0.05. Vertical line indicates log2 fold change threshold of 1. (**B**) Volcano plot of DEGs [log2 fold change (FC) > 1, adjusted $P < 0.05$] in whole lung tissue between *Mr1*$^{-/-}$ and WT mice lungs at **day 3**

post-bleomycin challenge. The top up and down-regulated genes are labelled. Horizontal line indicates *P* value threshold of 0.05. Vertical line indicates log2 fold change threshold of 1. (**C**) All significantly enriched ($P < 0.05$) upregulated pathways from Gene Ontology (GO) database (biological process) in upregulated DEGs in the lungs of $Mr1^{-/-}$ mice compared with WT mice lungs without bleomycin challenge (**Day 0**). (**D**) Top 25 significantly enriched ($P < 0.05$) pathways from GO database (biological process) in upregulated DEGs in the lungs of $Mr1^{-/-}$ mice compared with WT mice lungs at day 3 post-bleomycin challenge. For Figure 4.6C and D, colour intensity indicates the statistical significance of the enrichment, and dot size signifies the number of genes upregulated in the pathway. The x axis denotes the proportion of all DEGs included in the pathway (Gene Ratio).

Notably, expression of *Xcr1* and *Clec9a*, markers of DC (Merad *et al.*, 2013) – and *Flt3l* and *Ccr10*, both essential for DC development and recruitment (Liu *et al.*, 2021; Merad *et al.*, 2013), were significantly downregulated in $Mr1^{-/-}$ mice relative to WT mice at day 3 post-bleomycin (Figure 4.7), consistent with downregulation of the DC population in $Mr1^{-/-}$ mice relative to WT after bleomycin challenge shown in flow cytometry (Figure 4.4B and Figure 4.5C). My data imply that MAIT cells may modulate the accumulation of immune cells in the lung after sterile lung challenge, notably DCs, during sterile lung challenges.

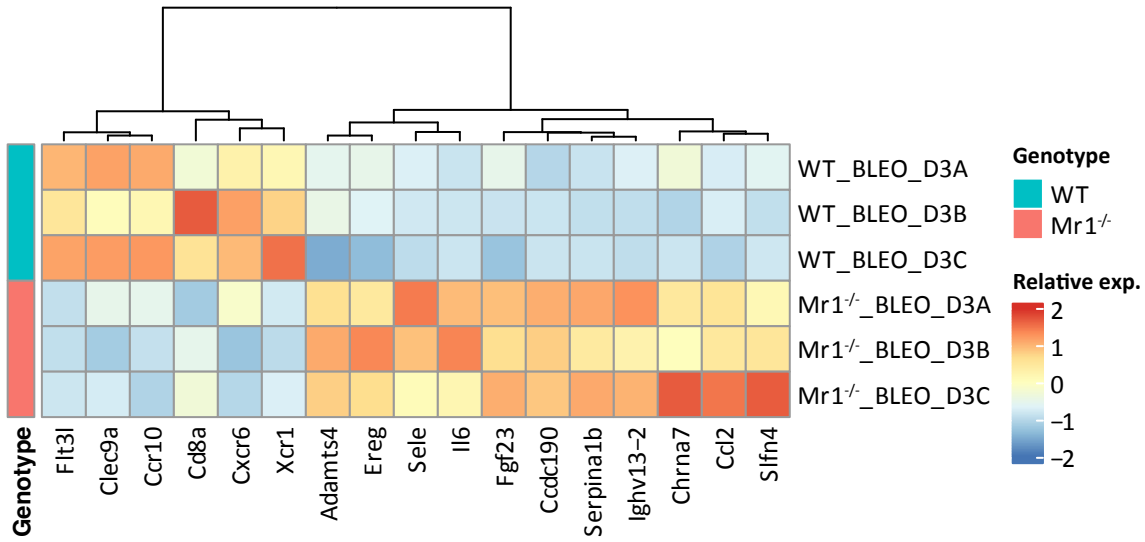

Figure 4.7 Heatmap depicting relative expression of selected genes in mice lungs (*Mr1*$^{-/-}$ versus WT).

4.3.2 Early accumulation of pulmonary CD103+ type 1 DCs is impaired in *Mr1*$^{-/-}$ mice

I subsequently aimed to explore the subpopulations of DCs to determine which subsets contributed to the decreased accumulation observed in *Mr1*$^{-/-}$ mice, following established guidelines (Cossarizza *et al.*, 2021) (Figure 4.8A). I noted an accumulation of CD45^{+} CD64^{-} CD11c^{+} MHCII^{+} cDCs (Figure 4.8B and E), particularly CD103^{+} cDC1, in lungs of WT mice on day 7 post-bleomycin. In contrast, *Mr1*$^{-/-}$ mice failed to accumulate CD103^{+} DCs, with significantly lower total count and percentage of pulmonary CD103^{+} DCs at day 7 post-challenge compared to WT counterparts (Figure 4.8C and F). There was also a tendency

towards impaired CD11b^{+} cDC2 accumulation in *Mr1*$^{-/-}$ lungs on day 7 post-bleomycin but this did not reach statistical significance (Figure 4.8D and G).

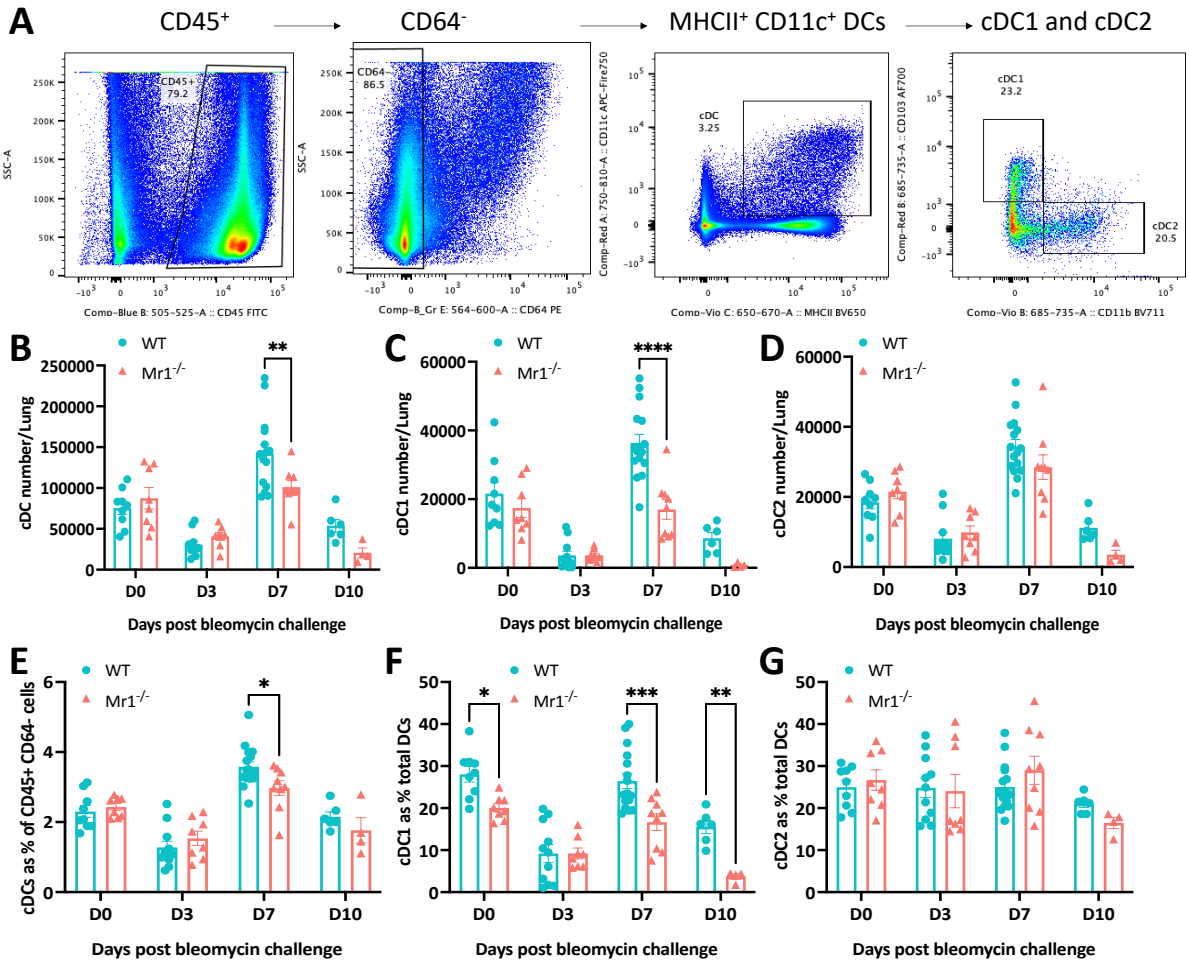

Figure 4.8 Early accumulation of CD103+ type 1 dendritic cells in the lungs upon bleomycin challenge is impaired in *Mr1*$^{-/-}$ mice.

(**A**) Representative flow cytometry plots of lung conventional dendritic cells (cDC), type 1 cDCs (cDC1) and type 2 cDCs (cDC2). (**B** to **D**) Absolute numbers of total cDCs (**B**), cDC1 (**C**) and cDC2 (**D**) in WT and *Mr1*$^{-/-}$ mice lungs post-bleomycin challenge. (**E**) Frequencies of

cDC as percentages of total $CD45^+$ $CD64^-$ cells in WT and *Mr1*$^{-/-}$ mice lungs. (**F** and **G**) Frequencies of cDC1 (**F**) and cDC2 (**G**) as percentages of total cDC population in WT and *Mr1*$^{-/-}$ mice lungs. Data (mean ± SEM) represent combined results from two independent experiments conducted on Days 0, 3, and 7, and one experiment on Day 10, with each group consisting of 3-6 mice.

Table 4-1 Top 20 upregulated and downregulated DEGs of total lung, *Salmonella* Typhimurium BRD509 pre-infected, *Mr1*$^{-/-}$ versus WT B6

DEGs MR1KO vs WT D0			DEGs MR1KO vs WT D3			DEGs MR1KO vs WT D7			DEGs MR1KO vs WT D14			DEGs MR1KO vs WT D14		
Gene	**Log2 Fold Change**	**Adjusted *P* value**	**Gene**	**Log2 Fold Change**	**Adjusted *P* value**	**Gene**	**Log2 Fold Change**	**Adjusted *P* value**	**Gene**	**Log2 Fold Change**	**Adjusted *P* value**	**Gene**	**Log2 Fold Change**	**Adjusted *P* value**
Ear-ps2	6.89	0.005	*Ccdc190*	4.83	4.64E-11	*Serpina1b*	4.26	0.0015	*Ighv1-84*	8.63	0.01	*Serpina1b*	4.23	0.0001
Rnase2a	6.56	0.02	*Fgf23*	4.40	5.61E-05	*Ccdc190*	4.09	7.90E-05	*Ear-ps2*	7.93	2.33E-05	*Ccdc190*	3.14	1.99E-05
Ccdc190	4.72	0.002	*Serpina1b*	3.98	1.33E-10	*Cd163l1*	2.25	0.0044	*Rnase2a*	3.00	0.04	*Zbtb16*	2.71	0.02
B3galt6	-1.29	0.02	*Ighv13-2*	3.40	0.0005	*Zbtb16*	1.59	0.0009	*Ccdc190*	2.66	0.010	*Cdh24*	2.06	0.0004
Adgrg5	-1.30	0.02	*Il6*	3.14	1.91E-05	*Rgs5*	1.27	0.04	*Igkv6-20*	2.50	0.01	*Per2*	1.85	7.41E-09
Klrd1	-1.34	0.04	*Ereg*	2.79	1.00E-05	*Fgfbp3*	1.20	0.03	*Ighv5-6*	2.38	0.01	*Tsc22d3*	1.72	1.73E-22
Gm10800	-6.32	0.0009	*Sele*	2.77	2.21E-05	*Ide*	1.08	1.08E-11	*Igkv3-4*	2.12	0.0006	*Ciart*	1.64	0.001
Jsrp1	-21.76	6.01E-05	*Adamts4*	2.73	4.32E-06	*Mmp28*	1.02	0.01	*Ighg1*	2.03	0.049	*Map3k6*	1.58	9.14E-07
Olfr518	-21.95	5.51E-05	*Slfn4*	2.64	3.70E-08	*Kif26a*	0.99	0.0001	*Sumo2*	1.83	0.002	*Hsph1*	1.50	0.0001
			Chrna7	2.51	0.003	*Rgs4*	0.93	0.047	*Krt79*	1.66	0.02	*Fam107a*	1.50	2.81E-05
			Ccl2	2.49	2.53E-12	*Slc16a9*	0.91	0.01	*AC160637.1*	1.62	0.04	*Mpp3*	1.50	0.008
			Fcrlb	2.48	0.008	*Hspa12b*	0.90	9.91E-06	*Klhl11*	1.56	0.04	*Fkbp5*	1.43	1.93E-10
			Hspa1b	2.43	0.003	*AC115954.1*	0.85	0.0079	*Pcdhgb2*	1.55	0.02	*Creb5*	1.41	0.003
			Dio2	2.39	0.003	*Tmod1*	0.82	0.02	*Pdpr*	1.46	0.002	*Per1*	1.40	2.92E-06
			Samd11	2.22	0.02	*Col4a3*	0.82	0.02	*Lrch3*	1.43	0.02	*Tmem181b-ps*	1.31	3.82E-05
			Chl1	2.20	0.006	*Fgd5*	0.81	0.0044	*Atp7a*	1.41	0.009	*Banp*	1.31	6.43E-05
			Serpina3h	2.20	8.12E-05	*Plpp1*	0.80	0.04	*Irs1*	1.41	0.04	*Nr4a3*	1.28	0.0004
			Has1	2.17	8.75E-08	*Timp3*	0.78	0.0069	*Nktr*	1.37	0.003	*Carmil3*	1.27	0.04
			Mmp8	2.17	0.001	*Frmd4a*	0.78	0.0015	*Vcl*	1.36	0.005	*Tmem252*	1.15	3.82E-05

Ifi27l2a	2.15	0.03	*Capn5*	0.76	0.04	*Gmpr2*	1.35	0.02	*Klf15*	1.12	1.79E-10
Igkj1	-1.89	0.003	*Rps27rt*	-1.10	0.01	*Ckap2*	-2.24	0.004	*Ppp1r3e*	-1.76	0.02
Ear1	-2.00	0.004	*Dnajb1*	-1.24	2.61E-09	*Inhba*	-2.26	0.0009	*Igkv4-72*	-1.77	0.0002
Tcrg-C2	-2.01	6.45E-05	*Rpl17-ps5*	-1.26	0.02	*S100a14*	-2.27	0.01	*Ighv1-39*	-1.79	0.01
Ighv1-52	-2.03	0.04	*Fhl2*	-1.27	0.045	*Matk*	-2.30	0.02	*Ighv7-3*	-1.80	3.24E-07
Nuggc	-2.14	0.002	*Fcrla*	-1.30	0.0052	*Ppp1r3e*	-2.34	1.79E-05	*Kcnc1*	-1.89	0.02
Igkv1-135	-2.22	0.04	*Igkv8-27*	-1.48	0.02	*Orm1*	-2.41	0.008	*Igkv6-15*	-1.91	2.16E-06
Iglc1	-2.24	0.0007	*mt-Tn*	-1.57	0.01	*Mmp12*	-2.44	0.01	*Ighv1-20*	-1.95	1.97E-08
Gjb6	-2.26	0.02	*Sh2d1b1*	-1.57	0.04	*Saa3*	-2.53	2.57E-12	*Igkv19-93*	-2.05	1.77E-07
Tnfrsf17	-2.29	7.23E-06	*Igkv14-126*	-1.67	0.048	*Fxyd4*	-2.66	0.002	*Rec8*	-2.32	3.34E-06
Rec8	-2.33	0.03	*Ighm*	-1.75	0.04	*Ccl7*	-2.67	0.04	*Igkv6-20*	-2.60	0.001
Iglj1	-2.47	3.69E-06	*Serpina9*	-1.78	0.03	*Cemip*	-2.81	0.007	*Igkv4-61*	-2.67	0.002
C030034L19Rik	-2.56	0.002	*Clca1*	-2.17	1.05E-05	*Krt83*	-2.87	0.02	*Igkv2-112*	-3.22	0.04
Igkv6-25	-2.60	4.62E-23	*Ighv14-1*	-2.27	1.05E-05	*Wnt10a*	-3.31	0.04	*Ighv2-3*	-3.33	0.004
Igkv6-23	-2.68	0.005	*Igkv4-53*	-2.51	2.01E-06	*Retnla*	-3.46	2.64E-05	*Igkv4-91*	-3.37	1.87E-10
Bex2	-2.69	1.57E-05	*Igkv4-68*	-2.70	2.28E-05	*Rec8*	-3.57	8.21E-18	*Serpina9*	-3.40	0.04
Kcnc1	-3.06	1.23E-06	*Hspa1b*	-2.73	1.57E-14	*Spp1*	-3.60	3.54E-18	*Igkv4-86*	-3.47	6.43E-05
Igkv8-27	-3.07	0.02	*Kcnc1*	-2.76	0.0062	*Thbs4*	-3.81	1.39E-05	*Ighv1-54*	-3.66	0.002
Igkv6-13	-3.18	0.03	*Hspa1a*	-2.95	4.18E-30	*Col11a1*	-4.92	0.009	*Igkv1-88*	-4.10	0.0004
AC160336.1	-4.60	1.01E-09	*Ighv1-54*	-3.92	0.0002	*Ighv1-54*	-5.41	0.003	*Igkv4-79*	-4.13	0.02
Igkv9-129	-6.03	0.01	*Ighv1-63*	-3.92	0.0010	*Gjb6*	-6.76	2.30E-09	*Igkv4-90*	-4.94	0.02

To assess functional differences in cDC1, I investigated surface expression of activation markers (Figure 4.9A). No discernible difference in the expression of co-stimulatory molecules CD86 (Figure 4.9B) or CD40 (Figure 4.9C) was observed in the first week. Additionally, I detected no variation in the levels of CCR2 (Figure 4.9D), known to facilitate DC migration and recruitment (Osterholzer *et al.*, 2008), or DNGR1 (Figure 4.9E), a C-type lectin receptor exclusively expressed in cDC1, which is encoded by *Clec9a* (Cueto *et al.*, 2019), on cDC1 between WT and *Mr1*$^{-/-}$ mice lungs at day 7 post-bleomycin. However, on day 10 post bleomycin-induced lung damage, I did see an upregulation of CD40 and CCR2 in lung cDC1 cells from *Mr1*$^{-/-}$ mice, suggesting that the cDC1s are showing a delayed inflammatory response in the *Mr1*$^{-/-}$ mice.

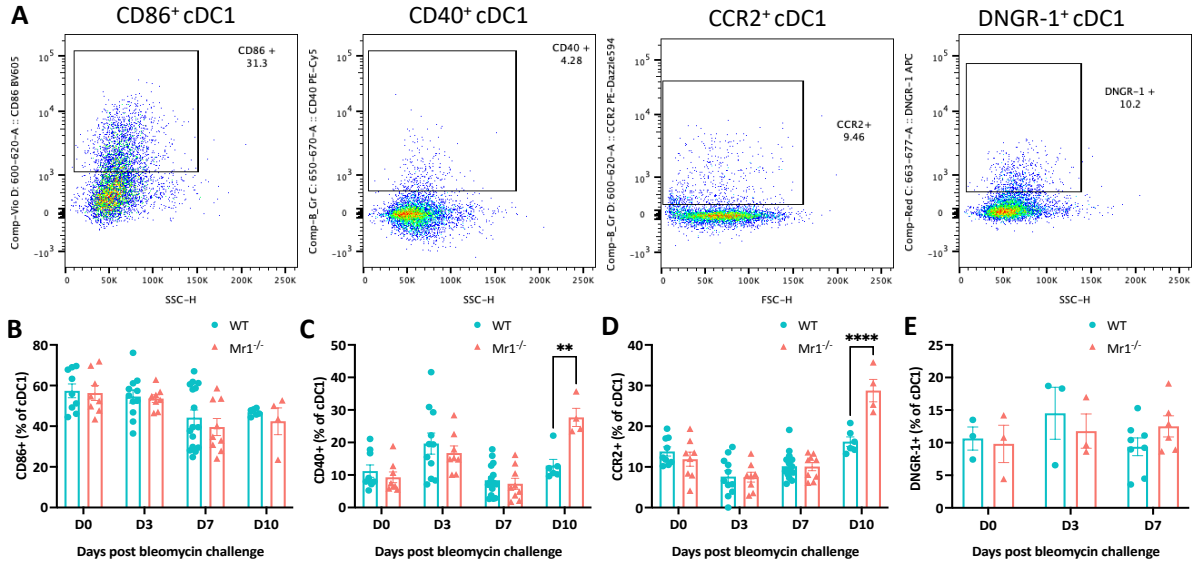

Figure 4.9 Expression of activation markers on lung cDC1 cells post-bleomycin challenge.

(**A**) Representative flow cytometry plots showing expression of CD86, CD40, CCR2 and DNGR-1, gated on live pulmonary $CD45^+$ $CD64^-$ $CD11c^+$ $MHCII^+$ $CD103^+$ cDC1 cells. Fraction of pulmonary cDC1 cells expressing CD86 (**B**), CD40 (**C**), CCR2 (**D**) and DNGR-1 (**E**) expressed as a percentage of pulmonary cDC1 in lungs of WT and *Mr1*$^{-/-}$ mice. For CD86, CD40 and CCR2 expression on cDC1 cells, data represent combined data from two (Day 0, 3 and 7) or one (Day 10) independent experiments, with 3-6 mice per group. For DNGR-1 expression on cDC1 cells, data represent combined results from two independent experiments on Day 7 and one independent experiment on Days 0 and 3, with 2-4 mice per group. Data are presented as mean ± SEM. Significance was tested by two-way ANOVA with Sidak's multiple comparisons test; *$P < 0.05$, **$P < 0.01$, ***$P < 0.001$, ****$P < 0.0001$.

4.3.3 Single-cell RNA Sequencing reveals diminished cDC1 proportions in *Mr1*$^{-/-}$ mice

To comprehensively delineate the cellular dynamics of major cell lineages post-bleomycin injury, I utilised single-cell RNA sequencing (scRNA-seq) (10x Genomics), Cellular Indexing of Transcriptomes and Epitopes by Sequencing (CITE-seq) and TCR sequencing. I again used the previously described MAIT-cell enriched mouse model and obtained single cell suspensions from both WT and *Mr1*$^{-/-}$ whole lungs of PBS-treated controls, as well as at days 3 and 7 post-injury, with three replicates for each time point (Figure 4.10A). I obtained transcriptomes from 117, 908 cells following quality control filtering. Principal component analysis highlighted variability influenced by both timepoints and mouse genotype (Figure 4.10B and C). Post-data integration and unsupervised clustering analysis, 27 cell type identities

were annotated using canonical marker genes and existing scRNA-seq datasets from mouse lungs (Angelidis *et al.*, 2019; Han *et al.*, 2018; Strunz *et al.*, 2020) (Figure 4.10D and Figure 4.11). All lineages were observed across both WT and *Mr1*$^{-/-}$ mice at all three timepoints (Figure 4.12). MAIT cells exhibited a single-cell transcriptional profile akin to γδ-T cells, leading to a shared cluster in the UMAP (Figure 4.11D). Expectedly, MAIT cells were absent in *Mr1*$^{-/-}$ mice (Figure 4.13), but there was a non-significant tendency towards an increase in CD4^{+} and CD8^{+} T cells in *Mr1*$^{-/-}$ mice compared to WT mice (Figure 4.14), possibly due to a compensatory mechanism.

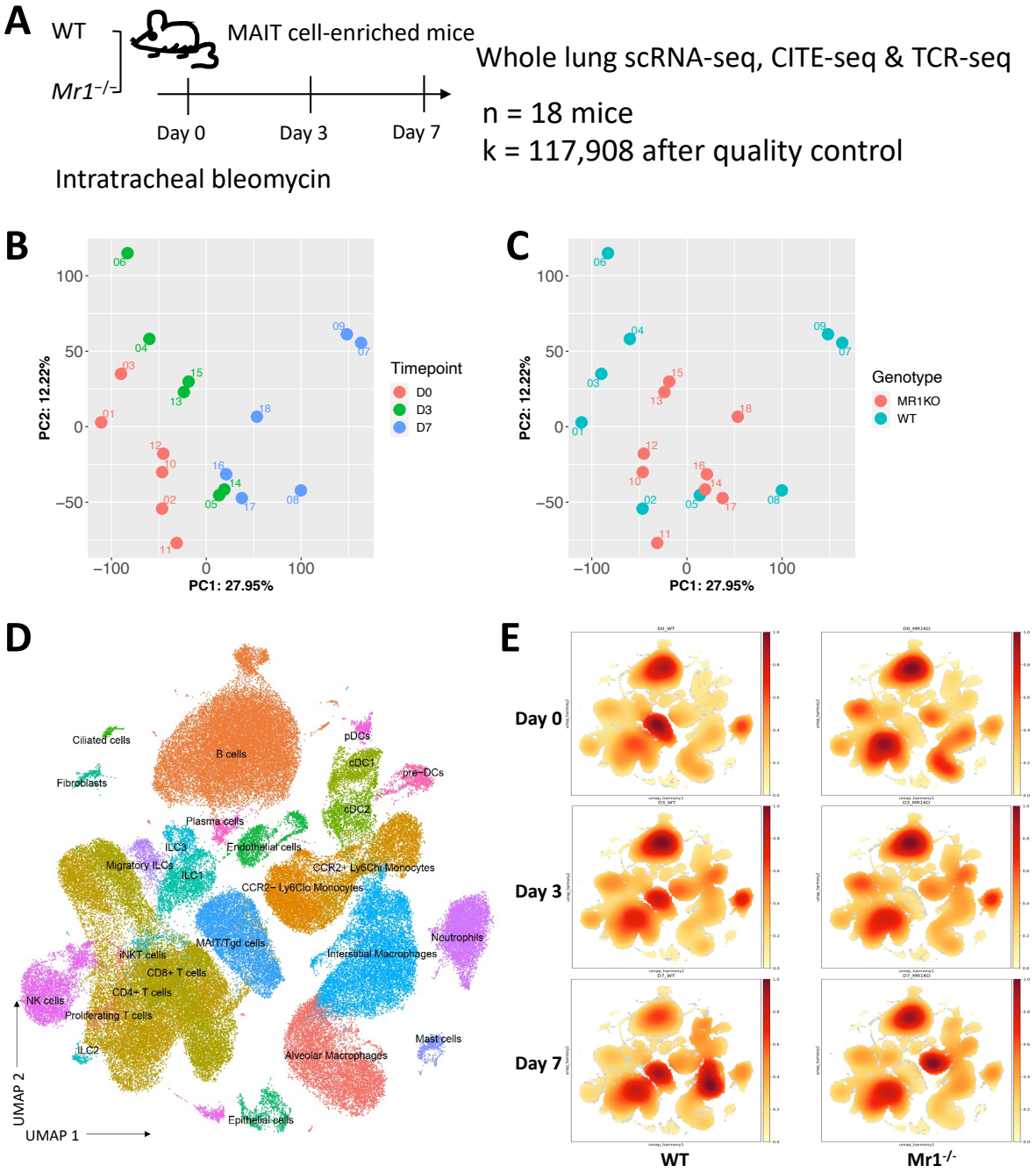

Figure 4.10 Single-cell RNA-sequencing analysis of total lung cells post-bleomycin challenge. (**A**) Single cell suspensions from whole-mouse lungs were analysed using scRNA-seq at the indicated time points after bleomycin-mediated lung injury. (**B** and **C**) Principal component

analysis on the overall transcriptomes of each sample coloured by timepoint (**B**) or mice genotype (**C**). (**D**) UMAP embedding of 117,908 high-quality single cells colour-coded by predicted cell lineage. (**E**) UMAP embedding of cell density displaying the proportion of each cell lineage at baseline (PBS control, Day 0) and post bleomycin challenge (Day 3 and 7), stratified by timepoint and mice genotype.

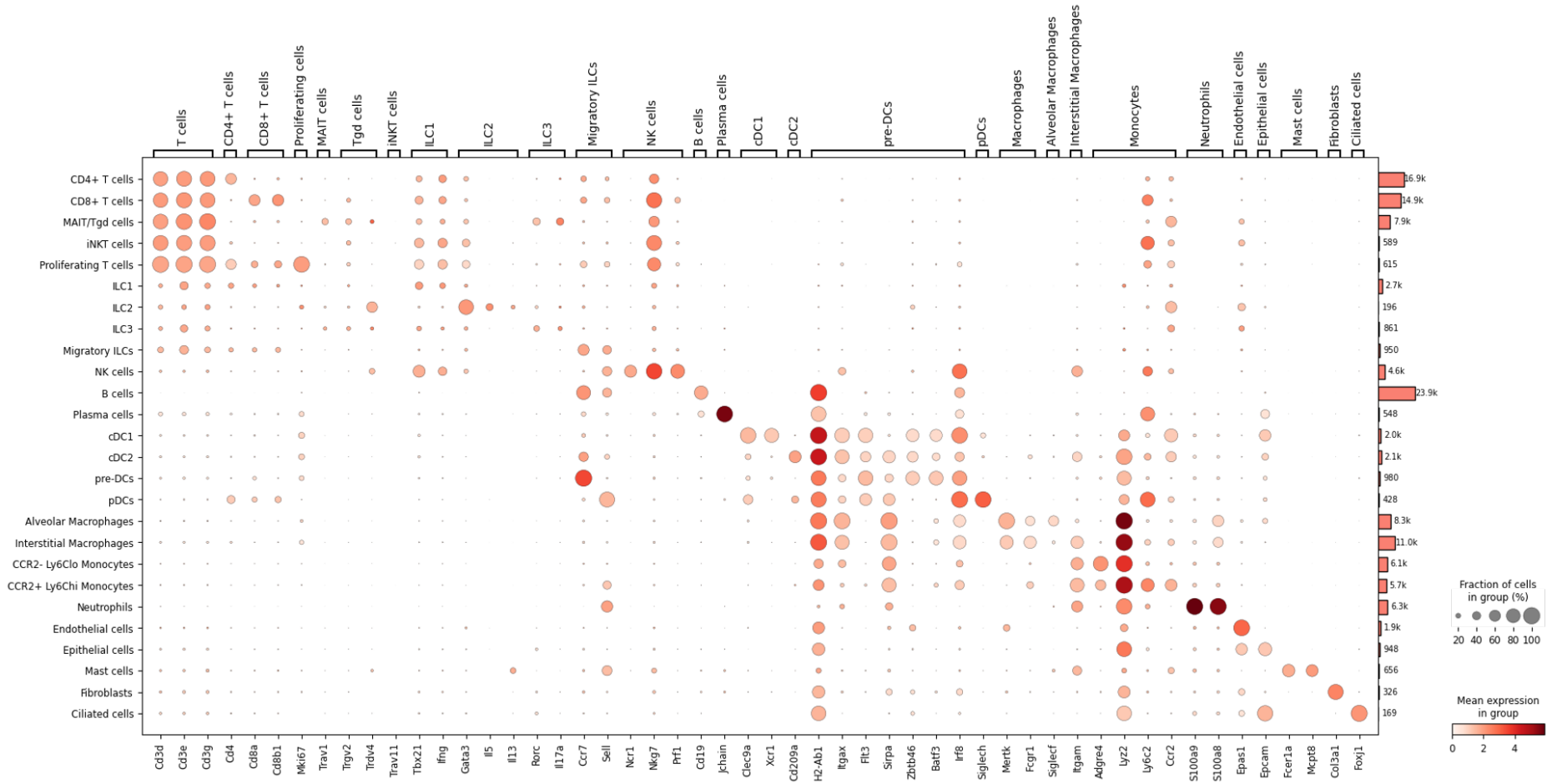
T cells
CD4+ T cells
CD8+ T cells
Proliferating cells
MAIT cells
Tgd cells
iNKT cells
ILC1
ILC2
ILC3
Migratory ILCs
NK cells
B cells
Plasma cells
cDC1
cDC2
pre-DCs
pDCs
Macrophages
Alveolar Macrophages
Interstitial Macrophages
Monocytes
Neutrophils
Endothelial cells
Epithelial cells
Mast cells
Fibroblasts
Ciliated cells
CD4+ T cells
CD8+ T cells
MAIT/Tgd cells
iNKT cells
Proliferating T cells
ILC1
ILC2
ILC3
Migratory ILCs
NK cells
B cells
Plasma cells
cDC1
cDC2
pre-DCs
pDCs
Alveolar Macrophages
Interstitial Macrophages
CCR2- Ly6Clo Monocytes
CCR2+ Ly6Chi Monocytes
Neutrophils
Endothelial cells
Epithelial cells
Mast cells
Fibroblasts
Ciliated cells
16.9k
14.9k
7.9k
589
615
2.7k
196
861
950
4.6k
23.9k
548
2.0k
2.1k
980
428
8.3k
11.0k
6.1k
5.7k
6.3k
1.9k
948
656
326
169
Cd3d
Cd3e
Cd3g
Cd4
Cd8a
Cd8b1
Mki67
Trav1
Trgv2
Trdv4
Trav11
Tbx21
Ifng
Gata3
Il5
Il13
Rorc
Il17a
Ccr7
Sell
Ncr1
Nkg7
Prf1
Cd19
Jchain
Clec9a
Xcr1
Cd209a
H2-Ab1
Itgax
Flt3
Sirpa
Zbtb46
Batf3
Irf8
Siglech
Mertk
Fcgr1
Siglecf
Itgam
Adgre4
Ly22
Ly6c2
Ccr2
S100a9
S100a8
Epas1
Epcam
Fcer1a
Mcpt8
Col3a1
Foxj1
Fraction of cells in group (%)
20 40 60 80 100
Mean expression in group
0 2 4

Figure 4.11 Dot plot showing the top discriminative gene sets for each cell lineage compared with every other lineage.

Dot size represents the fraction of cells in each group. Colour scales denote the normalised mean gene expression for each cluster. Bar chart on the right represents numbers of cells of each cell type in the single-cell RNA sequencing dataset.

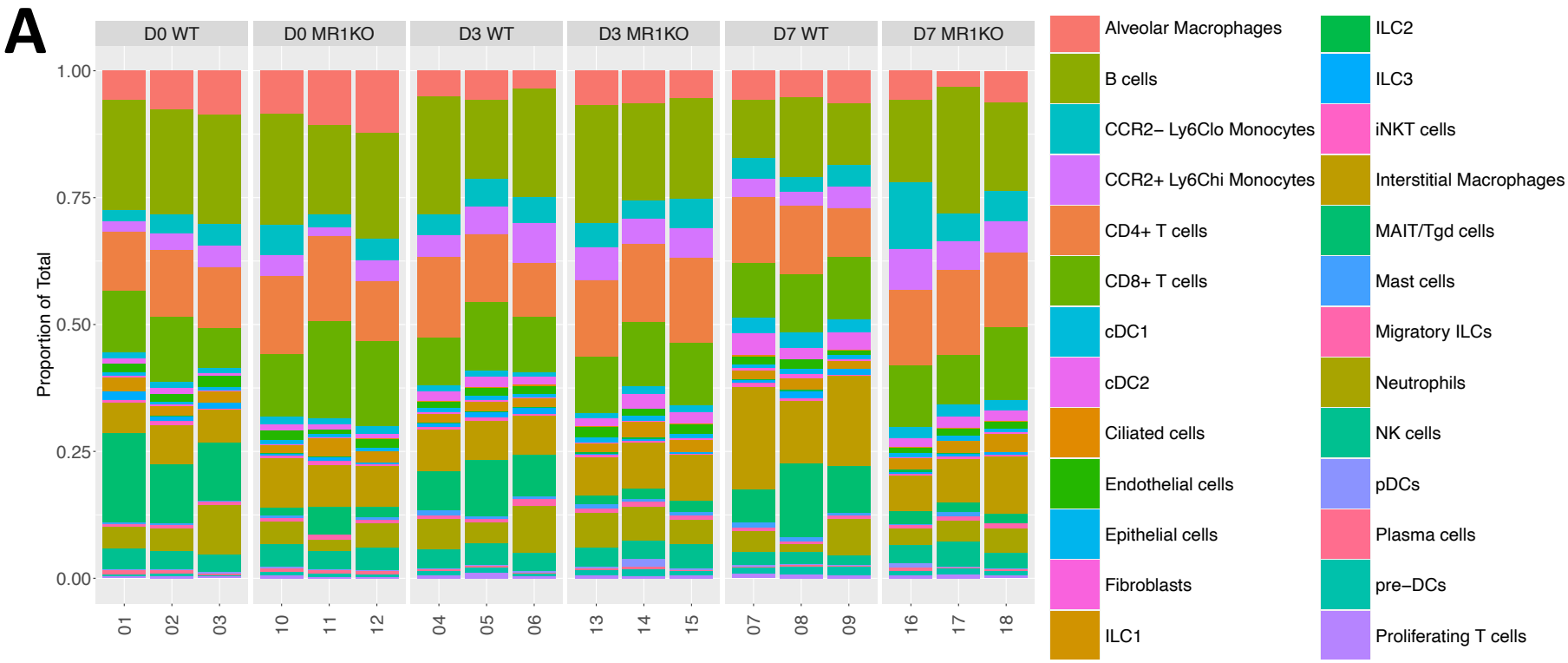
A
D0 WT
D0 MR1KO
D3 WT
D3 MR1KO
D7 WT
D7 MR1KO
Proportion of Total
1.00
0.75
0.50
0.25
0.00
01
02
03
10
11
12
04
05
06
13
14
15
07
08
09
16
17
18
Alveolar Macrophages
B cells
CCR2− Ly6Clo Monocytes
CCR2+ Ly6Chi Monocytes
CD4+ T cells
CD8+ T cells
cDC1
cDC2
Ciliated cells
Endothelial cells
Epithelial cells
Fibroblasts
ILC1
ILC2
ILC3
iNKT cells
Interstitial Macrophages
MAIT/Tgd cells
Mast cells
Migratory ILCs
Neutrophils
NK cells
pDCs
Plasma cells
pre−DCs
Proliferating T cells

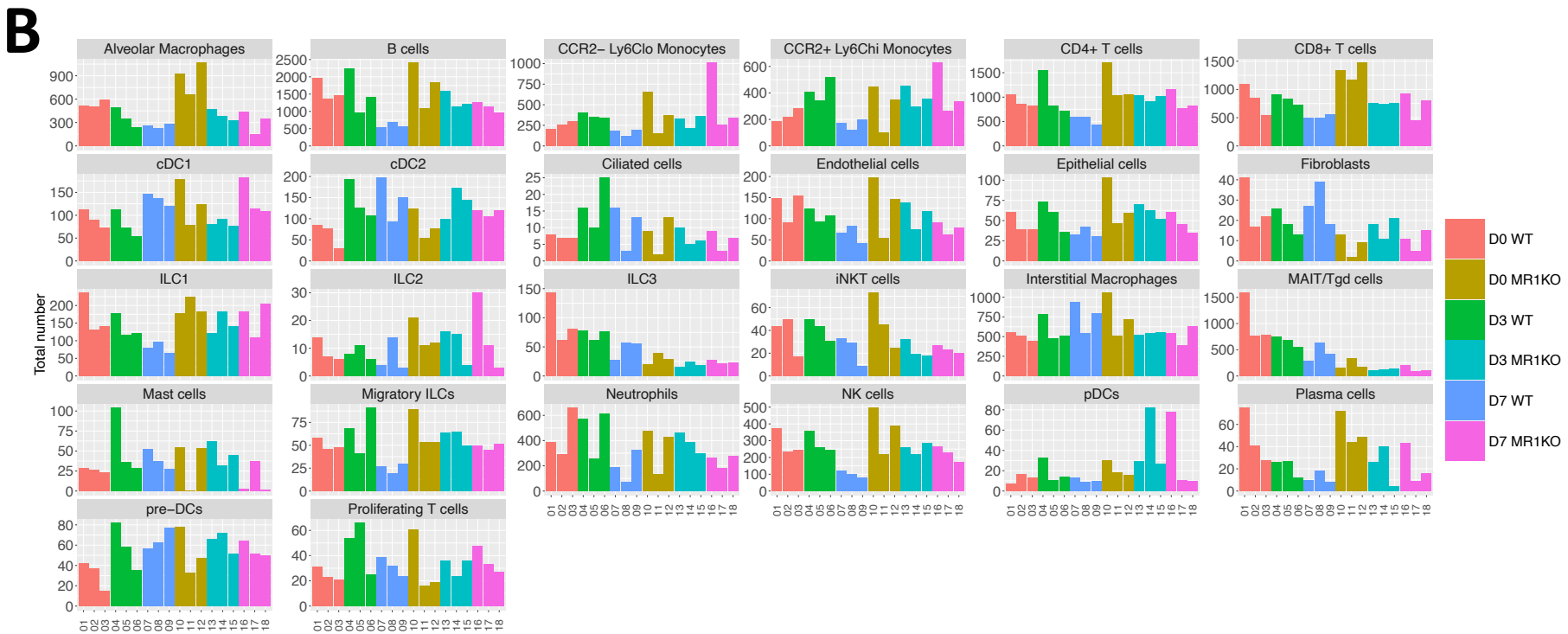

Figure 4.12 Proportion distribution and absolute number of the 27 cell lineages in each sample.

Proportion distribution (**A**) and absolute number (**B**) of the 27 cell lineages per sample. Bars represent the absolute number (**A**) or percentage (**B**) of cells assigned to each colour-coded cell lineage relative to the total cells for each sample.

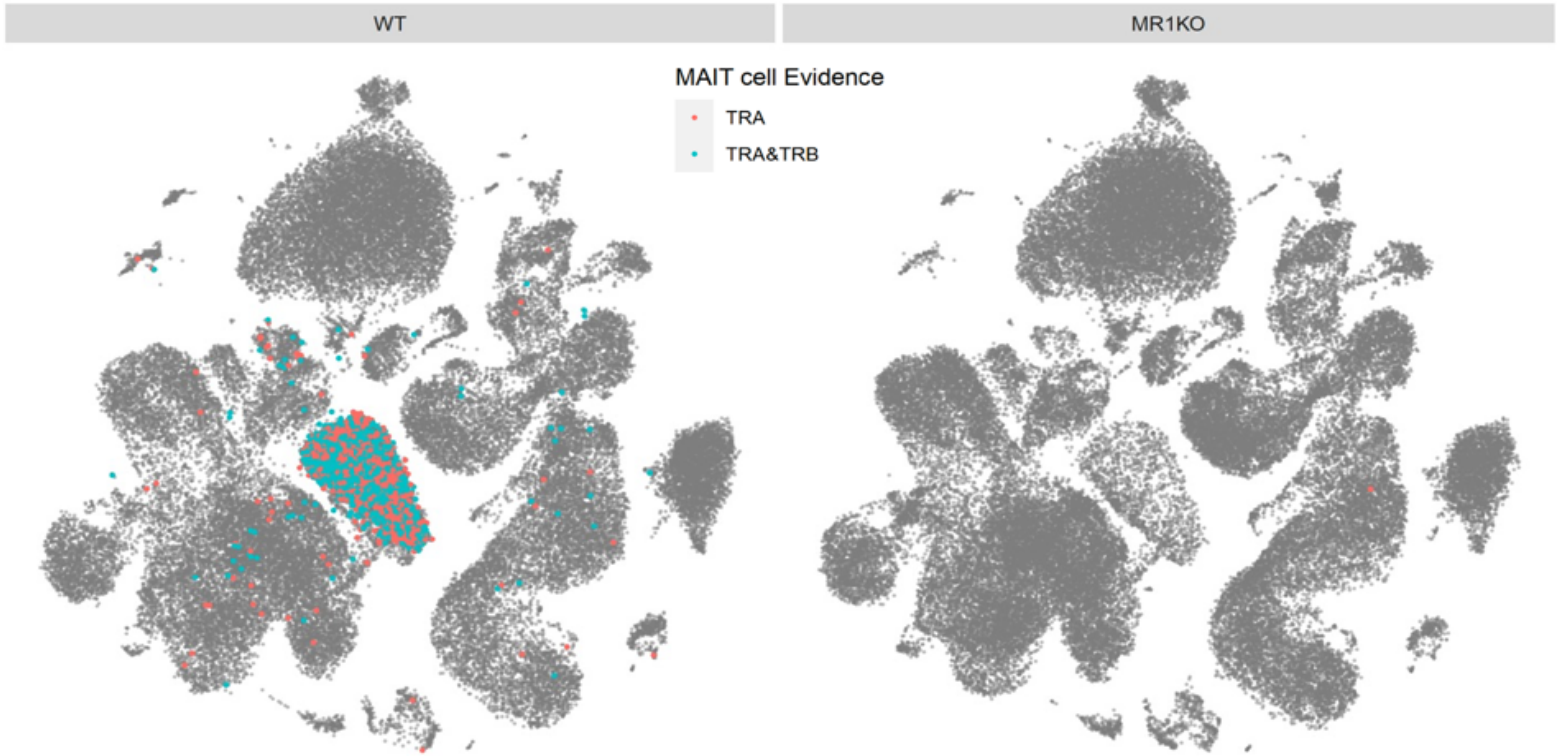

Figure 4.13 UMAP analysis showing presence of MAIT cells in both WT and *Mr1*$^{-/-}$ mice.

MAIT cells were identified using TCR sequencing results generated by Cell Ranger. A cell is classified as a MAIT cell if it belongs to a clonotype with expression of *Trav1* and *Traj33* (TRA), or a clonotype with the expression of *Trav1* and *Traj33*, paired with either *Trbv19* or *Trbv13* (TRA & TRB) (https://support.10xgenomics.com/single-cell-vdj/software/pipelines/latest/algorithms/inkt-mait).

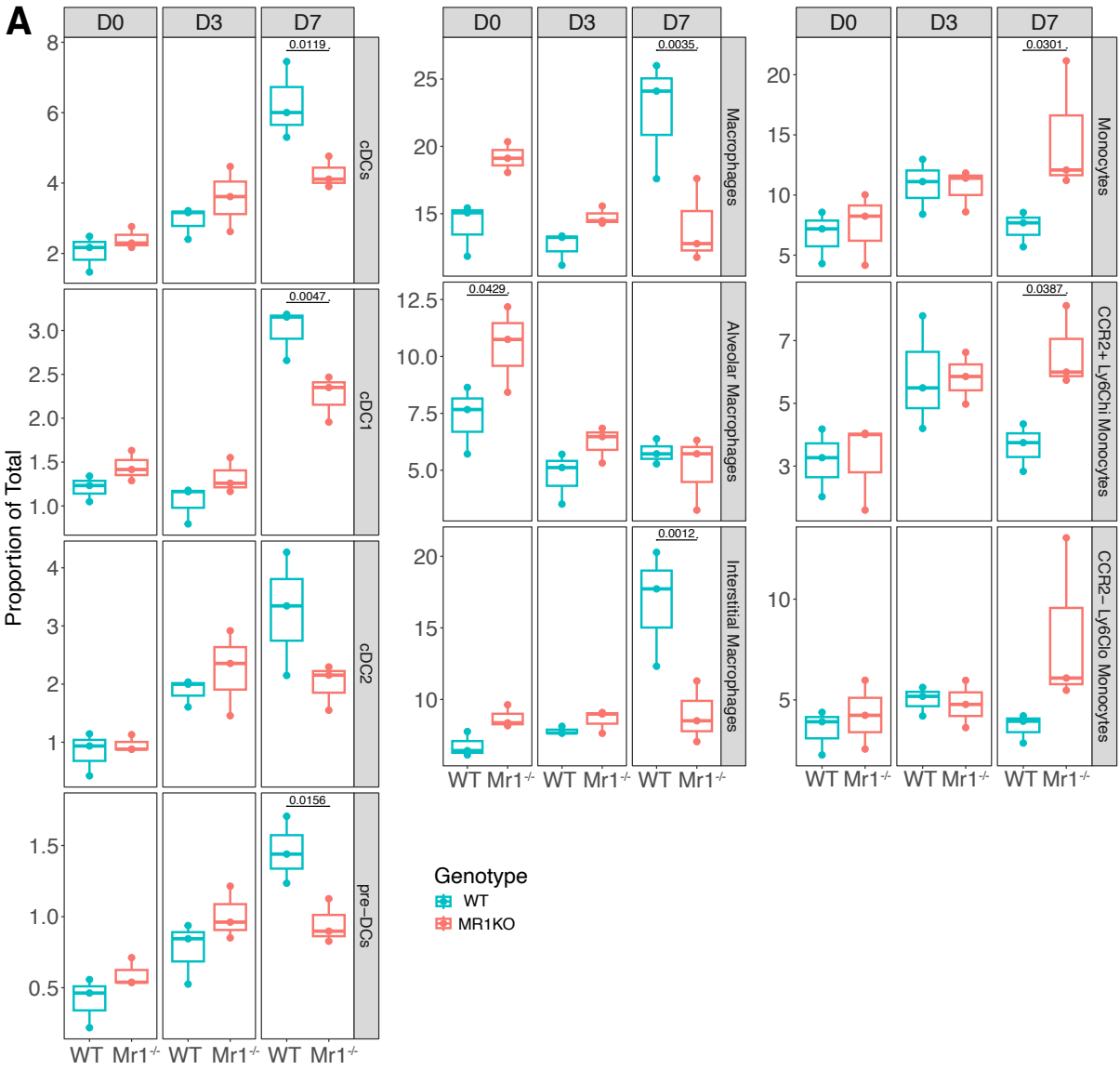
A
D0
D3
D7
cDCs
cDC1
cDC2
pre−DCs
Macrophages
Alveolar Macrophages
Interstitial Macrophages
Monocytes
CCR2+ Ly6Chi Monocytes
CCR2− Ly6Clo Monocytes
Proportion of Total
0.0119
0.0047
0.0156
0.0035
0.0429
0.0012
0.0301
0.0387
WT
Mr1-/-
Genotype
WT
MR1KO

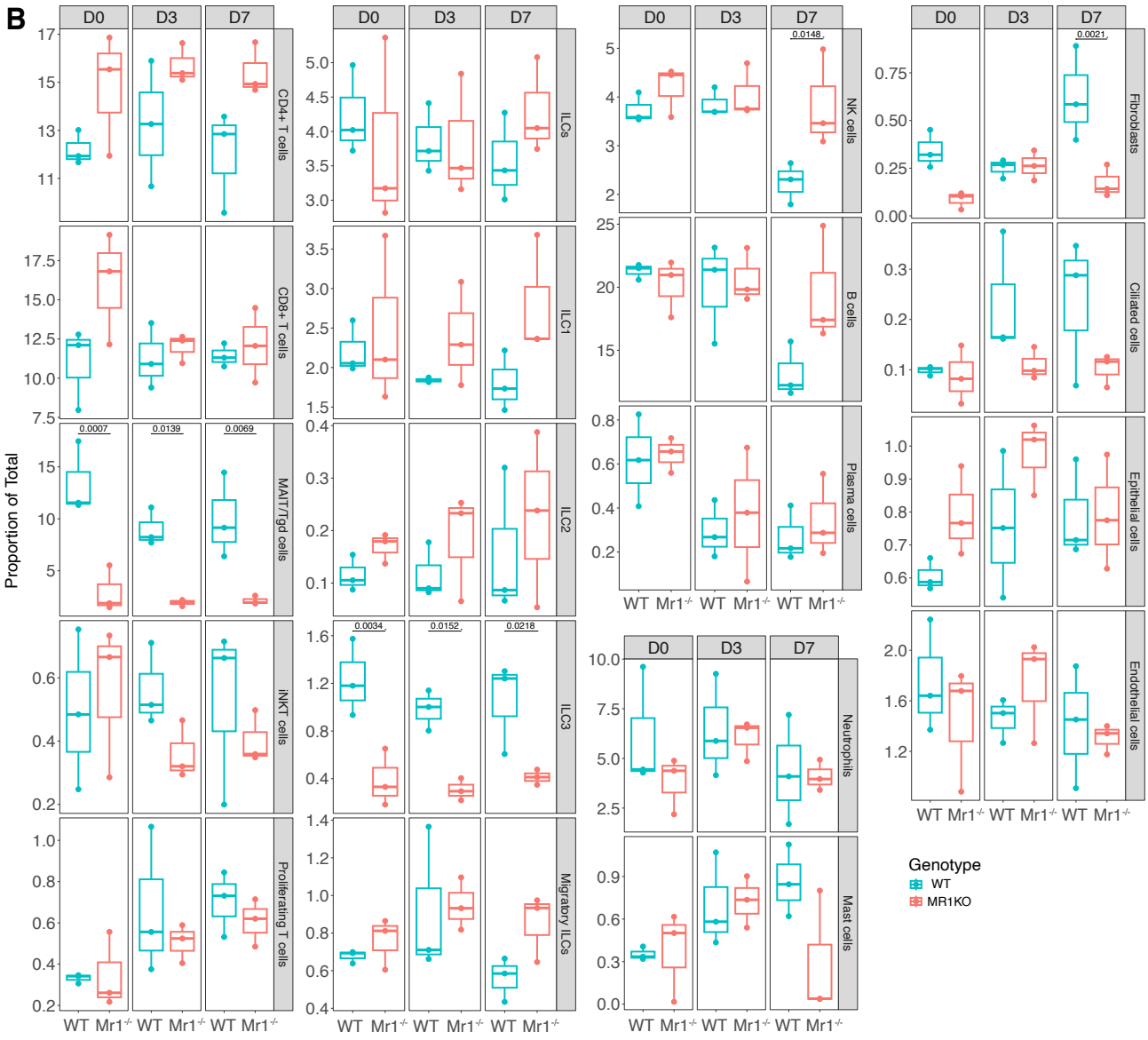

Figure 4.14 Cell type distribution in both WT and *Mr1*$^{-/-}$ mouse lungs post-bleomycin challenge.

Proportion of the indicated cell types of total lung cells was calculated for individual mice at the indicated time points at baseline (PBS control, Day 0) and after bleomycin challenge (Day 3 and 7) (n = 3 for each genotype). *P* values generated using a two-way ANOVA with Sidak's multiple comparisons test.

I observed an accumulation of cDC1 (P=0.0047) and cDC2 (non-significant) in the lungs of WT mice but not in *Mr1*$^{-/-}$ mice. These observations align with the flow cytometry data depicting a deficiency in cDC1 accumulation in *Mr1*$^{-/-}$ mice (Figure 4.8). Concomitantly, accumulation of monocyte and NK cells was prominently detected in the lungs of *Mr1*$^{-/-}$ mice, whereas this was not the case in WT counterparts (Figure 4.10E, Figure 4.14A and B). Furthermore, in the lungs of WT mice, there was a discernible expansion of both interstitial macrophages (Figure 4.14A) and fibroblasts (Figure 4.14B), and such expansions were absent in the *Mr1*$^{-/-}$ mice.

Next, I investigated the differences in cell type-specific DEGs (Data S1) between *Mr1*$^{-/-}$ and WT mice. Gene expression differences across most cell types were limited, with very few DEGs identified – fewer than 64 in any given cell type. Amongst pulmonary DCs and monocytes, I observed downregulation of genes in *Mr1*$^{-/-}$ mice on both day 3 and 7 post-bleomycin, including *Pbx1*, *Fcgr2b* and *Sh2d1b1* (Data S1, Figure 4.15). The inhibitory Fc receptor *Fcgr2b* was consistently downregulated in *Mr1*$^{-/-}$ cDC1 across all time points. This is paired with downregulation of *Cxcl1*/*Cxcl2* in cDC2 on day 7 post-challenge (Data S1, Figure 4.15), suggesting a disrupted chemokine expression profile within the cDC2 of *Mr1*$^{-/-}$ mice.

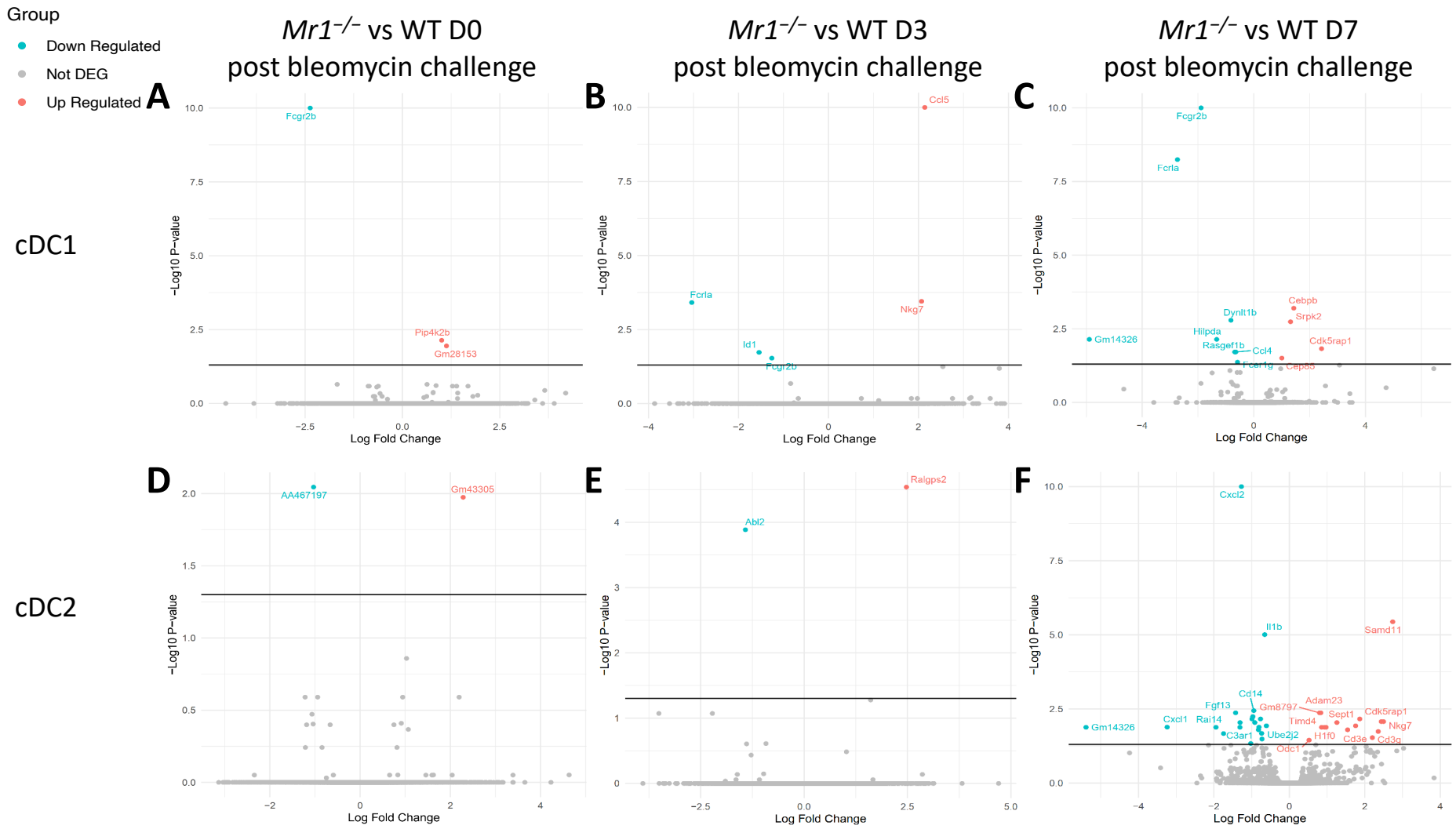
Group
Down Regulated
Not DEG
Up Regulated
Mr1−/− vs WT D0
post bleomycin challenge
Mr1−/− vs WT D3
post bleomycin challenge
Mr1−/− vs WT D7
post bleomycin challenge
A
B
C
D
E
F
cDC1
cDC2
−Log10 P−value
Log Fold Change
Fcgr2b
Pip4k2b
Gm28153
Ccl5
Fcrla
Nkg7
Id1
Cebpb
Srpk2
Dynlt1b
Hilpda
Rasgef1b
Ccl4
Cdk5rap1
Gm14326
Cep85
AA467197
Gm43305
Abl2
Ralgps2
Cxcl2
Il1b
Samd11
Cd14
Fgf13
Gm8797
Adam23
Sept1
Cdk5rap1
Cxcl1
Rai14
Timd4
Nkg7
C3ar1
Ube2j2
H1f0
Cd3e
Cd3g
Odc1

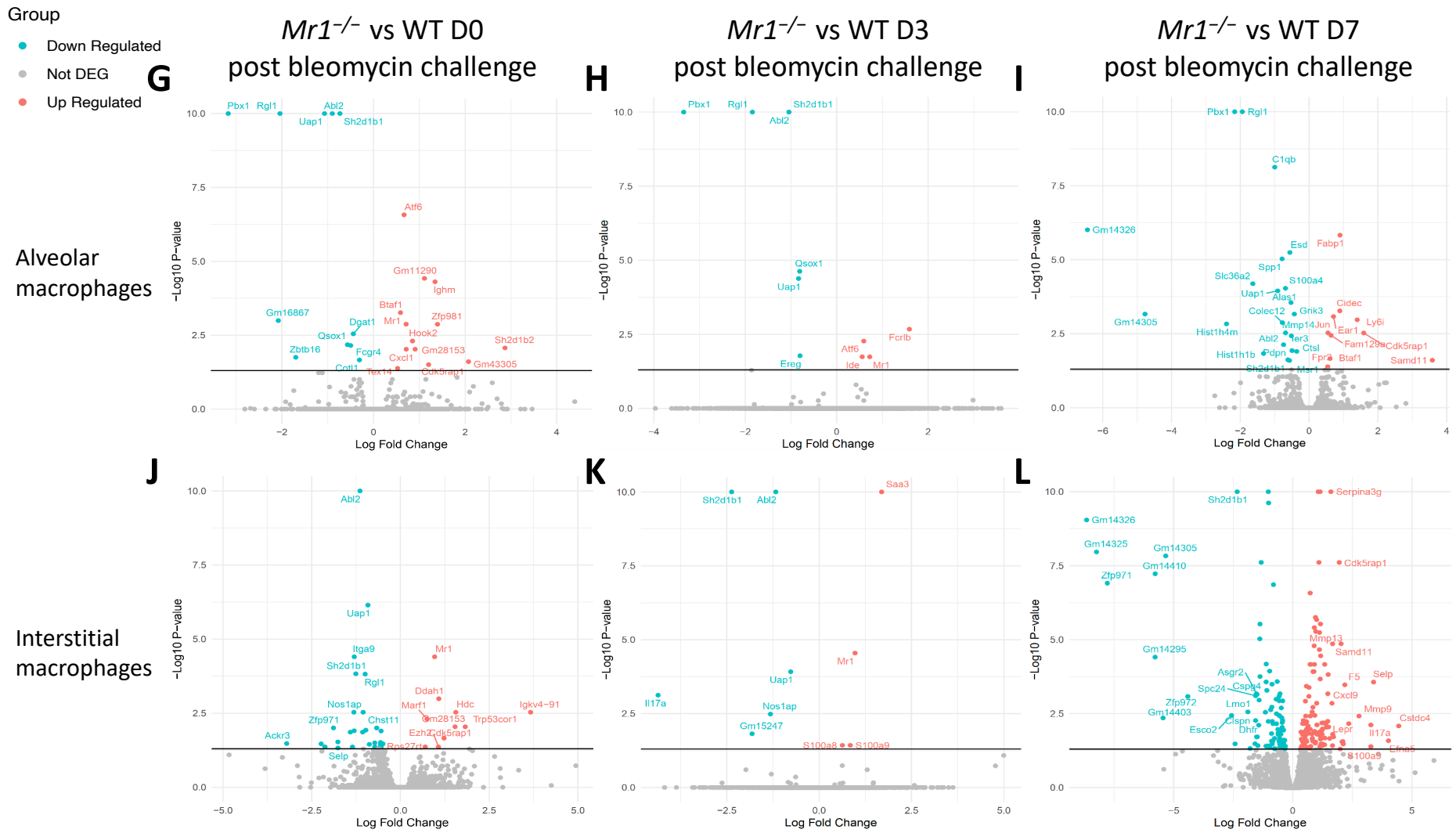
Group
Down Regulated
Not DEG
Up Regulated
G
Mr1-/- vs WT D0
post bleomycin challenge
H
Mr1-/- vs WT D3
post bleomycin challenge
I
Mr1-/- vs WT D7
post bleomycin challenge
Alveolar macrophages
J
K
L
Interstitial macrophages
−Log10 P−value
Log Fold Change

Figure 4.15 Differential gene expression in dendritic cell and macrophage populations in *Mr1*$^{-/-}$ vs. WT mice in response to bleomycin.

Volcano plots showing cDC1 (**A** to **C**), cDC2 (**D** to **F**), alveolar macrophages (**G** to **H**) and interstitial macrophage (**J** to **L**)-specific DEGs based on adjusted *P* value < 0.05 between *Mr1*$^{-/-}$ and WT mice before and post-bleomycin challenge. Horizontal line indicates *P* value threshold of 0.05.

I then looked at the precursor cells leading to cDCs – pre-DC population, in the lungs of both mice strains. Derived from CDP in the bone marrow, pre-DCs traffic to various tissues where they differentiate into cDC1 or cDC2, contingent upon tissue-specific and local environmental cues (Liu *et al.*, 2009; Onai *et al.*, 2013; Schlitzer *et al.*, 2015). Employing Monocle2 for trajectory analysis (Qiu *et al.*, 2017), I discerned a clear differentiation pathway commencing from pre-DCs (CD45^{+} MHCII^{+} CD11c^{-} Flt3^{hi} SIRP-α^{-}) and culminating in cDC1 and cDC2 subsets (Figure 4.16A). During the differentiation from pre-DCs into cDC1 and cDC2, I noticed that *Irf8* levels go up in cDC1 but go down in cDC2. Conversely, *Irf4* levels rise in cDC2 and fall in cDC1 (Figure 4.16B). Of particular interest, *Mr1*$^{-/-}$ mice exhibited a diminished pre-DC population at day 7 post bleomycin challenge (Figure 4.14A). However, when contrasting the transcriptomic profile of pre-DCs from WT and *Mr1*$^{-/-}$ mice, differential gene expression was minimal (Figure 4.17). This suggests that, during the bleomycin challenge, MAIT cells predominantly modulate the accumulation dynamics of the pre-DC population, without substantially altering their functional profile.

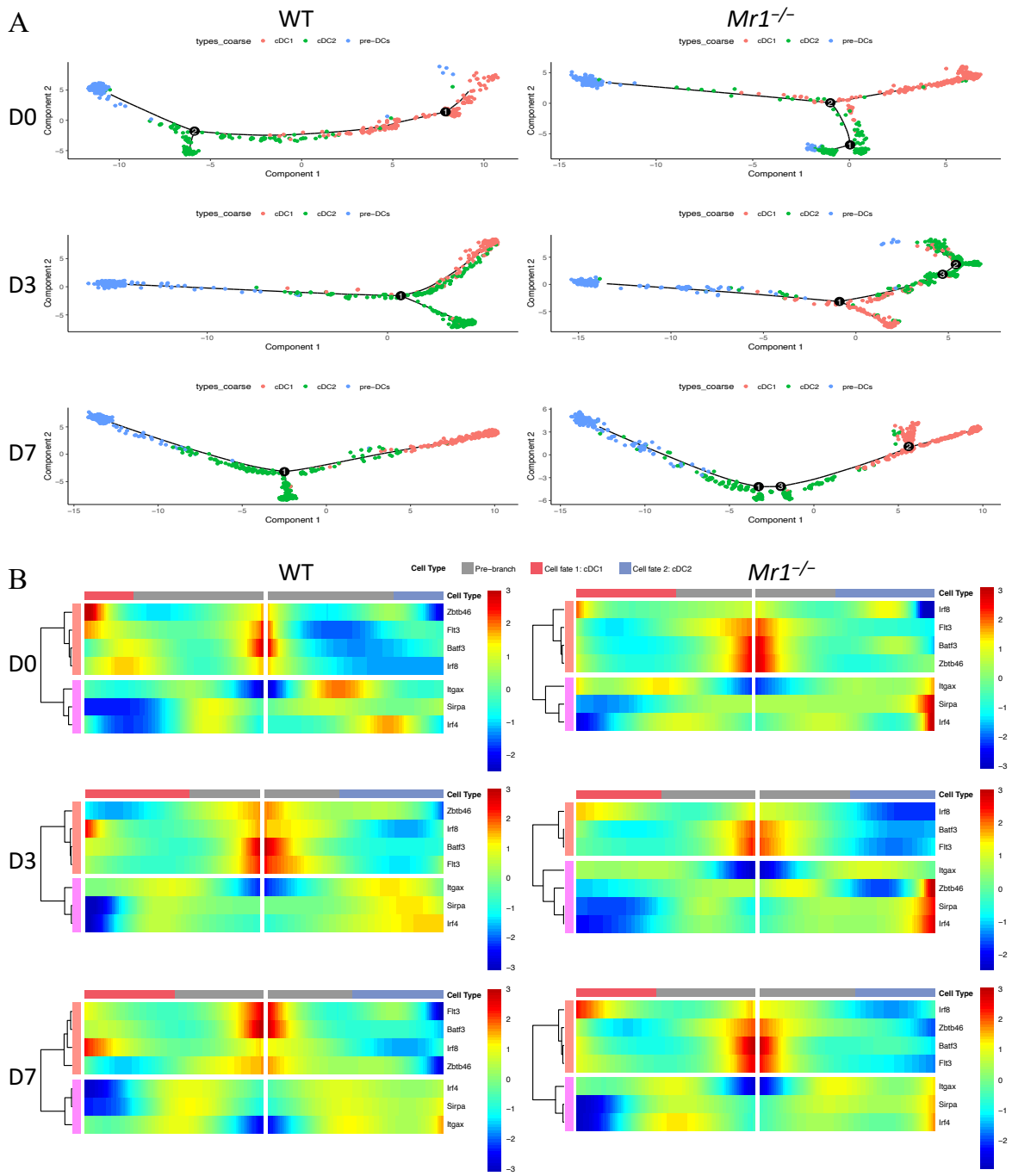

Figure 4.16 Differentiation trajectories and gene expression patterns of pre-DCs to cDC1 and cDC2 in WT and *Mr1*$^{-/-}$ mouse lungs.

(**A**) Analysis using Monocle2 (Qiu *et al.*, 2017) showing branches of differentiation trajectory from pre-DCs, the progenitors of cDCs, towards cDC1 and cDC2. (**B**) Heatmap showing dynamic change in gene expression of two differentiation branches (cDC1 and cDC2). Higher gene expression levels are denoted in red, while lower levels in blue.

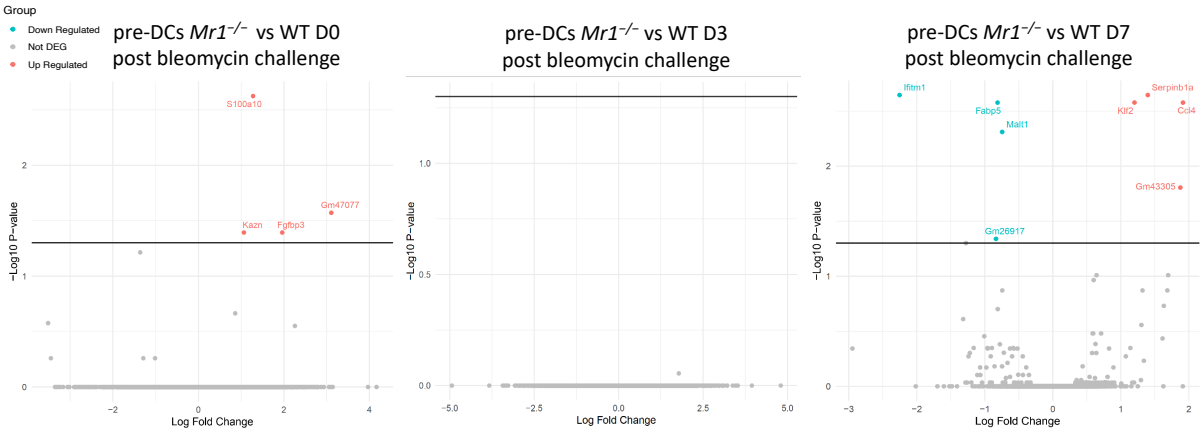

Figure 4.17 Volcano plots showing pre-DC-specific DEGs.

DEGs are identified based on adjusted *P* value < 0.05 between *Mr1*$^{-/-}$ and WT mice before and post-bleomycin challenge. Horizontal line indicates *P* value threshold of 0.05.

To test enrichment of pathways I performed GSEA analysis for all cell types across timepoints (Figure 4.18). A proinflammatory response was upregulated across various cell types in *Mr1*$^{-/-}$ mice compared with WT following bleomycin. Notably, NK cells, ciliated cells, and endothelial cells exhibited this exaggerated response on day 3, while monocytes and interstitial macrophages demonstrated a similar response on day 7, which would be expected to contribute to enhanced systemic inflammation. In summary, MAIT cells predominantly influence

accumulation of immune cells in response to sterile lung injury, particularly by increasing the number of cDC1s, pre-DCs and interstitial macrophages, but have more limited influence on the transcriptome of most cell types.

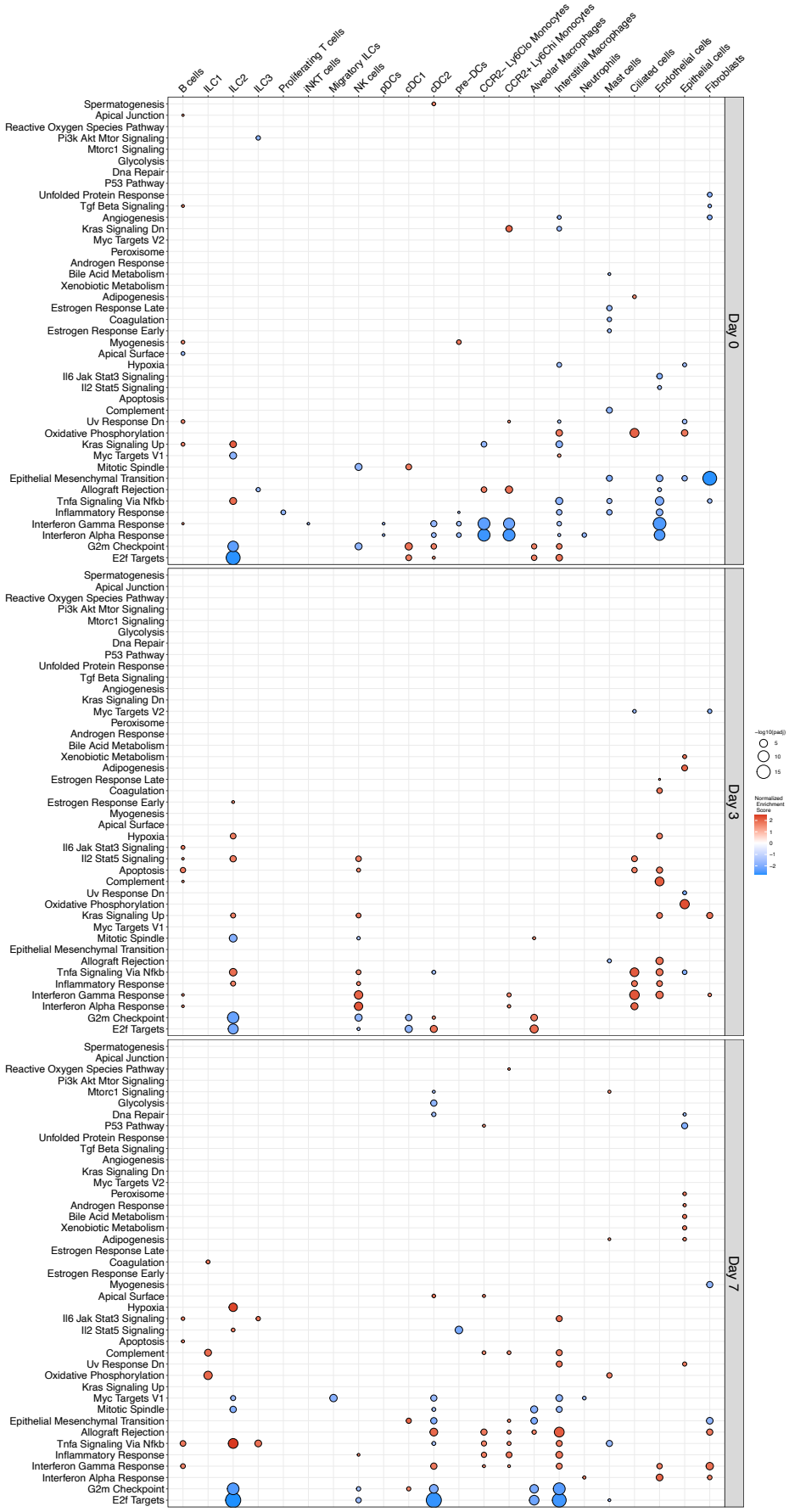
B cells
ILC1
ILC2
ILC3
Proliferating T cells
iNKT cells
Migratory ILCs
NK cells
pDCs
cDC1
cDC2
pre−DCs
CCR2− Ly6Clo Monocytes
CCR2+ Ly6Chi Monocytes
Alveolar Macrophages
Interstitial Macrophages
Neutrophils
Mast cells
Ciliated cells
Endothelial cells
Epithelial cells
Fibroblasts
Spermatogenesis
Apical Junction
Reactive Oxygen Species Pathway
Pi3k Akt Mtor Signaling
Mtorc1 Signaling
Glycolysis
Dna Repair
P53 Pathway
Unfolded Protein Response
Tgf Beta Signaling
Angiogenesis
Kras Signaling Dn
Myc Targets V2
Peroxisome
Androgen Response
Bile Acid Metabolism
Xenobiotic Metabolism
Adipogenesis
Estrogen Response Late
Coagulation
Estrogen Response Early
Myogenesis
Apical Surface
Hypoxia
Il6 Jak Stat3 Signaling
Il2 Stat5 Signaling
Apoptosis
Complement
Uv Response Dn
Oxidative Phosphorylation
Kras Signaling Up
Myc Targets V1
Mitotic Spindle
Epithelial Mesenchymal Transition
Allograft Rejection
Tnfa Signaling Via Nfkb
Inflammatory Response
Interferon Gamma Response
Interferon Alpha Response
G2m Checkpoint
E2f Targets
Day 0
Day 3
Day 7
−log10(padj)
5
10
15
Normalized Enrichment Score
2
1
0
−1
−2

Figure 4.18 Gene Set Enrichment Analysis in lung cells of *Mr1*$^{-/-}$ and WT mice post-bleomycin challenge.

GSEA performed on the *Mr1*$^{-/-}$ and wild-type (WT) mice across different time points utilizing the MSigDB Hallmark collection. Log2 fold changes in differential expression, as computed through DESeq2, served as the rank statistics. The colour of the dots represents the Normalised Enrichment Score (NES), while their size indicates the -log10-adjusted *P* value. *P* value was modified using the Benjamini-Hochberg method. The direction of the NES signifies the relative increase or decrease in the *Mr1*$^{-/-}$ mice when compared to the WT mice.

4.3.4 Cell-cell communication analysis reveals MAIT cell impact on cellular interaction during bleomycin challenge

I employed Tensor-cell2cell (Armingol *et al.*, 2022) to explore differences in cell-cell interactions between *Mr1*$^{-/-}$ and WT mice. I considered T cells as a single group due to the absence of MAIT cells in *Mr1*$^{-/-}$ mice. To ensure data reliability, cell types with limited numbers, such as fibroblasts, ciliated cells, and plasma cells, were excluded. Likewise, alveolar and interstitial macrophages, as well as CCR2^{+} Ly6C^{hi} and CCR2^{-} Ly6C^{lo} monocytes, were grouped and analysed collectively.

The deconstruction of the scRNA-seq dataset into 12 factors revealed cell-cell interaction patterns strongly associated with MAIT cell presence (Figure 4.19A). In this interaction landscape, baseline differences emerged in almost all factors (Figure 4.19B and C), with WT mice displaying more intact cell-cell communication network compared to their MAIT cell-

deficient counterparts, illustrating the fundamental role of MAIT cells in modulating cell-cell interaction during tissue injury. In particular, differences were significant in factors 3, 4, 6, 7 and 8.

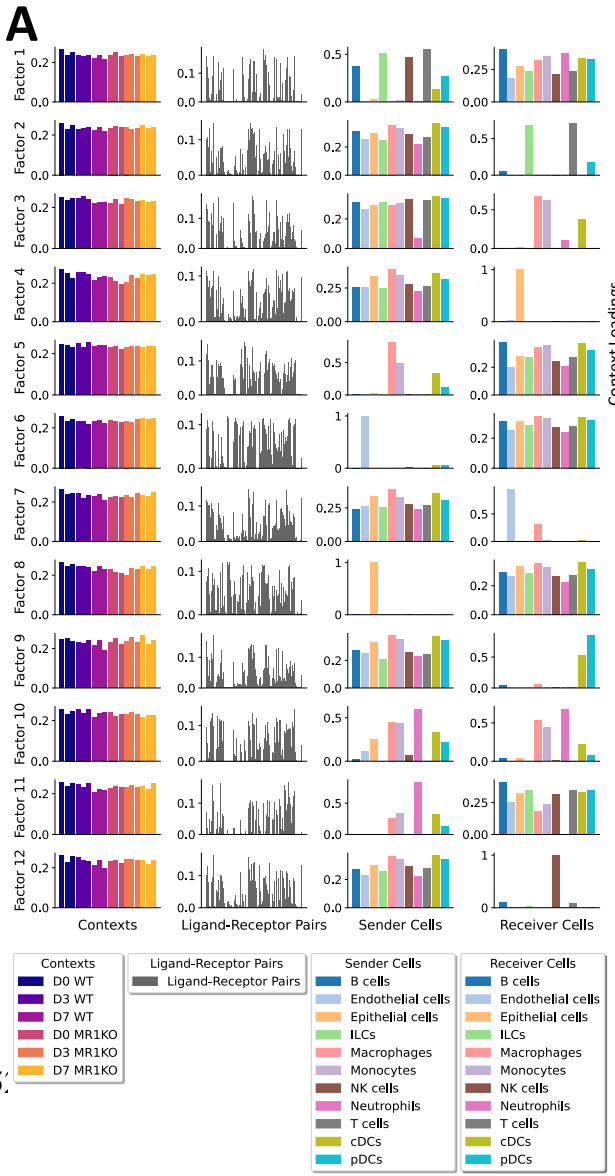

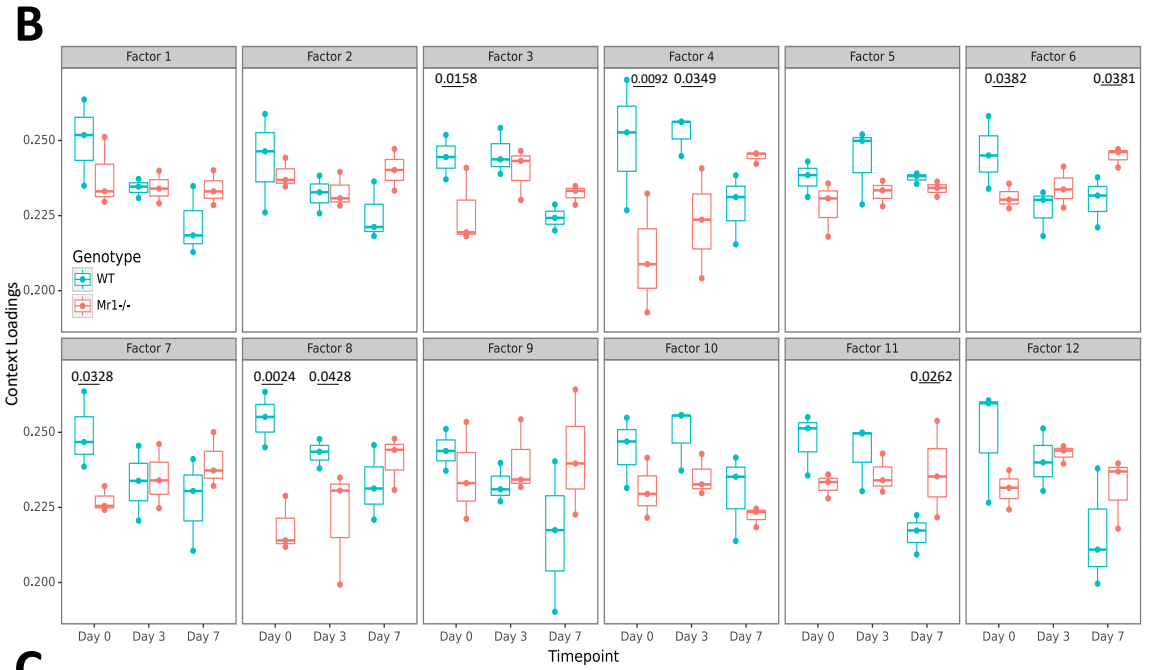

C

Top-10 Ligand-Receptor Pairs in each factor

Factor 1		Factor 2		Factor 3		Factor 4		Factor 5		Factor 6	
Lamb3 - Cd44	0.181	B2m - Cd3d	0.147	Hsp90b1 - Lrp1	0.173	Hspa8 - Lrp2	0.114	Fn1 - Cd44	0.153	Col4a1 - Cd47	0.120
Lgals1 - Ptprc	0.160	H2-K1 - Cd3d	0.147	Calr - Lrp1	0.171	Psap - Sort1	0.112	Adam15 - Itgb1	0.150	Cxcl12 - Itgb1	0.116
Adam10 - Cd44	0.158	B2m - Cd3g	0.145	Psap - Lrp1	0.161	Arpc5 - Lrp2	0.111	Fn1 - Itgav_Itgb1	0.142	Lamb2 - Rpsa	0.115
Vim - Cd44	0.158	H2-K1 - Cd3g	0.145	Lrpap1 - Lrp1	0.161	Hspa8 - Ldlr	0.111	Hgf - Cd44	0.139	Timp3 - Cd44	0.115
Arf6 - Smap1	0.157	B2m - Cd247	0.140	Hsp90b1 - Tlr2	0.160	Tgfb1 - Itgav_Itgb6	0.111	Fn1 - Itga4_Itgb1	0.137	Col4a1 - Cd44	0.115
Fam3c - Lamp1	0.156	H2-K1 - Cd8a	0.135	Copa - P2ry6	0.151	Gnai2 - Lpar3	0.111	Hgf - Itgb1	0.136	Col4a2 - Cd44	0.114
Pkm - Cd44	0.156	B2m - Klrc1	0.134	B2m - Hfe	0.150	Psap - Celsr1	0.110	F13a1 - Itgb1	0.134	Nid1 - Itgb1	0.114
Tgfb1 - Lpp	0.155	Psap - Ar	0.134	Actr2 - Ldlr	0.146	Actr2 - Lrp2	0.110	Adam15 - Itgav	0.133	Lama5 - Cd44	0.112
Adam10 - Tspan14	0.151	Hsp90aa1 - Itgb3	0.133	Arpc5 - Ldlr	0.146	Arpc5 - Ldlr	0.110	Lpl - Cd44	0.128	Vwf - Itgb1	0.112
Adam10 - Notch2	0.149	Alcam - Cd6	0.132	Hspa8 - Ldlr	0.146	Actr2 - Ldlr	0.109	F13a1 - Itga4	0.125	Cxcl12 - Itgav	0.111

Factor 7		Factor 8		Factor 9		Factor 10		Factor 11		Factor 12	
Gnai2 - Cav1	0.146	Col4a5 - Cd47	0.120	B2m - Klrd1	0.169	Vegfa - Sirpa	0.146	Tgm2 - Itgb1	0.166	B2m - Klrd1	0.162
Tgfb1 - Cav1	0.145	Col4a1 - Cd47	0.120	Adam10 - Cadm1	0.151	App - Fpr2	0.135	Cd14 - Ripk1	0.166	Gnai2 - S1pr4	0.158
Tgfb1 - Eng	0.140	Cgn - Tgfbr2	0.118	H2-M3 - Klrd1	0.142	Hp - Itgam	0.133	Cd14 - Itgb1	0.165	B2m - Klrc1	0.158
Icam1 - Cav1	0.140	Timp3 - Cd44	0.114	Lgals3 - Lag3	0.139	C3 - Itgam	0.127	Sirpa - Cd47	0.159	Gnai2 - Ccr5	0.157
Tgfb1 - Acvrl1	0.127	Hbegf - Cd44	0.114	Hspa8 - Ldlr	0.138	Anxa2 - Tlr2	0.121	App - Aplp2	0.158	B2m - Cd247	0.157
Tgfb1 - Acvr1b_Tgfbr2	0.125	Fgf1 - Cd44	0.114	Hsp90b1 - Tlr9	0.138	Ptpn6 - Cd300lf	0.121	App - Ncstn	0.157	Gnai2 - S1pr5	0.156
Ybx1 - Notch1	0.122	Lama5 - Cd44	0.114	Lrpap1 - Lrp8	0.137	Il1b - Il1r2_Il1rap	0.120	App - Lrp10	0.156	Icam1 - Spn	0.142
Gnas - Adcy9	0.121	Hbegf - Cd82	0.114	Arpc5 - Ldlr	0.136	Ccl4 - Ccr1	0.116	App - Rpsa	0.154	Icam1 - Itgam_Itgb2	0.140
Gnai2 - Adcy9	0.120	Col4a5 - Cd44	0.114	Actr2 - Ldlr	0.134	Selplg - Itgam	0.116	App - Lrp6	0.147	Icam1 - Itgax_Itgb2	0.138
Adam10 - Cadm1	0.117	Col4a1 - Cd44	0.114	H2-Aa - Lag3	0.134	S100a8 - Cd68	0.115	Spp1 - Itgav_Itgb1	0.143	Nampt - Adora2a	0.137

Figure 4.19 Cell-cell communication analysis reveals MAIT cell impact on cellular interaction during bleomycin challenge.

(**A**) Factors obtained after decomposing the tensor from the scRNA-seq dataset. 12 factors were selected for the analysis to show the representing dimension in samples, Ligand-Receptor (LR) pairs, sender cells, and receiver cells. Each row represents a factor, and each column represents the loadings for the given tensor dimensions. (**B**) Boxplot representation for WT and *Mr1*$^{-/-}$ mice post-bleomycin challenge. Each panel represents the sample loadings, grouped by mice genotype and timepoints, in each of the factors. Boxes represent the quartiles and whiskers show the rest of each distribution. Significance was tested by two-way ANOVA with Fisher's LSD test. (**C**) List of the top 10 Ligand-Receptor pairs ranked by loading for each factor. The corresponding ligands and receptors in these top-ranked pairs are mainly produced by sender and receiver cells with high loadings, respectively.

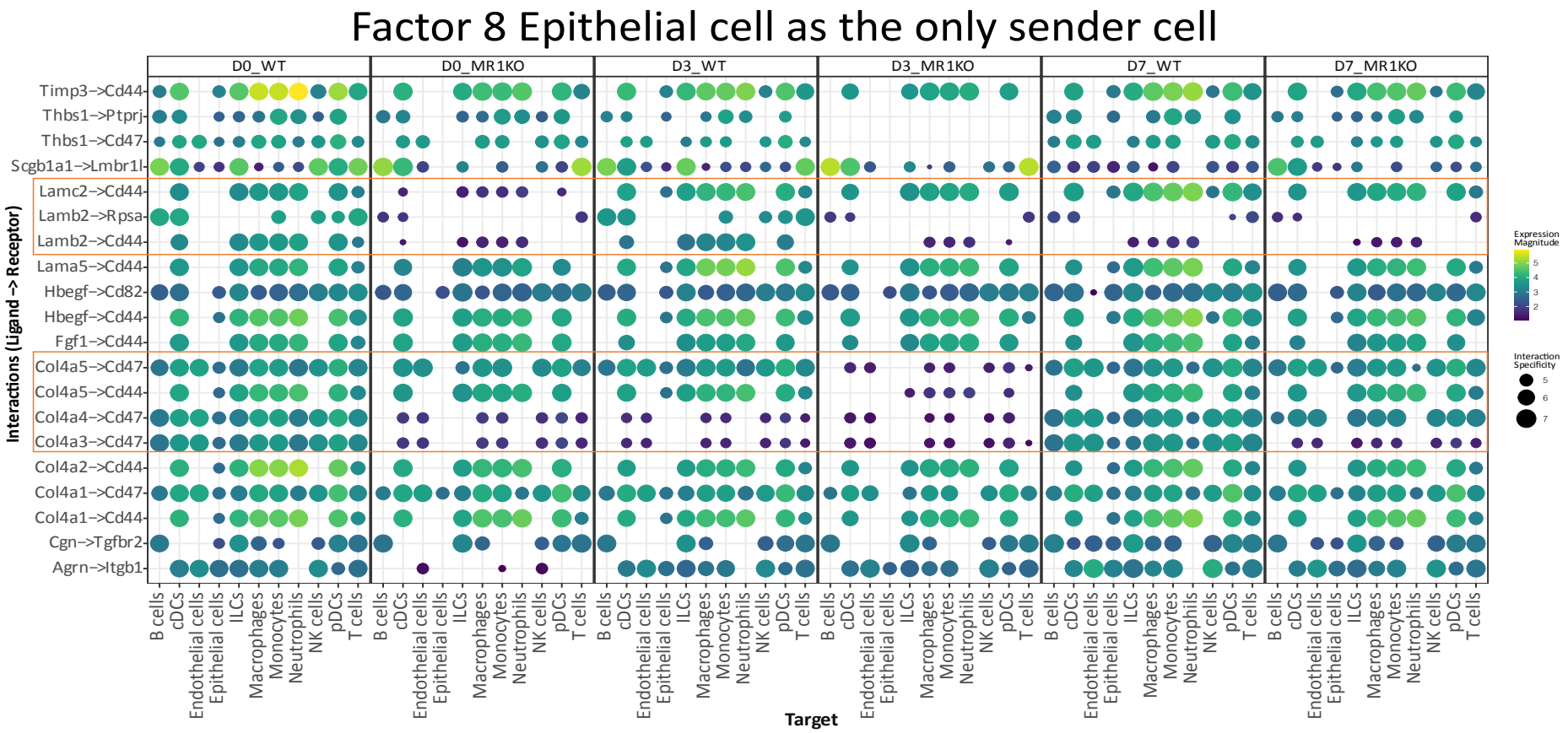
Factor 8 Epithelial cell as the only sender cell
D0_WT
D0_MR1KO
D3_WT
D3_MR1KO
D7_WT
D7_MR1KO
Timp3–>Cd44
Thbs1–>Ptprj
Thbs1–>Cd47
Scgb1a1–>Lmbr1l
Lamc2–>Cd44
Lamb2–>Rpsa
Lamb2–>Cd44
Lama5–>Cd44
Hbegf–>Cd82
Hbegf–>Cd44
Fgf1–>Cd44
Col4a5–>Cd47
Col4a5–>Cd44
Col4a4–>Cd47
Col4a3–>Cd47
Col4a2–>Cd44
Col4a1–>Cd47
Col4a1–>Cd44
Cgn–>Tgfbr2
Agrn–>Itgb1
Interactions (Ligand –> Receptor)
B cells
cDCs
Endothelial cells
Epithelial cells
ILCs
Macrophages
Monocytes
Neutrophils
NK cells
pDCs
T cells
Target
Expression Magnitude
5
4
3
2
Interaction Specificity
5
6
7

Figure 4.20 Dot plots showing predicted interactions between epithelial cells (sender cell) and other cell types (Factor 8) before and post bleomycin challenge in both WT and *Mr1*$^{-/-}$ mice.

Dot size indicates specificity of interaction to cell types. Colour intensity indicates the magnitude of the interaction. Significant discrepancies are emphasised by orange rectangles. Interactions that exhibited a specificity rank below 10^{-4} and differed between WT and *Mr1*$^{-/-}$ at any observed timepoints were presented.

Epithelial cells appeared as the primary sender cells in Factor 8 and the only receiver cells in Factor 4 (Figure 4.19A and Figure 4.20). Epithelial cells significantly contribute to the homeostatic and reparative processes in the lungs. Interactions between epithelial cells and various immune cell types were significantly disrupted in the absence of MAIT cells (Figure 4.20). For instance, *Col4a1/2/3/5* signals from epithelial cells to other immune cells were significantly reduced in *Mr1*$^{-/-}$ mice. Type IV collagens have a recognised role in regulating alveolar morphogenesis, epithelial cell proliferation and differentiation, and epithelial-mesenchymal association (Loscertales *et al.*, 2016). I also observed diminished epithelial-derived *Timp3*/*Hbegf* signals to *Cd44* on other immune cells in *Mr1*$^{-/-}$ mice. *Timp3* plays an essential role in the resolution of lung inflammation (Gill *et al.*, 2010), while *Hbegf* contributes to the differentiation of alveolar epithelial type II cells and is important for lung development (Leslie *et al.*, 1997; Wang *et al.*, 2009). Furthermore, the signals from *Lamb2* to *Rpsa* and *Cd44*, and from *Lamc2* to *Cd44*, are also diminished in *Mr1*$^{-/-}$ mice at baseline and on day 3 post-challenge. Both *Lamb2* and *Lamc2* are genes that encode epithelial basement membrane proteins. These proteins participate in a broad range of biological processes within the lung, including cell differentiation, adhesion, migration, and signalling (Moon *et al.*, 2015; Nguyen & Senior, 2006). Thus, reduced signals in *Mr1*$^{-/-}$ mice may result in compromised lung tissue integrity and disruption of normal cellular processes, exacerbating tissue damage following lung injury.

In a similar vein, endothelial cells were the main sender cells in Factor 6 and the primary receiver cell in Factor 7, and their key signals – *Col4α1/2*, *Cxcl12*, *Lamb2* for expression and *Cav1*, *Eng*, *Acvrl1*, *Tgfbr2*, *Notch1* for reception – were notably reduced in *Mr1*$^{-/-}$ mice at baseline (Day 0). These genes encode a diverse set of proteins: *Cav1* is a major component of

the inner surface of caveolae. *Notch1* is known to be involved in the development of numerous cell and tissue types. Macrophages, monocytes and cDCs emerged as the main receiver cells in Factor 3, suggesting more robust communication between myeloid cells and other immune and structural cells in WT mice compared to *Mr1*$^{-/-}$ mice.

The minimal changes in the gene expression profile across various cell types together with significant alterations in the proportion of these cells between WT and MAIT deficient *Mr1*$^{-/-}$ mice prompted us to further investigate the potential effects of MAIT cell deficiency on the interactions between T cells and myeloid cells. I found that the interactions between T cells and cDCs, which are mediated by several adhesion molecules and integrins such as *Icam1* in T cells and the *Itgax-Itgb2* complex in cDCs, along with chemokines and their receptors like *Xcl1* in T cells and *Xcr1* in cDCs, were downregulated in *Mr1*$^{-/-}$ mice compared to WT mice (Figure 4.21A). A similar trend was observed in the interactions between T cells and monocytes or macrophages prior to a bleomycin challenge (Figure 4.21B and C). Altogether, these findings imply that MAIT cells enhance intercellular communication among multiple cell types under homeostatic conditions.

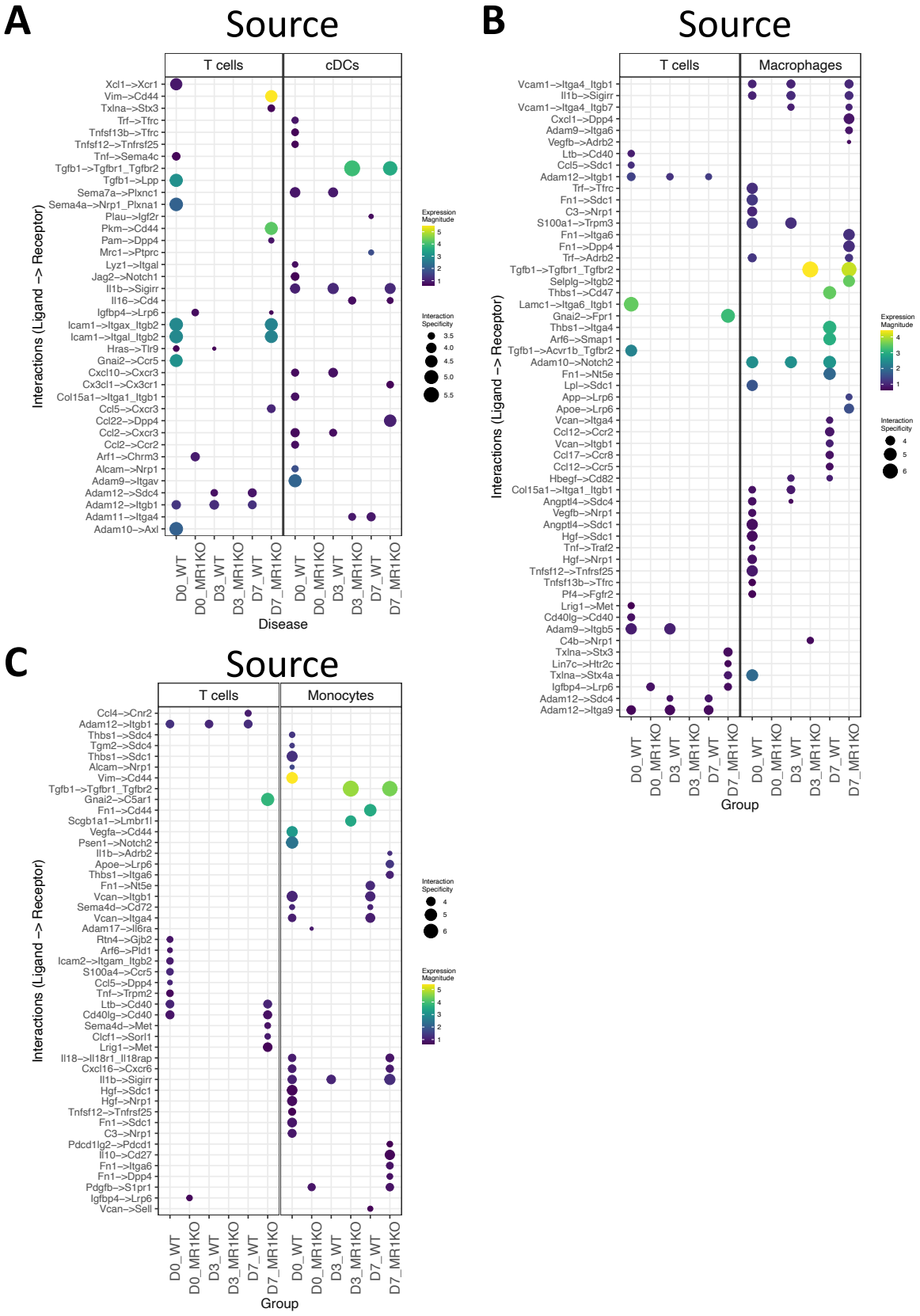
A
Source
T cells
cDCs
Interactions (Ligand –> Receptor)
Xcl1–>Xcr1
Vim–>Cd44
Txlna–>Stx3
Trf–>Tfrc
Tnfsf13b–>Tfrc
Tnfsf12–>Tnfrsf25
Tnf–>Sema4c
Tgfb1–>Tgfbr1_Tgfbr2
Tgfb1–>Lpp
Sema7a–>Plxnc1
Sema4a–>Nrp1_Plxna1
Plau–>Igf2r
Pkm–>Cd44
Pam–>Dpp4
Mrc1–>Ptprc
Lyz1–>Itgal
Jag2–>Notch1
Il1b–>Sigirr
Il16–>Cd4
Igfbp4–>Lrp6
Icam1–>Itgax_Itgb2
Icam1–>Itgal_Itgb2
Hras–>Tlr9
Gnai2–>Ccr5
Cxcl10–>Cxcr3
Cx3cl1–>Cx3cr1
Col15a1–>Itga1_Itgb1
Ccl5–>Cxcr3
Ccl22–>Dpp4
Ccl2–>Cxcr3
Ccl2–>Ccr2
Arf1–>Chrm3
Alcam–>Nrp1
Adam9–>Itgav
Adam12–>Sdc4
Adam12–>Itgb1
Adam11–>Itga4
Adam10–>Axl
D0_WT
D0_MR1KO
D3_WT
D3_MR1KO
D7_WT
D7_MR1KO
Disease
Expression Magnitude
Interaction Specificity
B
Source
T cells
Macrophages
Interactions (Ligand –> Receptor)
Vcam1–>Itga4_Itgb1
Il1b–>Sigirr
Vcam1–>Itga4_Itgb7
Cxcl1–>Dpp4
Adam9–>Itga6
Vegfb–>Adrb2
Ltb–>Cd40
Ccl5–>Sdc1
Adam12–>Itgb1
Trf–>Tfrc
Fn1–>Sdc1
C3–>Nrp1
S100a1–>Trpm3
Fn1–>Itga6
Fn1–>Dpp4
Trf–>Adrb2
Tgfb1–>Tgfbr1_Tgfbr2
Selplg–>Itgb2
Thbs1–>Cd47
Lamc1–>Itga6_Itgb1
Gnai2–>Fpr1
Thbs1–>Itga4
Arf6–>Smap1
Tgfb1–>Acvr1b_Tgfbr2
Adam10–>Notch2
Fn1–>Nt5e
Lpl–>Sdc1
App–>Lrp6
Apoe–>Lrp6
Vcan–>Itga4
Ccl12–>Ccr2
Vcan–>Itgb1
Ccl17–>Ccr8
Ccl12–>Ccr5
Hbegf–>Cd82
Col15a1–>Itga1_Itgb1
Angptl4–>Sdc4
Vegfb–>Nrp1
Angptl4–>Sdc1
Hgf–>Sdc1
Tnf–>Traf2
Hgf–>Nrp1
Tnfsf12–>Tnfrsf25
Tnfsf13b–>Tfrc
Pf4–>Fgfr2
Lrig1–>Met
Cd40lg–>Cd40
Adam9–>Itgb5
C4b–>Nrp1
Txlna–>Stx3
Lin7c–>Htr2c
Txlna–>Stx4a
Igfbp4–>Lrp6
Adam12–>Sdc4
Adam12–>Itga9
D0_WT
D0_MR1KO
D3_WT
D3_MR1KO
D7_WT
D7_MR1KO
Group
Expression Magnitude
Interaction Specificity
C
Source
T cells
Monocytes
Interactions (Ligand –> Receptor)
Ccl4–>Cnr2
Adam12–>Itgb1
Thbs1–>Sdc4
Tgm2–>Sdc4
Thbs1–>Sdc1
Alcam–>Nrp1
Vim–>Cd44
Tgfb1–>Tgfbr1_Tgfbr2
Gnai2–>C5ar1
Fn1–>Cd44
Scgb1a1–>Lmbr1l
Vegfa–>Cd44
Psen1–>Notch2
Il1b–>Adrb2
Apoe–>Lrp6
Thbs1–>Itga6
Fn1–>Nt5e
Vcan–>Itgb1
Sema4d–>Cd72
Vcan–>Itga4
Adam17–>Il6ra
Rtn4–>Gjb2
Arf6–>Pld1
Icam2–>Itgam_Itgb2
S100a4–>Ccr5
Ccl5–>Dpp4
Tnf–>Trpm2
Ltb–>Cd40
Cd40lg–>Cd40
Sema4d–>Met
Clcf1–>Sorl1
Lrig1–>Met
Il18–>Il18r1_Il18rap
Cxcl16–>Cxcr6
Il1b–>Sigirr
Hgf–>Sdc1
Hgf–>Nrp1
Tnfsf12–>Tnfrsf25
Fn1–>Sdc1
C3–>Nrp1
Pdcd1lg2–>Pdcd1
Il10–>Cd27
Fn1–>Itga6
Fn1–>Dpp4
Pdgfb–>S1pr1
Igfbp4–>Lrp6
Vcan–>Sell
D0_WT
D0_MR1KO
D3_WT
D3_MR1KO
D7_WT
D7_MR1KO
Group
Interaction Specificity
Expression Magnitude

Figure 4.21 Interactions of T cells with myeloid cells pre- and post-bleomycin challenge in both WT and *Mr1*$^{-/-}$ mice.

Interactions of T cells with cDCs (**A**), macrophages (**B**), and monocytes (**C**) pre- and post-bleomycin challenge in both WT and *Mr1*$^{-/-}$ mice. Dot size indicates specificity of interaction to cell types. Colour intensity indicates the magnitude of the interaction. In each subgraph, the initial block depicts interactions where T cells are the source and other cells serve as the targets. The subsequent block illustrates interactions where T cells are the targets and other cells are the source. Interactions that exhibited a specificity rank below 5×10^{-4} and differed between WT and *Mr1*$^{-/-}$ at any observed timepoints were presented.

4.3.5 Adoptive transfer of Flt3 ligand-generated bone marrow-derived dendritic cells to *Mr1*$^{-/-}$ mice reverts weight loss and reduces tissue damage

I reported compromised accumulation of cDC1 in *Mr1*$^{-/-}$ mice in the absence of MAIT cells. Given the exclusive presence of DNGR-1, a C-type lectin receptor, in cDC1 and its crucial role in managing tissue damage by detecting actin filaments exposed on necrotic cell death (Zhang *et al.*, 2012), I further probed its specific influence in my context. Previous studies have shown that DNGR-1 in DCs limits tissue damage in pancreatitis by dampening neutrophil recruitment, and DNGR-1 also controls neutrophil recruitment and pathology associated with systemic candidiasis (Del Fresno *et al.*, 2018). I therefore examined the role of cDC1-DNGR-1 in weight loss and tissue fibrosis in both WT and *Mr1*$^{-/-}$ mice following bleomycin challenge. Consistent with previous data (Figure 4.1A to D), *Mr1*$^{-/-}$ mice showed greater weight loss (Figure 4.22A and B), more pronounced tissue fibrosis (Figure 4.22C and D), and elevated gene expression

of *Col1α1* and *Col3α1* on D21 post-bleomycin challenge, compared to WT mice (Figure 4.22E and F). DNGR-1 is notably expressed in the $CD11b^{lo}$ $CD24^{hi}$ subset of Flt3L-generated bone marrow-derived dendritic cells (FLT3L-BMDC) (Figure 4.23A). For the adoptive transfer, CD11c-enriched FLT3L-BMDCs were utilized (Figure 4.23B), and I confirmed the presence of these cells on days 3 and 7 post-transfer (Figure 4.23C). Significantly, intranasal adoptive transfer of FLT3L-BMDCs on day 1 post-bleomycin challenge significantly alleviated weight loss and tissue fibrosis in $Mr1^{-/-}$ mice (Figure 4.22). This alleviating effect was abrogated by antibody blockade of DNGR-1 but persisted in $Mr1^{-/-}$ mice treated with isotype control (Figure 4.22). These results suggest that the protective effects offered by MAIT cells are mediated, at least partially, by regulating cDC1, and that cDC1s curb tissue damage through DNGR-1 signalling.

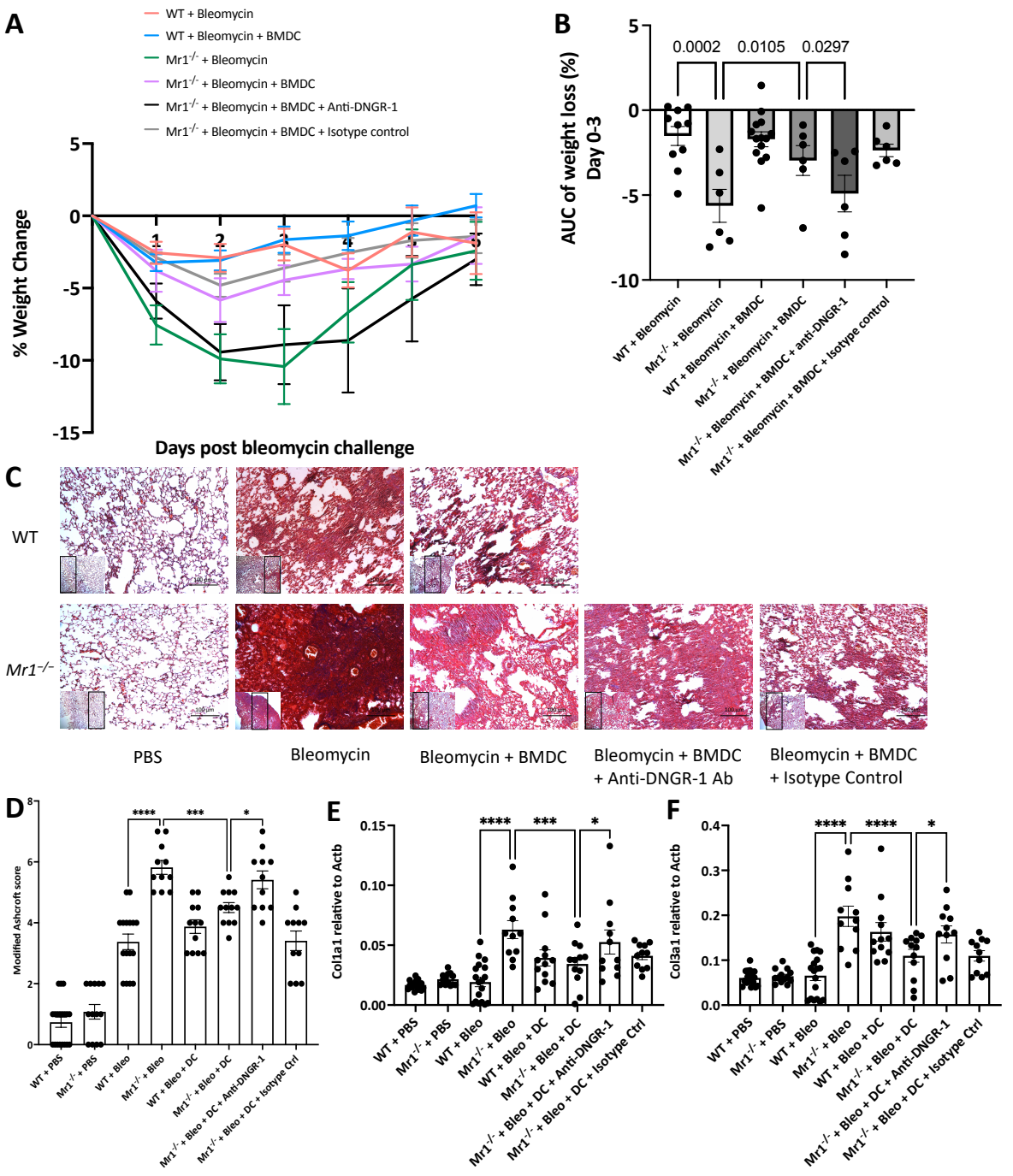

Figure 4.22 Adoptive transfer of bone marrow-derived dendritic cells (BMDC) to *Mr1*$^{-/-}$ mice reverts weight loss and reduces tissue damage.

(**A**) Body weight loss expressed as a percentage of the weight before bleomycin challenge. Adoptive transfer, conducted twice, utilized 5 × 10^5 BMDCs from the bone marrows of mice

infected with *Salmonella* Typhimurium BRD509 on day 28 post-infection. Cells were transferred 1-day post-bleomycin challenge. (**B**) Body weight loss as area under the curve (AUC). (**C**) Representative images of lung slices of PBS or bleomycin-challenged WT and *Mr1*$^{-/-}$ mice at D21, stained with Masson's trichrome. (**D**) Modified Ashcroft score of lung slices of PBS or bleomycin-challenged WT and *Mr1*$^{-/-}$ mice at day 21, stained with Masson's trichrome. (**E** and **F**) Gene expression of *Col1α1* (**E**), and *Col3α1* (**F**) in lung homogenates of PBS or bleomycin-challenged WT and *Mr1*$^{-/-}$ mice at day 21. *Actb* was used as a housekeeping gene. For weight loss results, data are one representative experiment of two independent experiments, with 4–6 mice per group in each replicate. For histology score and RT-qPCR results, data were pooled from two independent experiments (n=4-6 per group). Graphs show mean ± SEM. Statistical significance tested by one-way ANOVA with Holm-Sidak's multiple comparisons test; *$P < 0.05$, **$P < 0.01$, ***$P < 0.001$, ****$P < 0.0001$.

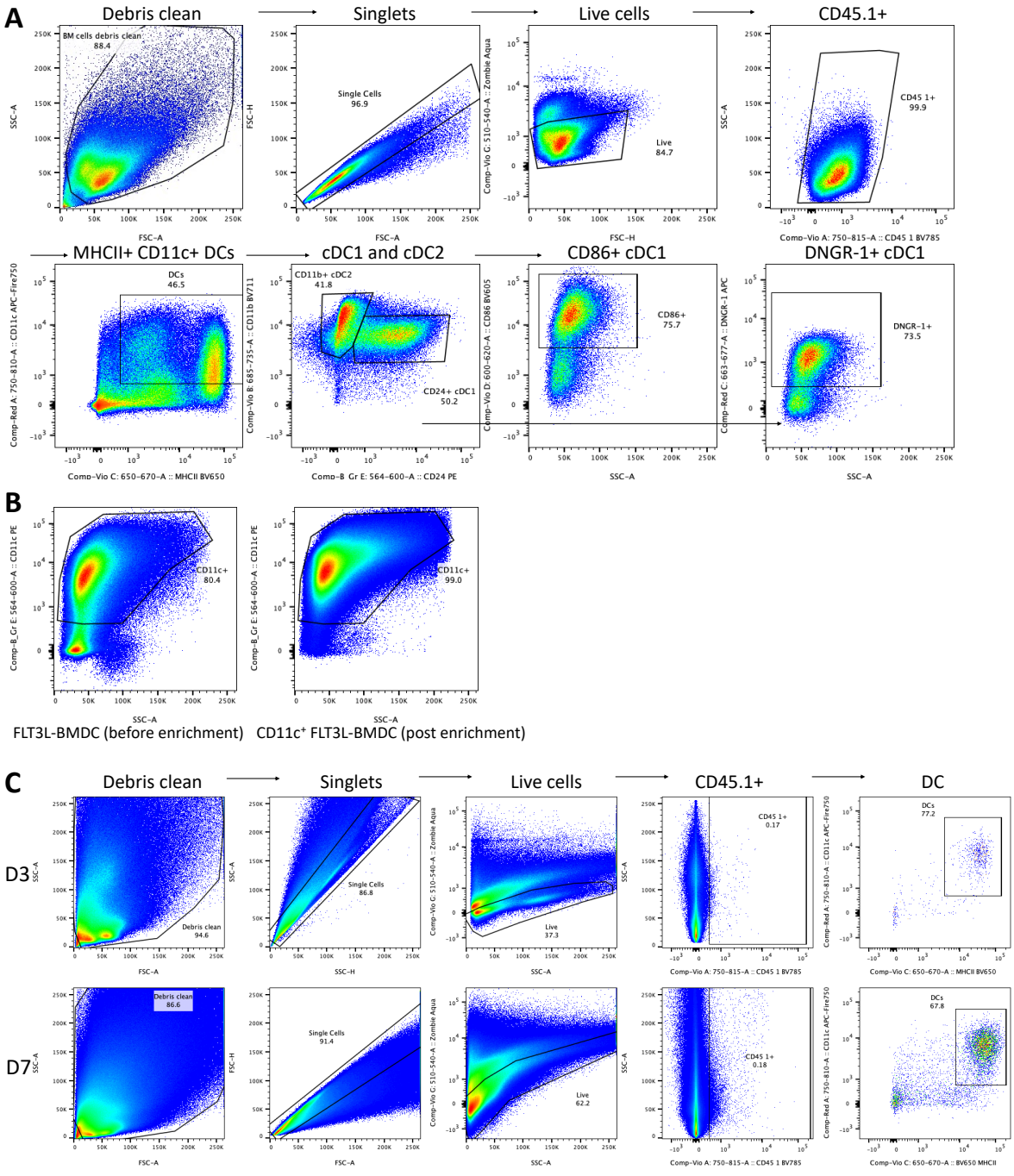

Figure 4.23 Flow cytometry plots of bone marrow-derived dendritic cells.

(**A**) Gating scheme for the identification of conventional dendritic cells (cDC) in Fms-like tyrosine kinase-3 ligand (Flt3L)-generated bone marrow-derived dendritic cells (FLT3L-

BMDC), and expression of CD86 and DNGR-1 on cDC1. cDCs are identified as $CD11c^+$ $MHCII^+$ cells and can be divided into cDC1 ($CD24^+$ $CD11b^-$) and cDC2 ($CD24^-$ $CD11b^+$). (**B**) Representative flow plot showing the $CD11c^+$ FLT3L-BMDC population before and post-CD11c enrichment (gated on all live $CD45.1^+$ cells). (**C**) Flow cytometric analysis of adoptive-transferred $CD11c^+$ bone marrow-derived dendritic cells (BMDC, gated as $CD45.1^+$ $MHCII^+$ $CD11c^+$ population) in *Mr1*$^{-/-}$ mice lungs at day 3 and day 7 post-adoptive transfer, respectively.

4.3.6 Spatial transcriptomic analysis reveals co-localization of T cells and cDC1

Structural cells and spatial information, which are often lost during single-cell preparations, can be captured by targeted spatial transcriptomics methods like MERFISH (Chen *et al.*, 2015). This technology delineates the topography of cell types and states within tissues at single-cell and subcellular resolutions by quantifying the expression of a predetermined gene set. Previous analyses of cell communication posited a significant role for MAIT cells in cellular interactions during sterile lung injury induced by bleomycin challenge. To elucidate this further, the following questions were asked: What is the spatial distribution of MAIT cells within lung tissue? How do MAIT cells interface with adjacent cells? In what way does gene expression pertaining to MAIT cell functionality vary across different lung regions, and does it associate with tissue damage? Moreover, how do MAIT cells interact with other immune cells in the lung, and what specific cell-cell interactions or signalling pathways are implicated?

For this investigation, I employed the MERSCOPE platform for spatial transcriptomic profiling (Figure 4.24) across both genotypes at baseline, and then on days 3, 5, 7, 10, 14, 21,

and 28 following bleomycin administration (Figure 4.25). I selected 500 genes based on marker genes from my prior scRNA-seq dataset annotations, bulk RNA-seq DEGs, markers in the TotalSeq™ Mouse Universal Cocktail (BioLegend, Cat. No. 199903), and literature. The majority of cell types from the scRNA-seq dataset were detectable via MERSCOPE (Figure 4.26). Notably, T cells and cDC1 exhibited distinct spatial colocalization in the mouse lung (Figure 4.27). This observation facilitated a temporal analysis of how such colocalization patterns evolve in WT and *Mr1*$^{-/-}$ mice after bleomycin challenge. Further data analysis is currently in progress.

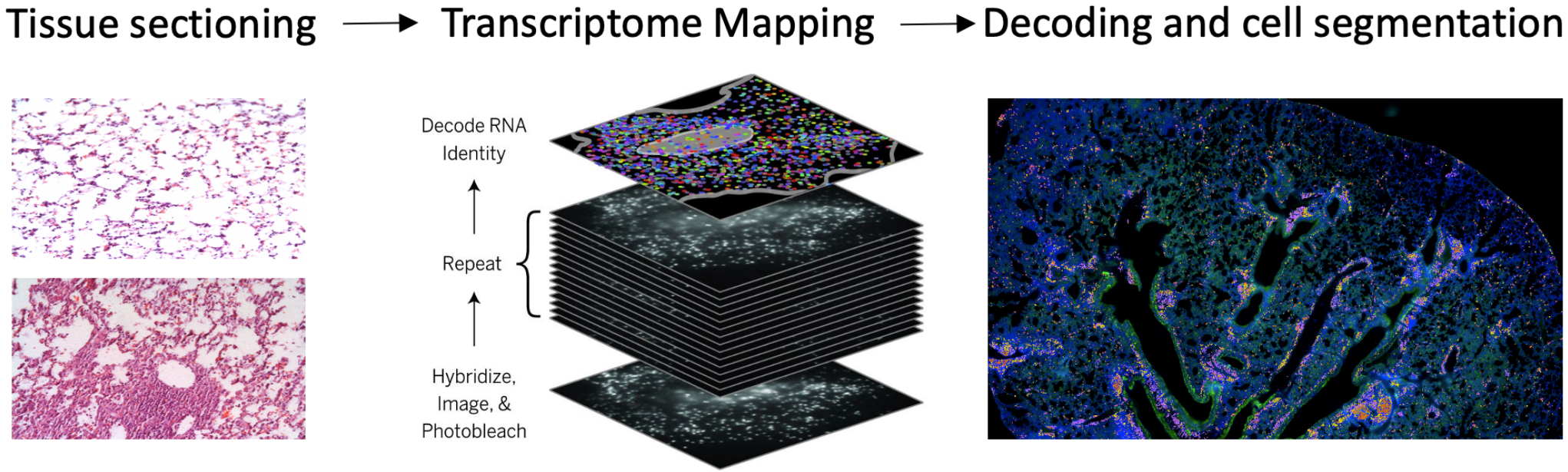

Figure 4.24 MERSCOPE experimental scheme.

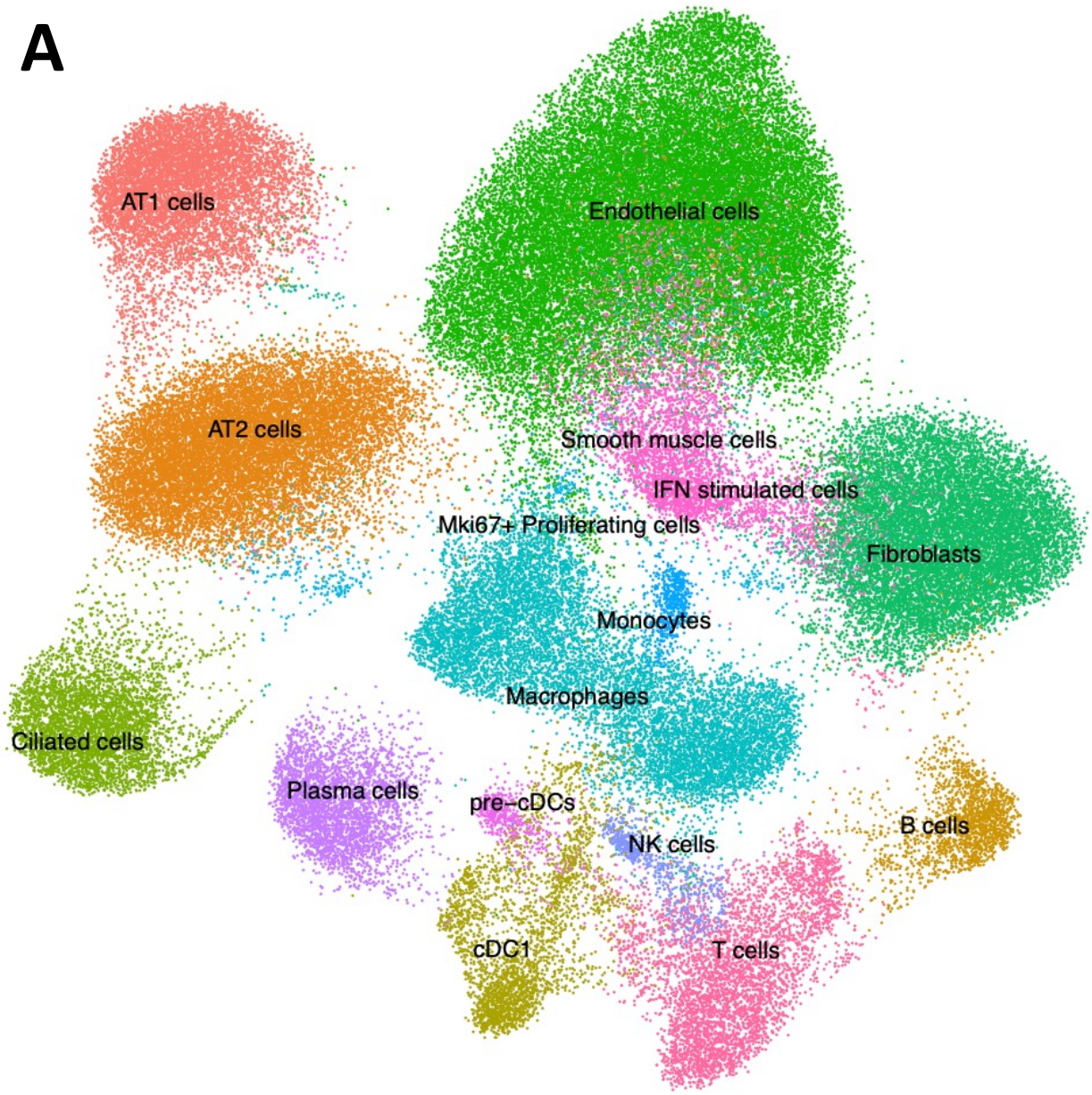
A
AT1 cells
Endothelial cells
AT2 cells
Smooth muscle cells
IFN stimulated cells
Mki67+ Proliferating cells
Fibroblasts
Monocytes
Macrophages
Ciliated cells
Plasma cells
pre−cDCs
NK cells
B cells
cDC1
T cells

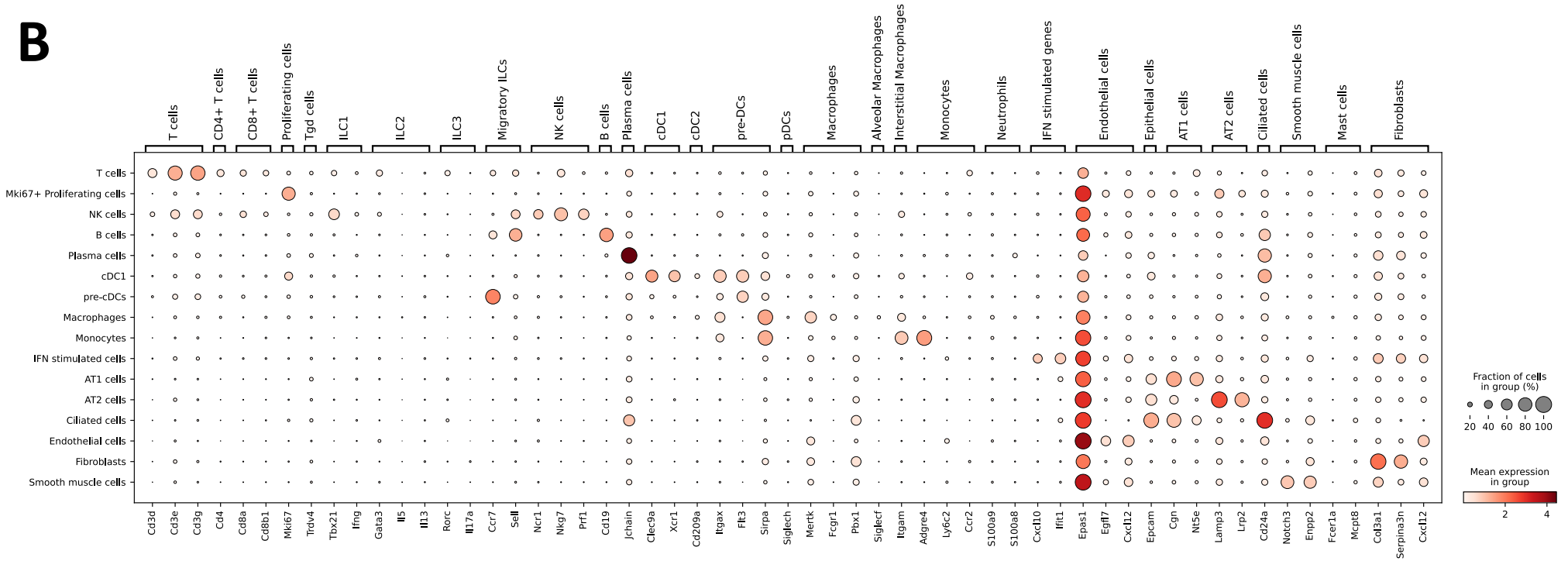

Figure 4.25 Annotation of major cell types in mouse lungs pre- and post-bleomycin challenge.

(**A**) UMAP embedding of 100,000 randomly sampled single cells from all MERSCOPE slides, color-coded by predicted cell lineage. (**B**) Dot plot illustrating the top discriminative gene sets for each cell lineage in comparison to all others. Dot size reflects the proportion of cells expressing the marker within each lineage. Colour scales represent the normalized mean gene expression across each cell lineage.

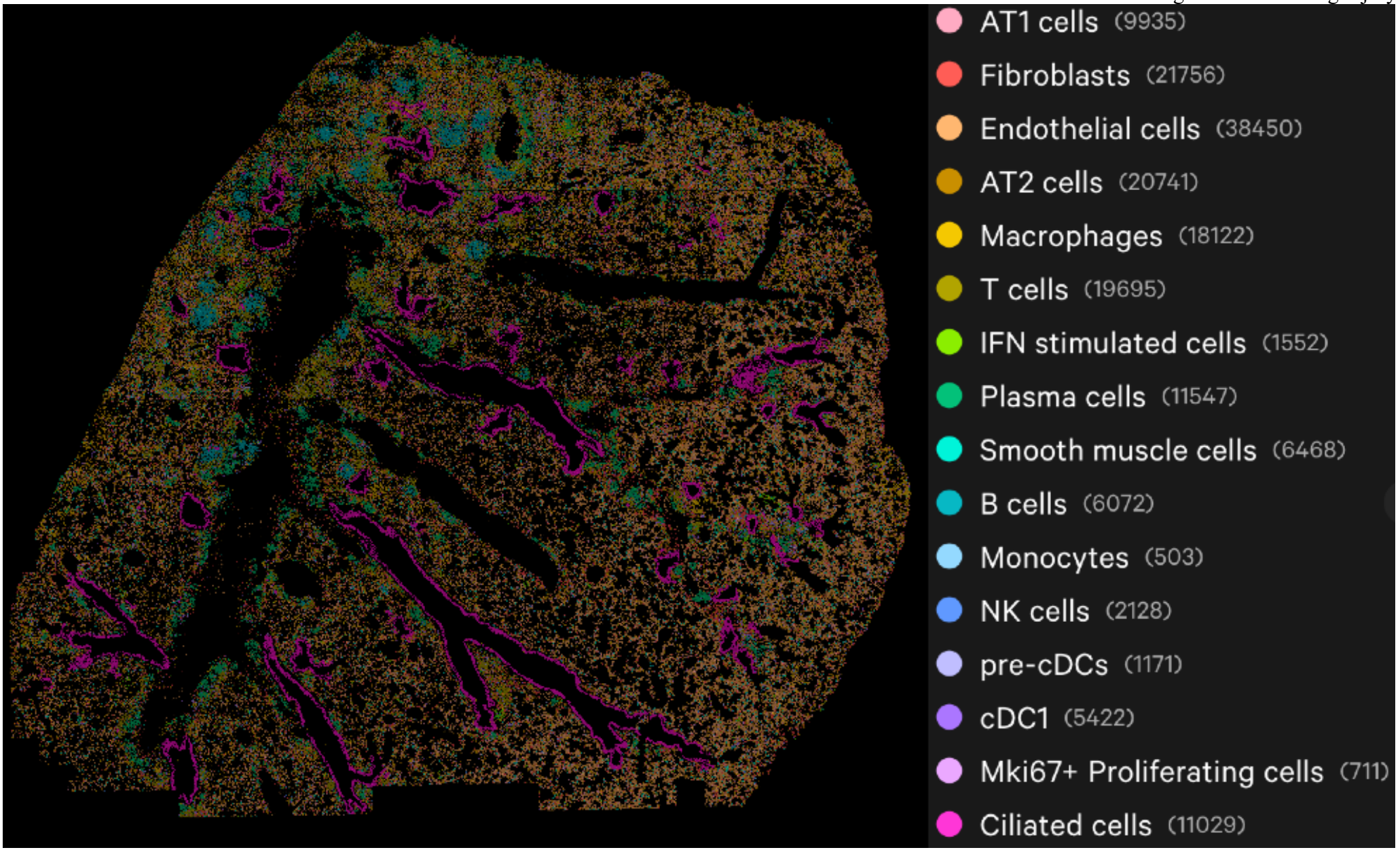
AT1 cells (9935)
Fibroblasts (21756)
Endothelial cells (38450)
AT2 cells (20741)
Macrophages (18122)
T cells (19695)
IFN stimulated cells (1552)
Plasma cells (11547)
Smooth muscle cells (6468)
B cells (6072)
Monocytes (503)
NK cells (2128)
pre-cDCs (1171)
cDC1 (5422)
Mki67+ Proliferating cells (711)
Ciliated cells (11029)

Figure 4.26 Spatial distribution of different cell types in the WT mouse lung pre-bleomycin challenge.

Colour indicates different cell types. The number in parentheses next to each cell type represents the count of cells of that type in the sample.

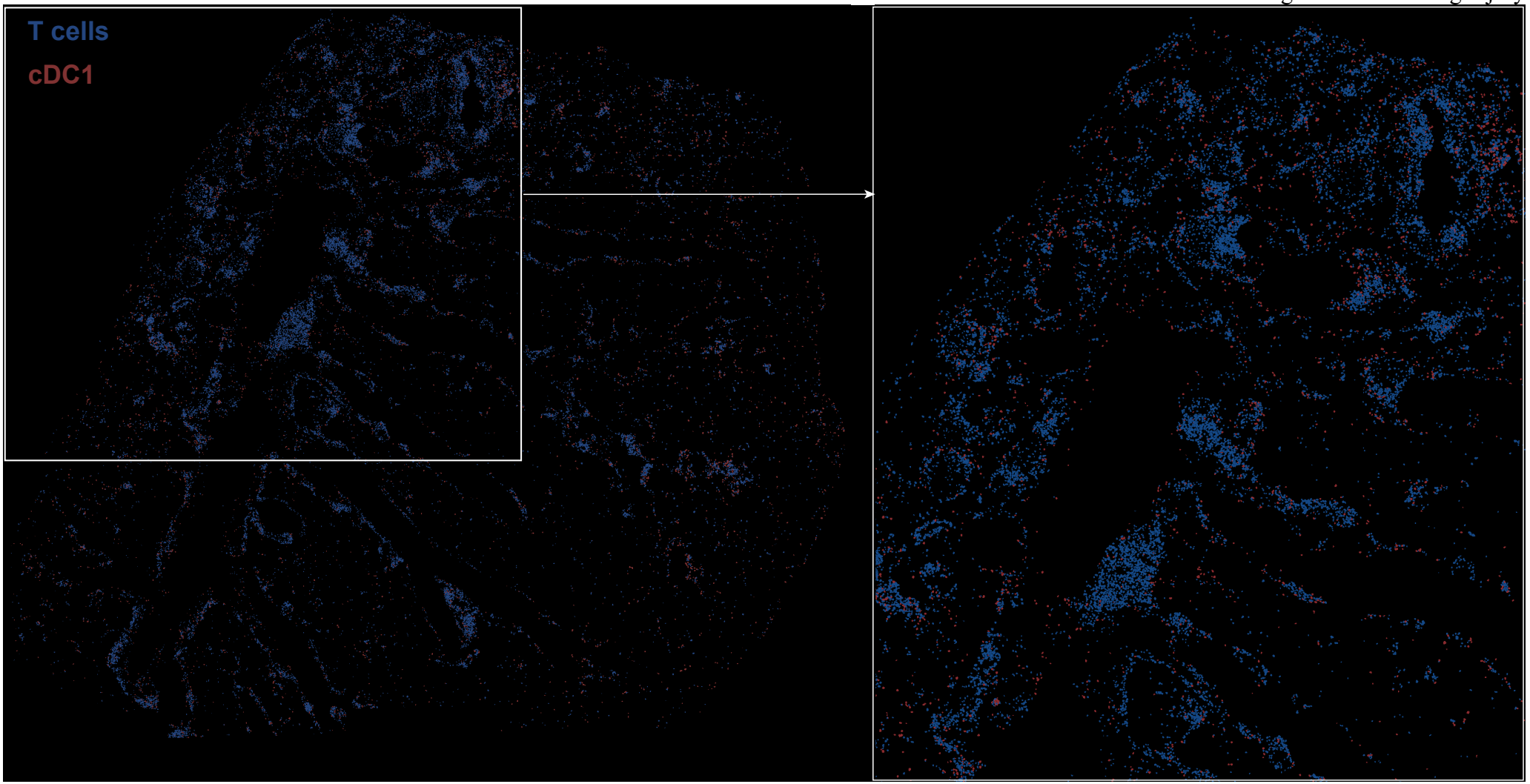
T cells
cDC1

Figure 4.27 Spatial distribution of T cells and cDC1 the WT mouse lung pre-bleomycin challenge.

4.4 Discussion

After bleomycin exposure, *Mr1*$^{-/-}$ mice not only suffer more severe weight loss, but also display an upregulated gene expression of *Col1a1* and *Col3a1*, suggesting intensified tissue damage in the lungs of *Mr1*$^{-/-}$ mice. Owing to their anatomical placement and resemblance to other tissue-resident lymphocytes (Hinks *et al.*, 2019), MAIT cells have been proposed to contribute to tissue protection (Constantinides *et al.*, 2019; Leng *et al.*, 2019). For instance, in the nonobese diabetic (NOD) mouse model of type 1 diabetes, *Mr1*$^{-/-}$ NOD mice have displayed impaired intestinal barrier integrity, accelerated disease progression, enhanced intestinal permeability, and augmented bacterial translocation, implying a protective role of MAIT cells in maintaining surface homeostasis (Rouxel *et al.*, 2017). Similarly, in scenarios involving allogeneic bone marrow transplantation, *Mr1*$^{-/-}$ mice showed compromised survival, escalated colonic graft versus host disease (GVHD), and diminished intestinal barrier integrity (Varelias *et al.*, 2018). These observations underscore the role of MAIT cells in preserving barrier integrity. Similar results have been observed in a mouse model of non-alcoholic steatohepatitis, where *Mr1*$^{-/-}$ mice on a diet deficient in methionine and choline exhibited more severe liver damage and disease intensity compared with WT. The underlying mechanism may involve an altered ratio of pro- and anti-inflammatory hepatic macrophages (Li *et al.*, 2018), though further research is needed to determine the exact role of MAIT cells in modulating macrophage function. Moreover, a recent study showed that MAIT cells were present in the meninges and expressed high levels of antioxidant molecules, and their absence led to meningeal ROS accumulation and barrier leakage, highlighting the function of MAIT cells in preserving meningeal homeostasis and cognitive function (Y. Zhang *et al.*, 2022). Collectively,

these findings point to an important role of MAIT cells in maintaining tissue homeostasis and reducing damage, especially in the context of inflammatory diseases.

Significant differences in weight loss were observed between *Mr1*$^{-/-}$ and WT mice in the initial days following bleomycin challenge, yet the notable decrease in cDC1 accumulation in *Mr1*$^{-/-}$ mice only occurred on day 7 post-challenge. This could indicate additional roles for MAIT cells in maintaining tissue homeostasis, in addition to the DNGR1-cDC1 mechanism elucidated here. As mentioned, my scRNA-seq dataset highlights baseline differences between *Mr1*$^{-/-}$ and WT mice, notably a reduced frequency of alveolar macrophages and diminished Pbx1 expression within these cells in *Mr1*$^{-/-}$ mice (Figure 4.15). Pbx1, a key transcriptional regulator in macrophages, initiates IL-10 transcription during apoptotic cell clearance via the apoptotic cell-response element (ACRE) in the Il10 promoter, indicating its significance in mitigating inflammation and maintaining tissue homeostasis during apoptosis (Chung *et al.*, 2007; Saraiva & O'Garra, 2010; Zhao *et al.*, 2014). My data suggest that MAIT cells might facilitate a constitutive anti-inflammatory state in alveolar macrophages during homeostasis, potentially crucial in shaping the lung's response to incident tissue injury. Additionally, my total lung RNA-seq dataset highlights an early upregulation (as soon as day 3 post-bleomycin challenge) of pro-inflammatory genes, *Il6* and *Ccl2*, in *Mr1*$^{-/-}$ mice. This rapid upregulation might contribute to the early onset of weight loss observed in these mice. Further scrutiny of the scRNA-seq data identifies mast cells, interstitial macrophages, fibroblasts and CCR2^{+} Ly6C^{hi} monocytes as the primary sources of these pro-inflammatory genes (Figure 4.28).

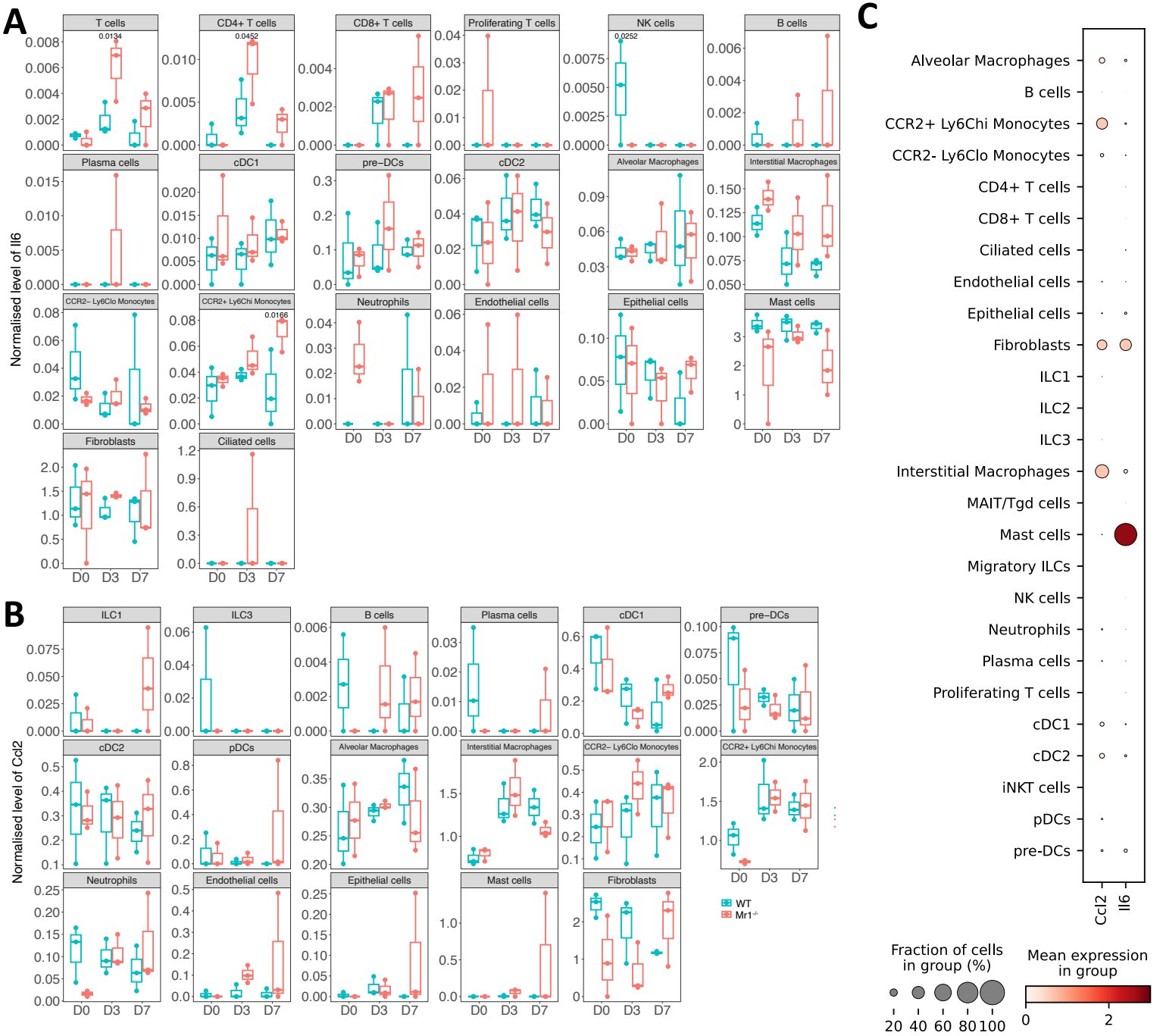
A
T cells
CD4+ T cells
CD8+ T cells
Proliferating T cells
NK cells
B cells
Plasma cells
cDC1
pre−DCs
cDC2
Alveolar Macrophages
Interstitial Macrophages
CCR2− Ly6Clo Monocytes
CCR2+ Ly6Chi Monocytes
Neutrophils
Endothelial cells
Epithelial cells
Mast cells
Fibroblasts
Ciliated cells
Normalised level of Il6
D0 D3 D7
B
ILC1
ILC3
B cells
Plasma cells
cDC1
pre−DCs
cDC2
pDCs
Alveolar Macrophages
Interstitial Macrophages
CCR2− Ly6Clo Monocytes
CCR2+ Ly6Chi Monocytes
Neutrophils
Endothelial cells
Epithelial cells
Mast cells
Fibroblasts
Normalised level of Ccl2
WT
Mr1-/-
C
Alveolar Macrophages
B cells
CCR2+ Ly6Chi Monocytes
CCR2- Ly6Clo Monocytes
CD4+ T cells
CD8+ T cells
Ciliated cells
Endothelial cells
Epithelial cells
Fibroblasts
ILC1
ILC2
ILC3
Interstitial Macrophages
MAIT/Tgd cells
Mast cells
Migratory ILCs
NK cells
Neutrophils
Plasma cells
Proliferating T cells
cDC1
cDC2
iNKT cells
pDCs
pre-DCs
Ccl2
Il6
Fraction of cells in group (%)
20 40 60 80 100
Mean expression in group
0
2

Figure 4.28 Differential expression of inflammatory markers *Il6* and *Ccl2* in lung cell types pre- and post-bleomycin challenge.

Bar plots showing the gene expression of *Il6* (**A**) and *Ccl2* (**B**) across various cell types pre- and post-bleomycin challenge. (**C**) Dot plot illustrating the combined gene expression levels of *Il6* and *Ccl2* across different cell types, collated from all time points and both WT and *Mr1*$^{-/-}$ mice.

MAIT cells and DCs coordinate in orchestrating immune responses against various pathogens and maintaining immune protection. During *Francisella tularensis* infection in mice, MAIT cell-dependent GM-CSF production contributed to monocyte differentiation into DCs, although MAIT cells were not explicitly identified as the GM-CSF source (Meierovics & Cowley, 2016). *In vitro* investigations with human MAIT cells revealed their capacity to induce DC maturation. When co-cultured with immature human DCs in the presence of 5-A-RU/methylglyoxal (MeG), MR1-dependent upregulation of CD86, CD80, CD40, and PD-L1 was observed on the DCs. Additionally, DC IL-12 production was contingent upon both MR1 and CD40L (Salio *et al.*, 2017). Furthermore, pulmonary MAIT cell stimulation *in vivo* with 5-A-RU/MeG or CpG led to the accumulation of CD11b^{+} DCs in the lung and migration of both CD11b^{+} and CD103^{+} DCs from the lung to the mediastinal lymph node. However this study did not explore the underlying mechanism driving the accumulation of DCs in response to MAIT cell activation (Philipp, 2020). My group have also shown MAIT cells amplify the early immune response to adenovirus vector vaccines, a mechanism necessitating pDC-derived IFN-α, monocyte-derived IL-18, and IFN-α-induced TNF from monocytes (Provine *et al.*,

2021). Additionally, intranasal immunisation with MAIT cell agonists and proteins activates DCs via CD40L, priming T follicular helper cells and inducing protective humoral immunity, establishing MAIT cells as potential cellular adjuvants in mucosal vaccines (Pankhurst *et al.*, 2023).

Currently, there are no *in vivo* studies examining the impact of MAIT cell and DC interactions within the context of sterile injury and tissue damage. In MAIT cell-deficient *Mr1*$^{-/-}$ mice, I observed an impaired early accumulation of CD103^{+} cDC1 and pre-DC populations in the lungs upon bleomycin challenge. Interestingly, there were minimal DEGs specific to pre-DC and cDC1 when comparing WT and *Mr1*$^{-/-}$ mice. This finding suggests that while MAIT cells are essential for the accumulation of cDC1, they may not modify the functional characteristics of these cells to influence their accumulation. The mechanism behind this remains to be elucidated: it is uncertain whether MAIT cells directly recruit DCs from the peripheral blood and bone marrow, indirectly draw in the precursor pre-DC population, or engage an alternative pathway. My findings highlight that MAIT cells produce GM-CSF, IFN-γ and IL17A in the context of bleomycin-induced lung injury. Both GM-CSF and IFN-γ are important for the maturation, differentiation, and recruitment of DCs to sites of inflammation (Cabeza-Cabrerizo *et al.*, 2021; Pan *et al.*, 2004). Moreover, IL-17 has been observed to augment the activation, migration, and overall functionality of airway DCs, which leads to more effective antigen-specific T cell activation and the progression of experimental allergic asthma (Jirmo *et al.*, 2020). My study also demonstrates an upregulation in the gene expression of *Ccrl2*, *Ccl3*, and *Cxcl2* in MAIT cells following bleomycin exposure (Figure 3.12). This upregulation could be instrumental in the accumulation of pre-DC and cDC1. Notably, *Ccrl2*, known as an inflammatory chemokine receptor, is implicated in the trafficking of lung DCs and in managing

excessive airway inflammatory responses (Otero *et al.*, 2010). *Ccl3*, on the other hand, has been identified as a significant mobilizer of DCs, facilitating their movement into the bloodstream and toward inflammation sites (Dieu *et al.*, 1998; Zhang *et al.*, 2004). I also noted a pronounced reduction in the ILC3 population in *Mr1*$^{-/-}$ mice relative to WT counterparts during sterile injury, suggesting a putative role of MAIT cells in maintaining ILC3 numbers. ILC3s are known to regulate the activity of various immune cells including DCs, macrophages, eosinophils, and neutrophils, contributing to their recruitment, movement, and tissue reparative functions. In steady-state conditions, ILC3s secrete Th17-associated cytokines such as IL-17A, IL-17F, IL-22, and GM-CSF, while during inflammatory responses, they are also capable of producing IFN-γ (Klose & Artis, 2016; Robinette *et al.*, 2015). These cytokines interact with respective receptors – IL-17R, IFN-γR, and GM-CSFR – on myeloid cells, which are particularly receptive to GM-CSF (Lavin *et al.*, 2014; Miller *et al.*, 2012). The GM-CSF produced by ILC3s has been implicated in bridging innate and adaptive immunity through its influence on myeloid cells (Mortha & Burrows, 2018). Thus, MAIT cells, through the production of cytokines such as GM-CSF, IFN-γ and IL17A, along with various chemokines, may exert a direct influence on the migration and functionality of DCs. Additionally, these factors could indirectly affect the function and maintenance of ILC3s, subsequently affecting the downstream accumulation and activity of diverse myeloid populations in response to sterile lung injury.

My research provides evidence that cDC1 cells contribute to tissue protection by mediating responses to cellular damage through DNGR-1 signalling. DNGR-1, or CLEC9A, a type II transmembrane protein categorized within the C-type lectin receptor (CLR) family's group V, is abundantly expressed on cDC1 cells. This receptor has a unique role in recognizing dead

cells by binding with its C-type lectin-like domain (CTLD) to F-actin, which becomes exposed upon disruption of cell membrane integrity (Zhang *et al.*, 2012). The subsequent phosphorylation of a hemITAM, especially at the tyrosine 7 residue, leads to SYK activation (Canton *et al.*, 2021; Iborra *et al.*, 2012; Sancho *et al.*, 2009). This triggers an intracellular response involving activation of NADPH oxidase and production of ROS, which induces lipid peroxidation, damages phagosomal membranes and causes the release of their contents into the cytosol (Canton *et al.*, 2021; Henry *et al.*, 2023). Consequently, this permits cross-presentation of antigens to $CD8^+$ T cells through the MHC-I pathway, traditionally used for presenting endogenous antigens. The ability of DNGR-1-mediated cDC1 signalling to detect and respond to cell damage not only mitigates the risk of excessive inflammation and collateral damage but also facilitates the prompt resolution of the immune response, underlying the critical role of cDC1s in adaptive immunity and tissue homeostasis.

I showed that intranasal adoptive transfer of FLT3L-BMDC ameliorated the weight loss and reduced tissue damage of *Mr1*$^{-/-}$ mice. The use of FLT3L-BMDC was important for this study because DNGR-1 is not expressed by GM-CSF-derived BMDCs but is highly expressed in the $CD11b^{lo}$ $CD24^{hi}$ subset of FLT3L-BMDCs (Figure 4.23A), which corresponds to cDC1 subset (Naik *et al.*, 2005; Sancho *et al.*, 2008). I administered BMDCs via intranasal adoptive transfer because this ensured their sustained presence in the lung in sufficient numbers to remain functional at the site of inflammation during the early stages of inflammation, as has been shown in previous studies in which pre-infected DCs successfully migrated to the mediastinal lymph nodes and activated antigen-specific CD4 T cells 60 hours post-transfer (Srivastava *et al.*, 2016). Understanding the role of MAIT cells in driving monocyte differentiation into cDC1 provides valuable insights into the complex interplay between innate and adaptive immunity.

The crosstalk between MAIT cells and DCs may contribute to the fine-tuning of immune responses, thus ensuring a balanced and effective defence against pathogens while minimising tissue damage.

4.5 Conclusion

- *Mr1*$^{-/-}$ mice show more severe tissue damage than WT mice. Early accumulation of cDC1 and pre-DCs in the lungs of *Mr1*$^{-/-}$ mice is impaired after pulmonary bleomycin challenge.

- Adoptive transfer of FLT3L-BMDC to *Mr1*$^{-/-}$ mice reverts weight loss and reduces tissue damage in a DNGR-1-dependent pathway.

5 Insights into Human MAIT Cell Functionality in Tissue Repair

5.1 Introduction

Building upon a comprehensive murine model that delineates the pivotal role of MAIT cells in sterile lung injury, I next sought to explore the clinical relevance of these findings by examining human scRNA-seq datasets. This transition from mouse models to human data represents an important step towards grasping the translational potential of preclinical observations. As previously mentioned, the bleomycin mouse model is frequently employed to mimic human IPF disease. By comparing the murine data with IPF patients' lung scRNA-seq datasets, using the Human Lung Cell Atlas (HLCA) (Sikkema *et al.*, 2023) and the IPF Cell Atlas (Neumark *et al.*, 2020), I aimed to characterise lung MAIT cells in the context of IPF.

Combining 49 datasets, the HLCA offers a comprehensive view of over 2.4 million cells from 486 individuals (Sikkema *et al.*, 2023). This expansive repository documents the cellular diversity of the human lung and uncovers novel cellular phenotypes and interactions via scRNA-seq. In a more focused approach, the IPF Cell Atlas compiles scRNA-seq data of 312,928 cells from 32 IPF patients, alongside 28 controls of smokers and non-smokers, and 18 COPD patients (Adams *et al.*, 2020). It provides a detailed perspective of the cellular changes that define IPF. These two atlases together play a crucial role in pinpointing abnormal cellular functions and gene expression in IPF lungs, offering essential insights for understanding the disease mechanisms and identifying potential therapeutic strategies.

In utilising these two powerful datasets, I am able to draw parallels between the animal model and human disease, particularly focusing on the role of MAIT cells within the fibrotic lung environment. This comparison is key to verifying whether the immunological insights gleaned

from mice are applicable to human IPF, thereby enhancing the integrity and applicability of the research findings. Through meticulous analysis of the HLCA and IPF Cell Atlas, I aim to deepen the understanding of MAIT cells in IPF and propel forward the development of innovative therapeutic strategies.

5.2 Aims

To understand the human relevance of murine studies regarding the role of MAIT cells in fibrotic lung disease.

5.3 Results

5.3.1 Human scRNA-sequencing datasets demonstrate differences in MAIT cells between IPF and non-fibrotic control lung tissues

To compare the murine findings with human clinical data from pulmonary fibrosis, I examined published scRNA-seq datasets of IPF in the HLCA (Sikkema *et al.*, 2023) and the IPF Cell Atlas (Neumark *et al.*, 2020). MAIT cells were prominently identified only in one dataset (Habermann *et al.*, 2020), where 176 MAIT cells were identified in non-fibrotic controls and 141 in IPF patients (GEO reference: GSE135893) (Figure 5.1A). Two datasets (Adams *et al.*, 2020; Habermann *et al.*, 2020) provided adequate participant numbers to compare cell proportions between IPF and controls (GEO reference: GSE135893 and GSE136831).

MAIT cells from IPF patients' lungs (n=10) exhibited 55 DEGs (49 up, 6 down, Table 5-1) compared to controls (n=6). Notably, the MAIT cell activation marker, *CD69*, was among the prominently upregulated genes (Figure 5.1B and C). I also observed a significant upregulation of chemokines in MAIT cells, including *CCL3*, *CCL4*, and *CCL4L2*, which play a pivotal role

in the recruitment and activation of immune cells. Additionally, MAIT cells demonstrated enhanced expression of *FOS*, *FOSB*, and *JUNB* – integral components of the AP-1 transcription factor complex, which might indicate alterations in cellular signalling and responses to lung injury. The elevated expression of *NFKBIA*, an inhibitor of the NF-kB transcription factor, suggests potential modulations in inflammatory response pathways. And the elevated anti-inflammatory genes *SCGB1A1* (Zhu *et al.*, 2019) and *ZFP36* (Cao *et al.*, 2021) in MAIT cells suggesting their modulatory role and a potential protective mechanism in the lungs of IPF patients.

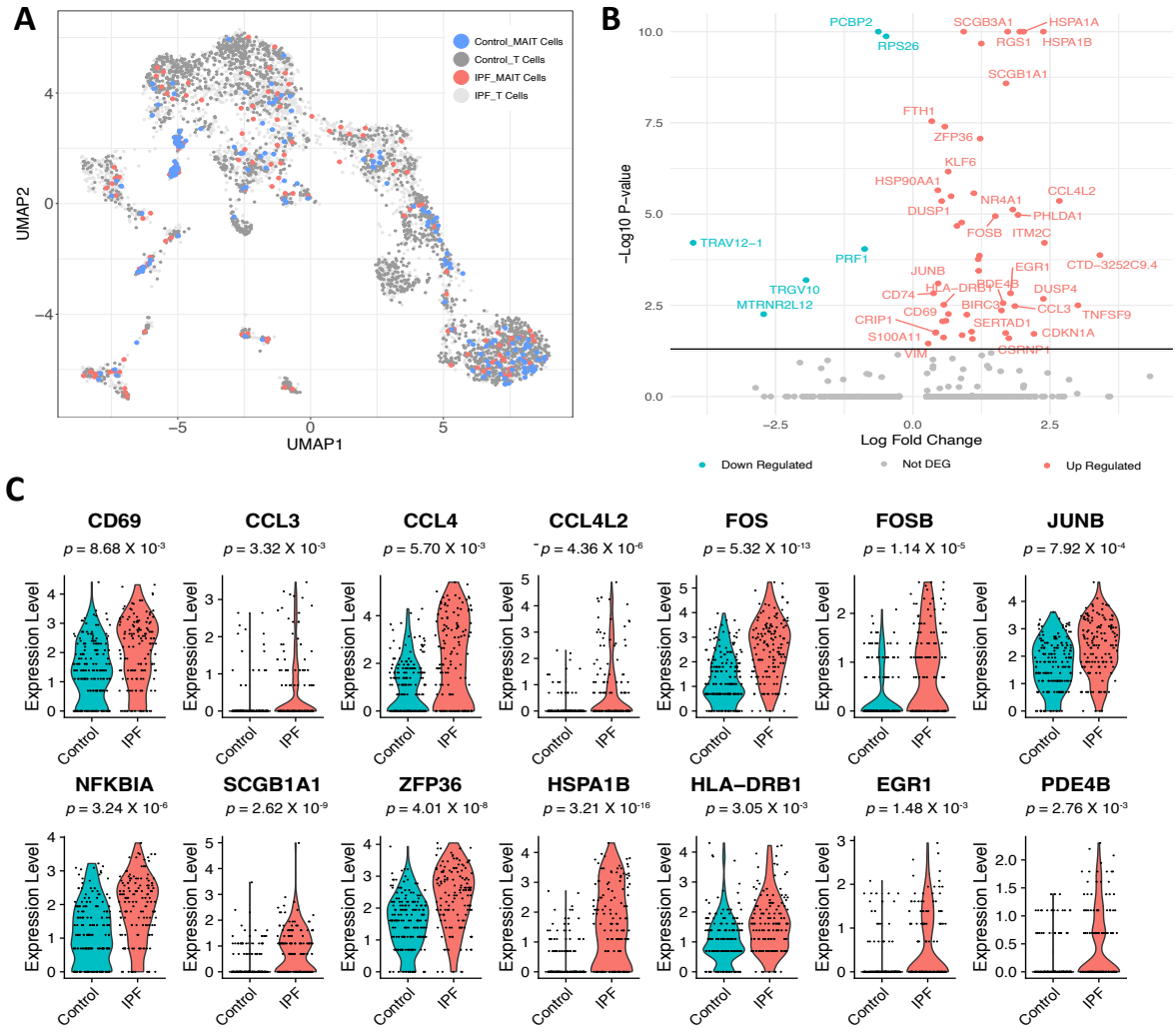

Figure 5.1 Differential gene expression in IPF patient lung MAIT cells.

(**A**) UMAP showing the MAIT cells and other T cells after reintegration. (**B**) Volcano plot displays DEGs (adjusted $P < 0.05$) in IPF lung MAIT cells relative to controls. The top upregulated and downregulated genes are annotated. (**C**) Violin plots illustrate expression levels of specified genes in MAIT cells, contrasting IPF with controls (GSE135893).

Table 5-1 DEGs of MAIT cells, IPF vs Control

	Log2 Fold Change	*P* value	Adjusted *P* value
CTD-3252C9.4	3.40847694	5.06E-09	0.00013339
TNFSF9 (4-1BBL)	3.00877575	1.20E-07	0.00316397
CCL4L2	2.67002871	1.65E-10	4.36E-06
ITM2C	2.39843978	2.32E-09	6.13E-05
HSPA1B	2.37900959	1.22E-20	3.21E-16
DUSP4	2.37889768	7.97E-08	0.0021023
CDKN1A	2.20750059	7.27E-07	0.01917007
HSPA1A	2.01768082	5.54E-17	1.46E-12
RGS1	1.95067011	4.28E-16	1.13E-11
PHLDA1	1.91687999	4.00E-10	1.06E-05
CCL3	1.86015604	1.26E-07	0.00332594
NR4A1	1.82189329	2.85E-10	7.51E-06
EGR1	1.78128101	5.63E-08	0.00148433
CSRNP1	1.74935216	9.58E-07	0.02526935
SCGB3A1	1.72801781	3.13E-17	8.25E-13
SCGB1A1	1.69915943	9.92E-14	2.62E-09
SERTAD1	1.69208413	6.91E-07	0.01821557
PDE4B	1.64592784	1.05E-07	0.00275658
BIRC3	1.61577906	1.66E-07	0.00437926
FOSB	1.50301559	4.32E-10	1.14E-05
DNAJB1	1.24869004	8.04E-15	2.12E-10
DNAJA1	1.22687395	3.24E-12	8.53E-08
RGCC	1.21337533	5.22E-09	0.00013778
RPS4Y1	1.20033202	1.36E-08	0.00035806
CORO1B	1.19148334	6.53E-09	0.00017236
BTG2	1.11280058	1.02E-10	2.68E-06
CAPG	1.08636027	9.99E-07	0.02635963
NR4A2	1.07056276	6.34E-07	0.01673196
CCL4	0.98464434	2.16E-07	0.00569644
FOS	0.92669826	2.02E-17	5.32E-13
PPP1R15A	0.89848942	7.88E-07	0.02077662
TNFAIP3	0.89036899	6.43E-10	1.70E-05
PTPRCAP	0.80498537	7.99E-10	2.11E-05
NFKBIA	0.69743629	1.23E-10	3.24E-06
LGALS1	0.64854233	2.07E-07	0.00547243
KLF6	0.64467035	2.59E-11	6.84E-07
ALOX5AP	0.60331068	3.17E-07	0.00837339
ZFP36	0.58343053	1.52E-12	4.01E-08
HLA-DRB1	0.56565865	1.16E-07	0.00305218

DYNLL1	0.56083732	9.13E-07	0.02409233
CD69	0.54163104	3.29E-07	0.00868113
DUSP1	0.52541753	1.67E-10	4.41E-06
JUNB	0.46129731	3.00E-08	0.00079207
HSP90AA1	0.45594655	8.42E-11	2.22E-06
CRIP1	0.42043194	6.61E-07	0.01744826
S100A11	0.41303276	6.73E-07	0.01775344
CD74	0.3775569	5.61E-08	0.00148106
FTH1	0.34485861	1.08E-12	2.84E-08
VIM	0.27986256	1.34E-06	0.03524605
RPS26	-0.4863287	5.11E-15	1.35E-10
PCBP2	-0.6295141	3.05E-16	8.04E-12
PRF1	-0.8782519	3.43E-09	9.05E-05
TRGV10	-1.9454736	2.45E-08	0.00064673
MTRNR2L12	-2.71823	2.10E-07	0.00553425
TRAV12-1	-4.0025993	2.32E-09	6.13E-05

I conducted an overrepresentation analysis of these DEGs using blood transcriptional modules (BTMs) (S. Li *et al.*, 2014). This analysis pinpointed a pronounced activation of the AP-1 transcription factor network, chemokines and inflammatory molecules in myeloid cells, as well as heightened activity related to pro-inflammatory dendritic cells and myeloid cell responses in IPF (Figure 5.2).

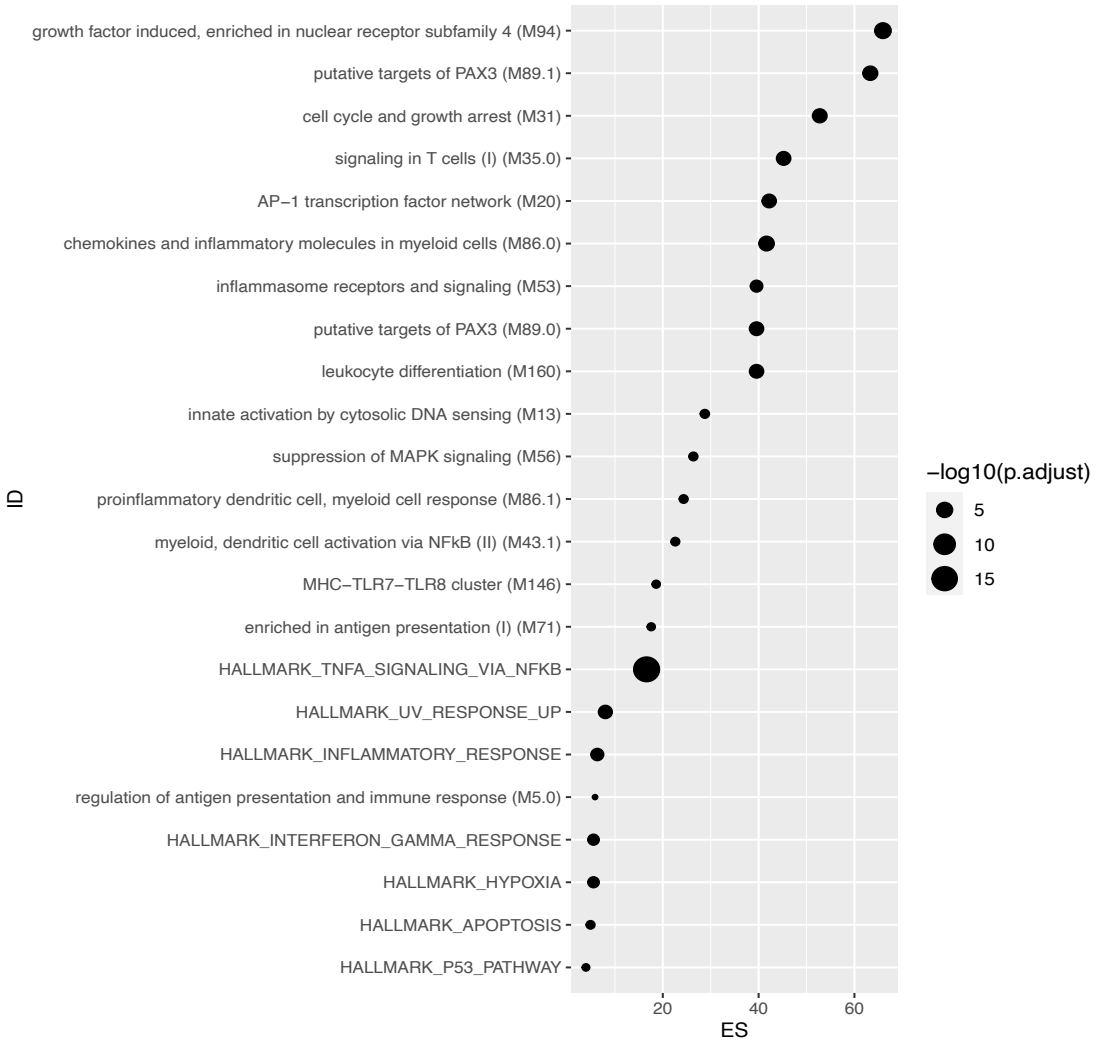

Figure 5.2 Analysis of DEGs for overrepresentation of blood transcriptional modules (BTM).

The top pathways significantly enriched ($P < 0.05$) from BTM are shown, contrasting IPF lung MAIT cells with controls. Dot size corresponds to the adjusted P value for each pathway, while the x-axis depicts the enrichment score (ES), calculated as the ratio of gene ratio to background ratio.

5.3.2 An increase of cDC population in IPF patients' lung tissues

In the GSE135893 dataset, cDC (marked by the genes: *FCER1A*, *CD1C*, and *CLEC9A*) emerged as the sole cell population with a significant increase in IPF patients' lungs (Figure 5.3A and B). Based on gene expression, these cDCs express *CD1C*, *PKIB*, and *CLEC10A*, suggesting that they are phenotypically cDC2 (Figure 5.3C). Analysis of the GSE136831 dataset revealed an elevation in the DC population within IPF patients' lungs, with significant accumulations specifically in cDC2 (marked by *FCGR2B*, *CLEC10A*, *FOXN3*, *ABHD12*) and Langerhans cells (indicated by *CD1A*, *FCER1A*, *CD1E*, *HLA-DQB2*, *S100B*). There was a non-significant tendency towards an increase in cDC1 (marked by *CADM1*, *SIPA1L3*, *CLEC9A*, *WDFY4*, *HDAC9*) or mature DC populations (marked by *CCL19*, *LAD1*, *CCR7*, *LAMP3*, *NCCRP1*) (Figure 5.4). This observation aligns with findings from my mouse lung scRNA-seq dataset, wherein DC accumulation was noted in WT mouse lungs post-bleomycin challenge, suggesting a potential role of DCs in modulating IPF-associated inflammation and fibrosis.

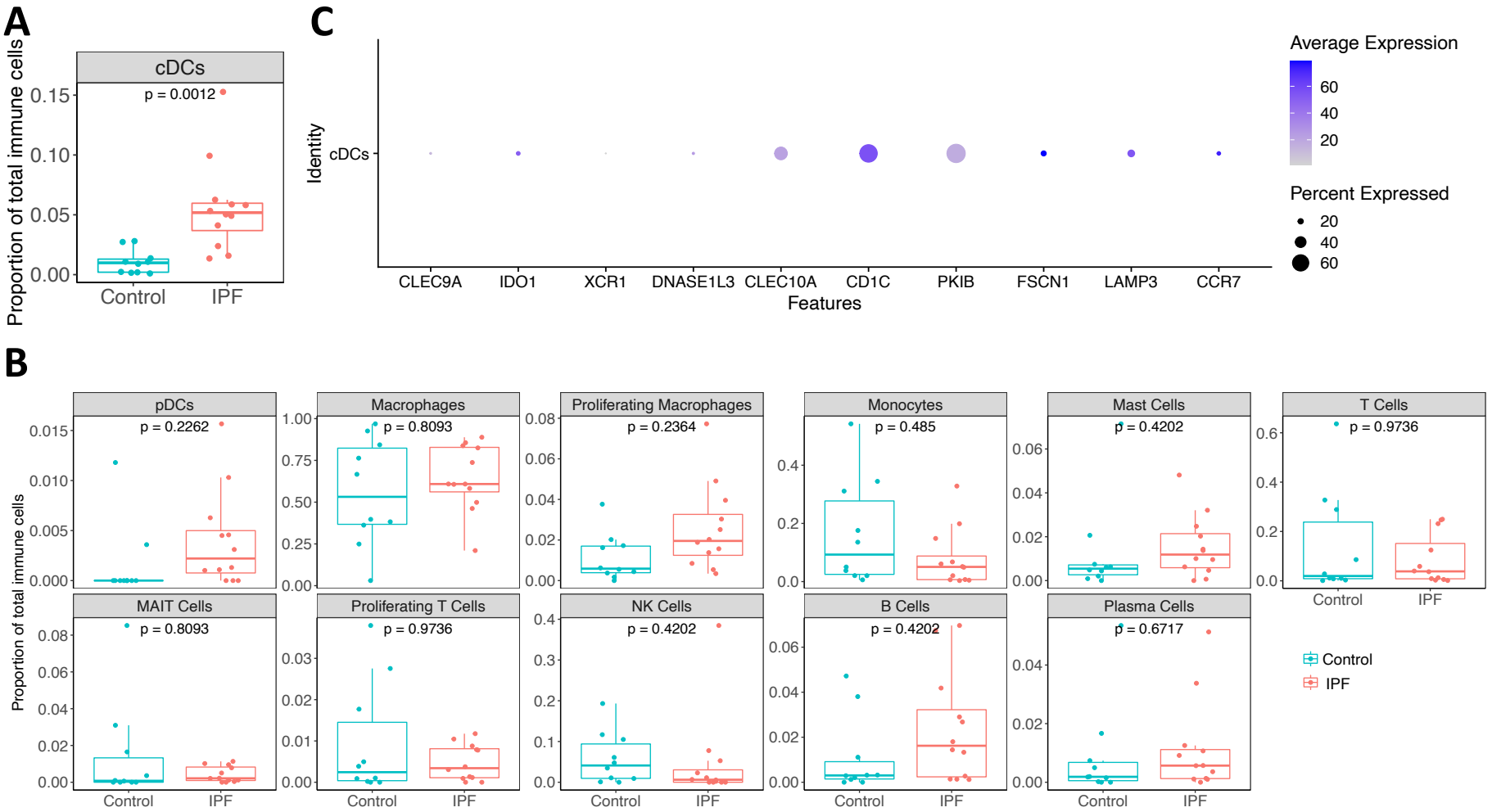
A
cDCs
p = 0.0012
Proportion of total immune cells
0.15
0.10
0.05
0.00
Control
IPF
C
Identity
cDCs
CLEC9A
IDO1
XCR1
DNASE1L3
CLEC10A
CD1C
PKIB
FSCN1
LAMP3
CCR7
Features
Average Expression
60
40
20
Percent Expressed
20
40
60
B
pDCs
p = 0.2262
Macrophages
p = 0.8093
Proliferating Macrophages
p = 0.2364
Monocytes
p = 0.485
Mast Cells
p = 0.4202
T Cells
p = 0.9736
MAIT Cells
p = 0.8093
Proliferating T Cells
p = 0.9736
NK Cells
p = 0.4202
B Cells
p = 0.4202
Plasma Cells
p = 0.6717
Proportion of total immune cells
Control
IPF

Figure 5.3 Analyses and frequencies of indicated cell types in in the GSE135893 dataset.

(**A**) Boxplots showing the proportion of cDC relative to total immune cells in lungs of IPF patients versus controls using data from GSE135893. (**B**) Boxplots present frequencies of indicated cell type, as proportions of total immune cells, in IPF patients versus controls, sourced from GSE135893. (**C**) Dot plot showing the gene expression profile for the cDCs in the GSE135893 dataset. Dot size represents percentage of expressed cells. Colour scales denote the average gene expression. *P* values generated using a two-way ANOVA with Sidak's multiple comparisons test.

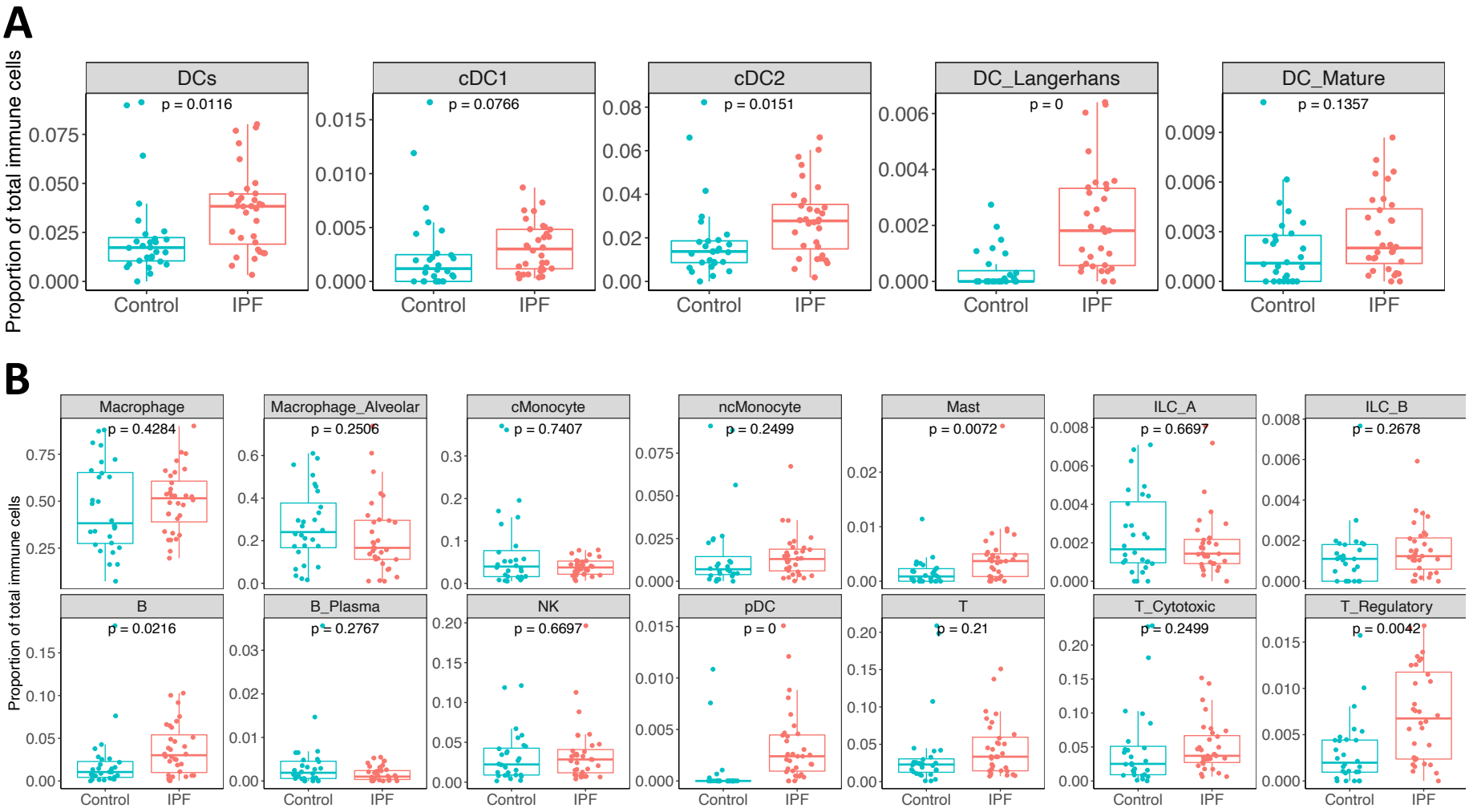
A
Proportion of total immune cells
DCs
p = 0.0116
cDC1
p = 0.0766
cDC2
p = 0.0151
DC_Langerhans
p = 0
DC_Mature
p = 0.1357
Control
IPF
B
Macrophage
p = 0.4284
Macrophage_Alveolar
p = 0.2506
cMonocyte
p = 0.7407
ncMonocyte
p = 0.2499
Mast
p = 0.0072
ILC_A
p = 0.6697
ILC_B
p = 0.2678
B
p = 0.0216
B_Plasma
p = 0.2767
NK
p = 0.6697
pDC
p = 0
T
p = 0.21
T_Cytotoxic
p = 0.2499
T_Regulatory
p = 0.0042

Figure 5.4 Frequencies of indicated cell types in in the GSE136831 dataset.

(A) Boxplots present frequencies of various DC subsets, including cDC1, cDC2, Langerhans, and mature DC, as proportions of total immune cells in lungs of IPF patients and controls, sourced from GSE136831. (**B**) Boxplots present frequencies of indicated cell type, as proportions of total immune cells, in IPF patients versus controls, sourced from GSE136831. *P* values generated using a two-way ANOVA with Sidak's multiple comparisons test.

Further analysis of cell-cell interactions revealed an active role of MAIT cells in mediating cellular communications within the lungs of IPF patients (Figure 5.5). I observed elevated interactions – including various chemokines, cytokines, and their corresponding receptors – between MAIT cells and myeloid cells including cDCs, macrophages, and monocytes in the lungs of IPF patients compared to those of healthy controls. For instance, *CCL20* in MAIT cells with *CCR6* in cDCs (Figure 5.5A), *CCL5* in MAIT cells with *CCR5* in macrophages (Figure 5.5B), and *CD40LG* in MAIT cells with *CD40* in monocytes (Figure 5.5C). These insights are consistent with data from our mouse lung scRNA-seq data, which highlighted a considerable alteration in cell-cell interactions in the mouse lung, both prior to and following a bleomycin challenge, due to MAIT cell deficiency.

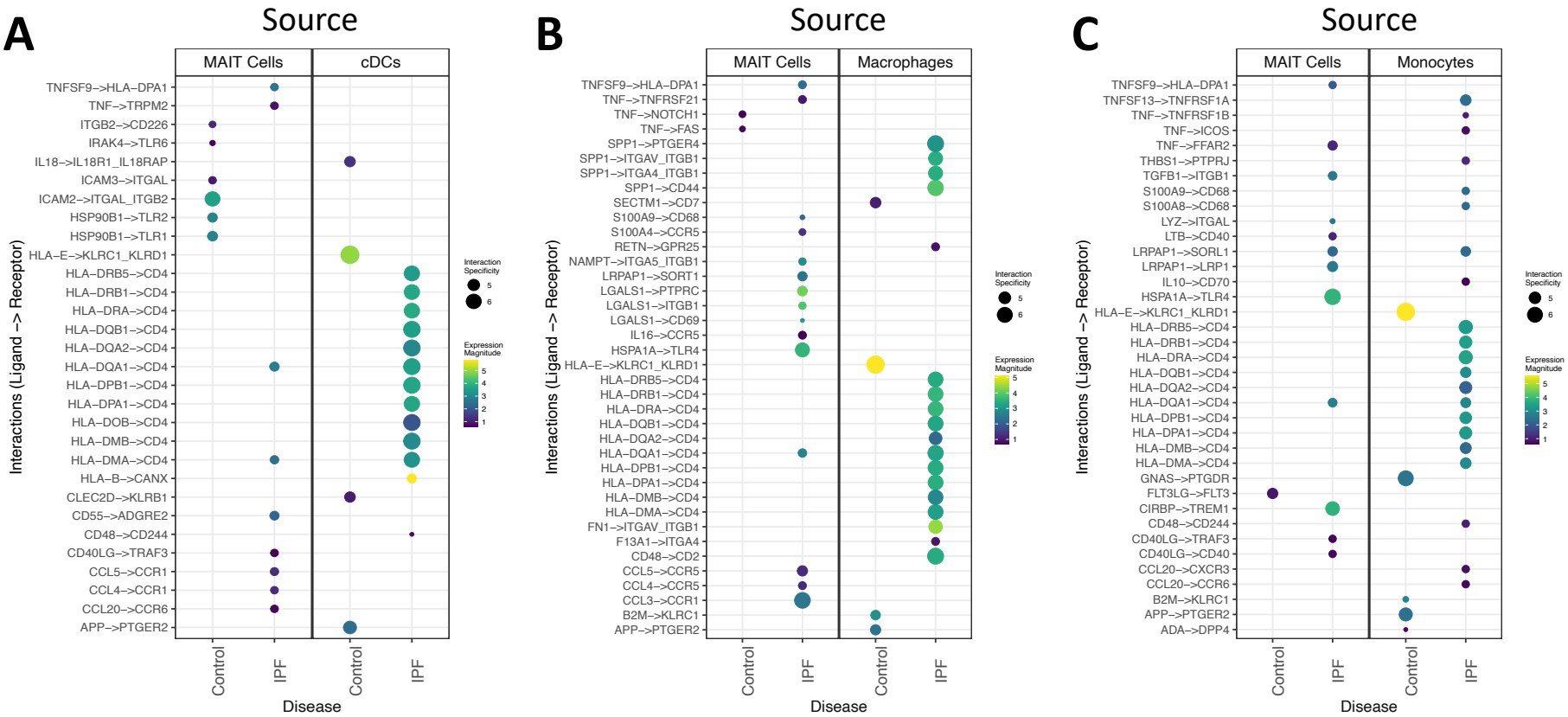

Figure 5.5 Interaction between MAIT cells and cDCs, and macrophages, and monocytes in the lungs of IPF patients and healthy controls.

Interaction between MAIT cells and cDCs (**A**), and macrophages (**B**), and monocytes (**C**) in the lungs of IPF patients and healthy controls. Dot size indicates specificity of interaction between MAIT cells and cDCs. Colour intensity indicates the magnitude of the interaction. In each subgraph, the initial block depicts interactions where T cells are the source and other cells serve as the targets. The subsequent block illustrates interactions where T cells are the targets and other cells are the source. Interactions that exhibited a specificity_rank below 10^{-4} and differed between WT and *Mr1*$^{-/-}$ at any observed timepoints were presented.

5.3.3 Human fibroblast cell line MRC-5 activated MAIT cells by 5-OP-RU antigen presentation

Fibroblasts play an important role in cell injury and wound healing (Li & Wang, 2011). To determine if fibroblast cells can present 5-OP-RU to MAIT cells and activate MAIT cells, I isolated TCR Vα7.2^{+} T cells from human PBMCs then co-cultured the cells with human fibroblast cell line MRC-5 and stimulated them with different conditions for 24 hours then detect expression of activation markers (CD25, CD69, IFN-γ, TNFα and Granzyme B) of MAIT cells by flow cytometry. MRC-5 activated MAIT cells by presenting 5-OP-RU, in a dose-dependent manner (Figure 5.6 and Figure 5.7).

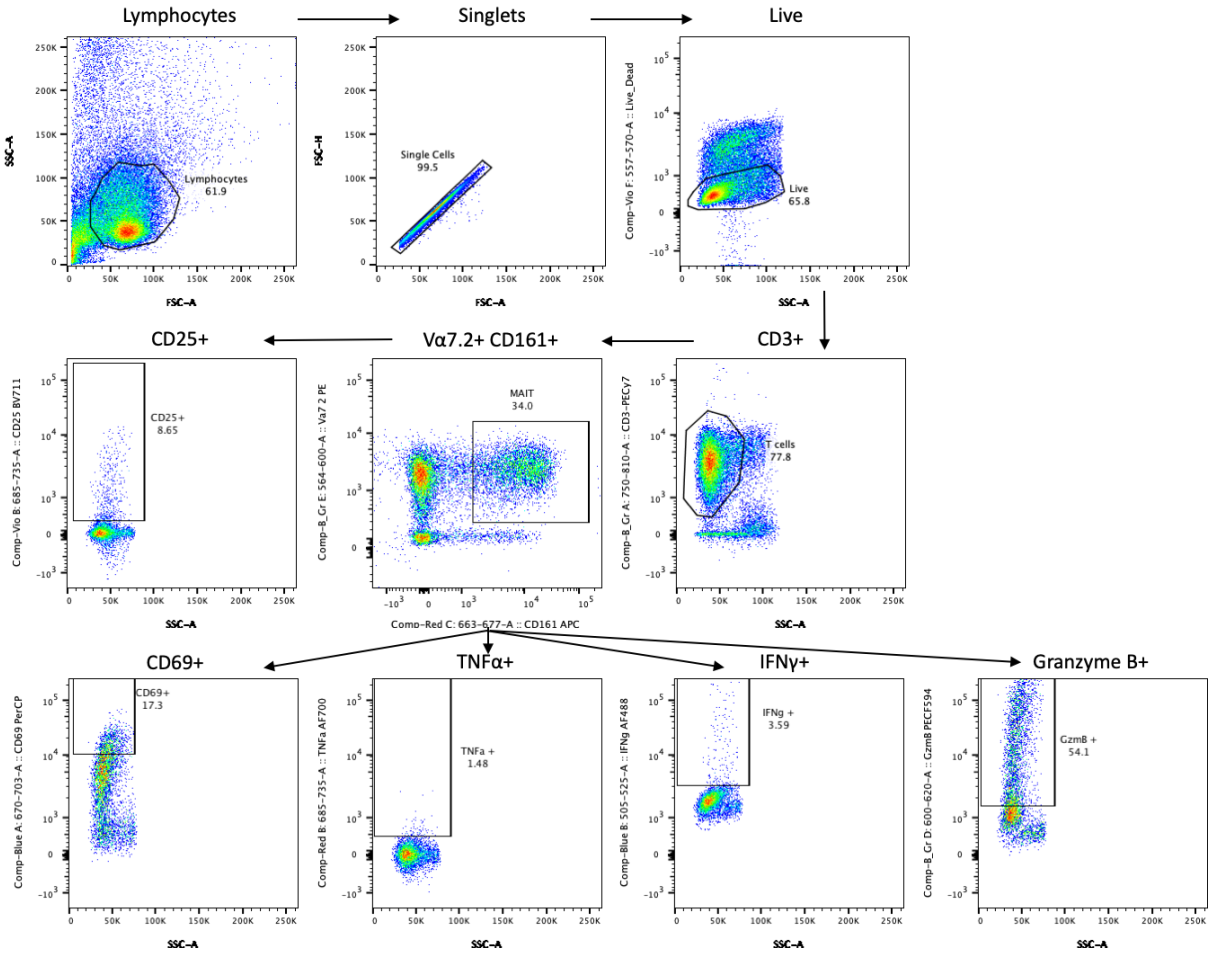

Figure 5.6 Representative flow plot showing the gating strategy of human MAIT cells ($CD3^+$ TCR $V\alpha7.2^+$ $CD161^+$ cells).

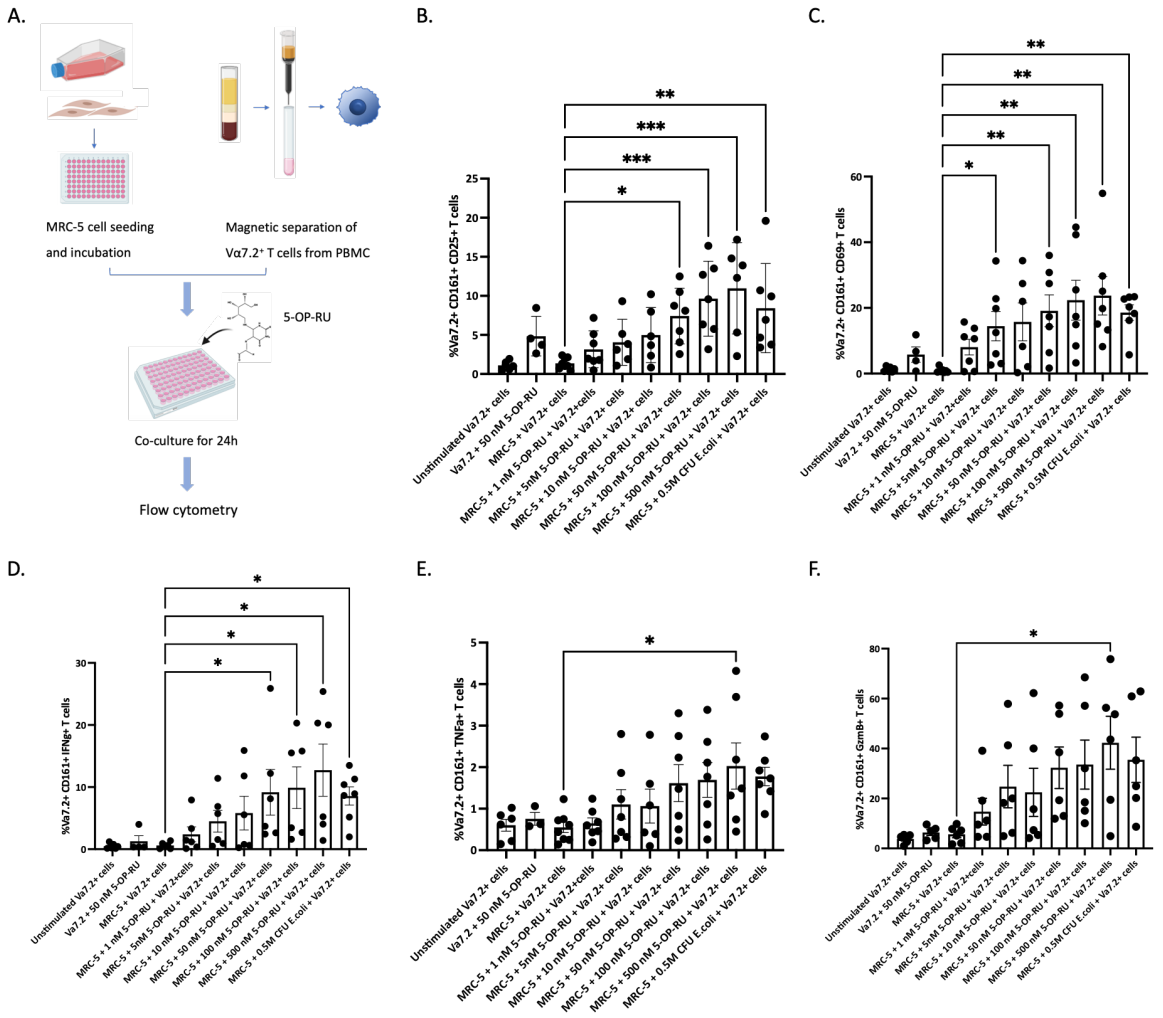

Figure 5.7 Human fibroblast cell line MRC-5 activated MAIT cells by 5-OP-RU antigen presentation.

(**A**) Experimental protocol schematic. Vα7.2^{+} T cells from human PBMCs were cocultured with MRC-5 cells and stimulated under various conditions for 24 hours. Activation markers of MAIT cells were then assessed via flow cytometry. (**B** to **F**) Bar plots showing the percentages of MAIT cells expressing activation markers: CD25 (**B**), CD69 (**C**), IFN-γ (**D**), TNF-α (**E**), and Granzyme B (**F**). Data are presented as mean ± SEM, combining results from three independent experiments, each with 2-3 biological replicates, yielding similar outcomes.

Statistical tests compare each time-point with control by one-way ANOVA with post hoc Dunnett's test or post hoc Dunn's tests; *$P < 0.05$, **$P < 0.01$, ***$P < 0.001$.

5.4 Discussion

My study indicates that MAIT cells are significantly activated in the lungs of IPF patients compared to non-fibrotic controls. To date, there has been limited literature examining the function of MAIT cells in IPF. One notable study reported decreased counts of MAIT cells in the peripheral blood of IPF patients, suggesting a potential migration to the lungs (Zhao *et al.*, 2023). Future research could delve into the involvement of MAIT cells in the onset and progression of pulmonary fibrosis. Another promising area of exploration is the interaction between MAIT cells and lung microbiota during fibrosis, given the known responsiveness of MAIT cells to bacterial and viral infections. Evaluating MAIT cells as potential therapeutic targets using synthetic blocking or activating ligands may also yield valuable insights.

In the bleomycin-induced lung injury mouse model, which parallels various aspects of human IPF, I observed an early accumulation of cDC1 cells in the lungs of WT mice following bleomycin administration. The cDC1 cells are known to excel in cross-presentation of antigens and can activate cytotoxic T cells. Their accumulation during the early stages of lung injury might suggest an attempt of the immune system to initiate a potent immune response against damaged lung tissue. Conversely, in human IPF patient-derived lung scRNA-seq data, there is a more pronounced accumulation of cDC2 rather than cDC1. cDC2s are adept at activating helper T cells and might be involved in generating and maintaining chronic inflammation, a hallmark of IPF. This discrepancy between mouse and human data could arise from difference

in species, disease dynamics or aetiological trigger. Bleomycin challenge in mice offers a snapshot of acute injury and subsequent fibrotic changes, while human IPF patients often present with chronic, established disease. The dynamics of DC infiltration and function could be different in these two scenarios. While murine models offer invaluable insights into the mechanisms of IPF, it is essential to interpret findings in the context of the chronic nature of human IPF. Further studies delving into the functional role of cDCs in both murine and human IPF settings will provide a clearer picture of their contributions to disease pathogenesis.

5.5 Conclusion

- Human scRNA-seq datasets demonstrate differences in MAIT cell and cDC population in IPF versus non-fibrotic control lungs tissues, with enhanced MAIT cell activation and MAIT-cDC cross talk in IPF.

- The human fibroblast cell line MRC-5 activated MAIT cells by 5-OP-RU antigen presentation.

6 DISCUSSION

In this, the first study of MAIT cells during sterile lung injury, I uncovered a novel role for MAIT cells; they are activated and promote pulmonary tissue repair, enhancing pulmonary accumulation of CD103^{+} cDC1, which limit pathology via DNGR-1 (Figure 6.1). Consistent with these findings, scRNA-seq data from IPF patients reveal activated MAIT cells, and increased cDC populations in the lungs of IPF patients compared with controls. My observations demonstrate the potential of MAIT cells as important orchestrators of tissue protection and modulators of inflammatory disease pathology.

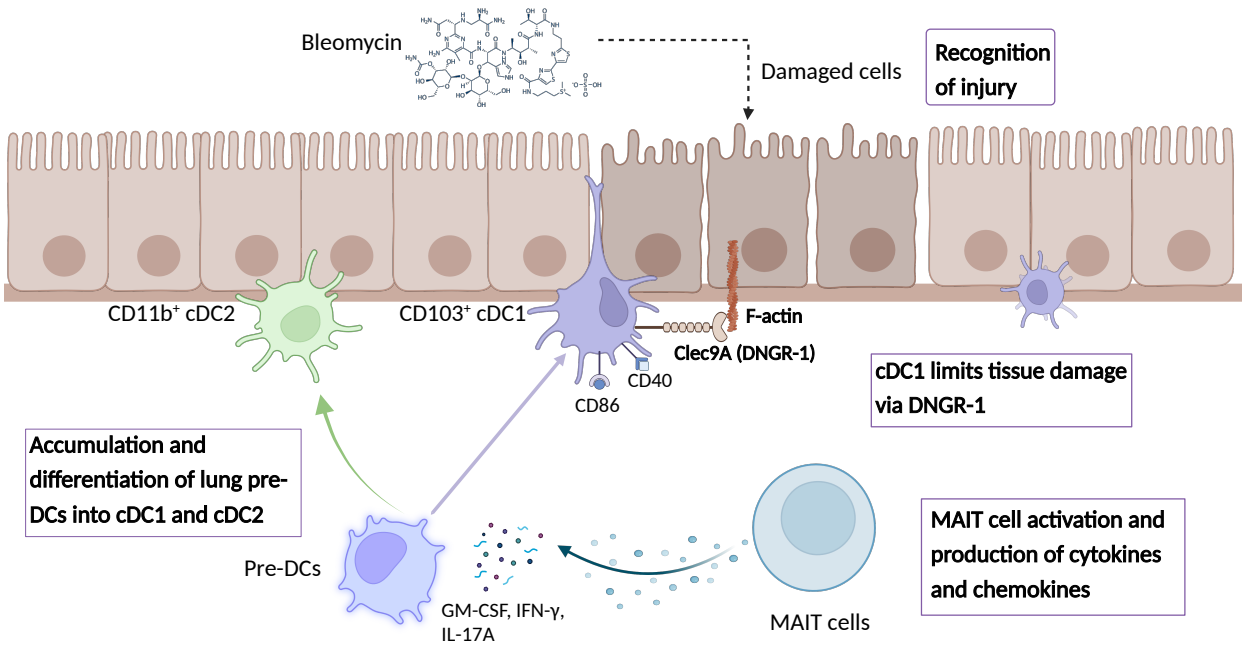

Figure 6.1 Model for how MAIT cells contribute to protection against bleomycin-induced lung tissue damage.

In vivo bleomycin challenge induced robust activation of murine pulmonary MAIT cells and its tissue repair programme. MAIT cells showed a protective role against bleomycin-induced lung tissue damage by mediating the accumulation of pre-DC and type 1 conventional dendritic cells (cDC1), which limited tissue damage via DNGR-1 signal.

My study has several limitations. Firstly, while I identified the central role of MAIT cells in the accumulation of $CD103^+$ cDC1 and pre-DC populations, the specific mechanisms through which MAIT cells influence this accumulation remain ambiguous. The exact interplay between MAIT cell-produced cytokines, such as GM-CSF and IFN-γ, and the accumulation of DC requires further elucidation. The potential interactions and crosstalk between MAIT cells and other myeloid cells also warrant a deeper investigation to comprehensively understand their combined roles in shaping immune responses to sterile challenge. Secondly, in contrast to the early accumulation of cDC1 in the lungs of WT mice subjected to bleomycin challenge, human IPF patient data show a more pronounced accumulation of cDC2, indicating species differences and the need for careful interpretation in the context of the chronic nature of human IPF and the dynamics of DC infiltration and function. Thirdly, the intricate processes of tissue damage and fibrosis, which involve numerous structural cells such as epithelial cells and fibroblasts, present difficulties for us to study.

Employing the bleomycin-challenged murine model, a well-accepted surrogate of interstitial lung disease (ILD) pathogenesis (Moore & Hogaboam, 2008), I have identified a crucial role for MAIT cells in counteracting lung injury. This offers invaluable insights into the complex mechanisms underpinning pulmonary tissue repair. Specifically, airway damage and tissue

remodelling emerge as common pathological traits across a wide spectrum of respiratory disorders, significantly contributing to their progression. While acting as a marker for disease progression, tissue remodelling is also a contributor to severe clinical symptoms and disease severity, causing impaired quality of life (James & Wenzel, 2007). These effects of remodelling are prominent in conditions such as ILD, pneumonia, and acute respiratory distress syndrome (Michalski *et al.*, 2022). Given the pathological importance of remodelling in lung diseases my findings are potentially important for the development of novel antifibrotic therapeutic strategies. For instance, the protective activities of MAIT cells could be enhanced by use of MAIT cell stimulating ligands, either synthetically produced, or administered through riboflavin-competent commensal organisms (Hinks, 2021), or through targeting the DNGR-1 pathway. Future studies will be required to further delineate the precise roles of MAIT cells in the context of human lung injury and repair, and to validate the translational potential of my findings in real-world clinical settings, but in summary I have for the first time generated *in vivo* data of MAIT cells protecting against lung damage, independently of a bacterial or viral pathogen.

7 REFERENCES

Adams, T. S., Schupp, J. C., Poli, S., Ayaub, E. A., Neumark, N., Ahangari, F., Chu, S. G., Raby, B. A., DeIuliis, G., Januszyk, M., Duan, Q., Arnett, H. A., Siddiqui, A., Washko, G. R., Homer, R., Yan, X., Rosas, I. O., & Kaminski, N. (2020). Single-cell RNA-seq reveals ectopic and aberrant lung-resident cell populations in idiopathic pulmonary fibrosis. *Sci Adv*, *6*(28), eaba1983. https://doi.org/10.1126/sciadv.aba1983

Adamson, I. Y., & Bowden, D. H. (1979). Bleomycin-induced injury and metaplasia of alveolar type 2 cells. Relationship of cellular responses to drug presence in the lung. *Am J Pathol*, *96*(2), 531-544.

Angelidis, I., Simon, L. M., Fernandez, I. E., Strunz, M., Mayr, C. H., Greiffo, F. R., Tsitsiridis, G., Ansari, M., Graf, E., Strom, T.-M., Nagendran, M., Desai, T., Eickelberg, O., Mann, M., Theis, F. J., & Schiller, H. B. (2019). An atlas of the aging lung mapped by single cell transcriptomics and deep tissue proteomics. *Nat Commun*, *10*(1), 963. https://doi.org/10.1038/s41467-019-08831-9

Armingol, E., Baghdassarian, H. M., Martino, C., Perez-Lopez, A., Aamodt, C., Knight, R., & Lewis, N. E. (2022). Context-aware deconvolution of cell–cell communication with Tensor-cell2cell. *Nat Commun*, *13*(1), 3665. https://doi.org/10.1038/s41467-022-31369-2

Ashburner, M., Ball, C. A., Blake, J. A., Botstein, D., Butler, H., Cherry, J. M., Davis, A. P., Dolinski, K., Dwight, S. S., Eppig, J. T., Harris, M. A., Hill, D. P., Issel-Tarver, L., Kasarskis, A., Lewis, S., Matese, J. C., Richardson, J. E., Ringwald, M., Rubin, G. M.,

& Sherlock, G. (2000). Gene Ontology: tool for the unification of biology. *Nature Genetics*, *25*(1), 25-29. https://doi.org/10.1038/75556

Balish, E., Wagner, R. D., Vazquez-Torres, A., Jones-Carson, J., Pierson, C., & Warner, T. (1999). Mucosal and systemic candidiasis in IL-8Rh−/− BALB/c mice. *J Leukoc Biol*, *66*(1), 144-150. https://doi.org/10.1002/jlb.66.1.144

Banki, Z., Krabbendam, L., Klaver, D., Leng, T., Kruis, S., Mehta, H., Mullauer, B., Orth-Holler, D., Stoiber, H., Willberg, C. B., & Klenerman, P. (2019). Antibody opsonization enhances MAIT cell responsiveness to bacteria via a TNF-dependent mechanism. *Immunol Cell Biol*, *97*(6), 538-551. https://doi.org/10.1111/imcb.12239

Bantsimba-Malanda, C., Marchal-Sommé, J., Goven, D., Freynet, O., Michel, L., Crestani, B., & Soler, P. (2010). A role for dendritic cells in bleomycin-induced pulmonary fibrosis in mice? *Am J Respir Crit Care Med*, *182*(3), 385-395. https://doi.org/10.1164/rccm.200907-1164OC

Becht, E., McInnes, L., Healy, J., Dutertre, C.-A., Kwok, I. W. H., Ng, L. G., Ginhoux, F., & Newell, E. W. (2019). Dimensionality reduction for visualizing single-cell data using UMAP. *Nat Biotechnol*, *37*(1), 38-44. https://doi.org/10.1038/nbt.4314

Bernal, I., Hofmann, J. D., Bulitta, B., Klawonn, F., Michel, A. M., Jahn, D., Neumann-Schaal, M., Bruder, D., & Jansch, L. (2018). Clostridioides difficile Activates Human Mucosal-Associated Invariant T Cells. *Front Microbiol*, *9*, 2532. https://doi.org/10.3389/fmicb.2018.02532

Blampey, Q., Mulder, K., Dutertre, C.-A., Gardet, M., André, F., Ginhoux, F., & Cournède, P.-H. (2023). Sopa: a technology-invariant pipeline for analyses of image-based spatial-omics. *bioRxiv*, 2023.2012.2022.571863. https://doi.org/10.1101/2023.12.22.571863

Brown, J. S. (2012). Community-acquired pneumonia. *Clin Med (Lond)*, *12*(6), 538-543. https://doi.org/10.7861/clinmedicine.12-6-538

Cabeza-Cabrerizo, M., Cardoso, A., Minutti, C. M., Costa, M. P. d., & Sousa, C. R. e. (2021). Dendritic Cells Revisited. *Annu Rev Immunol*, *39*(1), 131-166. https://doi.org/10.1146/annurev-immunol-061020-053707

Canton, J., Blees, H., Henry, C. M., Buck, M. D., Schulz, O., Rogers, N. C., Childs, E., Zelenay, S., Rhys, H., Domart, M. C., Collinson, L., Alloatti, A., Ellison, C. J., Amigorena, S., Papayannopoulos, V., Thomas, D. C., Randow, F., & Reis e Sousa, C. (2021). The receptor DNGR-1 signals for phagosomal rupture to promote cross-presentation of dead-cell-associated antigens. *Nat Immunol*, *22*(2), 140-153. https://doi.org/10.1038/s41590-020-00824-x

Cao, Y., Huang, W., Wu, F., Shang, J., Ping, F., Wang, W., Li, Y., Zhao, X., & Zhang, X. (2021). ZFP36 protects lungs from intestinal I/R-induced injury and fibrosis through the CREBBP/p53/p21/Bax pathway. *Cell Death Dis*, *12*(7), 685. https://doi.org/10.1038/s41419-021-03950-y

Carissimo, G., Xu, W., Kwok, I., Abdad, M. Y., Chan, Y.-H., Fong, S.-W., Puan, K. J., Lee, C. Y.-P., Yeo, N. K.-W., Amrun, S. N., Chee, R. S.-L., How, W., Chan, S., Fan, B. E., Andiappan, A. K., . . . Ng, L. F. P. (2020). Whole blood immunophenotyping uncovers

immature neutrophil-to-VD2 T-cell ratio as an early marker for severe COVID-19. *Nat Commun*, *11*(1), 5243. https://doi.org/10.1038/s41467-020-19080-6

Celli, B., Fabbri, L., Criner, G., Martinez, F. J., Mannino, D., Vogelmeier, C., Montes de Oca, M., Papi, A., Sin, D. D., Han, M. K., & Agusti, A. (2022). Definition and Nomenclature of Chronic Obstructive Pulmonary Disease: Time for Its Revision. *Am J Respir Crit Care Med*, *206*(11), 1317-1325. https://doi.org/10.1164/rccm.202204-0671PP

Chakraborty, K., Chatterjee, S., & Bhattacharyya, A. (2017). Modulation of CD11c+ lung dendritic cells in respect to TGF-β in experimental pulmonary fibrosis. *Cell Biol Int*, *41*(9), 991-1000. https://doi.org/10.1002/cbin.10800

Chang, M. Y., Brune, J. E., Black, M., Altemeier, W. A., & Frevert, C. W. (2023). Multicompartmental analysis of the murine pulmonary immune response by spectral flow cytometry. *Am J Physiol Lung Cell Mol Physiol*, *325*(4), L518-L535. https://doi.org/10.1152/ajplung.00317.2022

Chen, K. H., Boettiger, A. N., Moffitt, J. R., Wang, S., & Zhuang, X. (2015). Spatially resolved, highly multiplexed RNA profiling in single cells. *Science*, *348*(6233), aaa6090. https://doi.org/doi:10.1126/science.aaa6090

Chen, Z., Wang, H., D'Souza, C., Sun, S., Kostenko, L., Eckle, S. B., Meehan, B. S., Jackson, D. C., Strugnell, R. A., Cao, H., Wang, N., Fairlie, D. P., Liu, L., Godfrey, D. I., Rossjohn, J., McCluskey, J., & Corbett, A. J. (2017). Mucosal-associated invariant T-cell activation and accumulation after in vivo infection depends on microbial riboflavin

synthesis and co-stimulatory signals. *Mucosal Immunol*, *10*(1), 58-68. https://doi.org/10.1038/mi.2016.39

Chiba, A., Tajima, R., Tomi, C., Miyazaki, Y., Yamamura, T., & Miyake, S. (2012). Mucosal-associated invariant T cells promote inflammation and exacerbate disease in murine models of arthritis. *Arthritis Rheum*, *64*(1), 153-161. https://doi.org/10.1002/art.33314

Chua, W. J., Truscott, S. M., Eickhoff, C. S., Blazevic, A., Hoft, D. F., & Hansen, T. H. (2012). Polyclonal mucosa-associated invariant T cells have unique innate functions in bacterial infection. *Infect Immun*, *80*(9), 3256-3267. https://doi.org/10.1128/iai.00279-12

Chung, E. Y., Liu, J., Homma, Y., Zhang, Y., Brendolan, A., Saggese, M., Han, J., Silverstein, R., Selleri, L., & Ma, X. (2007). Interleukin-10 expression in macrophages during phagocytosis of apoptotic cells is mediated by homeodomain proteins Pbx1 and Prep-1. *Immunity*, *27*(6), 952-964. https://doi.org/10.1016/j.immuni.2007.11.014

Constantinides, M. G., Link, V. M., Tamoutounour, S., Wong, A. C., Perez-Chaparro, P. J., Han, S. J., Chen, Y. E., Li, K., Farhat, S., Weckel, A., Krishnamurthy, S. R., Vujkovic-Cvijin, I., Linehan, J. L., Bouladoux, N., Merrill, E. D., . . . Belkaid, Y. (2019). MAIT cells are imprinted by the microbiota in early life and promote tissue repair. *Science*, *366*(6464). https://doi.org/10.1126/science.aax6624

Corbett, A. J., Eckle, S. B., Birkinshaw, R. W., Liu, L., Patel, O., Mahony, J., Chen, Z., Reantragoon, R., Meehan, B., Cao, H., Williamson, N. A., Strugnell, R. A., Van Sinderen, D., Mak, J. Y., Fairlie, D. P., Kjer-Nielsen, L., Rossjohn, J., & McCluskey,

J. (2014). T-cell activation by transitory neo-antigens derived from distinct microbial pathways. *Nature*, *509*(7500), 361-365. https://doi.org/10.1038/nature13160

Cossarizza, A., Chang, H. D., Radbruch, A., Abrignani, S., Addo, R., Akdis, M., Andrä, I., Andreata, F., Annunziato, F., Arranz, E., Bacher, P., Bari, S., Barnaba, V., Barros-Martins, J., Baumjohann, D., . . . Yang, J. (2021). Guidelines for the use of flow cytometry and cell sorting in immunological studies (third edition). *Eur J Immunol*, *51*(12), 2708-3145. https://doi.org/10.1002/eji.202170126

Cueto, F. J., Del Fresno, C., Brandi, P., Combes, A. J., Hernández-García, E., Sánchez-Paulete, A. R., Enamorado, M., Bromley, C. P., Gomez, M. J., Conde-Garrosa, R., Mañes, S., Zelenay, S., Melero, I., Iborra, S., Krummel, M. F., & Sancho, D. (2021). DNGR-1 limits Flt3L-mediated antitumor immunity by restraining tumor-infiltrating type I conventional dendritic cells. *J Immunother Cancer*, *9*(5). https://doi.org/10.1136/jitc-2020-002054

Cueto, F. J., Del Fresno, C., & Sancho, D. (2019). DNGR-1, a Dendritic Cell-Specific Sensor of Tissue Damage That Dually Modulates Immunity and Inflammation. *Front Immunol*, *10*, 3146. https://doi.org/10.3389/fimmu.2019.03146

Davey, M. S., Morgan, M. P., Liuzzi, A. R., Tyler, C. J., Khan, M. W., Szakmany, T., Hall, J. E., Moser, B., & Eberl, M. (2014). Microbe-specific unconventional T cells induce human neutrophil differentiation into antigen cross-presenting cells. *J Immunol*, *193*(7), 3704-3716. https://doi.org/10.4049/jimmunol.1401018

Del Fresno, C., Saz-Leal, P., Enamorado, M., Wculek, S. K., Martínez-Cano, S., Blanco-Menéndez, N., Schulz, O., Gallizioli, M., Miró-Mur, F., Cano, E., Planas, A., & Sancho, D. (2018). DNGR-1 in dendritic cells limits tissue damage by dampening neutrophil recruitment. *Science*, *362*(6412), 351-356. https://doi.org/10.1126/science.aan8423

Deschler, S., Kager, J., Erber, J., Fricke, L., Koyumdzhieva, P., Georgieva, A., Lahmer, T., Wiessner, J. R., Voit, F., Schneider, J., Horstmann, J., Iakoubov, R., Treiber, M., Winter, C., Ruland, J., . . . Böttcher, K. (2021). Mucosal-Associated Invariant T (MAIT) Cells Are Highly Activated and Functionally Impaired in COVID-19 Patients. *Viruses*, *13*(2), 241. https://www.mdpi.com/1999-4915/13/2/241

Dias, J., Sobkowiak, M. J., Sandberg, J. K., & Leeansyah, E. (2016). Human MAIT-cell responses to Escherichia coli: activation, cytokine production, proliferation, and cytotoxicity. *J Leukoc Biol*, *100*(1), 233-240. https://doi.org/10.1189/jlb.4TA0815-391RR

Dieu, M. C., Vanbervliet, B., Vicari, A., Bridon, J. M., Oldham, E., Aït-Yahia, S., Brière, F., Zlotnik, A., Lebecque, S., & Caux, C. (1998). Selective recruitment of immature and mature dendritic cells by distinct chemokines expressed in different anatomic sites. *J Exp Med*, *188*(2), 373-386. https://doi.org/10.1084/jem.188.2.373

Dobin, A., Davis, C. A., Schlesinger, F., Drenkow, J., Zaleski, C., Jha, S., Batut, P., Chaisson, M., & Gingeras, T. R. (2013). STAR: ultrafast universal RNA-seq aligner. *Bioinformatics*, *29*(1), 15-21. https://doi.org/10.1093/bioinformatics/bts635

du Halgouet, A., Darbois, A., Alkobtawi, M., Mestdagh, M., Alphonse, A., Premel, V., Yvorra, T., Colombeau, L., Rodriguez, R., Zaiss, D., El Morr, Y., Bugaut, H., Legoux, F., Perrin, L., Aractingi, S., Golub, R., Lantz, O., & Salou, M. (2023). Role of MR1-driven signals and amphiregulin on the recruitment and repair function of MAIT cells during skin wound healing. *Immunity*, *56*(1), 78-92.e76. https://doi.org/10.1016/j.immuni.2022.12.004

Dündar, F., Skrabanek, L., & Zumbo, P. (2019). *Introduction to differential gene expression analysis using RNA-seq*. Weill Cornell Medical College.

Dusseaux, M., Martin, E., Serriari, N., Peguillet, I., Premel, V., Louis, D., Milder, M., Le Bourhis, L., Soudais, C., Treiner, E., & Lantz, O. (2011). Human MAIT cells are xenobiotic-resistant, tissue-targeted, CD161hi IL-17-secreting T cells. *Blood*, *117*(4), 1250-1259. https://doi.org/10.1182/blood-2010-08-303339

Eash, K. J., Greenbaum, A. M., Gopalan, P. K., & Link, D. C. (2010). CXCR2 and CXCR4 antagonistically regulate neutrophil trafficking from murine bone marrow. *J Clin Invest*, *120*(7), 2423-2431. https://doi.org/10.1172/jci41649

Eckle, S. B., Corbett, A. J., Keller, A. N., Chen, Z., Godfrey, D. I., Liu, L., Mak, J. Y., Fairlie, D. P., Rossjohn, J., & McCluskey, J. (2015). Recognition of Vitamin B Precursors and Byproducts by Mucosal Associated Invariant T Cells. *J Biol Chem*, *290*(51), 30204-30211. https://doi.org/10.1074/jbc.R115.685990

Ellis, J., Oyston, P. C., Green, M., & Titball, R. W. (2002). Tularemia. *Clin Microbiol Rev*, *15*(4), 631-646. https://doi.org/10.1128/cmr.15.4.631-646.2002

Ellis, T. N., & Beaman, B. L. (2004). Interferon-gamma activation of polymorphonuclear neutrophil function. *Immunology*, *112*(1), 2-12. https://doi.org/10.1111/j.1365-2567.2004.01849.x

Flament, H., Rouland, M., Beaudoin, L., Toubal, A., Bertrand, L., Lebourgeois, S., Rousseau, C., Soulard, P., Gouda, Z., Cagninacci, L., Monteiro, A. C., Hurtado-Nedelec, M., Luce, S., Bailly, K., Andrieu, M., . . . Lehuen, A. (2021). Outcome of SARS-CoV-2 infection is linked to MAIT cell activation and cytotoxicity. *Nat Immunol*, *22*(3), 322-335. https://doi.org/10.1038/s41590-021-00870-z

Galati, D., Zanotta, S., Polistina, G. E., Coppola, A., Capitelli, L., & Bocchino, M. (2020). Circulating dendritic cells are severely decreased in idiopathic pulmonary fibrosis with a potential value for prognosis prediction. *Clin Immunol*, *215*, 108454. https://doi.org/10.1016/j.clim.2020.108454

Gasse, P., Mary, C., Guenon, I., Noulin, N., Charron, S., Schnyder-Candrian, S., Schnyder, B., Akira, S., Quesniaux, V. F., Lagente, V., Ryffel, B., & Couillin, I. (2007). IL-1R1/MyD88 signaling and the inflammasome are essential in pulmonary inflammation and fibrosis in mice. *J Clin Invest*, *117*(12), 3786-3799. https://doi.org/10.1172/jci32285

Gasse, P., Riteau, N., Charron, S., Girre, S., Fick, L., Pétrilli, V., Tschopp, J., Lagente, V., Quesniaux, V. F., Ryffel, B., & Couillin, I. (2009). Uric acid is a danger signal activating NALP3 inflammasome in lung injury inflammation and fibrosis. *Am J Respir Crit Care Med*, *179*(10), 903-913. https://doi.org/10.1164/rccm.200808-1274OC

Giampazolias, E., Schulz, O., Lim, K. H. J., Rogers, N. C., Chakravarty, P., Srinivasan, N., Gordon, O., Cardoso, A., Buck, M. D., Poirier, E. Z., Canton, J., Zelenay, S., Sammicheli, S., Moncaut, N., Varsani-Brown, S., Rosewell, I., & Reis e Sousa, C. (2021). Secreted gelsolin inhibits DNGR-1-dependent cross-presentation and cancer immunity. *Cell*, *184*(15), 4016-4031.e4022. https://doi.org/https://doi.org/10.1016/j.cell.2021.05.021

Gideon, H. P., Hughes, T. K., Tzouanas, C. N., Wadsworth, M. H., 2nd, Tu, A. A., Gierahn, T. M., Peters, J. M., Hopkins, F. F., Wei, J. R., Kummerlowe, C., Grant, N. L., Nargan, K., Phuah, J. Y., Borish, H. J., Maiello, P., . . . Shalek, A. K. (2022). Multimodal profiling of lung granulomas in macaques reveals cellular correlates of tuberculosis control. *Immunity*, *55*(5), 827-846.e810. https://doi.org/10.1016/j.immuni.2022.04.004

Gill, S. E., Huizar, I., Bench, E. M., Sussman, S. W., Wang, Y., Khokha, R., & Parks, W. C. (2010). Tissue inhibitor of metalloproteinases 3 regulates resolution of inflammation following acute lung injury. *Am J Pathol*, *176*(1), 64-73. https://doi.org/10.2353/ajpath.2010.090158

Gnirck, A. C., Philipp, M. S., Waterhölter, A., Wunderlich, M., Shaikh, N., Adamiak, V., Henneken, L., Kautz, T., Xiong, T., Klaus, D., Tomczyk, P., Al-Bahra, M. M., Menche, D., Walkenhorst, M., Lantz, O., . . . Turner, J. E. (2023). Mucosal-associated invariant T cells contribute to suppression of inflammatory myeloid cells in immune-mediated kidney disease. *Nat Commun*, *14*(1), 7372. https://doi.org/10.1038/s41467-023-43269-0

Godfrey, D. I., Uldrich, A. P., McCluskey, J., Rossjohn, J., & Moody, D. B. (2015). The burgeoning family of unconventional T cells. *Nat Immunol*, *16*(11), 1114-1123. https://doi.org/10.1038/ni.3298

Gold, M. C., Cerri, S., Smyk-Pearson, S., Cansler, M. E., Vogt, T. M., Delepine, J., Winata, E., Swarbrick, G. M., Chua, W. J., Yu, Y. Y., Lantz, O., Cook, M. S., Null, M. D., Jacoby, D. B., Harriff, M. J., Lewinsohn, D. A., Hansen, T. H., & Lewinsohn, D. M. (2010). Human mucosal associated invariant T cells detect bacterially infected cells. *PLoS Biol*, *8*(6), e1000407. https://doi.org/10.1371/journal.pbio.1000407

Gold, M. C., Eid, T., Smyk-Pearson, S., Eberling, Y., Swarbrick, G. M., Langley, S. M., Streeter, P. R., Lewinsohn, D. A., & Lewinsohn, D. M. (2013). Human thymic MR1-restricted MAIT cells are innate pathogen-reactive effectors that adapt following thymic egress. *Mucosal Immunol*, *6*(1), 35-44. https://doi.org/10.1038/mi.2012.45

Gold, M. C., Napier, R. J., & Lewinsohn, D. M. (2015). MR1-restricted mucosal associated invariant T (MAIT) cells in the immune response to Mycobacterium tuberculosis. *Immunol Rev*, *264*(1), 154-166. https://doi.org/10.1111/imr.12271

Greenaway, H. Y., Ng, B., Price, D. A., Douek, D. C., Davenport, M. P., & Venturi, V. (2013). NKT and MAIT invariant TCRα sequences can be produced efficiently by VJ gene recombination. *Immunobiology*, *218*(2), 213-224. https://doi.org/10.1016/j.imbio.2012.04.003

Greer, A. M., Matthay, M. A., Kukreja, J., Bhakta, N. R., Nguyen, C. P., Wolters, P. J., Woodruff, P. G., Fahy, J. V., & Shin, J. S. (2014). Accumulation of BDCA1^{+} dendritic

cells in interstitial fibrotic lung diseases and Th2-high asthma. *PLoS One*, *9*(6), e99084. https://doi.org/10.1371/journal.pone.0099084

Guilliams, M., Lambrecht, B. N., & Hammad, H. (2013). Division of labor between lung dendritic cells and macrophages in the defense against pulmonary infections. *Mucosal Immunol*, *6*(3), 464-473. https://doi.org/10.1038/mi.2013.14

Habermann, A. C., Gutierrez, A. J., Bui, L. T., Yahn, S. L., Winters, N. I., Calvi, C. L., Peter, L., Chung, M. I., Taylor, C. J., Jetter, C., Raju, L., Roberson, J., Ding, G., Wood, L., Sucre, J. M. S., . . . Kropski, J. A. (2020). Single-cell RNA sequencing reveals profibrotic roles of distinct epithelial and mesenchymal lineages in pulmonary fibrosis. *Sci Adv*, *6*(28), eaba1972. https://doi.org/10.1126/sciadv.aba1972

Han, X., Wang, R., Zhou, Y., Fei, L., Sun, H., Lai, S., Saadatpour, A., Zhou, Z., Chen, H., Ye, F., Huang, D., Xu, Y., Huang, W., Jiang, M., Jiang, X., . . . Guo, G. (2018). Mapping the Mouse Cell Atlas by Microwell-Seq. *Cell*, *172*(5), 1091-1107.e1017. https://doi.org/10.1016/j.cell.2018.02.001

Hannaway, R. F., Wang, X., Schneider, M., Slow, S., Cowan, J., Brockway, B., Schofield, M. R., Morgan, X. C., Murdoch, D. R., & Ussher, J. E. (2020). Mucosal-associated invariant T cells and Vδ2(+) γδ T cells in community acquired pneumonia: association of abundance in sputum with clinical severity and outcome. *Clin Exp Immunol*, *199*(2), 201-215. https://doi.org/10.1111/cei.13377

Hao, Y., Hao, S., Andersen-Nissen, E., Mauck, W. M., 3rd, Zheng, S., Butler, A., Lee, M. J., Wilk, A. J., Darby, C., Zager, M., Hoffman, P., Stoeckius, M., Papalexi, E., Mimitou,

E. P., Jain, J., . . . Satija, R. (2021). Integrated analysis of multimodal single-cell data. *Cell*, *184*(13), 3573-3587.e3529. https://doi.org/10.1016/j.cell.2021.04.048

Harriff, M. J., Karamooz, E., Burr, A., Grant, W. F., Canfield, E. T., Sorensen, M. L., Moita, L. F., & Lewinsohn, D. M. (2016). Endosomal MR1 Trafficking Plays a Key Role in Presentation of Mycobacterium tuberculosis Ligands to MAIT Cells. *PLoS Pathog*, *12*(3), e1005524. https://doi.org/10.1371/journal.ppat.1005524

Hartmann, N., McMurtrey, C., Sorensen, M. L., Huber, M. E., Kurapova, R., Coleman, F. T., Mizgerd, J. P., Hildebrand, W., Kronenberg, M., Lewinsohn, D. M., & Harriff, M. J. (2018). Riboflavin Metabolism Variation Among Clinical Isolates of Streptococcus pneumoniae Results in Differential Activation of MAIT Cells. *Am J Respir Cell Mol Biol*. https://doi.org/10.1165/rcmb.2017-0290OC

Hashimoto, K., Hirai, M., & Kurosawa, Y. (1995). A gene outside the human MHC related to classical HLA class I genes. *Science*, *269*(5224), 693-695. https://doi.org/10.1126/science.7624800

Hay, J., Shahzeidi, S., & Laurent, G. (1991). Mechanisms of bleomycin-induced lung damage. *Arch Toxicol*, *65*(2), 81-94. https://doi.org/10.1007/bf02034932

Hay, J. G., Haslam, P. L., Dewar, A., Addis, B., Turner-Warwick, M., & Laurent, G. J. (1987). Development of acute lung injury after the combination of intravenous bleomycin and exposure to hyperoxia in rats. *Thorax*, *42*(5), 374-382. https://doi.org/10.1136/thx.42.5.374

Hegde, P., Weiss, E., Paradis, V., Wan, J., Mabire, M., Sukriti, S., Rautou, P.-E., Albuquerque, M., Picq, O., Gupta, A. C., Ferrere, G., Gilgenkrantz, H., Kiaf, B., Toubal, A., Beaudoin, L., Lettéron, P., Moreau, R., Lehuen, A., & Lotersztajn, S. (2018). Mucosal-associated invariant T cells are a profibrogenic immune cell population in the liver. *Nat Commun*, *9*(1), 2146. https://doi.org/10.1038/s41467-018-04450-y

Henry, C. M., Castellanos, C. A., & Reis e Sousa, C. (2023). DNGR-1-mediated cross-presentation of dead cell-associated antigens. *Semin Immunol*, *66*, 101726. https://doi.org/https://doi.org/10.1016/j.smim.2023.101726

Hinks, T. S., Wallington, J. C., Williams, A. P., Djukanović, R., Staples, K. J., & Wilkinson, T. M. (2016). Steroid-induced Deficiency of Mucosal-associated Invariant T Cells in the Chronic Obstructive Pulmonary Disease Lung. Implications for Nontypeable Haemophilus influenzae Infection. *Am J Respir Crit Care Med*, *194*(10), 1208-1218. https://doi.org/10.1164/rccm.201601-0002OC

Hinks, T. S., Zhou, X., Staples, K. J., Dimitrov, B. D., Manta, A., Petrossian, T., Lum, P. Y., Smith, C. G., Ward, J. A., Howarth, P. H., Walls, A. F., Gadola, S. D., & Djukanović, R. (2015). Innate and adaptive T cells in asthmatic patients: Relationship to severity and disease mechanisms. *J Allergy Clin Immunol*, *136*(2), 323-333. https://doi.org/10.1016/j.jaci.2015.01.014

Hinks, T. S. C. (2021). Boosting MAIT cells as immunotherapy: context is everything. *Mucosal Immunol*, *14*(1), 1-3. https://doi.org/10.1038/s41385-020-00337-8

Hinks, T. S. C., Marchi, E., Jabeen, M., Olshansky, M., Kurioka, A., Pediongco, T. J., Meehan, B. S., Kostenko, L., Turner, S. J., Corbett, A. J., Chen, Z., Klenerman, P., & McCluskey, J. (2019). Activation and In Vivo Evolution of the MAIT Cell Transcriptome in Mice and Humans Reveals Tissue Repair Functionality. *Cell Rep*, *28*(12), 3249-3262.e3245. https://doi.org/10.1016/j.celrep.2019.07.039

Hinks, T. S. C., van Wilgenburg, B., Wang, H., Loh, L., Koutsakos, M., Kedzierska, K., Corbett, A. J., & Chen, Z. (2020). Study of MAIT Cell Activation in Viral Infections In Vivo. *Methods Mol Biol*, *2098*, 261-281. https://doi.org/10.1007/978-1-0716-0207-2_17

Hinks, T. S. C., & Zhang, X.-W. (2020). MAIT Cell Activation and Functions [Mini Review]. *Front Immunol*, *11*(1014). https://doi.org/10.3389/fimmu.2020.01014

Holt, P. G., Schon-Hegrad, M. A., Phillips, M. J., & McMenamin, P. G. (1989). Ia-positive dendritic cells form a tightly meshed network within the human airway epithelium. *Clin Exp Allergy*, *19*(6), 597-601. https://doi.org/10.1111/j.1365-2222.1989.tb02752.x

Hoshino, T., Okamoto, M., Sakazaki, Y., Kato, S., Young, H. A., & Aizawa, H. (2009). Role of proinflammatory cytokines IL-18 and IL-1beta in bleomycin-induced lung injury in humans and mice. *Am J Respir Cell Mol Biol*, *41*(6), 661-670. https://doi.org/10.1165/rcmb.2008-0182OC

Huber, M. E., Larson, E., Lust, T. N., Heisler, C. M., & Harriff, M. J. (2023). Chronic Obstructive Pulmonary Disease and Cigarette Smoke Lead to Dysregulated Mucosal-

associated Invariant T-Cell Activation. *Am J Respir Cell Mol Biol*, *68*(1), 90-102. https://doi.org/10.1165/rcmb.2022-0131OC

Hübner, R. H., Gitter, W., El Mokhtari, N. E., Mathiak, M., Both, M., Bolte, H., Freitag-Wolf, S., & Bewig, B. (2008). Standardized quantification of pulmonary fibrosis in histological samples. *Biotechniques*, *44*(4), 507-511, 514-507. https://doi.org/10.2144/000112729

Hubrack, S., Al-Nesf, M. A., Agrebi, N., Raynaud, C., Khattab, M. A., Thomas, M., Ibrahim, T., Taha, S., Dermime, S., Merhi, M., Kulinski, M., Steinhoff, M., Tang, P., & Lo, B. (2021). In vitro Interleukin-7 treatment partially rescues MAIT cell dysfunction caused by SARS-CoV-2 infection. *Sci Rep*, *11*(1), 14090. https://doi.org/10.1038/s41598-021-93536-7

Iborra, S., Izquierdo, H. M., Martínez-López, M., Blanco-Menéndez, N., Reis e Sousa, C., & Sancho, D. (2012). The DC receptor DNGR-1 mediates cross-priming of CTLs during vaccinia virus infection in mice. *J Clin Invest*, *122*(5), 1628-1643. https://doi.org/10.1172/jci60660

Iborra, S., Martínez-López, M., Khouili, S. C., Enamorado, M., Cueto, F. J., Conde-Garrosa, R., Del Fresno, C., & Sancho, D. (2016). Optimal Generation of Tissue-Resident but Not Circulating Memory T Cells during Viral Infection Requires Crosspriming by DNGR-1(+) Dendritic Cells. *Immunity*, *45*(4), 847-860. https://doi.org/10.1016/j.immuni.2016.08.019

Ishimori, A., Harada, N., Chiba, A., Harada, S., Matsuno, K., Makino, F., Ito, J., Ohta, S., Ono, J., Atsuta, R., Izuhara, K., Takahashi, K., & Miyake, S. (2017). Circulating activated innate lymphoid cells and mucosal-associated invariant T cells are associated with airflow limitation in patients with asthma. *Allergol Int*, *66*(2), 302-309. https://doi.org/10.1016/j.alit.2016.07.005

Ivanov, S., Fontaine, J., Paget, C., Macho Fernandez, E., Van Maele, L., Renneson, J., Maillet, I., Wolf, N. M., Rial, A., Léger, H., Ryffel, B., Frisch, B., Chabalgoity, J. A., Sirard, J. C., Benecke, A., Faveeuw, C., & Trottein, F. (2012). Key role for respiratory CD103(+) dendritic cells, IFN-γ, and IL-17 in protection against Streptococcus pneumoniae infection in response to α-galactosylceramide. *J Infect Dis*, *206*(5), 723-734. https://doi.org/10.1093/infdis/jis413

Izbicki, G., Segel, M. J., Christensen, T. G., Conner, M. W., & Breuer, R. (2002). Time course of bleomycin-induced lung fibrosis. *Int J Exp Pathol*, *83*(3), 111-119. https://doi.org/https://doi.org/10.1046/j.1365-2613.2002.00220.x

Jahreis, S., Bottcher, S., Hartung, S., Rachow, T., Rummler, S., Dietl, A. M., Haas, H., Walther, G., Hochhaus, A., & von Lilienfeld-Toal, M. (2018). Human MAIT cells are rapidly activated by Aspergillus spp. in an APC-dependent manner. *Eur J Immunol*, *48*(10), 1698-1706. https://doi.org/10.1002/eji.201747312

James, A. L., & Wenzel, S. (2007). Clinical relevance of airway remodelling in airway diseases. *Eur Respir J*, *30*(1), 134-155. https://doi.org/10.1183/09031936.00146905

Jeffery, H. C., van Wilgenburg, B., Kurioka, A., Parekh, K., Stirling, K., Roberts, S., Dutton, E. E., Hunter, S., Geh, D., Braitch, M. K., Rajanayagam, J., Iqbal, T., Pinkney, T., Brown, R., Withers, D. R., Adams, D. H., Klenerman, P., & Oo, Y. H. (2016). Biliary epithelium and liver B cells exposed to bacteria activate intrahepatic MAIT cells through MR1. *J Hepatol*, *64*(5), 1118-1127. https://doi.org/10.1016/j.jhep.2015.12.017

Jesteadt, E., Zhang, I., Yu, H., Meierovics, A., Chua Yankelevich, W. J., & Cowley, S. (2018). Interleukin-18 Is Critical for Mucosa-Associated Invariant T Cell Gamma Interferon Responses to Francisella Species In Vitro but Not In Vivo. *Infect Immun*, *86*(5). https://doi.org/10.1128/iai.00117-18

Jiang, J., Cao, Z., Qu, J., Liu, H., Han, H., & Cheng, X. (2020). PD-1-expressing MAIT cells from patients with tuberculosis exhibit elevated production of CXCL13. *Scand J Immunol*, *91*(4), e12858. https://doi.org/10.1111/sji.12858

Jiang, J., Chen, X., An, H., Yang, B., Zhang, F., & Cheng, X. (2016). Enhanced immune response of MAIT cells in tuberculous pleural effusions depends on cytokine signaling. *Sci Rep*, *6*, 32320. https://doi.org/10.1038/srep32320

Jiang, J., Yang, B., An, H., Wang, X., Liu, Y., Cao, Z., Zhai, F., Wang, R., Cao, Y., & Cheng, X. (2016). Mucosal-associated invariant T cells from patients with tuberculosis exhibit impaired immune response. *J Infect*, *72*(3), 338-352. https://doi.org/10.1016/j.jinf.2015.11.010

Jilani, T. N., Avula, A., Zafar Gondal, A., & Siddiqui, A. H. (2024). Active Tuberculosis. In *StatPearls*. StatPearls Publishing. Copyright © 2024, StatPearls Publishing LLC.

Jirmo, A. C., Busse, M., Happle, C., Skuljec, J., Dalüge, K., Habener, A., Grychtol, R., DeLuca, D. S., Breiholz, O. D., Prinz, I., & Hansen, G. (2020). IL-17 regulates DC migration to the peribronchial LNs and allergen presentation in experimental allergic asthma. *Eur J Immunol*, *50*(7), 1019-1033. https://doi.org/https://doi.org/10.1002/eji.201948409

Jo, J., Tan, A. T., Ussher, J. E., Sandalova, E., Tang, X. Z., Tan-Garcia, A., To, N., Hong, M., Chia, A., Gill, U. S., Kennedy, P. T., Tan, K. C., Lee, K. H., De Libero, G., Gehring, A. J., Willberg, C. B., Klenerman, P., & Bertoletti, A. (2014). Toll-like receptor 8 agonist and bacteria trigger potent activation of innate immune cells in human liver. *PLoS Pathog*, *10*(6), e1004210. https://doi.org/10.1371/journal.ppat.1004210

Jouan, Y., Guillon, A., Gonzalez, L., Perez, Y., Boisseau, C., Ehrmann, S., Ferreira, M., Daix, T., Jeannet, R., François, B., Dequin, P. F., Si-Tahar, M., Baranek, T., & Paget, C. (2020). Phenotypical and functional alteration of unconventional T cells in severe COVID-19 patients. *J Exp Med*, *217*(12). https://doi.org/10.1084/jem.20200872

Kamphorst, A. O., Guermonprez, P., Dudziak, D., & Nussenzweig, M. C. (2010). Route of antigen uptake differentially impacts presentation by dendritic cells and activated monocytes. *J Immunol*, *185*(6), 3426-3435. https://doi.org/10.4049/jimmunol.1001205

Karmiol, S., Remick, D. G., Kunkel, S. L., & Phan, S. H. (1993). Regulation of rat pulmonary endothelial cell interleukin-6 production by bleomycin: effects of cellular fatty acid composition. *Am J Respir Cell Mol Biol*, *9*(6), 628-636. https://doi.org/10.1165/ajrcmb/9.6.628

Kawachi, I., Maldonado, J., Strader, C., & Gilfillan, S. (2006). MR1-restricted V alpha 19i mucosal-associated invariant T cells are innate T cells in the gut lamina propria that provide a rapid and diverse cytokine response. *J Immunol*, *176*(3), 1618-1627. https://doi.org/10.4049/jimmunol.176.3.1618

Keim, P., Johansson, A., & Wagner, D. M. (2007). Molecular epidemiology, evolution, and ecology of Francisella. *Ann N Y Acad Sci*, *1105*, 30-66. https://doi.org/10.1196/annals.1409.011

Kim, S. K., Choe, J. Y., & Park, K. Y. (2016). Rebamipide Suppresses Monosodium Urate Crystal-Induced Interleukin-1β Production Through Regulation of Oxidative Stress and Caspase-1 in THP-1 Cells. *Inflammation*, *39*(1), 473-482. https://doi.org/10.1007/s10753-015-0271-5

Kjer-Nielsen, L., Patel, O., Corbett, A. J., Le Nours, J., Meehan, B., Liu, L., Bhati, M., Chen, Z., Kostenko, L., Reantragoon, R., Williamson, N. A., Purcell, A. W., Dudek, N. L., McConville, M. J., O'Hair, R. A., Khairallah, G. N., Godfrey, D. I., Fairlie, D. P., Rossjohn, J., & McCluskey, J. (2012). MR1 presents microbial vitamin B metabolites to MAIT cells. *Nature*, *491*(7426), 717-723. https://doi.org/10.1038/nature11605

Klose, C. S. N., & Artis, D. (2016). Innate lymphoid cells as regulators of immunity, inflammation and tissue homeostasis. *Nat Immunol*, *17*(7), 765-774. https://doi.org/10.1038/ni.3489

Kong, G. L., Nguyen, T. T., Rosales, W. K., Panikar, A. D., Cheney, J. H. W., Curtiss, B. M., Carratt, S. A., Braun, T. P., & Maxson, J. E. (2022). CITE-Viz: Replicating the

Interactive Flow Cytometry Workflow in CITE-Seq. *bioRxiv*, 2022.2005.2015.491411. https://doi.org/10.1101/2022.05.15.491411

Korsunsky, I., Millard, N., Fan, J., Slowikowski, K., Zhang, F., Wei, K., Baglaenko, Y., Brenner, M., Loh, P.-r., & Raychaudhuri, S. (2019). Fast, sensitive and accurate integration of single-cell data with Harmony. *Nat Methods*, *16*(12), 1289-1296. https://doi.org/10.1038/s41592-019-0619-0

Kumar, L., & M, E. F. (2007). Mfuzz: a software package for soft clustering of microarray data. *Bioinformation*, *2*(1), 5-7. https://doi.org/10.6026/97320630002005

Kurioka, A., Ussher, J. E., Cosgrove, C., Clough, C., Fergusson, J. R., Smith, K., Kang, Y. H., Walker, L. J., Hansen, T. H., Willberg, C. B., & Klenerman, P. (2014). MAIT cells are licensed through granzyme exchange to kill bacterially sensitized targets. *Mucosal Immunol*. https://doi.org/10.1038/mi.2014.81

Kurioka, A., van Wilgenburg, B., Javan, R. R., Hoyle, R., van Tonder, A. J., Harrold, C. L., Leng, T., Howson, L. J., Shepherd, D., Cerundolo, V., Brueggemann, A. B., & Klenerman, P. (2018). Diverse Streptococcus pneumoniae Strains Drive a Mucosal-Associated Invariant T-Cell Response Through Major Histocompatibility Complex class I-Related Molecule-Dependent and Cytokine-Driven Pathways. *J Infect Dis*, *217*(6), 988-999. https://doi.org/10.1093/infdis/jix647

Kuwano, K., Hagimoto, N., Kawasaki, M., Yatomi, T., Nakamura, N., Nagata, S., Suda, T., Kunitake, R., Maeyama, T., Miyazaki, H., & Hara, N. (1999). Essential roles of the

Fas-Fas ligand pathway in the development of pulmonary fibrosis. *J Clin Invest*, *104*(1), 13-19. https://doi.org/10.1172/jci5628

Kwon, Y. S., Jin, H. M., Cho, Y. N., Kim, M. J., Kang, J. H., Jung, H. J., Park, K. J., Kee, H. J., Kee, S. J., & Park, Y. W. (2016). Mucosal-Associated Invariant T Cell Deficiency in Chronic Obstructive Pulmonary Disease. *Copd*, *13*(2), 196-202. https://doi.org/10.3109/15412555.2015.1069806

Lamichhane, R., Galvin, H., Hannaway, R. F., de la Harpe, S. M., Munro, F., Tyndall, J. D., Vernall, A. J., McCall, J. L., Husain, M., & Ussher, J. E. (2019). Type I interferons are important co-stimulatory signals during T cell receptor mediated human MAIT cell activation. *Eur J Immunol*. https://doi.org/10.1002/eji.201948279

Lamichhane, R., Schneider, M., de la Harpe, S. M., Harrop, T. W. R., Hannaway, R. F., Dearden, P. K., Kirman, J. R., Tyndall, J. D. A., Vernall, A. J., & Ussher, J. E. (2019). TCR- or Cytokine-Activated CD8(+) Mucosal-Associated Invariant T Cells Are Rapid Polyfunctional Effectors That Can Coordinate Immune Responses. *Cell Rep*, *28*(12), 3061-3076.e3065. https://doi.org/10.1016/j.celrep.2019.08.054

Lavin, Y., Winter, D., Blecher-Gonen, R., David, E., Keren-Shaul, H., Merad, M., Jung, S., & Amit, I. (2014). Tissue-resident macrophage enhancer landscapes are shaped by the local microenvironment. *Cell*, *159*(6), 1312-1326. https://doi.org/10.1016/j.cell.2014.11.018

Le Bourhis, L., Dusseaux, M., Bohineust, A., Bessoles, S., Martin, E., Premel, V., Coré, M., Sleurs, D., Serriari, N. E., Treiner, E., Hivroz, C., Sansonetti, P., Gougeon, M. L.,

Soudais, C., & Lantz, O. (2013). MAIT cells detect and efficiently lyse bacterially-infected epithelial cells. *PLoS Pathog*, *9*(10), e1003681. https://doi.org/10.1371/journal.ppat.1003681

Le Bourhis, L., Martin, E., Péguillet, I., Guihot, A., Froux, N., Coré, M., Lévy, E., Dusseaux, M., Meyssonnier, V., Premel, V., Ngo, C., Riteau, B., Duban, L., Robert, D., Huang, S., Rottman, M., Soudais, C., & Lantz, O. (2010). Antimicrobial activity of mucosal-associated invariant T cells. *Nat Immunol*, *11*(8), 701-708. https://doi.org/10.1038/ni.1890

Leeansyah, E., Svard, J., Dias, J., Buggert, M., Nystrom, J., Quigley, M. F., Moll, M., Sonnerborg, A., Nowak, P., & Sandberg, J. K. (2015). Arming of MAIT Cell Cytolytic Antimicrobial Activity Is Induced by IL-7 and Defective in HIV-1 Infection. *PLoS Pathog*, *11*(8), e1005072. https://doi.org/10.1371/journal.ppat.1005072

Leng, T., Akther, H. D., Hackstein, C. P., Powell, K., King, T., Friedrich, M., Christoforidou, Z., McCuaig, S., Neyazi, M., Arancibia-Carcamo, C. V., Hagel, J., Powrie, F., Peres, R. S., Millar, V., Ebner, D., . . . Klenerman, P. (2019). TCR and Inflammatory Signals Tune Human MAIT Cells to Exert Specific Tissue Repair and Effector Functions. *Cell Rep*, *28*(12), 3077-3091.e3075. https://doi.org/10.1016/j.celrep.2019.08.050

Lepore, M., Kalinicenko, A., Colone, A., Paleja, B., Singhal, A., Tschumi, A., Lee, B., Poidinger, M., Zolezzi, F., Quagliata, L., Sander, P., Newell, E., Bertoletti, A., Terracciano, L., De Libero, G., & Mori, L. (2014). Parallel T-cell cloning and deep sequencing of human MAIT cells reveal stable oligoclonal TCRbeta repertoire. *Nat Commun*, *5*, 3866. https://doi.org/10.1038/ncomms4866

Leslie, C. C., McCormick-Shannon, K., Shannon, J. M., Garrick, B., Damm, D., Abraham, J. A., & Mason, R. J. (1997). Heparin-binding EGF-like growth factor is a mitogen for rat alveolar type II cells. *Am J Respir Cell Mol Biol*, *16*(4), 379-387. https://doi.org/10.1165/ajrcmb.16.4.9115748

Lezmi, G., Abou Taam, R., Dietrich, C., Chatenoud, L., de Blic, J., & Leite-de-Moraes, M. (2018). Circulating IL-17-producing mucosal-associated invariant T cells (MAIT) are associated with symptoms in children with asthma. *Clin Immunol*, *188*, 7-11. https://doi.org/10.1016/j.clim.2017.11.009

Lezmi, G., Abou-Taam, R., Garcelon, N., Dietrich, C., Machavoine, F., Delacourt, C., Adel-Patient, K., & Leite-de-Moraes, M. (2019). Evidence for a MAIT-17-high phenotype in children with severe asthma. *J Allergy Clin Immunol*, *144*(6), 1714-1716.e1716. https://doi.org/10.1016/j.jaci.2019.08.003

Li, B., & Wang, J. H. C. (2011). Fibroblasts and myofibroblasts in wound healing: force generation and measurement. *Journal of tissue viability*, *20*(4), 108-120. https://doi.org/10.1016/j.jtv.2009.11.004

Li, D., Guabiraba, R., Besnard, A. G., Komai-Koma, M., Jabir, M. S., Zhang, L., Graham, G. J., Kurowska-Stolarska, M., Liew, F. Y., McSharry, C., & Xu, D. (2014). IL-33 promotes ST2-dependent lung fibrosis by the induction of alternatively activated macrophages and innate lymphoid cells in mice. *J Allergy Clin Immunol*, *134*(6), 1422-1432.e1411. https://doi.org/10.1016/j.jaci.2014.05.011

Li, S., Rouphael, N., Duraisingham, S., Romero-Steiner, S., Presnell, S., Davis, C., Schmidt, D. S., Johnson, S. E., Milton, A., Rajam, G., Kasturi, S., Carlone, G. M., Quinn, C., Chaussabel, D., Palucka, A. K., Mulligan, M. J., Ahmed, R., Stephens, D. S., Nakaya, H. I., & Pulendran, B. (2014). Molecular signatures of antibody responses derived from a systems biology study of five human vaccines. *Nat Immunol*, *15*(2), 195-204. https://doi.org/10.1038/ni.2789

Li, Y., Huang, B., Jiang, X., Chen, W., Zhang, J., Wei, Y., Chen, Y., Lian, M., Bian, Z., Miao, Q., Peng, Y., Fang, J., Wang, Q., Tang, R., Gershwin, M. E., & Ma, X. (2018). Mucosal-Associated Invariant T Cells Improve Nonalcoholic Fatty Liver Disease Through Regulating Macrophage Polarization. *Front Immunol*, *9*, 1994. https://doi.org/10.3389/fimmu.2018.01994

Liao, Y., Smyth, G. K., & Shi, W. (2014). featureCounts: an efficient general purpose program for assigning sequence reads to genomic features. *Bioinformatics*, *30*(7), 923-930. https://doi.org/10.1093/bioinformatics/btt656

Lim, K. H. J., Giampazolias, E., Schulz, O., Rogers, N. C., Wilkins, A., Sahai, E., Strid, J., & Reis e Sousa, C. (2022). Loss of secreted gelsolin enhances response to anticancer therapies. *J Immunother Cancer*, *10*(9). https://doi.org/10.1136/jitc-2022-005245

Linehan, J. L., Harrison, O. J., Han, S. J., Byrd, A. L., Vujkovic-Cvijin, I., Villarino, A. V., Sen, S. K., Shaik, J., Smelkinson, M., Tamoutounour, S., Collins, N., Bouladoux, N., Dzutsev, A., Rosshart, S. P., Arbuckle, J. H., . . . Belkaid, Y. (2018). Non-classical Immunity Controls Microbiota Impact on Skin Immunity and Tissue Repair. *Cell*, *172*(4), 784-796.e718. https://doi.org/10.1016/j.cell.2017.12.033

Liu, J., & Brutkiewicz, R. R. (2017). The Toll-like receptor 9 signalling pathway regulates MR1-mediated bacterial antigen presentation in B cells. *Immunology*, *152*(2), 232-242. https://doi.org/10.1111/imm.12759

Liu, J., Zhang, X., Cheng, Y., & Cao, X. (2021). Dendritic cell migration in inflammation and immunity. *Cellular & Molecular Immunology*, *18*(11), 2461-2471. https://doi.org/10.1038/s41423-021-00726-4

Liu, K., Victora, G. D., Schwickert, T. A., Guermonprez, P., Meredith, M. M., Yao, K., Chu, F. F., Randolph, G. J., Rudensky, A. Y., & Nussenzweig, M. (2009). In vivo analysis of dendritic cell development and homeostasis. *Science*, *324*(5925), 392-397. https://doi.org/10.1126/science.1170540

Liu, X., Das, A. M., Seideman, J., Griswold, D., Afuh, C. N., Kobayashi, T., Abe, S., Fang, Q., Hashimoto, M., Kim, H., Wang, X., Shen, L., Kawasaki, S., & Rennard, S. I. (2007). The CC chemokine ligand 2 (CCL2) mediates fibroblast survival through IL-6. *Am J Respir Cell Mol Biol*, *37*(1), 121-128. https://doi.org/10.1165/rcmb.2005-0253OC

Loh, L., Wang, Z., Sant, S., Koutsakos, M., Jegaskanda, S., Corbett, A. J., Liu, L., Fairlie, D. P., Crowe, J., Rossjohn, J., Xu, J., Doherty, P. C., McCluskey, J., & Kedzierska, K. (2016). Human mucosal-associated invariant T cells contribute to antiviral influenza immunity via IL-18-dependent activation. *Proc Natl Acad Sci U S A*, *113*(36), 10133-10138. https://doi.org/10.1073/pnas.1610750113

Loscertales, M., Nicolaou, F., Jeanne, M., Longoni, M., Gould, D. B., Sun, Y., Maalouf, F. I., Nagy, N., & Donahoe, P. K. (2016). Type IV collagen drives alveolar epithelial-

endothelial association and the morphogenetic movements of septation. *BMC Biol*, *14*, 59. https://doi.org/10.1186/s12915-016-0281-2

Love, M. I., Huber, W., & Anders, S. (2014). Moderated estimation of fold change and dispersion for RNA-seq data with DESeq2. *Genome Biol*, *15*(12), 550. https://doi.org/10.1186/s13059-014-0550-8

Lu, B., Liu, M., Wang, J., Fan, H., Yang, D., Zhang, L., Gu, X., Nie, J., Chen, Z., Corbett, A. J., Zhan, M. J., Zhang, S., Bryant, V. L., Lew, A. M., McCluskey, J., Luo, H. B., Cui, J., Zhang, Y., Zhan, Y., & Lu, G. (2020). IL-17 production by tissue-resident MAIT cells is locally induced in children with pneumonia. *Mucosal Immunol*, *13*(5), 824-835. https://doi.org/10.1038/s41385-020-0273-y

Mabire, M., Hegde, P., Hammoutene, A., Wan, J., Caër, C., Sayegh, R. A., Cadoux, M., Allaire, M., Weiss, E., Thibault-Sogorb, T., Lantz, O., Goodhardt, M., Paradis, V., de la Grange, P., Gilgenkrantz, H., & Lotersztajn, S. (2023). MAIT cell inhibition promotes liver fibrosis regression via macrophage phenotype reprogramming. *Nat Commun*, *14*(1), 1830. https://doi.org/10.1038/s41467-023-37453-5

Maggio, S., Takeda, K., Stark, F., Meierovics, A. I., Yabe, I., & Cowley, S. C. (2015). Control of Francisella tularensis Intracellular Growth by Pulmonary Epithelial Cells. *PLoS One*, *10*(9), e0138565. https://doi.org/10.1371/journal.pone.0138565

Mak, J. Y., Xu, W., Reid, R. C., Corbett, A. J., Meehan, B. S., Wang, H., Chen, Z., Rossjohn, J., McCluskey, J., Liu, L., & Fairlie, D. P. (2017). Stabilizing short-lived Schiff base

derivatives of 5-aminouracils that activate mucosal-associated invariant T cells. *Nat Commun*, *8*, 14599. https://doi.org/10.1038/ncomms14599

Malka-Ruimy, C., Ben Youssef, G., Lambert, M., Tourret, M., Ghazarian, L., Faye, A., Caillat-Zucman, S., & Houdouin, V. (2019). Mucosal-Associated Invariant T Cell Levels Are Reduced in the Peripheral Blood and Lungs of Children With Active Pulmonary Tuberculosis. *Front Immunol*, *10*, 206. https://doi.org/10.3389/fimmu.2019.00206

Marchal-Sommé, J., Uzunhan, Y., Marchand-Adam, S., Kambouchner, M., Valeyre, D., Crestani, B., & Soler, P. (2007). Dendritic cells accumulate in human fibrotic interstitial lung disease. *Am J Respir Crit Care Med*, *176*(10), 1007-1014. https://doi.org/10.1164/rccm.200609-1347OC

Martin, E., Treiner, E., Duban, L., Guerri, L., Laude, H., Toly, C., Premel, V., Devys, A., Moura, I. C., Tilloy, F., Cherif, S., Vera, G., Latour, S., Soudais, C., & Lantz, O. (2009). Stepwise development of MAIT cells in mouse and human. *PLoS Biol*, *7*(3), e54. https://doi.org/10.1371/journal.pbio.1000054

Matsuyama, H., Isshiki, T., Chiba, A., Yamaguchi, T., Murayama, G., Akasaka, Y., Eishi, Y., Sakamoto, S., Homma, S., & Miyake, S. (2019). Activation of mucosal-associated invariant T cells in the lungs of sarcoidosis patients. *Sci Rep*, *9*(1), 13181. https://doi.org/10.1038/s41598-019-49903-6

Mayassi, T., Barreiro, L. B., Rossjohn, J., & Jabri, B. (2021). A multilayered immune system through the lens of unconventional T cells. *Nature*, *595*(7868), 501-510. https://doi.org/10.1038/s41586-021-03578-0

McElroy, R., Talesh, G. A., Harpur, C. M., Carzino, R., Corbett, A. J., Pellicci, D. G., Ranganathan, S., & Sutton, P. (2022). Unconventional T Cell Immunity in the Lungs of Young Children with Cystic Fibrosis. *FBL*, *27*(5). https://doi.org/10.31083/j.fbl2705149

McWilliam, H. E., Eckle, S. B., Theodossis, A., Liu, L., Chen, Z., Wubben, J. M., Fairlie, D. P., Strugnell, R. A., Mintern, J. D., McCluskey, J., Rossjohn, J., & Villadangos, J. A. (2016). The intracellular pathway for the presentation of vitamin B-related antigens by the antigen-presenting molecule MR1. *Nat Immunol*, *17*(5), 531-537. https://doi.org/10.1038/ni.3416

Meermeier, E. W., Harriff, M. J., Karamooz, E., & Lewinsohn, D. M. (2018). MAIT cells and microbial immunity. *Immunol Cell Biol*, *96*(6), 607-617. https://doi.org/10.1111/imcb.12022

Meierovics, A., Yankelevich, W. J., & Cowley, S. C. (2013). MAIT cells are critical for optimal mucosal immune responses during in vivo pulmonary bacterial infection. *Proc Natl Acad Sci U S A*, *110*(33), E3119-3128. https://doi.org/10.1073/pnas.1302799110

Meierovics, A. I., & Cowley, S. C. (2016). MAIT cells promote inflammatory monocyte differentiation into dendritic cells during pulmonary intracellular infection. *J Exp Med*, *213*(12), 2793-2809. https://doi.org/10.1084/jem.20160637

Merad, M., Sathe, P., Helft, J., Miller, J., & Mortha, A. (2013). The dendritic cell lineage: ontogeny and function of dendritic cells and their subsets in the steady state and the

inflamed setting. *Annu Rev Immunol*, *31*, 563-604. https://doi.org/10.1146/annurev-immunol-020711-074950

Mi, S., Li, Z., Yang, H. Z., Liu, H., Wang, J. P., Ma, Y. G., Wang, X. X., Liu, H. Z., Sun, W., & Hu, Z. W. (2011). Blocking IL-17A promotes the resolution of pulmonary inflammation and fibrosis via TGF-beta1-dependent and -independent mechanisms. *J Immunol*, *187*(6), 3003-3014. https://doi.org/10.4049/jimmunol.1004081

Michalski, J. E., Kurche, J. S., & Schwartz, D. A. (2022). From ARDS to pulmonary fibrosis: the next phase of the COVID-19 pandemic? *Transl Res*, *241*, 13-24. https://doi.org/10.1016/j.trsl.2021.09.001

Miller, J. C., Brown, B. D., Shay, T., Gautier, E. L., Jojic, V., Cohain, A., Pandey, G., Leboeuf, M., Elpek, K. G., Helft, J., Hashimoto, D., Chow, A., Price, J., Greter, M., Bogunovic, M., . . . the Immunological Genome, C. (2012). Deciphering the transcriptional network of the dendritic cell lineage. *Nat Immunol*, *13*(9), 888-899. https://doi.org/10.1038/ni.2370

Moon, Y. W., Rao, G., Kim, J. J., Shim, H. S., Park, K. S., An, S. S., Kim, B., Steeg, P. S., Sarfaraz, S., Changwoo Lee, L., Voeller, D., Choi, E. Y., Luo, J., Palmieri, D., Chung, H. C., Kim, J. H., Wang, Y., & Giaccone, G. (2015). LAMC2 enhances the metastatic potential of lung adenocarcinoma. *Cell Death Differ*, *22*(8), 1341-1352. https://doi.org/10.1038/cdd.2014.228

Moore, B. B., & Hogaboam, C. M. (2008). Murine models of pulmonary fibrosis. *Am J Physiol Lung Cell Mol Physiol*, *294*(2), L152-160. https://doi.org/10.1152/ajplung.00313.2007

Mortha, A., & Burrows, K. (2018). Cytokine Networks between Innate Lymphoid Cells and Myeloid Cells [Review]. *Front Immunol*, *9*. https://doi.org/10.3389/fimmu.2018.00191

Moseley, P. L. (1989). Augmentation of bleomycin-induced DNA damage in intact cells. *Am J Physiol*, *257*(5 Pt 1), C882-887. https://doi.org/10.1152/ajpcell.1989.257.5.C882

Mulè, M. P., Martins, A. J., & Tsang, J. S. (2022). Normalizing and denoising protein expression data from droplet-based single cell profiling. *Nat Commun*, *13*(1), 2099. https://doi.org/10.1038/s41467-022-29356-8

Naik, S. H., Proietto, A. I., Wilson, N. S., Dakic, A., Schnorrer, P., Fuchsberger, M., Lahoud, M. H., O'Keeffe, M., Shao, Q. X., Chen, W. F., Villadangos, J. A., Shortman, K., & Wu, L. (2005). Cutting edge: generation of splenic CD8+ and CD8- dendritic cell equivalents in Fms-like tyrosine kinase 3 ligand bone marrow cultures. *J Immunol*, *174*(11), 6592-6597. https://doi.org/10.4049/jimmunol.174.11.6592

Neumark, N., Cosme, C., Jr., Rose, K. A., & Kaminski, N. (2020). The Idiopathic Pulmonary Fibrosis Cell Atlas. *Am J Physiol Lung Cell Mol Physiol*, *319*(6), L887-l893. https://doi.org/10.1152/ajplung.00451.2020

Nguyen, N. M., & Senior, R. M. (2006). Laminin isoforms and lung development: All isoforms are not equal. *Developmental Biology*, *294*(2), 271-279. https://doi.org/https://doi.org/10.1016/j.ydbio.2006.03.032

Nie, Y., Hu, Y., Yu, K., Zhang, D., Shi, Y., Li, Y., Sun, L., & Qian, F. (2019). Akt1 regulates pulmonary fibrosis via modulating IL-13 expression in macrophages. *Innate Immun*, *25*(7), 451-461. https://doi.org/10.1177/1753425919861774

Onai, N., Kurabayashi, K., Hosoi-Amaike, M., Toyama-Sorimachi, N., Matsushima, K., Inaba, K., & Ohteki, T. (2013). A clonogenic progenitor with prominent plasmacytoid dendritic cell developmental potential. *Immunity*, *38*(5), 943-957. https://doi.org/10.1016/j.immuni.2013.04.006

Ortiz, L. A., Lasky, J., Hamilton, R. F., Jr., Holian, A., Hoyle, G. W., Banks, W., Peschon, J. J., Brody, A. R., Lungarella, G., & Friedman, M. (1998). Expression of TNF and the necessity of TNF receptors in bleomycin-induced lung injury in mice. *Exp Lung Res*, *24*(6), 721-743. https://doi.org/10.3109/01902149809099592

Osterholzer, J. J., Curtis, J. L., Polak, T., Ames, T., Chen, G. H., McDonald, R., Huffnagle, G. B., & Toews, G. B. (2008). CCR2 mediates conventional dendritic cell recruitment and the formation of bronchovascular mononuclear cell infiltrates in the lungs of mice infected with Cryptococcus neoformans. *J Immunol*, *181*(1), 610-620. https://doi.org/10.4049/jimmunol.181.1.610

Otero, K., Vecchi, A., Hirsch, E., Kearley, J., Vermi, W., Del Prete, A., Gonzalvo-Feo, S., Garlanda, C., Azzolino, O., Salogni, L., Lloyd, C. M., Facchetti, F., Mantovani, A., & Sozzani, S. (2010). Nonredundant role of CCRL2 in lung dendritic cell trafficking. *Blood*, *116*(16), 2942-2949. https://doi.org/10.1182/blood-2009-12-259903

Ouyang, L., Wu, M., Shen, Z., Cheng, X., Wang, W., Jiang, L., Zhao, J., Gong, Y., Liang, Z., Weng, X., Yu, M., & Wu, X. (2021). Activation and Functional Alteration of Mucosal-Associated Invariant T Cells in Adult Patients With Community-Acquired Pneumonia. *Front Immunol*, *12*, 788406. https://doi.org/10.3389/fimmu.2021.788406

Oyston, P. C. F. (2008). Francisella tularensis: unravelling the secrets of an intracellular pathogen. *J Med Microbiol*, *57*(Pt 8), 921-930. https://doi.org/10.1099/jmm.0.2008/000653-0

Palla, G., Spitzer, H., Klein, M., Fischer, D., Schaar, A. C., Kuemmerle, L. B., Rybakov, S., Ibarra, I. L., Holmberg, O., Virshup, I., Lotfollahi, M., Richter, S., & Theis, F. J. (2022). Squidpy: a scalable framework for spatial omics analysis. *Nat Methods*, *19*(2), 171-178. https://doi.org/10.1038/s41592-021-01358-2

Pan, J., Zhang, M., Wang, J., Wang, Q., Xia, D., Sun, W., Zhang, L., Yu, H., Liu, Y., & Cao, X. (2004). Interferon-γ is an autocrine mediator for dendritic cell maturation. *Immunol Lett*, *94*(1), 141-151. https://doi.org/https://doi.org/10.1016/j.imlet.2004.05.003

Pankhurst, T. E., Buick, K. H., Lange, J. L., Marshall, A. J., Button, K. R., Palmer, O. R., Farrand, K. J., Montgomerie, I., Bird, T. W., Mason, N. C., Kuang, J., Compton, B. J., Comoletti, D., Salio, M., Cerundolo, V., Quiñones-Mateu, M. E., Painter, G. F., Hermans, I. F., & Connor, L. M. (2023). MAIT cells activate dendritic cells to promote T(FH) cell differentiation and induce humoral immunity. *Cell Rep*, *42*(4), 112310. https://doi.org/10.1016/j.celrep.2023.112310

Paquin-Proulx, D., Costa, P. R., Terrassani Silveira, C. G., Marmorato, M. P., Cerqueira, N. B., Sutton, M. S., O'Connor, S. L., Carvalho, K. I., Nixon, D. F., & Kallas, E. G. (2018). Latent Mycobacterium tuberculosis Infection Is Associated With a Higher Frequency of Mucosal-Associated Invariant T and Invariant Natural Killer T Cells. *Front Immunol*, *9*, 1394. https://doi.org/10.3389/fimmu.2018.01394

Park, D., Kim, H. G., Kim, M., Park, T., Ha, H.-H., Lee, D. H., Park, K.-S., Park, S. J., Lim, H. J., & Lee, C. H. (2019). Differences in the molecular signatures of mucosal-associated invariant T cells and conventional T cells. *Sci Rep*, *9*(1), 7094. https://doi.org/10.1038/s41598-019-43578-9

Parrot, T., Gorin, J. B., Ponzetta, A., Maleki, K. T., Kammann, T., Emgård, J., Perez-Potti, A., Sekine, T., Rivera-Ballesteros, O., Gredmark-Russ, S., Rooyackers, O., Folkesson, E., Eriksson, L. I., Norrby-Teglund, A., Ljunggren, H. G., . . . Sandberg, J. K. (2020). MAIT cell activation and dynamics associated with COVID-19 disease severity. *Sci Immunol*, *5*(51). https://doi.org/10.1126/sciimmunol.abe1670

Pauline, T., Sylvie, L., Loïc, G., Thomas, F., Julie, M., Youen, J., Antoine, G., Mustapha, S.-T., & Christophe, P. (2021). Frequency and phenotypical alterations of unconventional T cells in cystic fibrosis. *Eur Respir J*, *58*(suppl 65), OA1497. https://doi.org/10.1183/13993003.congress-2021.OA1497

Petley, E. V., Koay, H.-F., Henderson, M. A., Sek, K., Todd, K. L., Keam, S. P., Lai, J., House, I. G., Li, J., Zethoven, M., Chen, A. X. Y., Oliver, A. J., Michie, J., Freeman, A. J., Giuffrida, L., . . . Darcy, P. K. (2021). MAIT cells regulate NK cell-mediated tumor immunity. *Nat Commun*, *12*(1), 4746. https://doi.org/10.1038/s41467-021-25009-4

Petukhov, V., Xu, R. J., Soldatov, R. A., Cadinu, P., Khodosevich, K., Moffitt, J. R., & Kharchenko, P. V. (2022). Cell segmentation in imaging-based spatial transcriptomics. *Nat Biotechnol*, *40*(3), 345-354. https://doi.org/10.1038/s41587-021-01044-w

Philipp, M.-S. (2020). *MAIT cell diversity, function and impact on dendritic cells* [Dissertation, The Rheinische Friedrich-Wilhelms-Universität Bonn, The University of Melbourne]. https://nbn-resolving.org/urn:nbn:de:hbz:5-58010

Pincikova, T., Parrot, T., Hjelte, L., Högman, M., Lisspers, K., Ställberg, B., Janson, C., Malinovschi, A., & Sandberg, J. K. (2022). MAIT cell counts are associated with the risk of hospitalization in COPD. *Respir Res*, *23*(1), 127. https://doi.org/10.1186/s12931-022-02045-2

Provine, N. M., Amini, A., Garner, L. C., Spencer, A. J., Dold, C., Hutchings, C., Silva Reyes, L., FitzPatrick, M. E. B., Chinnakannan, S., Oguti, B., Raymond, M., Ulaszewska, M., Troise, F., Sharpe, H., Morgan, S. B., . . . Klenerman, P. (2021). MAIT cell activation augments adenovirus vector vaccine immunogenicity. *Science*, *371*(6528), 521-526. https://doi.org/10.1126/science.aax8819

Qiu, W., Kang, N., Wu, Y., Cai, Y., Xiao, L., Ge, H., & Zhu, H. (2021). Mucosal Associated Invariant T Cells Were Activated and Polarized Toward Th17 in Chronic Obstructive Pulmonary Disease. *Front Immunol*, *12*, 640455. https://doi.org/10.3389/fimmu.2021.640455

Qiu, X., Hill, A., Packer, J., Lin, D., Ma, Y.-A., & Trapnell, C. (2017). Single-cell mRNA quantification and differential analysis with Census. *Nat Methods*, *14*(3), 309-315. https://doi.org/10.1038/nmeth.4150

Rahimpour, A., Koay, H. F., Enders, A., Clanchy, R., Eckle, S. B., Meehan, B., Chen, Z., Whittle, B., Liu, L., Fairlie, D. P., Goodnow, C. C., McCluskey, J., Rossjohn, J.,

Uldrich, A. P., Pellicci, D. G., & Godfrey, D. I. (2015). Identification of phenotypically and functionally heterogeneous mouse mucosal-associated invariant T cells using MR1 tetramers. *J Exp Med*, *212*(7), 1095-1108. https://doi.org/10.1084/jem.20142110

Reantragoon, R., Corbett, A. J., Sakala, I. G., Gherardin, N. A., Furness, J. B., Chen, Z., Eckle, S. B., Uldrich, A. P., Birkinshaw, R. W., Patel, O., Kostenko, L., Meehan, B., Kedzierska, K., Liu, L., Fairlie, D. P., Hansen, T. H., Godfrey, D. I., Rossjohn, J., McCluskey, J., & Kjer-Nielsen, L. (2013). Antigen-loaded MR1 tetramers define T cell receptor heterogeneity in mucosal-associated invariant T cells. *J Exp Med*, *210*(11), 2305-2320. https://doi.org/10.1084/jem.20130958

Reinert, T., Baldotto, C. S. d. R., Nunes, F. A. P., & Scheliga, A. A. d. S. (2013). Bleomycin-induced lung injury. *J Cancer Res*, *2013*.

Ren, X., Wen, W., Fan, X., Hou, W., Su, B., Cai, P., Li, J., Liu, Y., Tang, F., Zhang, F., Yang, Y., He, J., Ma, W., He, J., Wang, P., . . . Zhang, Z. (2021). COVID-19 immune features revealed by a large-scale single-cell transcriptome atlas. *Cell*, *184*(7), 1895-1913.e1819. https://doi.org/10.1016/j.cell.2021.01.053

Riegert, P., Wanner, V., & Bahram, S. (1998). Genomics, isoforms, expression, and phylogeny of the MHC class I-related MR1 gene. *J Immunol*, *161*(8), 4066-4077.

Riffelmacher, T., Paynich Murray, M., Wientjens, C., Chandra, S., Cedillo-Castelán, V., Chou, T.-F., McArdle, S., Dillingham, C., Devereaux, J., Nilsen, A., Brunel, S., Lewinsohn, D. M., Hasty, J., Seumois, G., Benedict, C. A., Vijayanand, P., & Kronenberg, M. (2023). Divergent metabolic programmes control two populations of MAIT cells that

protect the lung. *Nature Cell Biology*, *25*(6), 877-891. https://doi.org/10.1038/s41556-023-01152-6

Ritchie, M. E., Phipson, B., Wu, D., Hu, Y., Law, C. W., Shi, W., & Smyth, G. K. (2015). limma powers differential expression analyses for RNA-sequencing and microarray studies. *Nucleic Acids Res*, *43*(7), e47-e47. https://doi.org/10.1093/nar/gkv007

Riteau, N., Gasse, P., Fauconnier, L., Gombault, A., Couegnat, M., Fick, L., Kanellopoulos, J., Quesniaux, V. F., Marchand-Adam, S., Crestani, B., Ryffel, B., & Couillin, I. (2010). Extracellular ATP is a danger signal activating P2X7 receptor in lung inflammation and fibrosis. *Am J Respir Crit Care Med*, *182*(6), 774-783. https://doi.org/10.1164/rccm.201003-0359OC

Robinette, M. L., Fuchs, A., Cortez, V. S., Lee, J. S., Wang, Y., Durum, S. K., Gilfillan, S., Colonna, M., Shaw, L., Yu, B., Goldrath, A., Mostafavi, S., Regev, A., Kim, E. Y., Dwyer, D. F., . . . the Immunological Genome, C. (2015). Transcriptional programs define molecular characteristics of innate lymphoid cell classes and subsets. *Nat Immunol*, *16*(3), 306-317. https://doi.org/10.1038/ni.3094

Robinson, M. D., McCarthy, D. J., & Smyth, G. K. (2010). edgeR: a Bioconductor package for differential expression analysis of digital gene expression data. *Bioinformatics*, *26*(1), 139-140. https://doi.org/10.1093/bioinformatics/btp616

Rouxel, O., Da Silva, J., Beaudoin, L., Nel, I., Tard, C., Cagninacci, L., Kiaf, B., Oshima, M., Diedisheim, M., Salou, M., Corbett, A., Rossjohn, J., McCluskey, J., Scharfmann, R., Battaglia, M., Polak, M., Lantz, O., Beltrand, J., & Lehuen, A. (2017). Cytotoxic and

regulatory roles of mucosal-associated invariant T cells in type 1 diabetes. *Nat Immunol*, *18*(12), 1321-1331. https://doi.org/10.1038/ni.3854

Ruf, B., Catania, V. V., Wabitsch, S., Ma, C., Diggs, L. P., Zhang, Q., Heinrich, B., Subramanyam, V., Cui, L. L., Pouzolles, M., Evans, C. N., Chari, R., Sakai, S., Oh, S., Barry, C. E., III, Barber, D. L., & Greten, T. F. (2021). Activating Mucosal-Associated Invariant T Cells Induces a Broad Antitumor Response. *Cancer Immunol Res*, *9*(9), 1024-1034. https://doi.org/10.1158/2326-6066.Cir-20-0925

Ryu, J. H., Colby, T. V., & Hartman, T. E. (1998). Idiopathic pulmonary fibrosis: current concepts. *Mayo Clin Proc*, *73*(11), 1085-1101. https://doi.org/10.4065/73.11.1085

Sadeghipour, A., & Babaheidarian, P. (2019). Making Formalin-Fixed, Paraffin Embedded Blocks. In W. H. Yong (Ed.), *Biobanking: Methods and Protocols* (pp. 253-268). Springer New York. https://doi.org/10.1007/978-1-4939-8935-5_22

Saito, F., Tasaka, S., Inoue, K., Miyamoto, K., Nakano, Y., Ogawa, Y., Yamada, W., Shiraishi, Y., Hasegawa, N., Fujishima, S., Takano, H., & Ishizaka, A. (2008). Role of interleukin-6 in bleomycin-induced lung inflammatory changes in mice. *Am J Respir Cell Mol Biol*, *38*(5), 566-571. https://doi.org/10.1165/rcmb.2007-0299OC

Sakai, S., Kauffman, K. D., Oh, S., Nelson, C. E., Barry, C. E., & Barber, D. L. (2021). MAIT cell-directed therapy of Mycobacterium tuberculosis infection. *Mucosal Immunol*, *14*(1), 199-208. https://doi.org/10.1038/s41385-020-0332-4

Sakai, S., Lora, N. E., Kauffman, K. D., Dorosky, D. E., Oh, S., Namasivayam, S., Gomez, F., Fleegle, J. D., Arlehamn, C. S. L., Sette, A., Sher, A., Freeman, G. J., Via, L. E., Barry

Iii, C. E., & Barber, D. L. (2021). Functional inactivation of pulmonary MAIT cells following 5-OP-RU treatment of non-human primates. *Mucosal Immunol*, *14*(5), 1055-1066. https://doi.org/10.1038/s41385-021-00425-3

Sakamoto, H., Zhao, L. H., Jain, F., & Kradin, R. (2002). IL-12p40(-/-) mice treated with intratracheal bleomycin exhibit decreased pulmonary inflammation and increased fibrosis. *Exp Mol Pathol*, *72*(1), 1-9. https://doi.org/10.1006/exmp.2001.2409

Salerno-Goncalves, R., Rezwan, T., & Sztein, M. B. (2014). B cells modulate mucosal associated invariant T cell immune responses. *Front Immunol*, *4*, 511. https://doi.org/10.3389/fimmu.2013.00511

Salio, M., Gasser, O., Gonzalez-Lopez, C., Martens, A., Veerapen, N., Gileadi, U., Verter, J. G., Napolitani, G., Anderson, R., Painter, G., Besra, G. S., Hermans, I. F., & Cerundolo, V. (2017). Activation of Human Mucosal-Associated Invariant T Cells Induces CD40L-Dependent Maturation of Monocyte-Derived and Primary Dendritic Cells. *J Immunol*, *199*(8), 2631-2638. https://doi.org/10.4049/jimmunol.1700615

Samstein, M., Schreiber, H. A., Leiner, I. M., Susac, B., Glickman, M. S., & Pamer, E. G. (2013). Essential yet limited role for CCR2(+) inflammatory monocytes during Mycobacterium tuberculosis-specific T cell priming. *Elife*, *2*, e01086. https://doi.org/10.7554/eLife.01086

Sancho, D., Joffre, O. P., Keller, A. M., Rogers, N. C., Martínez, D., Hernanz-Falcón, P., Rosewell, I., & Reis e Sousa, C. (2009). Identification of a dendritic cell receptor that

couples sensing of necrosis to immunity. *Nature*, *458*(7240), 899-903. https://doi.org/10.1038/nature07750

Sancho, D., Mourão-Sá, D., Joffre, O. P., Schulz, O., Rogers, N. C., Pennington, D. J., Carlyle, J. R., & Reis e Sousa, C. (2008). Tumor therapy in mice via antigen targeting to a novel, DC-restricted C-type lectin. *J Clin Invest*, *118*(6), 2098-2110. https://doi.org/10.1172/jci34584

Saraiva, M., & O'Garra, A. (2010). The regulation of IL-10 production by immune cells. *Nat Rev Immunol*, *10*(3), 170-181. https://doi.org/10.1038/nri2711

Sattler, A., Dang-Heine, C., Reinke, P., & Babel, N. (2015). IL-15 dependent induction of IL-18 secretion as a feedback mechanism controlling human MAIT-cell effector functions. *Eur J Immunol*, *45*(8), 2286-2298. https://doi.org/10.1002/eji.201445313

Savani, R. C., Hou, G., Liu, P., Wang, C., Simons, E., Grimm, P. C., Stern, R., Greenberg, A. H., DeLisser, H. M., & Khalil, N. (2000). A role for hyaluronan in macrophage accumulation and collagen deposition after bleomycin-induced lung injury. *Am J Respir Cell Mol Biol*, *23*(4), 475-484. https://doi.org/10.1165/ajrcmb.23.4.3944

Scheule, R. K., Perkins, R. C., Hamilton, R., & Holian, A. (1992). Bleomycin stimulation of cytokine secretion by the human alveolar macrophage. *Am J Physiol*, *262*(4 Pt 1), L386-391. https://doi.org/10.1152/ajplung.1992.262.4.L386

Schlitzer, A., Sivakamasundari, V., Chen, J., Sumatoh, H. R., Schreuder, J., Lum, J., Malleret, B., Zhang, S., Larbi, A., Zolezzi, F., Renia, L., Poidinger, M., Naik, S., Newell, E. W., Robson, P., & Ginhoux, F. (2015). Identification of cDC1- and cDC2-committed DC

progenitors reveals early lineage priming at the common DC progenitor stage in the bone marrow. *Nat Immunol*, *16*(7), 718-728. https://doi.org/10.1038/ni.3200

Schulz, O., Hanč, P., Böttcher, J. P., Hoogeboom, R., Diebold, S. S., Tolar, P., & Reis e Sousa, C. (2018). Myosin II Synergizes with F-Actin to Promote DNGR-1-Dependent Cross-Presentation of Dead Cell-Associated Antigens. *Cell Rep*, *24*(2), 419-428. https://doi.org/10.1016/j.celrep.2018.06.038

Sergushichev, A. A. (2016). An algorithm for fast preranked gene set enrichment analysis using cumulative statistic calculation. *bioRxiv*, 060012. https://doi.org/10.1101/060012

Shaler, C. R., Choi, J., Rudak, P. T., Memarnejadian, A., Szabo, P. A., Tun-Abraham, M. E., Rossjohn, J., Corbett, A. J., McCluskey, J., McCormick, J. K., Lantz, O., Hernandez-Alejandro, R., & Haeryfar, S. M. M. (2017). MAIT cells launch a rapid, robust and distinct hyperinflammatory response to bacterial superantigens and quickly acquire an anergic phenotype that impedes their cognate antimicrobial function: Defining a novel mechanism of superantigen-induced immunopathology and immunosuppression. *PLoS Biol*, *15*(6), e2001930. https://doi.org/10.1371/journal.pbio.2001930

Sharma, P. K., Wong, E. B., Napier, R. J., Bishai, W. R., Ndung'u, T., Kasprowicz, V. O., Lewinsohn, D. A., Lewinsohn, D. M., & Gold, M. C. (2015). High expression of CD26 accurately identifies human bacteria-reactive MR1-restricted MAIT cells. *Immunology*, *145*(3), 443-453. https://doi.org/10.1111/imm.12461

Shi, J., Zhou, J., Zhang, X., Hu, W., Zhao, J. F., Wang, S., Wang, F. S., & Zhang, J. Y. (2021). Single-Cell Transcriptomic Profiling of MAIT Cells in Patients With COVID-19. *Front Immunol*, *12*, 700152. https://doi.org/10.3389/fimmu.2021.700152

Shimizu, Y., Horigane-Konakai, Y., Ishii, Y., Sugimoto, C., & Wakao, H. (2022). Mucosal-associated invariant T cells repress group 2 innate lymphoid cells in Alternaria alternata-induced model of allergic airway inflammation. *Front Immunol*, *13*, 1005226. https://doi.org/10.3389/fimmu.2022.1005226

Shinkai, Y., Rathbun, G., Lam, K. P., Oltz, E. M., Stewart, V., Mendelsohn, M., Charron, J., Datta, M., Young, F., Stall, A. M., & et al. (1992). RAG-2-deficient mice lack mature lymphocytes owing to inability to initiate V(D)J rearrangement. *Cell*, *68*(5), 855-867. https://doi.org/10.1016/0092-8674(92)90029-c

Shteinberg, M., Haq, I. J., Polineni, D., & Davies, J. C. (2021). Cystic fibrosis. *Lancet*, *397*(10290), 2195-2211. https://doi.org/10.1016/s0140-6736(20)32542-3

Sikkema, L., Ramírez-Suástegui, C., Strobl, D. C., Gillett, T. E., Zappia, L., Madissoon, E., Markov, N. S., Zaragosi, L.-E., Ji, Y., Ansari, M., Arguel, M.-J., Apperloo, L., Banchero, M., Bécavin, C., Berg, M., . . . Lung Biological Network, C. (2023). An integrated cell atlas of the lung in health and disease. *Nat Med*, *29*(6), 1563-1577. https://doi.org/10.1038/s41591-023-02327-2

Sleijfer, S. (2001). Bleomycin-induced pneumonitis. *Chest*, *120*(2), 617-624. https://doi.org/10.1378/chest.120.2.617

Slichter, C. K., McDavid, A., Miller, H. W., Finak, G., Seymour, B. J., McNevin, J. P., Diaz, G., Czartoski, J. L., McElrath, M. J., Gottardo, R., & Prlic, M. (2016). Distinct activation thresholds of human conventional and innate-like memory T cells. *JCI Insight*, *1*(8). https://doi.org/10.1172/jci.insight.86292

Smith, D. J., Hill, G. R., Bell, S. C., & Reid, D. W. (2014). Reduced mucosal associated invariant T-cells are associated with increased disease severity and Pseudomonas aeruginosa infection in cystic fibrosis. *PLoS One*, *9*(10), e109891. https://doi.org/10.1371/journal.pone.0109891

Sonnenberg, G. F., Fouser, L. A., & Artis, D. (2010). Functional biology of the IL-22-IL-22R pathway in regulating immunity and inflammation at barrier surfaces. *Adv Immunol*, *107*, 1-29. https://doi.org/10.1016/b978-0-12-381300-8.00001-0

Soudais, C., Samassa, F., Sarkis, M., Le Bourhis, L., Bessoles, S., Blanot, D., Herve, M., Schmidt, F., Mengin-Lecreulx, D., & Lantz, O. (2015). In Vitro and In Vivo Analysis of the Gram-Negative Bacteria-Derived Riboflavin Precursor Derivatives Activating Mouse MAIT Cells. *J Immunol*, *194*(10), 4641-4649. https://doi.org/10.4049/jimmunol.1403224

Spagnolo, P., Rossi, G., Trisolini, R., Sverzellati, N., Baughman, R. P., & Wells, A. U. (2018). Pulmonary sarcoidosis. *Lancet Respir Med*, *6*(5), 389-402. https://doi.org/10.1016/s2213-2600(18)30064-x

Srivastava, S., Grace, P. S., & Ernst, J. D. (2016). Antigen Export Reduces Antigen Presentation and Limits T Cell Control of M. tuberculosis. *Cell Host Microbe*, *19*(1), 44-54. https://doi.org/10.1016/j.chom.2015.12.003

Steimle, V., Siegrist, C. A., Mottet, A., Lisowska-Grospierre, B., & Mach, B. (1994). Regulation of MHC class II expression by interferon-gamma mediated by the transactivator gene CIITA. *Science*, *265*(5168), 106-109. https://doi.org/10.1126/science.8016643

Stringer, C., Wang, T., Michaelos, M., & Pachitariu, M. (2021). Cellpose: a generalist algorithm for cellular segmentation. *Nat Methods*, *18*(1), 100-106. https://doi.org/10.1038/s41592-020-01018-x

Strunz, M., Simon, L. M., Ansari, M., Kathiriya, J. J., Angelidis, I., Mayr, C. H., Tsidiridis, G., Lange, M., Mattner, L. F., Yee, M., Ogar, P., Sengupta, A., Kukhtevich, I., Schneider, R., Zhao, Z., . . . Schiller, H. B. (2020). Alveolar regeneration through a Krt8+ transitional stem cell state that persists in human lung fibrosis. *Nat Commun*, *11*(1), 3559. https://doi.org/10.1038/s41467-020-17358-3

Subramanian, A., Tamayo, P., Mootha, V. K., Mukherjee, S., Ebert, B. L., Gillette, M. A., Paulovich, A., Pomeroy, S. L., Golub, T. R., Lander, E. S., & Mesirov, J. P. (2005). Gene set enrichment analysis: a knowledge-based approach for interpreting genome-wide expression profiles. *Proc Natl Acad Sci U S A*, *102*(43), 15545-15550. https://doi.org/10.1073/pnas.0506580102

Sugimoto, C., Murakami, Y., Ishii, E., Fujita, H., & Wakao, H. (2022). Reprogramming and redifferentiation of mucosal-associated invariant T cells reveal tumor inhibitory activity. *eLife*, *11*, e70848. https://doi.org/10.7554/eLife.70848

Suliman, S., Murphy, M., Musvosvi, M., Gela, A., Meermeier, E. W., Geldenhuys, H., Hopley, C., Toefy, A., Bilek, N., Veldsman, A., Hanekom, W. A., Johnson, J. L., Boom, W. H., Obermoser, G., Huang, H., Hatherill, M., Lewinsohn, D. M., Nemes, E., & Scriba, T. J. (2019). MR1-Independent Activation of Human Mucosal-Associated Invariant T Cells by Mycobacteria. *J Immunol*, *203*(11), 2917-2927. https://doi.org/10.4049/jimmunol.1900674

Svedberg, F. R., Brown, S. L., Krauss, M. Z., Campbell, L., Sharpe, C., Clausen, M., Howell, G. J., Clark, H., Madsen, J., Evans, C. M., Sutherland, T. E., Ivens, A. C., Thornton, D. J., Grencis, R. K., Hussell, T., Cunoosamy, D. M., Cook, P. C., & MacDonald, A. S. (2019). The lung environment controls alveolar macrophage metabolism and responsiveness in type 2 inflammation. *Nat Immunol*, *20*(5), 571-580. https://doi.org/10.1038/s41590-019-0352-y

Szabó, M., Sárosi, V., Balikó, Z., Bodó, K., Farkas, N., Berki, T., & Engelmann, P. (2017). Deficiency of innate-like T lymphocytes in chronic obstructive pulmonary disease. *Respir Res*, *18*(1), 197. https://doi.org/10.1186/s12931-017-0671-1

Tang, X. Z., Jo, J., Tan, A. T., Sandalova, E., Chia, A., Tan, K. C., Lee, K. H., Gehring, A. J., De Libero, G., & Bertoletti, A. (2013). IL-7 licenses activation of human liver intrasinusoidal mucosal-associated invariant T cells. *J Immunol*, *190*(7), 3142-3152. https://doi.org/10.4049/jimmunol.1203218

Tashiro, J., Rubio, G. A., Limper, A. H., Williams, K., Elliot, S. J., Ninou, I., Aidinis, V., Tzouvelekis, A., & Glassberg, M. K. (2017). Exploring Animal Models That Resemble Idiopathic Pulmonary Fibrosis. *Front Med (Lausanne)*, *4*, 118. https://doi.org/10.3389/fmed.2017.00118

Tilloy, F., Treiner, E., Park, S. H., Garcia, C., Lemonnier, F., de la Salle, H., Bendelac, A., Bonneville, M., & Lantz, O. (1999). An invariant T cell receptor alpha chain defines a novel TAP-independent major histocompatibility complex class Ib-restricted alpha/beta T cell subpopulation in mammals. *J Exp Med*, *189*(12), 1907-1921. https://doi.org/10.1084/jem.189.12.1907

Tort Tarrés, M., Aschenbrenner, F., Maus, R., Stolper, J., Schuette, L., Knudsen, L., Lopez Rodriguez, E., Jonigk, D., Kühnel, M. P., DeLuca, D., Prasse, A., Welte, T., Gauldie, J., Kolb, M. R., & Maus, U. A. (2019). The FMS-like tyrosine kinase-3 ligand/lung dendritic cell axis contributes to regulation of pulmonary fibrosis. *Thorax*, *74*(10), 947-957. https://doi.org/10.1136/thoraxjnl-2018-212603

Traag, V. A., Waltman, L., & van Eck, N. J. (2019). From Louvain to Leiden: guaranteeing well-connected communities. *Sci Rep*, *9*(1), 5233. https://doi.org/10.1038/s41598-019-41695-z

Treiner, E., Duban, L., Bahram, S., Radosavljevic, M., Wanner, V., Tilloy, F., Affaticati, P., Gilfillan, S., & Lantz, O. (2003). Selection of evolutionarily conserved mucosal-associated invariant T cells by MR1. *Nature*, *422*(6928), 164-169. https://doi.org/10.1038/nature01433

Tsoumakidou, M., Karagiannis, K. P., Bouloukaki, I., Zakynthinos, S., Tzanakis, N., & Siafakas, N. M. (2009). Increased bronchoalveolar lavage fluid CD1c expressing dendritic cells in idiopathic pulmonary fibrosis. *Respiration*, *78*(4), 446-452. https://doi.org/10.1159/000226244

Turtle, C. J., Delrow, J., Joslyn, R. C., Swanson, H. M., Basom, R., Tabellini, L., Delaney, C., Heimfeld, S., Hansen, J. A., & Riddell, S. R. (2011). Innate signals overcome acquired TCR signaling pathway regulation and govern the fate of human CD161(hi) CD8alpha(+) semi-invariant T cells. *Blood*, *118*(10), 2752-2762. https://doi.org/10.1182/blood-2011-02-334698

Twentyman, P. R. (1983). Bleomycin--mode of action with particular reference to the cell cycle. *Pharmacol Ther*, *23*(3), 417-441. https://doi.org/10.1016/0163-7258(83)90022-0

Umezawa, H., Maeda, K., Takeuchi, T., & Okami, Y. (1966). New antibiotics, bleomycin A and B. *J Antibiot (Tokyo)*, *19*(5), 200-209.

Ussher, J. E., Bilton, M., Attwod, E., Shadwell, J., Richardson, R., de Lara, C., Mettke, E., Kurioka, A., Hansen, T. H., Klenerman, P., & Willberg, C. B. (2014). CD161++ CD8+ T cells, including the MAIT cell subset, are specifically activated by IL-12+IL-18 in a TCR-independent manner. *Eur J Immunol*, *44*(1), 195-203. https://doi.org/10.1002/eji.201343509

Ussher, J. E., van Wilgenburg, B., Hannaway, R. F., Ruustal, K., Phalora, P., Kurioka, A., Hansen, T. H., Willberg, C. B., Phillips, R. E., & Klenerman, P. (2016). TLR signalling in human antigen-presenting cells regulates MR1-dependent activation of MAIT cells

[Research Article]. *Eur J Immunol*, *46*(7), 1600-1614. https://doi.org/10.1002/eji.201545969

Ussher, J. E., Willberg, C. B., & Klenerman, P. (2018). MAIT cells and viruses. *Immunol Cell Biol*, *96*(6), 630-641. https://doi.org/10.1111/imcb.12008

van Wilgenburg, B., Loh, L., Chen, Z., Pediongco, T. J., Wang, H., Shi, M., Zhao, Z., Koutsakos, M., Nussing, S., Sant, S., Wang, Z., D'Souza, C., Jia, X., Almeida, C. F., Kostenko, L., . . . Hinks, T. S. C. (2018). MAIT cells contribute to protection against lethal influenza infection in vivo. *Nat Commun*, *9*(1), 4706. https://doi.org/10.1038/s41467-018-07207-9

van Wilgenburg, B., Scherwitzl, I., Hutchinson, E. C., Leng, T., Kurioka, A., Kulicke, C., de Lara, C., Cole, S., Vasanawathana, S., Limpitikul, W., Malasit, P., Young, D., Denney, L., Moore, M. D., Fabris, P., . . . Klenerman, P. (2016). MAIT cells are activated during human viral infections. *Nat Commun*, *7*, 11653. https://doi.org/10.1038/ncomms11653

Varelias, A., Bunting, M. D., Ormerod, K. L., Koyama, M., Olver, S. D., Straube, J., Kuns, R. D., Robb, R. J., Henden, A. S., Cooper, L., Lachner, N., Gartlan, K. H., Lantz, O., Kjer-Nielsen, L., Mak, J. Y., . . . Hill, G. R. (2018). Recipient mucosal-associated invariant T cells control GVHD within the colon. *J Clin Invest*, *128*(5), 1919-1936. https://doi.org/10.1172/jci91646

Venkatesan, P. (2023). 2023 GINA report for asthma. *Lancet Respir Med*, *11*(7), 589. https://doi.org/10.1016/s2213-2600(23)00230-8

von Garnier, C., Filgueira, L., Wikstrom, M., Smith, M., Thomas, J. A., Strickland, D. H., Holt, P. G., & Stumbles, P. A. (2005). Anatomical location determines the distribution and function of dendritic cells and other APCs in the respiratory tract. *J Immunol*, *175*(3), 1609-1618. https://doi.org/10.4049/jimmunol.175.3.1609

Wang, H. (2018). *Mucosal associated invariant T cell-mediated vaccination and protection against pathogenic bacteria* [Dissertation, The University of Melbourne].

Wang, H., D'Souza, C., Lim, X. Y., Kostenko, L., Pediongco, T. J., Eckle, S. B. G., Meehan, B. S., Shi, M., Wang, N., Li, S., Liu, L., Mak, J. Y. W., Fairlie, D. P., Iwakura, Y., Gunnersen, J. M., . . . Chen, Z. (2018). MAIT cells protect against pulmonary Legionella longbeachae infection. *Nat Commun*, *9*(1), 3350. https://doi.org/10.1038/s41467-018-05202-8

Wang, H., Kjer-Nielsen, L., Shi, M., D'Souza, C., Pediongco, T. J., Cao, H., Kostenko, L., Lim, X. Y., Eckle, S. B. G., Meehan, B. S., Zhu, T., Wang, B., Zhao, Z., Mak, J. Y. W., Fairlie, D. P., . . . Chen, Z. (2019). IL-23 costimulates antigen-specific MAIT cell activation and enables vaccination against bacterial infection. *Sci Immunol*, *4*(41). https://doi.org/10.1126/sciimmunol.aaw0402

Wang, X., Park, J., Susztak, K., Zhang, N. R., & Li, M. (2019). Bulk tissue cell type deconvolution with multi-subject single-cell expression reference. *Nat Commun*, *10*(1), 380. https://doi.org/10.1038/s41467-018-08023-x

Wang, Y., Maciejewski, B. S., Soto-Reyes, D., Lee, H. S., Warburton, D., & Sanchez-Esteban, J. (2009). Mechanical stretch promotes fetal type II epithelial cell differentiation via

shedding of HB-EGF and TGF-alpha. *J Physiol*, *587*(Pt 8), 1739-1753. https://doi.org/10.1113/jphysiol.2008.163899

Wen, X., Nian, S., Wei, G., Kang, P., Yang, Y., Li, L., Ye, Y., Zhang, L., Wang, S., & Yuan, Q. (2022). Changes in the phenotype and function of mucosal-associated invariant T cells in neutrophilic asthma. *Int Immunopharmacol*, *106*, 108606. https://doi.org/https://doi.org/10.1016/j.intimp.2022.108606

Wijsenbeek, M., Suzuki, A., & Maher, T. M. (2022). Interstitial lung diseases. *Lancet*, *400*(10354), 769-786. https://doi.org/10.1016/s0140-6736(22)01052-2

Williamson, J. D., Sadofsky, L. R., & Hart, S. P. (2015). The pathogenesis of bleomycin-induced lung injury in animals and its applicability to human idiopathic pulmonary fibrosis. *Exp Lung Res*, *41*(2), 57-73.

Wilson, M. S., Madala, S. K., Ramalingam, T. R., Gochuico, B. R., Rosas, I. O., Cheever, A. W., & Wynn, T. A. (2010). Bleomycin and IL-1β–mediated pulmonary fibrosis is IL-17A dependent. *J Exp Med*, *207*(3), 535-552. https://doi.org/10.1084/jem.20092121

Wolf, F. A., Angerer, P., & Theis, F. J. (2018). SCANPY: large-scale single-cell gene expression data analysis. *Genome Biol*, *19*(1), 15. https://doi.org/10.1186/s13059-017-1382-0

Wolock, S. L., Lopez, R., & Klein, A. M. (2019). Scrublet: Computational Identification of Cell Doublets in Single-Cell Transcriptomic Data. *Cell Systems*, *8*(4), 281-291.e289. https://doi.org/https://doi.org/10.1016/j.cels.2018.11.005

Won, E. J., Ju, J. K., Cho, Y. N., Jin, H. M., Park, K. J., Kim, T. J., Kwon, Y. S., Kee, H. J., Kim, J. C., Kee, S. J., & Park, Y. W. (2016). Clinical relevance of circulating mucosal-associated invariant T cell levels and their anti-cancer activity in patients with mucosal-associated cancer. *Oncotarget*, *7*(46), 76274-76290. https://doi.org/10.18632/oncotarget.11187

Wong, E. B., Gold, M. C., Meermeier, E. W., Xulu, B. Z., Khuzwayo, S., Sullivan, Z. A., Mahyari, E., Rogers, Z., Kløverpris, H., Sharma, P. K., Worley, A. H., Lalloo, U., Baijnath, P., Ambaram, A., Naidoo, L., . . . Lewinsohn, D. M. (2019). TRAV1-2(+) CD8(+) T-cells including oligoconal expansions of MAIT cells are enriched in the airways in human tuberculosis. *Commun Biol*, *2*, 203. https://doi.org/10.1038/s42003-019-0442-2

Wu, T., Hu, E., Xu, S., Chen, M., Guo, P., Dai, Z., Feng, T., Zhou, L., Tang, W., Zhan, L., Fu, X., Liu, S., Bo, X., & Yu, G. (2021). clusterProfiler 4.0: A universal enrichment tool for interpreting omics data. *Innovation (Camb)*, *2*(3), 100141. https://doi.org/10.1016/j.xinn.2021.100141

Yan, J., Allen, S., McDonald, E., Das, I., Mak, J. Y. W., Liu, L., Fairlie, D. P., Meehan, B. S., Chen, Z., Corbett, A. J., Varelias, A., Smyth, M. J., & Teng, M. W. L. (2020). MAIT Cells Promote Tumor Initiation, Growth, and Metastases via Tumor MR1. *Cancer Discov*, *10*(1), 124-141. https://doi.org/10.1158/2159-8290.Cd-19-0569

Yang, S., Corbett, S. E., Koga, Y., Wang, Z., Johnson, W. E., Yajima, M., & Campbell, J. D. (2020). Decontamination of ambient RNA in single-cell RNA-seq with DecontX. *Genome Biol*, *21*(1), 57. https://doi.org/10.1186/s13059-020-1950-6

Ye, L., Pan, J., Pasha, M. A., Shen, X., D'Souza, S. S., Fung, I. T. H., Wang, Y., Guo, B., Tang, D. D., & Yang, Q. (2020). Mucosal-associated invariant T cells restrict allergic airway inflammation. *J Allergy Clin Immunol*, *145*(5), 1469-1473.e1464. https://doi.org/10.1016/j.jaci.2019.12.891

Youngs, J., Provine, N. M., Lim, N., Sharpe, H. R., Amini, A., Chen, Y. L., Luo, J., Edmans, M. D., Zacharopoulou, P., Chen, W., Sampson, O., Paton, R., Hurt, W. J., Duncan, D. A., McNaughton, A. L., . . . Bicanic, T. (2021). Identification of immune correlates of fatal outcomes in critically ill COVID-19 patients. *PLoS Pathog*, *17*(9), e1009804. https://doi.org/10.1371/journal.ppat.1009804

Zamoyska, R. (1998). CD4 and CD8: modulators of T-cell receptor recognition of antigen and of immune responses? *Curr Opin Immunol*, *10*(1), 82-87. https://doi.org/10.1016/s0952-7915(98)80036-8

Zelenay, S., Keller, A. M., Whitney, P. G., Schraml, B. U., Deddouche, S., Rogers, N. C., Schulz, O., Sancho, D., & Reis e Sousa, C. (2012). The dendritic cell receptor DNGR-1 controls endocytic handling of necrotic cell antigens to favor cross-priming of CTLs in virus-infected mice. *J Clin Invest*, *122*(5), 1615-1627. https://doi.org/10.1172/jci60644

Zhang, J. G., Czabotar, P. E., Policheni, A. N., Caminschi, I., Wan, S. S., Kitsoulis, S., Tullett, K. M., Robin, A. Y., Brammananth, R., van Delft, M. F., Lu, J., O'Reilly, L. A., Josefsson, E. C., Kile, B. T., Chin, W. J., . . . Lahoud, M. H. (2012). The dendritic cell receptor Clec9A binds damaged cells via exposed actin filaments. *Immunity*, *36*(4), 646-657. https://doi.org/10.1016/j.immuni.2012.03.009

Zhang, Q., Li, P., Zhou, W., Fang, S., & Wang, J. (2022). Participation of Increased Circulating MAIT Cells in Lung Cancer: a Pilot Study. *J Cancer*, *13*(5), 1623-1629. https://doi.org/10.7150/jca.69415

Zhang, Y., Bailey, J. T., Xu, E., Singh, K., Lavaert, M., Link, V. M., D'Souza, S., Hafiz, A., Cao, J., Cao, G., Sant'Angelo, D. B., Sun, W., Belkaid, Y., Bhandoola, A., McGavern, D. B., & Yang, Q. (2022). Mucosal-associated invariant T cells restrict reactive oxidative damage and preserve meningeal barrier integrity and cognitive function. *Nat Immunol*, *23*(12), 1714-1725. https://doi.org/10.1038/s41590-022-01349-1

Zhang, Y., Yoneyama, H., Wang, Y., Ishikawa, S., Hashimoto, S., Gao, J. L., Murphy, P., & Matsushima, K. (2004). Mobilization of dendritic cell precursors into the circulation by administration of MIP-1alpha in mice. *J Natl Cancer Inst*, *96*(3), 201-209. https://doi.org/10.1093/jnci/djh024

Zhao, A. Y., Unterman, A., Abu Hussein, N., Sharma, P., Flint, J., Yan, X., Adams, T. S., Justet, A., Sumida, T. S., Zhao, J., Schupp, J. C., Raredon, M. S. B., Ahangari, F., Zhang, Y., Buendia-Roldan, I., . . . Kaminski, N. (2023). Peripheral Blood Single-Cell Sequencing Uncovers Common and Specific Immune Aberrations in Fibrotic Lung Diseases. *bioRxiv*. https://doi.org/10.1101/2023.09.20.558301

Zhao, Y., Xiong, Z., Lechner, E. J., Klenotic, P. A., Hamburg, B. J., Hulver, M., Khare, A., Oriss, T., Mangalmurti, N., Chan, Y., Zhang, Y., Ross, M. A., Stolz, D. B., Rosengart, M. R., Pilewski, J., Ray, P., Ray, A., Silverstein, R. L., & Lee, J. S. (2014). Thrombospondin-1 triggers macrophage IL-10 production and promotes resolution of

experimental lung injury. *Mucosal Immunol*, *7*(2), 440-448. https://doi.org/10.1038/mi.2013.63

Zhu, L., An, L., Ran, D., Lizarraga, R., Bondy, C., Zhou, X., Harper, R. W., Liao, S. Y., & Chen, Y. (2019). The Club Cell Marker SCGB1A1 Downstream of FOXA2 is Reduced in Asthma. *Am J Respir Cell Mol Biol*, *60*(6), 695-704. https://doi.org/10.1165/rcmb.2018-0199OC